ABSTRACT

Title of Document: DEVELOPMENT OF A SHIFTING MELTING POINT Ag-In PASTE VIA TRANSIENT LIQUID PHASE SINTERING FOR HIGH TEMPERATURE ENVIRONMENTS

Pedro O. Quintero, Doctor of Philosophy, 2008

Directed By: Associate Professor F. Patrick McCluskey, Department of Mechanical Engineering

The increasing demand for electronic devices capable of operating at temperatures above the traditional 125°C limit is driving major efforts in research and development. Devices based on wide band gap semiconductors have been demonstrated to operate at temperatures up to 500°C, but packaging still remains a major hurdle for product development. Recent regulations, such as RoHS and WEEE, increase the complexity of the packaging task as they prohibit the use of certain materials in electronic products such as lead (Pb), which has traditionally been used in high temperature solder attach. The successful development of new attach materials and manufacturing processes will enable the realization of next generation products capable of operating reliably at elevated temperatures. In this investigation a shifting melting point silver (Ag) - indium (In) solder paste that uses a Transient Liquid Phase Sintering (TLPS) process was developed. This novel material and

manufacturing process constitutes a major advancement over the conventional soldering process temperature hierarchy, in which the maximum allowable application temperature is limited by the melting point of the attach material. By virtue of a shifting melting temperature, which results from isothermal solidification during the TLPS process, this attach material can be processed at a relatively low temperature while being capable of sustaining much higher temperatures in use, limited only by its new melting point. In order to develop an empirical kinetics model of the Ag-In TLPS process, a design of experiments (DOE) was used to study the effect of multiple factors on the solidification reaction. These factors include particle size, weight fraction of solute, heating rate, holding time, and processing temperature. The physical implications of the empirical model were confirmed by constructing a diffusion based mechanistic model. Pivotal microstructural information was obtained from metallographic analysis where a transition from an In-rich matrix to an Ag-rich solid solution was observed. The metallographic characteristics, mechanical strength, and electrical conductivity of the resulting Ag-In TLPS material were assessed. This study has resulted in the creation of a novel attach material and method that will enable future development of electronic packaging for high temperature environments. The quantitative description of the reaction kinetics during the TLPS process provided a valuable tool for future development and an optimization of this system.

DEVELOPMENT OF A SHIFTING MELTING POINT Ag-In PASTE VIA TRANSIENT LIQUID PHASE SINTERING FOR HIGH TEMPERATURE ENVIRONMENTS

By

Pedro O. Quintero

Dissertation submitted to the Faculty of the Graduate School of the
University of Maryland, College Park, in partial fulfillment
of the requirements for the degree of
Doctor of Philosophy
2008

Advisory Committee:
Dr. F. Patrick McCluskey, Chair and Advisor
Dr. Mohamad Al-Sheikhly
Dr. Peter Sandborn
Dr. Hugh A. Bruck
Dr. Santiago Solares

Dedication

To my wife, Raisha, for her understanding and continuous support during this journey.

To Mayito, for teaching me how to handle life.

Acknowledgements

I am indebted to my research advisor, Dr. F. Patrick McCluskey, for his support, assistance, and encouragement throughout this investigation. I also express my sincere thanks to Rui Wu and Tim Oberc for been always there. I wish to thank the Department of Mechanical Engineering at the University of Maryland and the CALCE research center for the opportunity to complete my graduate studies.

I would like to thank Dr. Paul A. Sundaram from the University of Puerto Rico-Mayaguez for his encouragement and full support during all these years.

Table of Contents

List of Tables

List of Figures

Chapter 1: Introduction

The development of electronics and microsystems that can operate at temperatures in excess of the traditional maximum [1] of 125°C is a critical enabling technology for the creation of next generation systems. These next generation systems will be used for a wide range of military and commercial applications, including avionics, hybrid-electric automotive electronics, deep well drilling, chemical processing systems, and space/earth explorations. Critical elements of these systems are the sub-assemblies for power control, distribution, and management. The last several years have resulted in the advent of silicon carbide (SiC) power devices operating at temperatures well above 125°C [2]. These devices provide higher switching speed and lower on-state losses with higher thermal conductivity. However, the lack of reliable device packaging materials and methods for these operating conditions is a major reason for the slower acceptance of these devices [3].

1.1 Background

This work will focus on the first-level interconnection process known as die attach. The primary function of die attach is to secure the semiconductor chip to a lead frame or substrate, and to ensure that it does not detach or fracture over an operational lifetime that may include power and temperature cycle excursions. From a design point of view, an ideal die attach material should have good adhesion to both the die and the substrate to avoid delamination, be compliant to provide strain energy absorption, possess a high thermal conductivity so that the heat can be rapidly dissipated from the chip, have an appropriate processing temperature, and maintain

good thermal stability to fit into the soldering process hierarchy. Meeting this last requirement is hindered by a design rule [$T_m > T_a$] that has been identified as a major constraint for the development of high temperature electronic packaging. This constraint results from the fact that the maximum application temperature (T_a) must be less than the melting temperature (T_m) of the selected die attach material. In addition, the utility and reliability of die attach materials may be compromised at temperatures below the solidus, melting, or decomposition temperature, as a result of failure mechanisms related to the thermal stresses induced by temperature cycling and initial die bond cool down [1]. Die fracture and fatigue mechanisms depend primarily on the modulus of the die attach, which determines the fraction of the stress imparted to the die, and on the difference in the coefficient of thermal expansion of the die and substrate, which determines the total thermo-mechanical stress.

Bonding materials can be classified as hard solders, soft solders, glasses, and polymers, which include epoxies and polyimide [4] . Epoxies are the most widely used in commercial applications due to their low cost and their ability to absorb stress by plastic deformation, thus preventing damage to the die. However they cannot withstand high temperature environments without decomposing. Glass materials are stable at high temperature and can tolerate harsh environments, but processing temperatures (T_p) ranging from 400 - 600°C are required. These high temperatures induce which induces residual stresses during cool down. This limits glass material usage to packages completely built from high temperature resistant materials. Soft solders are generally inexpensive, have acceptable thermal conductivity, but are

mechanically weak. Though stiff at low temperatures, they become more compliant and lose strength above 100°C. When these solders are used to bond the die, most of the stress occurs in the bonding layer because they are more compliant than the die and the substrate. However, this propensity for plastic deformation makes them prone to thermal fatigue and creep rupture causing long term reliability problems. Packages intended for elevated temperature applications tend to contain stiffer (hard solder) die attach materials with higher melting temperatures such as gold eutectics (Au-Sn, Au-Ge, Au-Si). These systems have higher moduli, thus higher flow stresses can be tolerated before fatigue and creep damage occurs at elevated temperatures. However, they transfer more stress to the die, often causing failure to occur by die fracture.

1.2 Problem Statement and Motivation

When metallic solders are used as die attach, the application temperature (T_a) dictates the material selection as well as the assembly process. This limitation arises due to the nature of the bonding mechanism, in which the attach material has to melt in order to form a reliable metallurgical interconnection as it solidifies. This implies a design rule in which the melting temperature (T_m) needs to be higher than the T_a, and the processing temperature (T_p) above T_m; [$T_p > T_m > T_a$]. For example, based on this rule, a device intended for a 350°C application will require an attach material with a melting point of ~ 400°C (to avoid re-melting during operation) and a processing temperature close to 450°C. These extreme processing temperatures will result in built-in residual stresses during the cool down stage, which may accelerate thermally activated failure mechanisms yielding reliability problems [5]. Typically, these

temperatures are above the maximum allowable limits for most of the materials used in electronic packaging, causing an economic impact when customized materials are required for such products.

An alternative for the above temperature hierarchy rule is needed for the advancement of high temperature die attach processes, where increasing application temperature is dictating the development of new technologies. Solid state sintering of silver particles has been identified as an alternative [6] because of its excellent thermal and electrical properties. This low temperature joining technique is based on the principle of diffusion welding, where a material is subjected to a temperature below its melting point and assisted by an external pressure to consolidate it into a solid. However, pressures of 40 MPa are required to form a reliable die attach joint, frequently causing catastrophic damage to the devices. An alternative that does not require a high pressure and is based on silver nano-particles has been studied by several researchers [7][8][9]. This technique utilizes the reduction of total free energy as the driving force for the sintering reaction. Nano particles possess a high surface-to-volume ratio and thus a high surface energy due to their size, making them reactive by nature. Therefore, thermodynamics dictates that agglomeration and further growth will occur without the need for external pressure. Actual experimental data have demonstrated partial coagulation of the material in which the continuous metallic film was interrupted by physical ridges that yielded isolated regions. The presence of the organic binder, required for the colloidal suspension, has been suggested as the root cause for reliability problems [9][10].

A transient liquid phase sintering process (TLPS) will be presented in this work as an alternative for high temperature solder attach. Powder mixtures consisting primarily of a high melting point base metal powder (constituent B) can be more easily sintered when in the presence of a low melting point additive powder (constituent A). The TLPS of powder mixtures depends on the formation of a liquid phase at the processing temperature (T_p) that is set to be below the melting point of the base metal powder (T_{mB}) yet above that of the additive phase (T_{mA}). The presence of the liquid enhances mass transport rates and densification (compared to the solid-solid sintering) by exerting a capillary pull to rearrange powder particles [11][12]. This liquid isothermally solidifies over time (transient process) by solute diffusion into the base metal particles as T_p is held above T_{mA}. The advantages offered by TLPS over conventional solid state sintering include rapid densification during sintering because of the capillary action and enhanced mass transport created by the liquid phase, lower sintering temperatures, and reduced microstructural coarsening attributed to shorter and lower temperature sintering. The most significant advantage of TLPS is that the liquid solidifies isothermally, resulting in an in-situ alloying process that yields an alloy having an equilibrium bulk composition that corresponds to the initial mixing ratio of its elemental constituents. This new alloy exhibits a higher melting point (T_{mC}) that permits application temperatures well above the processing temperature. This material also overcomes the traditional temperature hierarchy paradigm by permitting solder attachment at temperatures below the final melting point of the newly formed alloy. This enhanced temperature rule is given by: $T_p > T_{mA}$ which

shifts to $T_{mC} > T_a$, where T_a is, in the end, constrained by T_{mC}. The result is that T_{mC} can then be much higher than T_{mA}. The processing temperature (T_p) is defined by the lower T_{mA}, resulting in $T_m / T_p > 1$. Figure 1 shows a graphical representation of the concept.

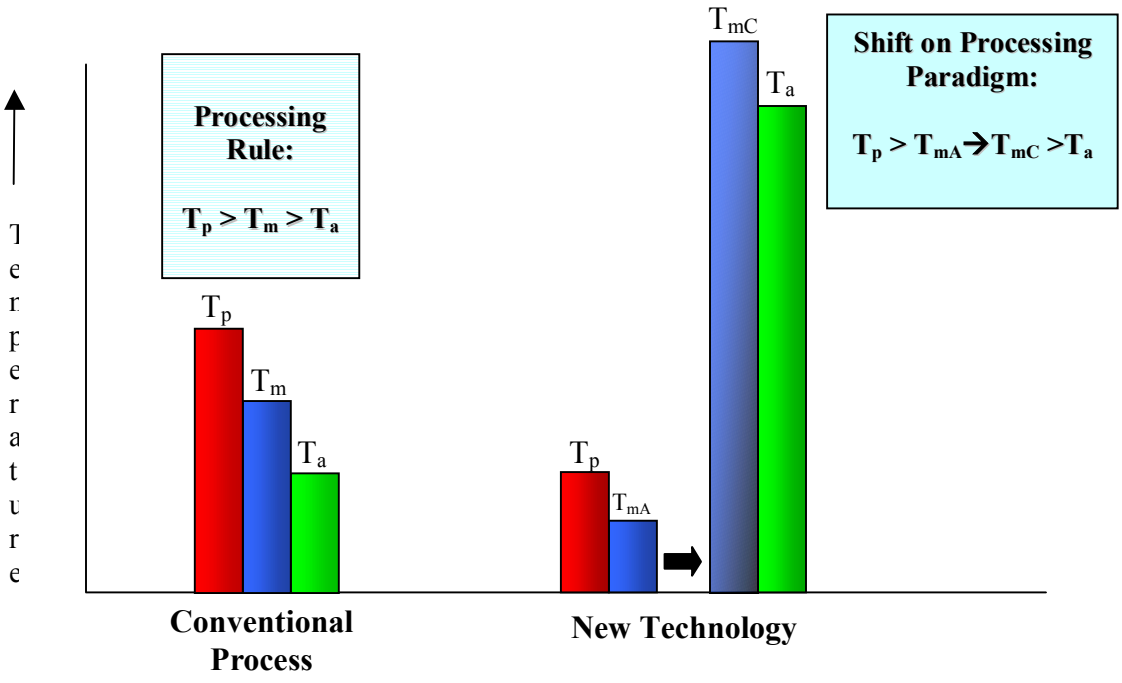

Figure 1. Graphical representation of the conventional process vs. the proposed TLPS technique.

This research will use the fundamental knowledge of TLPS to develop a lead-free silver (Ag) – indium (In) shifting melting point solder paste suitable for high temperature applications. Throughout the investigation, both experimental and analytical methods will be used to study the reaction kinetics so that an appropriate model can be provided as an optimization tool of the completion time for the isothermal solidification process. Understanding the process kinetics as function of

controllable parameters will enable the successful deployment of this process without the uncertainty associated with current trial and error approaches. A microstructural evaluation of the system will assist the interpretation of the experimental observations and shall provide the necessary morphological information as it progresses towards equilibrium. The structure of the sintered material, along with its effect on mechanical, electrical, and thermal properties will be studied.

Chapter 2: Literature Review

The need for high temperature die attach materials and manufacturing processes for packaging devices based on SiC and III – V compound semiconductors where the operating temperature has been raised to 400°C and above, has been acknowledged by several researchers [3][4][6][7][13][14][15][16]. These high temperature devices provide performance advantages in numerous applications in military, commercial, automotive, and avionics. However, to support these devices in packages, high temperature joints are needed. Such joints conventionally require a processing temperature exceeding the melting point of the chosen alloy. The elevated temperatures encountered during the assembly process tend to induce high stresses as the system is cooled down to room temperature. This stress is primarily due to thermal expansion mismatch between the different materials. Novel attach technologies (both materials and processes) that can be used to produce high temperature joints at relative low process temperature for stress reduction and package reliability are desired. Lee [4] presented a synopsis of available attach technologies and their classification, along with some critical properties. From his work, it is evident (based on melting point data) that a new technology is required for high temperature applications such as those discuss above. Table 1 summarizes the physical properties of widely used hard and soft solder alloys.

Table 1. Properties of some commonly used hard and soft solder alloys [4]

Alloy	Melting Point (°C)	Thermal Conductivity (W / m-°C)	CTE (10^{-6} / °C)	Yield Strength (MPa) @: 23°C	100°C	150°C
Hard Solders						
Au - 20Sn	280	57.3	15.9	275	217	165
Au – 12Ge	356	44.4	13.3	185	177	170
Au-3Si	363	27.2	12.3	220	207	195
Soft Solders						
Pb-60Sn	183-188	50.6	24.7	1.5	-	-
Pb-5Sn	308-312	23	29.8	14.8	10.4	5.0

2.1 Sintering as die attach alternative:

A novel low temperature joining technique based on the principles of diffusion welding was proposed by Schwarzbauer [6][17]. Silver was used in this technique as an attach material because it is a comparatively cheap noble metal with excellent thermal and electrical properties, and a melting point of 962°C. In addition, it is readily available in powder form and is soft and malleable facilitating cold welding. High shear and tensile strength values of diffusion-welded thin silver layers have been reported by Crane [18] and O'Brien [19] confirming it as a suitable joining material. The process consists of the deposition of a flake-shaped silver powder paste followed by a drying step at 250°C. Once the organic solvent is removed from the bonding layer, the final sintering step is executed. In this process, the die is compressed at a temperature ranging from 200 - 250°C to ensure that full densification occurs. Pressures of 40 MPa were required to obtain the desired final properties of the die attach. Even though the objective of creating high temperature resistant joints using a low temperature process was attained, the extreme pressure requirements make it a risky operation for the fragile dice. Therefore, a pressureless

approach has been investigated [7]. In this approach, silver nano-particles were introduced as an alternative to the μ-sized flakes to reduce the external pressures required for the solid-solid diffusion mechanism governing the sintering process. In this work [7], the driving force for sintering was provided by the reduction in the total free energy of a system through reduction of the surface energy by particle coalescence. The driving force (DF) is a function of the applied pressure and a geometrical factor (K), which is proportional to the inverse of the particle size (K α 1/r). An expression for this driving force was provided by GQ Lu et al. [7]:

$$DF = P_a\varphi + \gamma_{sv}K$$

where P_a is the applied pressure, φ is the stress intensification factor, γ_{sv} is the surface energy, and K is 1/r where r is the particle radius. Increasing the densification rate is crucial in a sintering process, where the time-to-full compaction must be minimized. Higher processing temperatures will result in faster densification, but the desired low temperature for the die attach process inhibits the usage of this approach. With temperature restricted to a relatively low level, the densification rate is dependant on the driving force. This term can be maximized either by applying a large external pressure or by reducing the particle size (r), the latter being more desirable due to dice cracking problems attributed to large pressures.

The strategy of using nanosilver paste has been discussed previously [7][10][13][20][21], where agglomeration was identified as a critical factor affecting both manufacturability and reliability. The powder has a tendency to absorb a large amount of the fugitive binding solvent required to obtain satisfactory viscosity for

dispersion, so an ultrasonic bath was used to assist in dispersion of the paste. The material consisted of silver nano-particles ranging in size from 10nm to 30 nm and specimens were assembled using a pressure-less sintering process at 280°C. Despite the theoretical advantages of this approach, particle agglomeration combined with the formation of a discontinuous film at the die-substrate interface are still an impediment to reliable implementation. Efforts to improve the assembly process and colloidal formulation are underway by several researchers [10][20][21] who are investigating parameters such as pressure, sintering time, and processing temperature. Metallographic characterization of these specimens have shown a partial coagulation of the material at the joint interface, but the formation of isolated "grain like" structures has been a major concern [9]. Incomplete densification of the attach material, in addition to the lack of a repeatable manufacturing process, has been a driver for further investigation in this area. Nevertheless, the usage of a silver rich material is still desirable due to its excellent thermal and electrical properties.

2.2 Transient liquid phase sintering (TLPS):

Packed powders bond together when heated to temperatures above half of the absolute melting temperature, in a phenomenon known as sintering. A common characteristic of all forms of sintering is a reduction in surface area with accompanying compact-strengthening effect, driven by the formation of inter-particle bonds due to atomic motion at the sintering temperature [11]. During liquid phase sintering, a liquid coexists with a particulate solid at the sintering temperature, enhancing the rate of inter-particle bonding. Liquid phase sintering creates sufficient internal force through liquid capillary action on the particulate solid, thus external

forces are not required. This enhancement in process kinetics, along with the theoretical elimination of external pressure, make this technology a preferred alternative to pure silver sintering for die attach. There are two common ways for obtaining the liquid phase: the use of mixed elemental powders in which the liquid is formed by either melting one of the constituents or by the formation of a eutectic composition, or the use of pre-alloyed powders. The use of elemental powders is often preferred due to its lower cost and availability. The formation of a liquid phase may be transient or persistent during the process depending on the solubility relationship between the main constituents. For the case of high temperature applications, the formation of a persistent low melting temperature phase is detrimental due to the inherent low melting point limitation. Formation of a transient low melting phase is desired since it provides the advantage of low temperature processing, while the elimination of the liquid with time results in a melting point shift that yields a high temperature resistant material. Despite the importance and wide industrial utilization of TLPS as an advanced powder processing method, a fundamental understanding of the process and the critical variables controlling it has not been achieved [11][22][23]. The following section will discuss the fundamental theoretical steps and critical variables that govern the process. The overall intent, however, is to develop a quantitative description of this phenomenon as it pertains to its application in the development of a lead free high temperature die attachment.

2.2.1. Theoretical description of TLPS:

Transient liquid phase joints are formed when a melting point depressant (MPD) in the interlayer diffuses into the surrounding bulk and isothermal solidification results

[24]. A phenomenological description of the TLPS has been presented by Tuah-Poku et al. [25] in which the process has been divided into three stages: dissolution, isothermal solidification, and homogenization as described in Figure 2.

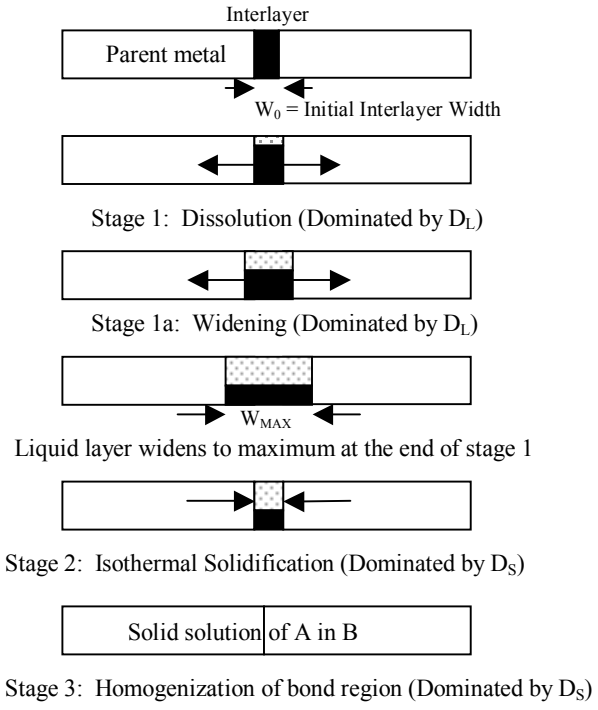

Figure 2. Schematic representation of the TLPS stages as defined by W.D. MacDonald [24]. The width of the regions can be interpreted as the phase volume fraction, whereas the dark indicator (vertical) corresponds to the MPD composition in terms of solute.

The rationale for this theoretical description is based on the evaluation of a binary eutectic phase diagram as shown in Figure 3. In this instance, the parent metal was identified as constituent B, whereas the MPD additive (solute) was referred to as A; this is in accordance with the convention previously used in an earlier section.

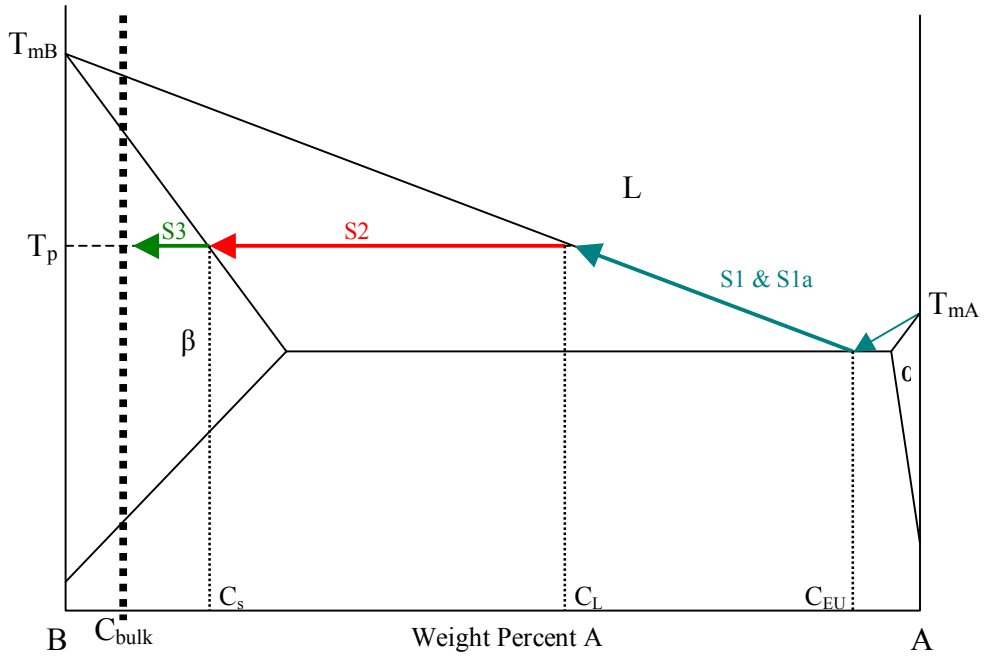

Figure 3. Schematic binary eutectic phase diagram showing the stages in TLPS bonding.

Pure metal A (MPD) is placed between structures of dominant base metal B. Note that the interlayer can be provided in a variety of forms including foil, electroplate film, sputter coat, powder, paste, or any other method that produces a film at the facing surfaces. Upon heating to the processing temperature (T_p) there is an initial solid state reaction that is dominated by interdiffusion resulting in the formation of a eutectic composition (C_{EU}). The formation of a liquid phase comes from the melting of the formed eutectic, as the temperature keeps rising the composition of the liquid phase changes along the liquidus line as presented in the above diagram. During this stage (S1 and S1a) the diffusion mechanism is dominated by the material transport of solid (B) into the liquid. This has been referenced as an erosion phenomenon [11]. As the dissolution progresses, the liquid phase becomes richer in base metal atoms

and widens (due to mass balance) to a maximum value at T_p. The time required for this step has been estimated to be on the order of seconds [25] since it is dominated by the diffusion of a solid into a liquid, i.e. the dominant parameter is diffusivity D_L, which is orders of magnitudes larger [26] than D_S due to the atomic structure differences. The presence of this liquid is the key enabler for this technology. The liquid spreads by capillary action through the powder compact (in the case of powder paste) causing particle rearrangement, enhanced mass transport, and densification. Once the sintering enhancement is accomplished by the spreading liquid and equilibrium is reached, the second stage starts. The isothermal solidification (S2) is the most critical aspect of the process as it requires the greatest amount of time, mainly due to the rate of diffusion into the bulk (D_S). From Figure 3, it is observed that this stage occurs at a constant temperature (T_p) at which the composition of the liquid is constant at C_L and MPD (A) atoms diffuse into the base metal (B). The kinetics of these reactions are controlled by various transport mechanisms, but the bulk diffusion has been demonstrated to be the dominant one [27]. During this stage, the average composition of the system shifts along the arrow identified as S2 in Figure 3. Continuous calculation of liquid weight fraction along this line will result in a fraction that approaches zero, meaning that the liquid would have completely solidified into a solid with composition C_s. Since the isothermal solidification stage depends on the diffusion of the solute in the solid base metal, it is orders of magnitude longer than the dissolution and widening steps. Due to the criticality of this step as it pertains to obtaining the desired results in a reasonable time, the focus of research in this area is on understanding the effects of processing variables such as

solid solubility, particle size, sintering temperature, and composition on the transformation kinetics. Both analytical and experimental methods will be discussed in the following sections. The last stage of the process is homogenization as given by the horizontal representation in Figure 3 (S3). Through solid state diffusion at $T_{p,}$ the whole system homogenizes to a final bulk composition (C_{bulk}), eliminating compositional gradients and providing the desired physical properties of the resulting solid solution of A in a B matrix.

2.2.2. Analytical approach to the TLPS process:

Figure 2 shows the different stages that have been identified in the TLPS process [24][25] in which each step is dominated by specific critical parameters that, when combined as a whole, dictate the kinetics of the process. Base metal particle size, solute diffusivity, processing temperature, heating rate, and bulk solute content of the mixture have been found to influence the amount of liquid formed as well as the length of time required for it to isothermally solidify [23][24][25][27][28]. Being a diffusion bonding problem, TLPS has been examined by analytical models where mass transport at the interlayer, governed by compositional gradients and interdiffusion coefficients, has been used to describe the phenomenon. In the proposed models [23][24][25][27], the condition of local equilibrium at the interface is assumed between the liquid and the solid such that the composition of each phase at the interface can be directly calculated from the phase diagram. It has also been assumed that due to the small thickness of the interlayer, the effect of convection in the liquid is negligible so the problem can be considered as one of pure diffusion. Table 2 provides a summary of the work performed by Tuah-Poku [25].

Table 2. Stages of the TLPS bonding process and its controlling parameters.

Stage	Controlling Parameters	Rapidity	Feature Controlled during the Stage
Dissolution of Interlayer (S1)	D_L	Very fast	Maximum width of the transient interlayer
Homogenization of the Liquid (S1a)	D_L	Fast	
Isothermal Solidification	D_S	Slow	Total time needed for TLPS bonding
Homogenization of the Bond	D_S	Slow	

The derivation of analytical models assumed "sandwiched" structures in which the base metal and additive materials were mated in a planar fashion. A planar interlayer growth was also assumed. Analytical models are useful because they develop an understanding of the effects of various parameters in the process and can be used to validate experimental observations. In this investigation, emphasis will be on the isothermal solidification stage which is the rate controlling step of the process.

2.2.2.1. Mathematics of diffusion:

Transient liquid phase sintering is a diffusion driven process in which the mathematics of diffusion can be used to develop analytical models to describe the governing reactions. Fick's unidirectional first law gives the mass flux (J) of the diffusing solute [29]:

Equation 1

$$J = -D \cdot \left(\frac{\partial C}{\partial x} \right)$$

where D is the diffusion coefficient (assumed to be independent of composition), C is the concentration of the diffusing material (solute), and x is the direction of the mass transfer assuming uni-dimensional diffusion. Fick's second law describes the case of non-steady diffusion in which the concentration changes with position and time. For the one-dimensional case and constant D, it is given by:

Equation 2

$$\partial C / \partial t = D \cdot (\partial^2 C / \partial x^2)$$

Fick's first and second laws provide the basis for all of the analytical work in this area. A comprehensive summary of the modeling efforts on TLPS was given by Zhou et al.[30]. For all analytical methods, a series of assumptions are necessary for the mathematical solution of the resulting partial differential equations. Of critical importance is the assumption of a semi-infinite media which implies that all of the available solute can be absorbed by the solid, and that the process obeys a general square root law, i.e. the reaction rate is proportional to $\sqrt{t}$ for the entire process. A condition of local equilibrium at the solid/liquid interface is also assumed; the position of the interface [X(t)] is defined by a solute mass balance (conservation of solute). The mass balance at the solid/liquid interface as shown in Figure 4 is given by Equation 3 [23][25][27][30][31], where C_L and C_s are the liquid and solid compositions at the solid/liquid interface for a particular processing temperature as given schematically in Figure 3. D_L and D_s are the solute diffusivities in the liquid and solid, respectively.

Equation 3

$$(C_L - C_S) \cdot \frac{dX(t)}{dt} = D_S \cdot \frac{\partial C_S}{\partial x} - D_L \cdot \frac{\partial C_L}{\partial x}$$

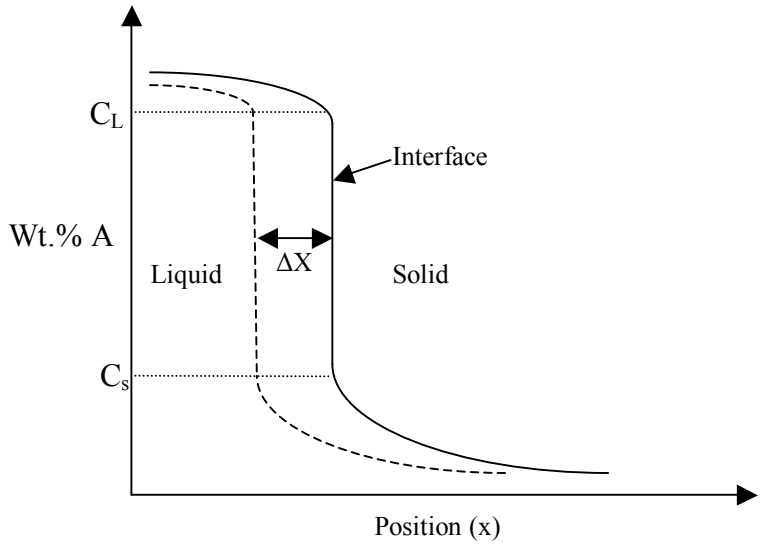

Figure 4. Solid/liquid moving interface schematic showing the migration of the interface by a distance ΔX [31].

Figure 4 shows a schematic of the moving solid/liquid interface, in which the solid line represents the position of the boundary at time, t. After an isothermal solidification interval, dt, the new interface has shifted a distance ΔX as shown by the dotted line. From the above diagram, it can be observed that with increased holding time the liquid can is consumed by the diffusional solidification of the moving boundary. The direction of the interface motion is driven by the concentration gradient as expressed in Equation 3.

2.2.2.2. Dissolution stage (S1):

Zhou et al. [31] have shown that there are no suitable analytical solutions for the heating portion, i.e. heating from the melting point to the processing temperature. The reason for this lack of models stems from the difficulty of this task, where both the concentration of solute at the interface (C_s and C_L) and the diffusivity values varies as temperature rises. This can be observed by inspection of Figure 3.

However, if a fast heating rate is assumed, the time to reach T_p becomes negligible; thus an instantaneous T_p can be considered for the model. There then exists a period of time required to reach a homogeneous liquid state with an equilibrium composition of C_L at T_p. Tuah-Poku et al. [25] used a method proposed by Lesoult [32] to predict this time. In his work, he assumed that the dissolution stops when the interlayer width reaches its maximum (W_{max}) in Figure 2. This dissolution is controlled by the diffusion of the base metal into the liquid (D_L). From this approach it was estimated that the time to complete dissolution of the interlayer is on the order of seconds (less than 2 minutes) [25]. Nakagawa [30][33] used a numerical finite difference model in which both the heating and dissolution were combined. In his work, he concluded that the time for completion of this stage is dependent upon the diffusivity of the base metal into the liquid (C_L), as well as on the heating rate used to reach T_p. Although none of these modeling attempts can be applied with confidence during the dissolution stage, there is a general agreement on the fact that the time for dissolution can be considered negligible when compared to the duration of the subsequent stages. This is provided that the process takes place at a high enough heating rate (above ~20°C/min.) [28][30].

2.2.2.3. Isothermal solidification stage (S2):

The isothermal solidification stage is the most critical step of the TLPS process. It is during this stage that the in-situ alloying takes place, which results in the desired shift in melting point. The solidification reaction, or transformation into the final solid solution, occurs by diffusion of solute atoms into the solid matrix. This can be a lengthy process. Thus, estimation or modeling of this stage is a critical enabler for

the successful practical development of this technique. From reviewing the relevant literature in this topic, it was found that all analytical models are based on solutions to Fick's diffusion laws for semi-infinite media with constant surface composition. There have been two basic approaches, a simplistic formulation in which a stationary interface is assumed and a more rigorous solution that considers a moving interface as a result of the atomic flux. Both approaches used a similar method for the mathematical formulation of the problem; a description of this method follows.

If local equilibrium is assumed to be established at the solid/liquid interface, the composition of the solid phase at the interface (C_s) during the isothermal (T_p) solidification stage is fixed by the tie line on the equilibrium phase diagram (horizontal S2 line at T_p in Figure 3). In this case, diffusion of solute (A) into the base material (B) may be modeled as a semi-infinite medium with constant surface composition. Solution to this problem requires the definition of initial and boundary conditions, which are given below:

Initial Condition:

Equation 4

$$C(x,0) = C_o$$

Boundary Conditions:

Equation 5

$$C(0,t) = C_S$$

Equation 6

$$C(\infty,t) = C_o$$

Where C_o is the initial composition of solute in the base metal and C_S is the solidus composition at the processing temperature, T_p. Initial condition t = 0 refers to the start of the isothermal stage, i.e. it assumes that the time for S1 is negligible. The boundary condition at the interface, x = 0, is valid under the assumption that local equilibrium is maintained, thus the composition C_S is given by the tie line from the phase diagram. The second boundary condition, x = ∞, is valid for the semi-infinitely large media, which implies that there is no net effect on the composition of the base material far from the interface. The solution of Fick's second law (Equation 2) for the above initial and boundary conditions, assuming constant D and semi-infinite media, was derived by Crank [29]:

Equation 7

$$C(x,t) = C_S + (C_o - C_S) \cdot erf\left(\frac{x}{2\sqrt{Dt}}\right)$$

A general form of Equation 7 can be used to develop a common solution for the isothermal solidification stage for the different initial and boundary conditions that may be encountered; this will be explained in greater detail in section 2.2.2.5.

2.2.2.4. Analytical solution for the stationary interface:

The simplest treatment of the isothermal solidification process assumes that the solid/liquid interface is fixed. For this scenario, Tuah-Poku [25] developed a method to find the time required for completion of the solidification stage based on the fundamental work presented by Lesoult [32]. Differentiating Equation 7 with respect to position (x) results in the following expression:

Equation 8

$$\frac{\partial C}{\partial x} = (C_o - C_S) \cdot \frac{\partial}{\partial x} erf\left(\frac{x}{2\sqrt{Dt}}\right)$$

Solution to Equation 8 is given by [29]:

Equation 9

$$\frac{\partial C}{\partial x} = \frac{(C_o - C_S)}{\sqrt{\pi Dt}} \cdot \exp\left(\frac{-x^2}{4Dt}\right)$$

By substituting the solution of Equation 9 into Fick's first law (Equation 1) at x = 0 (stationary interface), the solute mass flux through the boundary is given by:

Equation 10

$$J = (C_S - C_o) \cdot \sqrt{\frac{D}{\pi \cdot t}}$$

Considering that the isothermal solidification stage is complete when all of the initial solute in the liquid has diffused across the interface, a time to solidification can be calculated by knowing the total mass transferred during this stage. The mass across the interface is given by integrating the flux over time:

Equation 11

$$M = \int J \cdot dt = \int (C_S - C_o) \cdot \sqrt{\frac{D}{\pi \cdot t}} \cdot dt$$

The solution to Equation 11 is given by:

Equation 12

$$M = 2 \cdot (C_S - C_o) \cdot \sqrt{\frac{D \cdot t}{\pi}}$$

From a conservation of mass argument, the total initial mass of solute in the system, i.e. $(C_{Li} \cdot W_i)$, must equal the total mass of solute transferred through the interface, i.e. M from Equation 12. By making these substitutions and considering the symmetry

plane at the center line of Figure 2, the total time for isothermal solidification assuming a stationary interface is given by:

Equation 13

$$t = \frac{\pi}{16 \cdot D} \cdot \left(\frac{C_{Li} \cdot W_i}{C_S - C_o} \right)^2$$

There exists a significant error associated with this solution [23][24][28][31] due to the fact that the moving solid/liquid interface was neglected. This stationary interface resulted in a systematic overestimation of the time required for the isothermal solidification, yielding disappointing results for practical applications. A more rigorous and accurate treatment is required for more useful predictions of the TLPS system.

2.2.2.5. Analytical formulation for the moving boundary problem:

When a solid and a liquid are brought together in a planar fashion, as shown in Figure 2, and held isothermally for a period of time, there will be an atomic potential gradient at the interface that will induce a net atomic flux. If local equilibrium at the interface is assumed, the solute concentration of each phase is given by the phase diagram. Figure 4 shows the general schematic representation of this condition in which both concentration profiles within the solid and liquid phases are given by a penetration curve from the error function solution of Fick's second law. It has been demonstrated [34] that the concentration gradient within the liquid can be assumed constant due to the openness of its structure in which complete mixing is possible. With that condition, an updated schematic of the "sandwiched" structure is given in Figure 5.

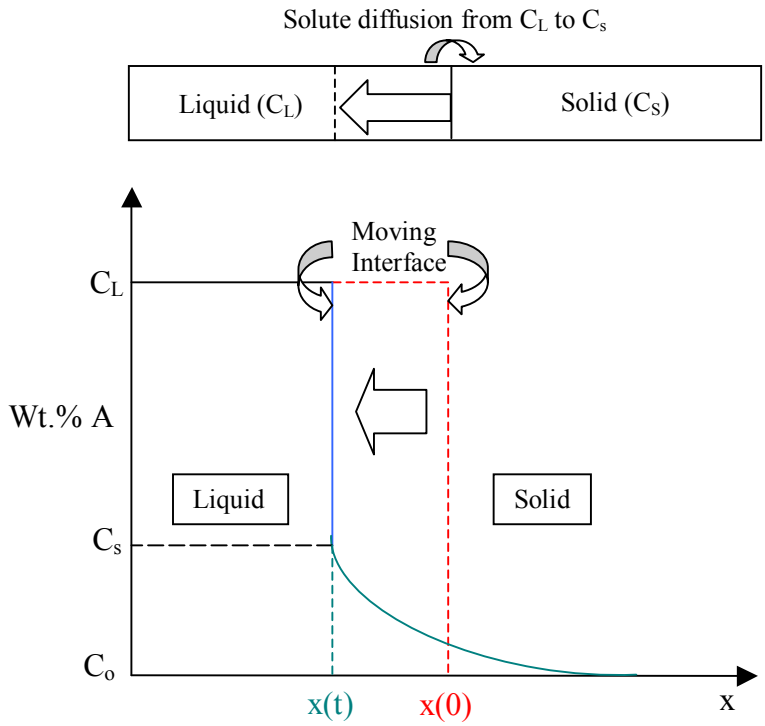

Figure 5. Schematic representation of the moving interface. The large arrow indicates the direction of the interface movement with time while the vertical scale represents the composition percent in terms of additive material (solute A).

A zero concentration gradient within the solid implies a $\partial C_L / \partial x$ equals to zero, which, when substituted in Equation 3, results in an interface motion always in the direction of the liquid as given by the arrows in the above schematic. This interface motion can be explained by the equilibrium assumption together with the conservation of solute principle. Initially, at t = 0, the liquid has a composition C_L whereas the solid's composition is C_o. This condition is represented by the dotted line in Figure 5, where the position of the interface is given by x(0) = 0. At some later time increment dt, the boundary moves into the liquid through a distance dx to a new position x(t). Note that at this instant, the concentration of the liquid is constant with no gradient within the liquid and the concentration at the new interface position (solid vertical line) is constant at C_s. The vertical magnitude of this line represents

the solute compositional gradient across the interface, i.e. $C_L - C_s$. Away from the interface, at increasing distance into the solid, the solute content decreases towards C_o following the penetration curve from the solution of Fick's second law. For this investigation, the solution of the penetration curve [C(x,t)] is not critical since it deals with a solid solution of A in B, which has already attained the desired effect of a shift in its melting point. What is desired is to obtain the rate at which the liquid solidifies isothermally, a parameter that is related to the movement of the boundary. The movement of the interface has the effect of converting a volume of material, equivalent to $A \cdot dx$, from a composition C_L to a composition C_s. In order for this to occur, a total of $(C_L - C_s) \cdot A \cdot dx$ atoms of solute must diffuse across the interface (conservation of solute). From Fick's first law (Equation 1), this number of atoms for an incremental time step (dt) should be equal to:

Equation 14

$$J \cdot dt = D \cdot \left(\frac{\partial C}{\partial x} \right) \cdot dt$$

Equating these two quantities and assuming unit area (A =1) gives us:

Equation 15

$$(C_L - C_S) \cdot dx = D \cdot \left(\frac{\partial C}{\partial x} \right) \cdot dt$$

Rewriting the above equation gives an expression for the interface velocity; this is the derivation of the expression given in Equation 3.

Equation 16

$$(C_L - C_S) \cdot \frac{dx}{dt} = D \cdot \left(\frac{\partial C}{\partial x} \right)$$

As mentioned above, the real interest of the analytical model is to obtain an estimation of the interface rate parameter, i.e. estimate the reaction rate for the transformation or consumption of the liquid. The derivation for the method is as follows, based on the work of several researchers in this area [27][31][32]. From Figure 5, the position of the interface can be defined as x = x(t), where x(0) = 0 is the initial position at the start of the isothermal solidification stage, i.e. end of the dissolution stage. For this system the boundary conditions now becomes:

Equation 17

$$C(x(t),t) = C_S$$

Equation 18

$$C(\infty,t) = C_o$$

The solute concentration profile in the base metal is given by the solution of Fick's second law, which can be assumed to take a general form of Equation 7 [29][32]. This results in:

Equation 19

$$C(x,t) = A + B \cdot erf\left(\frac{x}{2\sqrt{Dt}}\right)$$

Where A and B are constants that depend on the particular boundary conditions. The boundary condition given by Equation 17 implies that at any time during the isothermal solidification stage, the composition of the solid at the interface is a constant (C_s), which when substituted in Equation 19 yields the following expression:

Equation 20

$$C(x(t),t) = A + B \cdot erf\left(\frac{x(t)}{2\sqrt{Dt}}\right) = C_S$$

Equation 20 can only be true if the argument of the error function is constant; thus, an expression for this constant (K), which is the interface rate parameter, has been defined as [34]:

Equation 21

$$K = \frac{x(t)}{2\sqrt{Dt}}$$

Equation 21 shows the origin of the relationship between the reaction rate and the square root of time, a condition typically assumed for all diffusion driven mechanisms. As was demonstrated here, it comes from the assumption of local equilibrium at the interface and from the application of an error function solution to Fick's second law. This solution is valid for the time period governed by the isothermal solidification process, as given by the initial and boundary conditions assumed for the mathematical formulation of the problem. With the above boundary conditions and the definition of the rate parameter (K), the values for constants A and B are given [31][32]:

Equation 22

$$A = C_o - \frac{C_S - C_o}{erf(K) - 1}$$

Equation 23

$$B = \frac{C_S - C_o}{erf(K) - 1}$$

With A and B defined, the solution to Fick's second law for a semi-infinite media with a constant surface composition and a moving interface is:

Equation 24

$$C(x,t) = C_o - \frac{C_S - C_o}{erf(K) - 1} + \frac{C_S - C_o}{erf(K) - 1} \cdot erf\left(\frac{x}{2\sqrt{Dt}}\right)$$

Solving Equation 21 for x(t) and taking its derivative with time gave an expression for dx(t)/dt, whereas a partial derivative of Equation 24 with respect to position (x) yielded an expression for $\partial C/\partial x$. Substituting these results into the mass balance function (Equation 16) resulted in an equation for the interface rate parameter (K). This function requires a numerical solution for the evaluation of K [23][27][35][36].

Equation 25

$$\frac{C_S - C_o}{C_L - C_S} = \sqrt{\pi} \cdot \frac{K \cdot (1 + erf(K))}{\exp(-K^2)}$$

From inspecting Equation 25, it can be observed that the rate parameter (K) can be evaluated for any system during the isothermal solidification stage in which the local equilibrium condition permits the usage of the phase diagram to obtain all the necessary constant compositions (left hand side term). Note that from this analytical approach, the solidification rate (K) depends only on the dimensionless concentration potential term; no geometrical effects are considered. This is an artifact of the semi-infinite media assumption for the Crank solution. Illingworth et al.[36] defined the compositional potential as a dimensionless thermodynamic parameter, Ω:

Equation 26

$$\Omega = \frac{C_S - C_o}{C_L - C_S}$$

In their work [36] a graphical solution for Equation 25 was given. This solution allows the K value to be found for any particular Ω. Lesoult [32] also provided tabulated results for K for given compositional gradients. From this work it could be

possible to obtain an estimate of the solidification rate during the isothermal solidification process provided that C_s, C_L, and C_o are known. Tuah-Poku [25] used this analytical approach to calculate the time for the completion of isothermal solidification for a planar Ag/Cu/Ag structure. In his work, he estimated the K value from the tabulated data given by Lesoult. The estimated time obtained from this method was on the order of hours, which led to some interesting conclusions. First, it was confirmed that the isothermal solidification stage is in fact the rate controlling step of the process so emphasis should be on its optimization. Second, it is evident that a planar system is not an efficient set up since the interface area available for diffusion is constrained, resulting in a major delaying effect. Sandwiched structures are typically used for their ability to closely control composition and surface roughness. Furthermore they are modeled with relative ease. However, from a processing stand point, the effective surface area available for diffusion is greatly increased by using fine powders. For the current investigation, a powder method will be introduced. In this method the particles not only provide the solute material but also the base metal matrix into which diffusion occurs. This allows for solidification time to be reduced by over two orders of magnitude when compared to planar surfaces [37]. Controlling and modeling powder systems is major challenge due to the nature of particles, in which the assumption of mono-sized and perfectly shaped particles is far from reality.

2.2.3. Experimental approach for studying TLPS kinetics:

One of the major drawbacks of TLPS is its sensitivity to processing conditions, making it a complex problem in terms of process control and optimization. These

complexities explain the current lack of quantitative scientific description of its stages. Savitskii [38] summarized the experimental work that has been performed in the investigation of TLPS where the dominant experimental technique is dilatometry. In this approach, the formation of a liquid phase can only be inferred by measuring the dimensional changes of the samples as function of time and temperature, but no emphasis has been placed on the duration of the liquid phase remaining in the specimen [28]. This lack of emphasis in previous work has been attributed [28] to (a) the difficulties in experimentally measuring of the quantity of liquid present at a given time, and (b) for most current commercial applications, the fact that the amount of liquid does not represents an important variable [11]. However, for our intended application it has been explained that the amount of liquid is important for the enhancement of the sintering process in terms of wetting forces and mass transport; its remaining fraction during the isothermal solidification process dictates the rate constant as well as the ability to form a variable melting point alloy. Therefore, understanding liquid formation and duration is fundamental in our effort to develop the proposed solution for the high temperature applications attach system.

An experimental technique to measure liquid phase formation directly and quantitatively using differential scanning calorimetry (DSC) has been developed by Corbin and Kuntz [22][31][39][40]. This method allows the determination of initial liquid formation as well as its duration, i.e. the kinetics of the isothermal solidification step. This technique has enabled characterization of the process

kinetics, resulting in advancement of the understanding of the progression of TLPS process [40].

Initial attempts to study the process kinetics of TLPS used metallographic techniques [24][25] where evolution of the phases was analyzed on quenched specimens at particular elapsed times during the process. This method was subject to large errors of measurement since the solid-liquid interface is not planar but scalloped instead. This fact, along with being a tedious time consuming technique, provides incentive to further investigate feasible experimental methods. The use of the DSC technique provides a more accurate and relatively simple method that can be used to optimize parameters, such as temperature and time, in lieu of its capacity to describe the process kinetics [39].

Chapter 3: Objectives and Statement of Work

In this research, a silver-indium (Ag-In) paste is proposed as an alternative attach material for high temperature applications. Developing a material in the form of a paste provides some advantages over the traditional planar systems. From a reaction kinetics perspective, it should decrease the time to solidification, thus making it a feasible alternative for volume manufacturing. From an assembly process perspective, a paste can be handled and processed using standard techniques and equipment such as stencil printing and reflow furnaces. This represents a key advantage over the thin film techniques required for the deposition of materials, both in economical terms and throughput. This proposed system is to be processed at a relatively low temperature via a Transient Liquid Phase Sintering (TLPS) technique. The in-situ alloying process that takes place during the isothermal hold results in a variable melting point material with a shift on its initial melting temperature ($T_{mA} \rightarrow T_{mC}$). Powder equilibrium composition, particle shape and size, along with the processing temperature and time profile, are the critical factors in the formation of a solid compact that can be used for attachment of electronic devices for high temperature applications. The fact that the melting point of the material changes dramatically during the process explains the novel feature of this proposed research. In this instance, the processing temperature is well below the new melting temperature that defines the operating limit of the system. Experimental observations with different techniques will provide the required data for the scientific study in the evolution of the proposed system. A theoretical diffusion based model, considering the physics of the process, will serve as a reference for the experimental results. The

combination of empirical data and the results from theoretical models, will provide the necessary information to quantitatively describe the phenomenological aspects of the proposed attach system, so it can be controlled for the particular application conditions. The statement of work for this investigation is as follows:

- Use a TLPS technique to develop a shifting melting point Ag-In die attach in the form of a solder paste suitable for high temperature environment.
- Study the interface kinetics of this binary system using a DSC experimental technique to estimate the reaction rate (k) of the solidification process.
- Use metallurgical techniques to complement and assist the analysis of the obtained data in an effort to provide physical evidence of the theoretical stages of the TLPS process.
- Develop an empirical model of the process as a function of controllable parameters using a response surface methodology. This model will provide the scientific community with a parameter optimization tool for a more efficient implementation on practical applications. Metallurgical and analytical methods will be used to verify the adequacy and physical significance of the proposed model.
- Characterize the resulting sintered material in terms of structural morphology and its corresponding electrical, thermal, and mechanical properties.
- Utilize the kinetics model in combination with measured physical properties to recommend an optimal system in terms of minimization or processing time while providing acceptable properties.

- Assess the reliability of the Ag-In sintered material by passive thermal cycling of die attach specimens.

Chapter 4: TLPS of the Ag-In Binary System

Transient liquid phase sintered joints are formed when a melting point depressant (MPD) diffuses into the surrounding base metal and isothermal solidification results; the kinetics of the process are thus controlled by diffusion of the MPD into the base material. This technology can be applied to any system where the driving force inherently leads to solid state equilibrium [24]. One of the first uses of liquid phase sintering for metals is attributed to the Incas, who converted platinum grains into consolidated form by the use of gold bonds. Artifacts from this process indicate its use over 500 years ago [11]. The first attempt to use this technology as a semi-conductor attach is attributed to Bernstein [41]. In his work, solid-liquid interdiffusion (SLID) was used, however, persistent liquid was documented as a drawback for this application. When appropriate constituents are selected, TLPS produces "invisible" joints that have strengths and other properties similar to the base material [24]. In fact, the interlayer must meet the following criteria:

1) At least one element, (MPD), must have solid solubility in the base metal.
2) The MPD must have a significant diffusivity at the bonding temperature to ensure reasonable processing time. MacDonald and Eagar [24] reported that to achieve an acceptable time, the solute diffusivity into the base metal (isothermal solidification stage) must be in the order of 10^{-14} m^2/s.
3) The elements in the interlayer must not be detrimental to the physical and mechanical properties of the base material.
4) The interface between the two metals must be clean and free of oxides.

5) Bulk composition of the metallurgical system should be selected to minimize bonding time (dominated by the isothermal solidification stage) and to provide adequate wetting forces.

In their fundamental work regarding TLPS, MacDonald et al. [24] presented a synopsis of key conditions that have proven to be critical: (a) for fast processing times, an interstitial diffuser is helpful during the initial alloying stage; (b) selection criteria for the applicability of TLPS bonding to a particular system should include the assessment of the system's stability at Tp as well as the solubility of the MPD into the base; (c) intermetallic formation can be tolerated in binary systems with peritectic reactions, but may require extended homogenization; (d) base metal mechanical properties can be achieved, but the joint always remains susceptible to reduced toughness.

Based on the literature review, previous work in the area of high temperature attachment, and its favorable properties, the Ag-In binary system has been selected as a suitable alternative to develop an attach material by means of transient liquid phase sintering. In the following sections, the electrical, mechanical, and physical properties of both silver and indium will be presented along with the analysis of the equilibrium phase diagram. This metallurgical system will be further analyzed according to the critical conditions required for a successful application of TLPS; the formulation of a solder paste will also be discussed. Finally the phase evolution along the stages of the process will be presented based on the study of the equilibrium

phase diagram as well as a qualitative description of the progression of the system towards the equilibrium composition.

4.1 Properties of silver (Ag) and indium (In):

A successful development of a TLPS attach requires both a high melting point base material with a substantial solid solubility of the melting point depressant, and properties for specific design applications. The MPD constituent must posses a relatively low melting point, should diffuse easily through the base metal matrix, and must form a stable solid-solution with the main constituent. For the case of a semi-conductor power device attach, the metallic joint must not only provide the mechanical integrity, but also a good thermal and electrical conduction path. These requirements, along with the lead free constraints of the Restriction of Hazardous Substance (RoHS) and WEEE regulations, are all reasons for the selection of the Ag-In binary system for our TLPS die attach. This is a result of the excellent properties of the pure elements individually, and for the system's capacity to form the intended structure based on the study of its binary phase diagram. Table 3 provides the critical properties of the two main constituents of the proposed metallurgical system.

Table 3. Properties of the main elemental constituents of the attach system [42][43][44].

Properties	Indium (In)	Silver (Ag)
Physical Properties		
Atomic Number	49	47
Atomic Mass	114.82	107.87
Density (g/cc)	7.31	10.49
Crystal Structure (25°C)	FCT (a = b = 0.325nm, c = 0.495nm)	FCC (a = b = c = 0.409nm)
Mechanical Properties		
Hardness (Vickers)	10	25
UTS (Annealed)	4.5 MPa	140 MPa
Modulus of Elasticity (E)	12.7 GPa	76 GPa
Poisson's Ratio	0.45	0.37
Shear Modulus (G)	4.4 GPa	27.8 GPa

Properties	Indium (In)	Silver (Ag)
Electrical Properties		
Electrical Resistivity (25°C)	9 X 10^{-6} ohm-cm	1.55 X 10^{-6} ohm-cm
Thermal Properties		
Heat of Fusion	28.5 J/g	105 J/g
CTE (25°C)	33 µm/m-°C	19.6 µm/m-°C
Specific Heat	0.239 J/g-°C	0.234 J/g-°C
Thermal Conductivity (25°C)	83.7 W/m-K	419 W/m-K
Melting Point	156.6 °C	962 °C

4.2 Ag-In binary system:

In order to study the kinetics and evolution of the process, it is critical to understand the phases present in the binary system and their transformations as a function of composition and temperature. Equilibrium phase diagrams represent the relationship between the temperature and composition, as well as the quantities of phases present at equilibrium. Phase diagrams also are helpful in predicting phase transformation and the resulting microstructures, which may have equilibrium or non-equilibrium character [45]. Figure 6 depicts the equilibrium phase diagram of the Ag-In binary system [46], which will be a crucial instrument throughout this investigation. This diagram will provide the basis for the selection of possible compositions based on the solubility limits, will suggest possible processing temperatures based on the phase transformations, will provide compositional data necessary for theoretical calculations of amount of phases present, and will serve as reference for the experimental findings from the DSC testing.

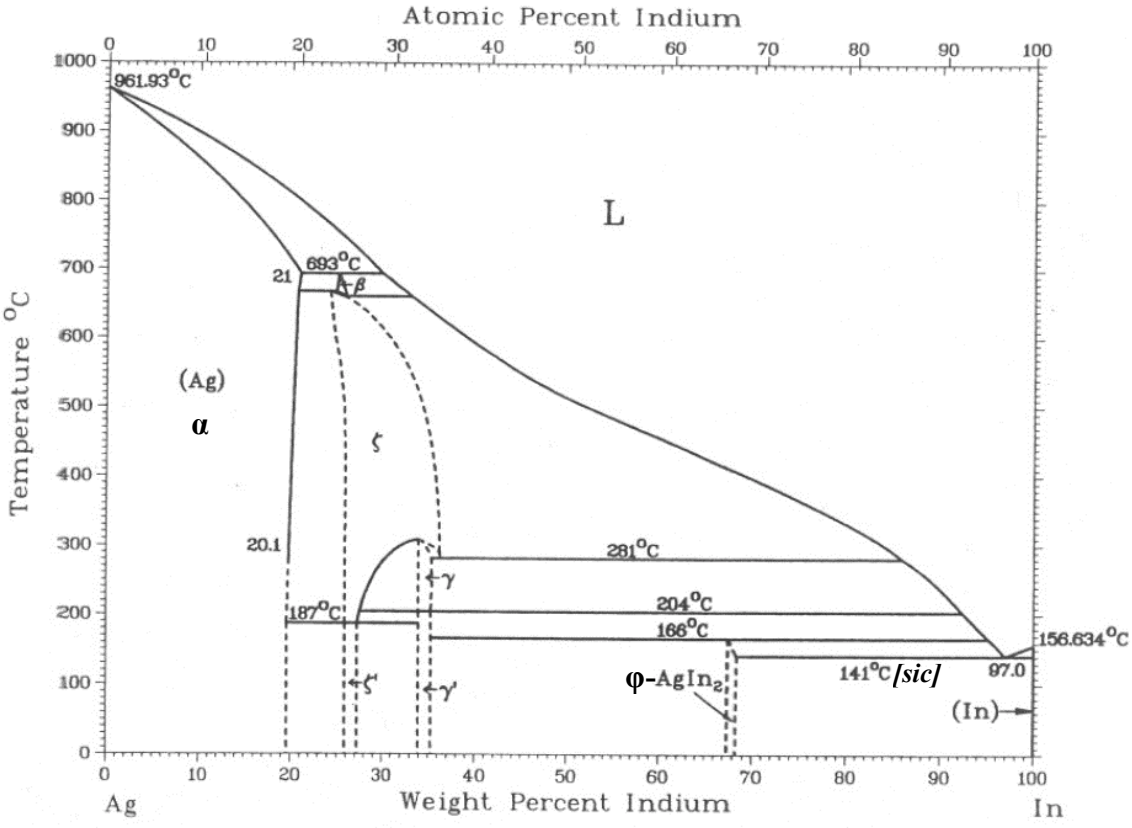

Figure 6. Equilibrium phase diagram of the Ag-In binary system [46].

From the above figure, it is evident that silver has a relatively high melting temperature (961.9°C) while that of indium (156.6°C) is relatively low. This is a good indication of a possible TLPS process in which the base material will be silver and the melting point depressant will be indium. By inspection, it can be seen that the maximum solid solubility of indium into the ζ phase is given at 37 Wt. % In, although Baren [47] reported it at 40 Wt.% In, where silver is present as a Ag-rich solid solution. At 300°C the ζ phase, which has an HCP structure, undergoes an allotropic transformation into γ phase (rhombohedral) that is stable to room temperature. It can be observed that the solvus lines of the Ag-rich phases are not sensitive to temperature, as suggested by their steep slope which is almost vertical along the

temperature scale. For a successful TLPS system, it has been demonstrated that the solubility of the MPD into the base material is very important since it provides the capacity of having a stable final solid solution with no low melting point material precipitating out as a second phase. In this case, a solid solubility limit larger than 25 Wt. % In is a favorable characteristic. The formation of a eutectic at 97 Wt. % In with a melting point of 147°C [47] (erroneously reported in Figure 6 as 141°C) is a key factor in the proposed system. This eutectic has a composition very close to 100 Wt. % In, which will only require minimal solid state interdiffusion for its formation, a critical factor in the proposed system since it means that negligible time will be required for this transformation. Based on the initial inspection of the phase diagram and considering the requirements for a successful development of a TLPS process, it can be inferred that the proposed system should be considered for further investigation.

4.3 Diffusion and interactions of the Ag-In couples:

Most material reactions and processes rely on the transfer of mass either within a specific solid or from a liquid, a gas, or another solid phase. This mechanism is known as diffusion, the phenomenon of material transport by atomic motion. This physical mechanism can be demonstrated with the use of a diffusion couple, which is formed by the joining of two different materials to make an interface contact. Concentrations of both metals vary with position, suggesting that atoms of one material have migrated into the other and vice versa. This process, whereby atoms of one metal diffuse into another, is termed interdiffusion. From an atomic perspective, diffusion is the stepwise migration of atoms from lattice site to lattice site. For an

atom to make this move, two conditions must be met: (1) there must be an empty adjacent site, and (2) the atom must have sufficient energy to break bonds with its neighbor atoms and then cause some lattice distortion during the displacement [45]. Several different models for this atomic motion have been proposed, of these possibilities, two dominate for metallic diffusion. In vacancy diffusion there is an interchange of an atom from a normal lattice position to an adjacent vacant lattice site. The likelihood or probability of having a vacant site present at a particular time and location is a constraint for this mechanism. A second type of diffusion involves atoms that migrate from an interstitial site to a neighboring one that is empty. In most metal alloys, interstitial diffusion occurs more rapidly than vacancy diffusion, since the interstitial atoms are smaller and thus more mobile. Furthermore, there are more empty interstitial positions than vacancies; hence the probability of interstitial atomic movement is greater. A third type of atomic migration may also occur along dislocations and grain boundaries; this is called "short circuit" diffusion paths because the diffusion rates are much faster than in the above mechanisms mentioned previously. A phenomenon explained by the open structure at these defects which provide empty sites and minimizes lattice distortion during displacement.

Diffusion is a time-dependant process, i.e. the quantity of an element that is transported within another is a function of time. In studying the kinetics of the proposed binary system, it is necessary to know how fast the diffusion occurs. This is important because diffusion is the dominant mechanism in the progression of the TLPS. This rate of mass transfer is known as diffusion flux (J), which is the number

of atoms (M) diffusing through a perpendicular cross sectional area (A) per unit time (t). Mathematically it is expressed as: $J = M / (A \cdot t)$. If the diffusion flux (J) does not change with time, a steady state condition exists. When the concentration of solute (diffusing species) versus position within the base material is plotted, the resulting curve is termed the concentration profile; the slope at a particular point on this curve is the concentration gradient. The mathematics of uni-dimensional steady-state diffusion is given by Equation 1, where the flux is proportional to the concentration gradient and the constant of proportionality D is called the diffusion coefficient. This expression is known as Fick's first law of diffusion. The concentration gradient of solute is the driving force of this reaction; thus it will be the basis for the theoretical approach in developing a model for the TLPS process for the Ag-In system. However, in most practical diffusion situations, the diffusion flux and the concentration gradient vary with time, resulting in a net accumulation or depletion of the diffusing species. This non-steady state situation can not be described by Equation 1. Instead the partial differential Equation 2, known as Fick's second law, is used. The magnitude of the diffusion coefficient is indicative of the rate at which atoms diffuse, which is sensitive to both the diffusing species and the base material. Temperature has the most profound influence on the coefficients and diffusion rates; the temperature dependency of the diffusion coefficient is given by the Arrhenius expression:

Equation 27

$$D = D_o \cdot \exp\left(\frac{-Q}{RT}\right)$$

Where D_o is a temperature independent pre-exponential (m^2/s), Q is the activation energy for diffusion (eV/atom), R is the gas constant, and T is absolute temperature. Activation energy for this relation may be thought of as the energy required to produce the diffusive motion of one mole of atoms. Large activation energy results in a relatively small diffusion coefficient. The proposed alternative of TLPS for high temperature attachment relies on the fundamentals of a diffusion couple, where a non-steady state situation is observed at the interface of a MPD and a base material. The kinetics of this process have to be studied in terms of a series of stages that are dominated initially by solid state interdiffusion. This is followed by a dissolution stage that is characterized by the diffusion of the base material into the liquid. Once this system reaches equilibrium at a particular processing temperature, the diffusion mechanism shifts back to a movement of atoms from the MPD (liquid) into the solid base metal until all of the solute is consumed by the isothermal solidification process. From the above description it is evident that this is a complex, multi-stage process with a reaction rate that is driven by the ability of the materials to diffuse. Several researchers have investigated the kinetics of formation for silver-indium couples and have provided experimental results of their findings in terms of diffusion coefficients, activation energies, and preferred diffusion mechanisms.

It has been shown [48] that group Ib (copper, silver, and gold) impurity metals can diffuse rapidly into group IIIa (indium) and IVa (tin and lead) base metals via an interstitial mechanism. This interdiffusion has shown to be even faster in thin films than in bulk due to the high densities of defects such as grain boundaries and

dislocations. Previous work [49] on the Ag/In couple suggested a silver-indium reaction at room temperature which was proven to be a diffusion-controlled growth mechanism. From their experimental work on diffusion couples, Rita et al. [48] reported that the activation energy of lattice diffusion of silver into bulk indium is about 0.55 eV. Although the lattice diffusion of silver in bulk indium is favorable (Q = 0.55 eV) with a pre-exponential factor (D_o) of 0.52 X 10^{-4} m^2/s, the solubility of silver in indium is negligible, therefore resulting in a limited solid state reaction during the first stage (S1a) of the TLPS process. Indium diffuses through the silver grain boundaries [48][50] at higher temperatures with a reported pre exponential factor (D_o) of 2.79 X 10^{-14} m^2/s and an activation energy of 0.34 eV. This grain boundary activation energy is smaller than the 1.77 eV reported [48] for the bulk, meaning that with a rise in temperature, the diffusion is predominantly indium into silver through a grain boundary path. Table 4 summarizes the dominant diffusion mechanisms along with the critical parameters for the Ag/In couples.

Table 4. Summary of diffusion data on the Ag/In system.

Couple	Diffusion Mechanism	D_o (m^2/s)	Q (eV)	Rate
Ag into In	Interstitial	0.52 X 10^{-4}	0.55	Slower
In into Ag	Grain Boundary	2.79 X 10^{-14}	0.34	Faster

4.4 Phase transformations in the Ag-In binary system:

A review of the Ag-In binary system, along with its intermediate phases is introduced in this section before presenting the proposed solder paste alternative. As previously discussed, Ag-rich solid solution (ζ or γ at temperatures below 300°C) can take up to 37 - 40 Wt. % In over a wide temperature range, whereas the indium (In) solid

solution has negligible solubility of silver. At temperatures between the melting points of indium (156.7°C) and silver (961.9°C), silver atoms are dissolved by the molten indium in a dissolution process (erosion) that is highly temperature dependent. The interaction between the solid silver and the molten indium results in the formation of a fraction of material with an eutectic composition as well as an In-rich intermediate phase (φ). The melting point of these phases increases with silver content [46][47][51], i.e. eutectic (147°C) < φ [BCT] (166°C) < ζ [HCP] (670°C) < β (693°C). When this information is compared to common soldering alloys such as Sn-Pb or the lead-free SAC replacement, the Ag-In systems provides a lower eutectic point (147°C < 183°C < 217°C), which gives the possibility of lower processing temperatures. The sequentially increasing melting point phases provide the basis for the realization of the shifting melting point alloy at the end of the diffusional solidification process when a final equilibrium composition is achieved. The advantages of such a system can be summarized as follows: (1) the joint is obtained at a lower temperature; (2) the soldered bond becomes stronger [51][52][53][54] and is able to withstand higher temperatures if more silver diffuses into the bond; (3) it is a lead-free solution.

For the formulation of an effective solder paste using the Ag-In binary system, it is important to understand the evolution of phases as a function of temperature and solute concentration. The precipitation and decomposition of these phases will determine the final microstructure of the equilibrated system, which indeed controls the strength of the joint and determines the resulting melting point of the alloy. The

following description goes through the transformations of a hypothetical Ag-In planar couple with an initial equilibrium bulk composition of 75 Wt. % Ag – 25 Wt. % In, as temperature is raised from room temperature to some processing temperature between the indium and the silver melting point. In this qualitative description, the effect of holding time will be assessed in terms of the inspection of the phase diagram. From this phase diagram, the composition and mass fraction of each phase can be calculated by the lever rule at a particular equilibrium state. Figure 7 provides a schematic representation of the microstructural progression of an Ag-In couple processed at a particular T_p after isothermal holds of varying length and subsequently cooled to room temperature. The descriptive evolution is based on both the phase diagram in Figure 6 and previous research [36][48][51][53].

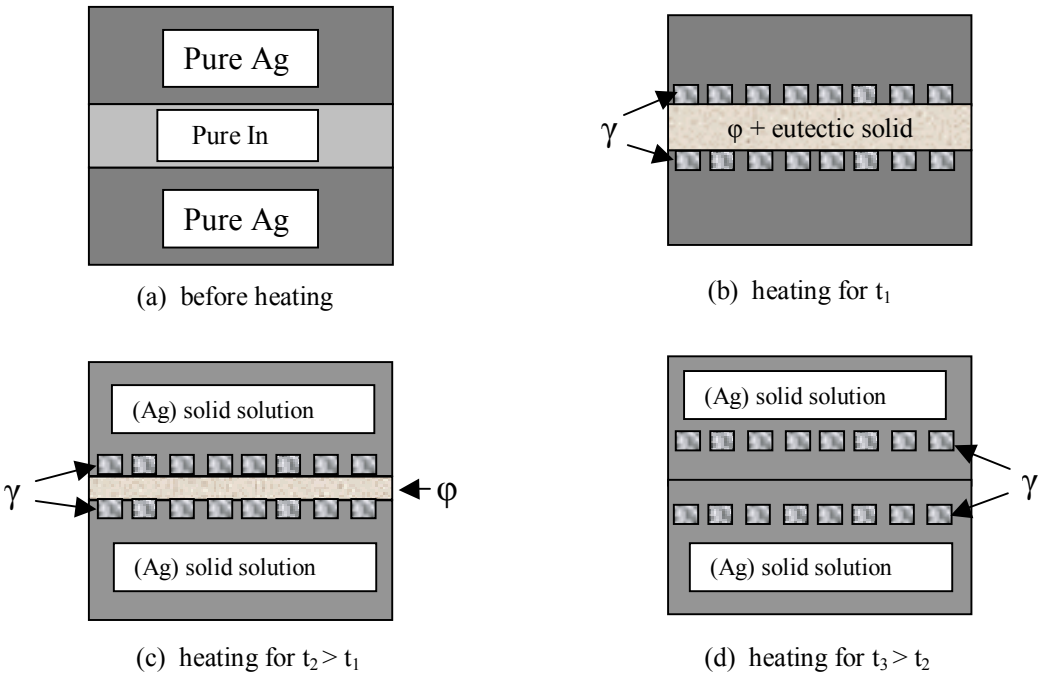

Figure 7. Schematic microstructure of the Ag-In couple (25 Wt. % In) after isothermal holds of varying length (t_i) at T_p. (a) initial conditions, the interface between silver and indium will contain φ from the solid sate reaction; (b) after heating for some time t_1; (c) after heating for a

longer period, not in equilibrium, (d) heating for long enough time so that complete transformation of the In-rich phase is achieved.

When the elemental materials are mixed in the solid state, there is some initial interdiffusion, resulting in the formation of the stable φ-phase. Initial heating to T_p results in the formation of an indium rich liquid from a eutectic reaction at 147 °C, φ (66 at.% In) + In (100 at.% In) → L (97 at.% In) [55]. The amount of liquid formed during this melting event is proportional to the fraction of material having the eutectic composition. As the temperature is raised past 166°C, a peritectic reaction occurs in which φ transforms as follows: φ (66 at.% In) → γ (33.5 at.% In) + L (96.2 at.% In). The initial liquid formed from the eutectic reaction combines with the peritectic liquid to fill up the gap between the solid base material, enhancing the sintering and densification of the compact. These two melting reactions constitute the transformation of the totality of the indium material that was initially added to the mixture. The γ phase, which is Ag-rich, nucleates at the solid-liquid interface as a result of indium diffusion into the silver, this is depicted in Figure 7 (b). The extent of Ag-In interdiffusion in such an isothermal system is determined by the holding time, processing temperature, initial solute composition, and particle size, which will dictate the progression of the TLPS in any practical application. Studying this progression (reaction kinetics) is one of objectives of this investigation. When the extent of the isothermal holding time is not enough, solute diffusion (In → Ag) is limited; thus, the result is a persistent mass fraction of liquid within the structure. Upon cooling from T_p, a primary φ will precipitate from the In-rich liquid as temperature gets below 166°C. For short isothermal holding times, the surplus liquid undergoes a eutectic reaction at 147°C as it cools down, leading to a mixture of low

melting point solid phases (φ + eutectic solid) that is stable at room temperature. This is illustrated in the interlayer in Figure 7 (b), the resulting persistent material is detrimental for the proposed high temperature application environments due to its low melting point. For longer periods of times at T_p (condition (c) in Figure 7), the indium diffusion into silver results in the consumption of more liquid, therefore less amount of indium is available for the solidification reaction upon cooling. This smaller remaining amount of indium material will result in precipitation of φ-phase with no eutectic solid. The presence of the low melting point φ still represents a hurdle for the proposed attachment technology. Condition (d) on Figure 7 represents the condition of a sufficiently long isothermal hold at T_p. In this case, all of the indium diffused into the base metal and the isothermal solidification process is complete, leaving no In-rich liquid for further transformations upon cooling. When the system is treated for a long enough time, equilibrium of the diffusion species is attained, i.e. there is no further concentration gradient driving the movement of atoms. This equilibrium state is defined by the initial bulk composition of the mixture that will exhibit a new melting point given by the phase diagram. It is important to recognize that the complete isothermal solidification is not only a function of holding time, but is also dependent on the initial amount of solute present. If the initial indium addition exceeds the solubility limit in the Ag-rich phases (ζ or γ), there will be some fraction of persistent liquid that upon cooling, will transform into a persistent In-rich φ phase. Formation of this phase not only limits the maximum application temperature of the system, but as reported by Lin et al. [51], it also weakens the interface. From this qualitative description of the evolution of

phases, it is evident that for the successful development of a high temperature attach material, the fraction of remaining low melting point In-rich phases must be minimized. Minimization of these phases requires a full understanding of their kinetics of formation and decomposition, along with the study of how they are affected by other critical parameters throughout this transient process.

Previous researchers [48][51] have attempted to describe the phase evolution of this system. In their investigations, samples were heat treated and quenched from varying time intervals at the holding temperature. Microstructural evaluation was used to describe the phases present, but no quantitative data was presented as function of time, temperature, or initial bulk composition. The transient nature of this liquid phase sintering method does not allows the usage of the equilibrium phase diagram for the calculation of the dynamic fractions of the phases during the process. This explains the necessity for an alternative method to study the kinetics of this transient diffusional solidification process. This investigation will use the DSC as the experimental tool to measure the low melting point mass fraction and its variation as function of input parameters.

4.5 Solder paste development:

The reliable attachment of electronic devices to a substrate that is capable of withstanding elevated application temperatures has been identified as a key enabler for future electronic system developments. In previous sections, it was shown that a TLPS technique provides a relatively low processing temperature that results in a melting point shift. This new higher melting point material can resist application

temperatures well above the initial processing temperature. Initial work on this technique [48][51][52][53][54] used thin films deposited on both the device (die) and substrate, with the primary joining mechanism being the interdiffusion at the facing surfaces. This approach provided information about the diffusion mechanism and kinetics, but proved to be an inefficient technique for the microelectronic industry. When exotic materials, such as gold, silver, and titanium are deposited on a substrate and die, there is an initial investment (money and time) that will not necessarily pay back in an acceptable time frame. This is a result of aging from the time of metallization to the time of its final usage in the assembly process. At that time, the quality of the metallized layer may be affected by oxides or foreign materials, ruining the high initial investment. A second disadvantage of this approach results from the limited surface area for diffusion on a planar contact. This limitation results in a slower process that may not fulfill industry throughput and cycle time requirements.

A well known technique that is widely accepted in the electronic industry is the usage of solder paste for device attachment. In a solder paste, the effective surface area available for diffusion is greatly increased by using a powder. This way, solidification time may be reduced by over two orders of magnitude when compared to planar surfaces [37]. Another advantage of a solder paste is that the main constituent powders are mixed in a flux medium that enhances its shelf life. The paste is strictly deposited as required (controllable size, shape, volume, and method) at the time of manufacturing, making it a more efficient mechanism to protect the investment when compared to the thin film planar method discusses earlier.

Instead of assuming the planar sandwiched structure depicted in Figure 2, consider a mixture of elemental powders in which particles of the base metal (B) and additive (A) are combined. A key advantage over the thin film approach is that the average composition of the mixture can be easily controlled by weighing each constituent during the mixing process, whereas in the planar method, the composition of the system is defined by the thicknesses of the deposited interlayer. This is costly and difficult to control when physical vapor deposition techniques are used. Figure 8 depicts a schematic representation of the proposed paste along with its progression during the TLPS process.

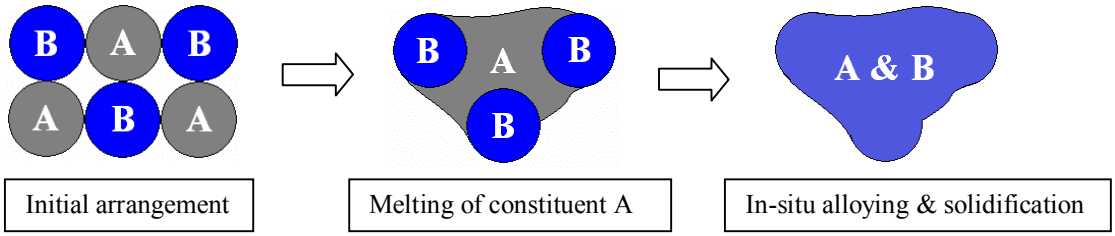

Figure 8. Schematic representation of the powder mixture alternative for the TLPS technique. The direction of the arrows indicate the progression of the process with increasing temperature and time, the diagram in the center is during heating and early period at Tp, whereas the right most cartoon indicates the culmination of the in-situ alloying process.

From the above figure, it can be observed that as temperature (direction of the arrows) rises to T_p, the additive material, A, melts and by capillary flow it wets and pulls the solid B particles together. The result is a rearranged denser structure. During the isothermal solidification stage, the diffusion of A atoms into B results in an in-situ alloying process that culminates with the complete solidification (disappearance of the A-rich material) and the formation of the final solid solution. This newly formed alloy will exhibit a bulk composition corresponding to the initial

mixing ratio (equilibrium) and a new melting temperature. This is the fundamental concept behind the proposed approach, in which the A and B will be given by indium and silver, respectively. Upcoming chapters will discuss the details of the particular Ag-In powder mixture in terms of reaction kinetics and physical properties.

4.5.1 Fundamentals of solder paste:

A conventional solder paste comprises a powder, made of pre-alloyed particles of certain shape and size, which are suspended in a viscous flux vehicle [56]. This flux vehicle is a complex system whose main composition consists of a resin, solvents, rheological agents, and activators. The flux provides a matrix to hold the metallic powder, provides the necessary viscous characteristics required for the application method, and protects the metallic surfaces from oxidation during the process. Solvents from the flux evaporate as the paste is heated to the processing temperature while the remaining constituents flow out by capillary action as the metallic powder consolidates. This effect was confirmed by EDS analysis from which the carbon based resin was detected in the periphery of the joint. This paste can be applied to a substrate by either stencil printing or dispensing. The metal-to-flux ratio is an important parameter that needs to be considered depending on the deposition technique. When devices are placed on the paste and the whole assembly is heated above the melting point of the pre-alloyed particles, a dense metallic liquid wets the surfaces. Upon cooling, the molten solder solidifies and a solid joint is formed. It is important to point out that each of the particles forming the powder has an identical composition defined by the alloy being used, meaning that they all have a single

reproducible melting point. This description of the conventional solder paste and its behavior upon processing explains the conventional processing rule depicted in Figure 1. The following section presents a novel approach in which a solder paste composed of silver and indium elemental powders is proposed as a high temperature attach material.

4.5.2 Ag-In transient liquid high temperature solder paste attach:

In this alternative, a powder mixture of elemental indium particles having a pre-selected maximum particle size and elemental silver particles, having a pre-selected particle size are mixed together to a specific (controllable) mass ratio together with a flux medium. The mass fraction of elemental constituents is selected based on the theory presented in the previous chapters, where the metal load is defined by the consistency of the mixture and its ability to be stencil printed. Previous attempts to form this type of material have been published [14][57][58], being Pb-Sn, Sn-Bi, Cu-Ni, Sn-Sb, and Cu-Sn the tested binary systems.

The key aspect of the proposed system is that upon heating above the melting point of the In-rich phases (both the eutectic and φ-phase), the newly formed liquid spreads throughout the paste consolidating the powder mixture and joining the components together (Figure 8). With further heating, the In-rich liquid and the high temperature silver solid undergo in-situ alloying. This alloying process transforms the liquid to a solid phase and thus the solder solidifies isothermally. This process occurs to the extent that no (or negligible) liquid remains to solidify during the cool down step.

The absence of any remaining In-rich phase during cool down avoids the formation of low temperature phases that can segregate resulting in detriment of physical and mechanical properties. This explains the usage of remaining In-rich phase as the response variable in the experimental approach (section 5.2.2). Upon reheating, the attach material will not re-melt until a temperature greater than the new melting point is exceeded. This can be proven with the DSC test.

During the process, enough In-rich liquid must initially form to consolidate the paste and spread over the base silver particles to form the joint. However, there is a limit to the amount of liquid present because it will affect the time to solidification as well as the structure of the resulting material. A fraction of persistent In-rich liquid, which cannot solidify by the diffusion reaction, will result when the indium addition exceeds the maximum solubility of the Ag-rich matrix. When the maximum solid solubility is not exceeded, an indium addition below certain level may not provide the necessary consolidation. Conversely, over loading the system with indium may result in a time-to-solidification beyond an acceptable or practical period. Therefore, understanding the kinetics of this problem is a critical aspect of the development of a suitable technology. The effects of input variables in the time to completion of the solidification process, as measured by the fractional In-rich remaining, will provide the tools to develop a response model to predict the behavior of this system.

Particle size has been identified as a dominant variable in the diffusion process [23] [25][27]. In this case, powder size of the main constituent should be chosen such that

the maximum amount of initial melting occurs (enhance densification) and the solidification rate (k) is maximized (minimize the time to completion).

Chapter 5: Solidification Kinetics of the TLPS Process for an Ag-In Paste

5.1 Introduction:

In recent years, there has been an increasing demand for high temperature resistant systems. Smart point-of-use micro electromechanical systems (MEMS), high temperature / high power electronics such as those used in hybrid vehicles, control systems for deep well drilling, and high temperature fuel cells are examples of the wide field of applications. The vast majority of these engineering systems are complex structures composed of a myriad of materials joined together. In the presence of temperature gradients, thermomechanical stresses are induced in these systems due to the mismatch in the coefficients of thermal expansion (CTE) of their main constituents. The first, and possibly the most damaging of these excursions usually happens during fabrication. Joining of the main components of these systems is typically accomplished by means of a soldering process, during which a filler (in the form of a thin film layer, paste, or foil) is sandwiched between the solid materials to be joined. It is assumed that the melting temperature of the filler is lower than that of the components, such that a reflow process can be used for the joining operation. The processing temperature is thus defined by the melting point of the solder, which also limits the maximum allowable application temperature of the system. This traditional joining process, which was described in Figure 1, is given by $T_m / T_p < 1$, where T_p is the processing temperature and T_m is the melting point of the solder.

Inspection of the above rule suggests that, for increasing application temperatures, higher melting point materials that require even higher processing temperatures will be needed. Cooling an assembly from such elevated processing temperatures results in built-in residual stresses that might be above the tolerable limits of the materials. Thus, an alternative to the above paradigm was presented as the motivation for this research.

Transient liquid phase sintering is a powder metallurgy technique that has a relatively limited commercial exploitation mainly due to its incomplete fundamental understanding [11][22][23][36]. However, a phenomenological description of the process has been given [24][25]. This description of the process includes a series of discrete stages, each dominated by a diffusion controlled mechanism [25].

In this chapter, the Ag-In binary system is introduced as an alternative for high temperature applications using a TLPS solder paste approach. The low melting point of indium (156°C), together with its good wettability, make it a suitable candidate as a melting point depressant (MPD), whereas the high melting temperature of silver (962°C), its thermal conductivity (419 W/m-K), and electrical resistivity (1.55 X 10^{-6} Ω-cm) [59] make it a promising prospect as a base metal. Although sintering is not an equilibrium process, it does approach equilibrium; thus, the phase diagram can aid in defining critical process variables. In order to study the kinetics and the evolution of the process, it is critical to understand the phases present in the binary system along with their transformations as function of composition and temperature. Phase

diagrams are helpful in predicting phase transformation and the resulting microstructures, which may have equilibrium or non-equilibrium character [45]. Figure 6 depicts the equilibrium phase diagram of the Ag-In binary system. This diagram served as a tool for the selection of possible compositions (based on the solubility limits), processing temperatures (based on the phase transformations), compositional data necessary for theoretical calculations, and also as reference for the experimental findings from the DSC test.

In this stage of the investigation, the kinetics of the TLPS reaction will be experimentally studied using a differential scanning calorimetry (DSC) technique as function of base metal particle size and isothermal holding time. A reaction rate for the process will be estimated experimentally, whereas a diffusion based analytical rate will be calculated for comparison purposes. A microstructural evaluation of the system will assist the interpretation of the experimental data and shall provide the necessary morphological information about the system as it progresses towards equilibrium. The thermal stability of the newly formed alloy and the achievement of the melting point shift will be studied by thermal analysis from the DSC.

5.2 Experimental methods:

5.2.1. Solder paste formulation and characterization:

Previous work on TLPS of the Ag-In binary system was presented by Chuang and Lee [54] with the materials deposited as thin films in facing surfaces. They provided a theoretical evolution of the system towards its equilibrium state based on the phase

diagram and reported a time for completion in the order of 26 to 30 hours. The duration of the process to reach the final composition has been identified as a major drawback to commercial feasibility. The planar nature of the interface contributed to its rapid saturation. In addition, it limited the surface area available for diffusion, delaying the overall process. In a paste, the main constituents are given in the form of nearly spherical particles, indicating that the effective surface area available for diffusion is greatly increased by using a powder. This way, the solidification time can be significantly reduced when compared to that of planar surfaces [37]. During this phase of the investigation, three solder pastes mixed to a composition of 75 Wt.% Ag – 25 Wt. % In (68 Vol. % Ag – 32 Vol. % In) and variable silver particle sizes were fabricated. Powders were characterized by the supplier (Alfa-Aesar) using the standard ASTM-B214. For this study they were conventionally identified by their maximum particle diameter, but the existence of a distribution was also recognized. Characterization of the powders was confirmed by scanning electron microscopy on the as-received material, in which particle size and shape were validated. The indium powder size was fixed to 50 μm (Mesh -325 or Type III). Elemental powders were dry mixed to the above mass ratio (~ 25 Wt. % In); a no clean rosin mildly activated flux (RMA) [Indium Corp. TAC Flux 007] was later added to the mixture to form a paste. The metal content of this paste was set to 91% by weight with the remaining portion being the flux. TLPS is a complex metallurgical process governed by multiple variables such as heating rate, composition, processing temperature, holding time, and particle size [11]; for this stage of the investigation, the heating rate, composition, and processing temperature were deliberately set as constants. These

parameters were set to typical values used for the standard reflow process. The composition was chosen such that an (Ag) solid solution plus γ is obtained at the end of the transient process. Details of the three solder pastes formulated for this investigation are given in Table 5 in which the amounts of the main components were measured using a Mettler AE100 analytical balance with a precision of 0.1mg.

Table 5. Solder paste formulations for experimental testing.

Solder Paste	Wt.% In	Wt.% Ag	In Powder Mesh (Shape*)	In Particle Dia.* (μm)	In Purity (%)	Ag Powder Mesh (Shape*)	Ag Particle Dia.* (μm)	Ag Purity	Wt. % Flux	Metal Load (by Wt.)
A	25	75	-325 (rounded and ligamental)	50*	99.99	-1250 (Agglomerated aggregates)	5	99.95	9	91%
B	25	75	-325	50*	99.99	-325 (Spherical)	50	99.9	9	91%
C	25	75	-325	50*	99.99	-500 (Spherical)	25	99.9	9	91%

* Particle maximum diameter is based on ASTM-B214, there is a distribution attributed to this value which is tabulated as "Less than 1% particles bigger than xx", "Maximum Particle Size", and "80% Minimum Between". Due to agglomeration and screening problems attributed to particle shapes the exact measurement of powder particles is beyond the scope of this work. Maximum values will be used for theoretical calculations, whereas shape description was based on the work of RM German in Powder Metallurgy [60].

The main difference among the pastes was the maximum particle size of the base material (silver). Paste A was specified by an aggregate of silver particles with a maximum diameter of 5 μm. Pastes B and C, both contained spherical silver particles with a maximum diameter of 50 μm and 25 μm, respectively. All of the pastes contained the same indium material, a rounded and ligamentally shaped powder with a maximum particle size of 50 μm. The following scanning electron images illustrate the as-received powders used for paste formulation. This qualitative information was used to validate the specifications given by the supplier.

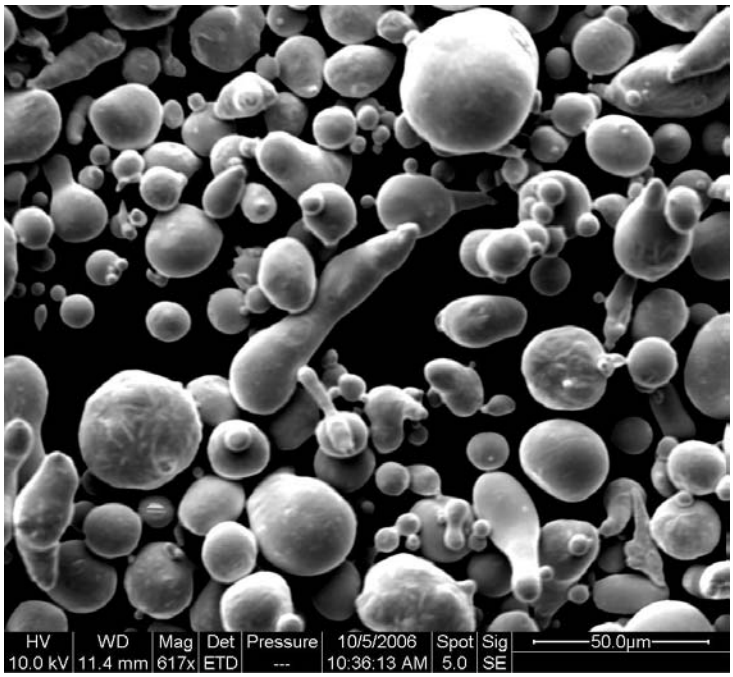

Figure 9. SEM image of the elemental indium powder used for all three solder pastes. This material was specified as -325 mesh (50 µm maximum diameter) by the supplier with a rounded ligamental shape [60].

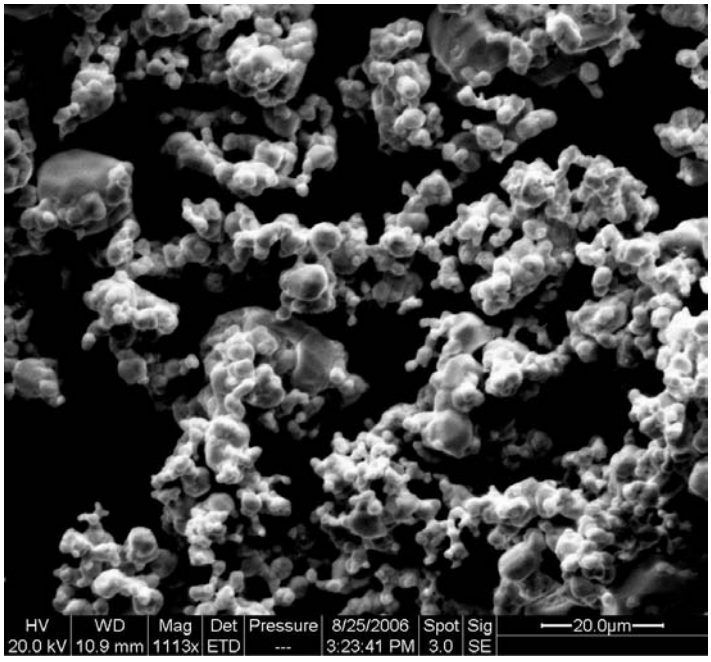

Figure 10. SEM image of the silver powder used on Paste A, in this instance the powder was specified as -1250 mesh (5 µm maximum diameter) with an agglomerated aggregate shape [60].

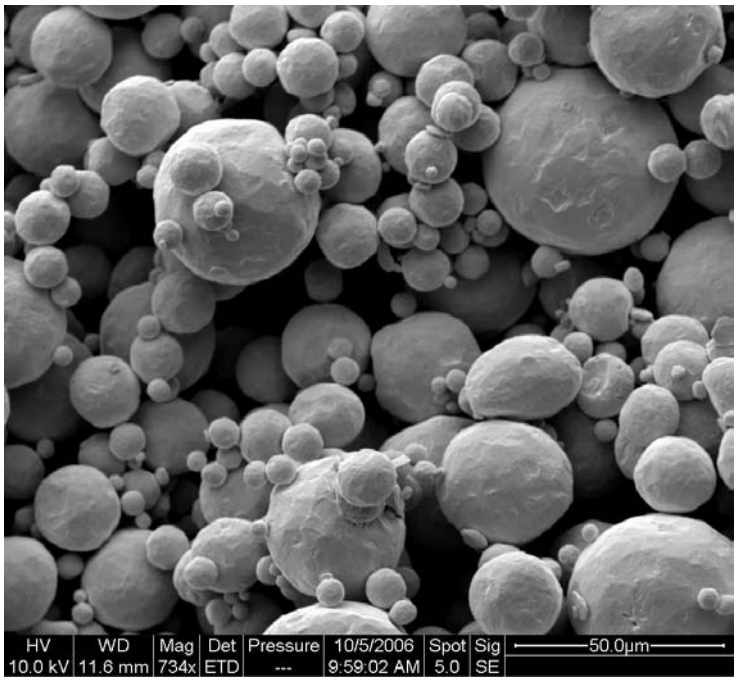

Figure 11. SEM image of the silver powder used on Paste B, in this instance the powder was specified as -325 mesh (50 µm maximum diameter) with a spherical shape [60]. Note the problem of agglomeration of smaller particles that affects the screening process and indeed the mesh sizing.

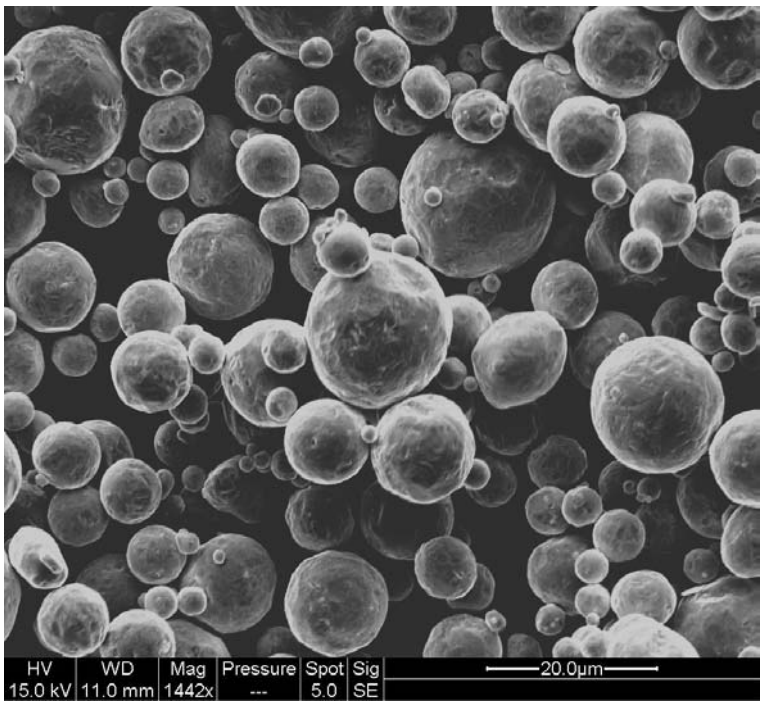

Figure 12. SEM image of the silver powder used on Paste C, in this instance the powder was specified as -500 mesh (25 µm maximum diameter) with a spherical shape [60].

Solid powders were initially mixed to a 75%Ag - 25%In mass ratio (the true final composition of each batch was then measured form the DSC for further calculations). The addition of a no-clean rosin mildly activated (RMA) flux (Indium Corp. TAC-007) completed the formulation of the paste. The selection of the flux medium was based on the properties of the activators and their ability to resist elevated processing temperatures for prolonged periods of time without burning off. In this case, processing temperatures ranging from 250°C to 300°C and holding times of over 60 minutes were used for flux selection. Indium Corporation TAC flux 007 was chosen based on company's recommendations and the fact this flux is used in their commercial die attach solder paste products.

A sample of solder paste A was analyzed using the ESEM; energy dispersive spectroscopy (EDS) was used for elemental composition of the mixture. A dot map over the region of interest confirmed the presence and distribution of the main constituents. Figure 13 and Figure 14 depict the ESEM micrographs over the region of interest and the dot maps.

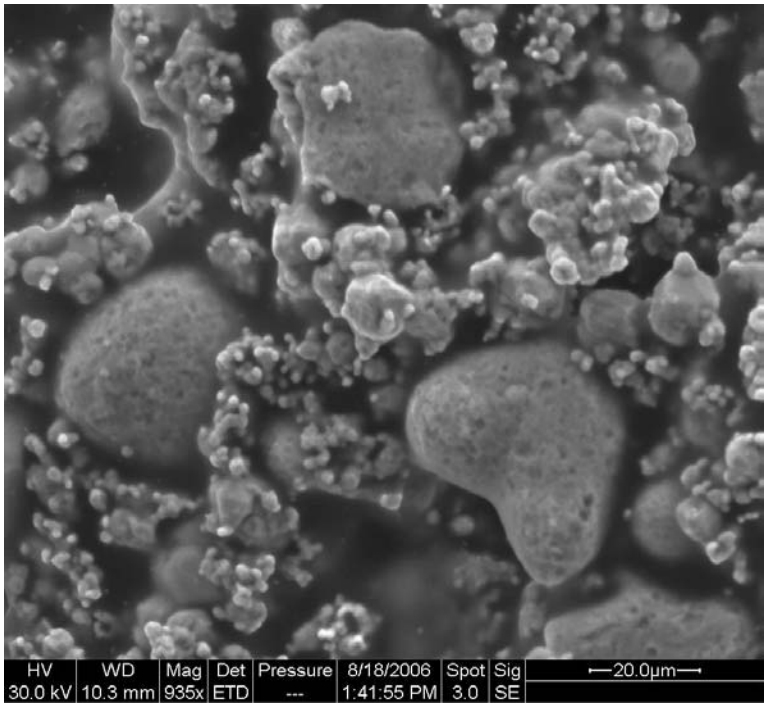

Figure 13. SEM image of Paste A sample, as can be observed there is a larger amount of the fine silver powder surrounding the larger near spherical indium particles.

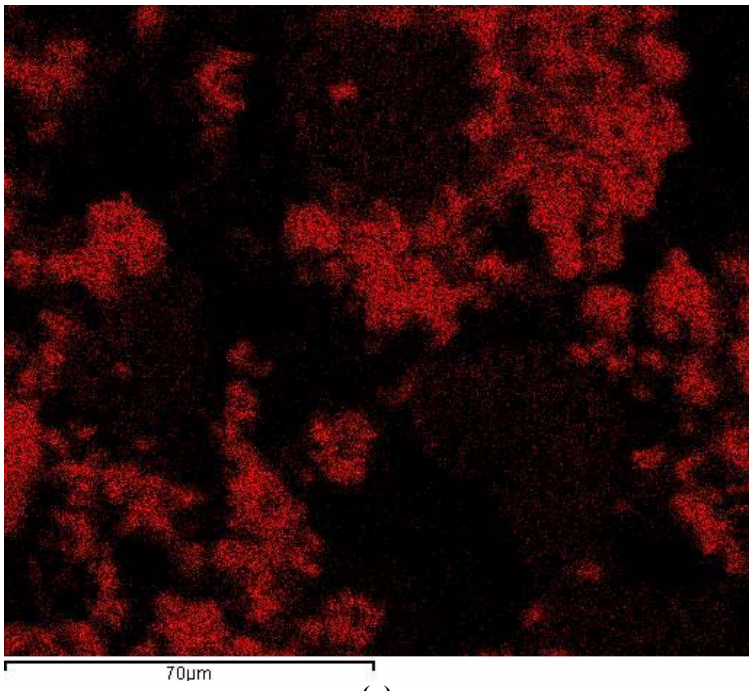

(a)

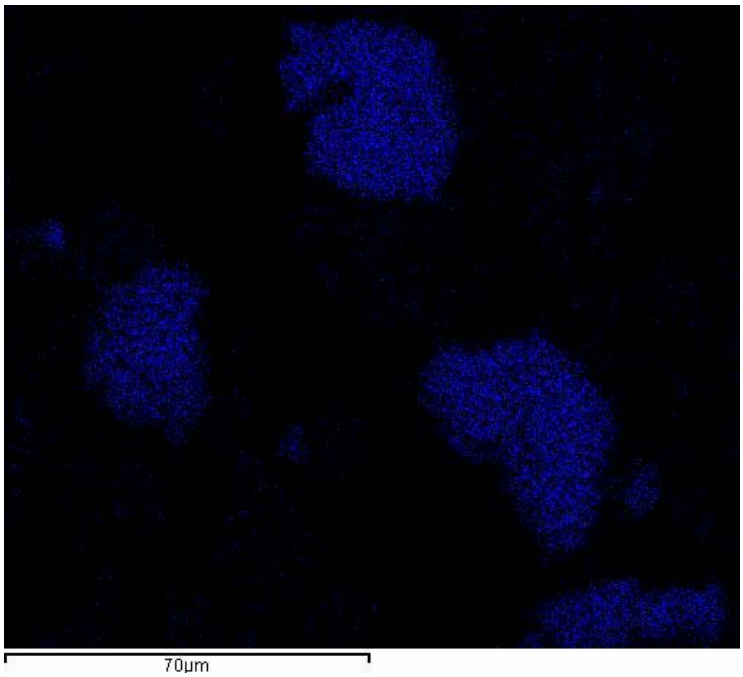

(b)

Figure 14. EDS dot map over the region depicted in Figure 13. (a) Dots denote the presence of silver as given by the EDS analysis; (b) Dots represents the presence of indium given by the larger particles in the mixture.

As seen from these figures, it is evident that the shape and size of the particles are in accordance with Table 5, where the near spherical indium particles (~ 50µm) are seen in Figure 14 (b) and the agglomerated smaller silver particles are depicted by the dots in Figure 14 (a). An important factor in solder paste blending is the homogeneity of the mixture, i.e. each sample taken from the batch should have approximately the same of 75%Ag - 25%In by weight. Using the densities of both elements and the rule of mixtures based on the pre-defined weight ratio, a volume fraction calculation was performed. Theoretical volume fractions were found to be 67.7% Ag and 32.3% In. Mixing for sufficient time has been proposed by powder metallurgists [60] as a solution for the homogeneity of the system; for this investigation all powders were dry mixed for 30 minutes. To validate the effectiveness of the mixing and to

calculate the true final composition of the mixture, DSC tests were used to obtain empirical amounts of indium present in randomly taken samples from all three batches. A description of this test and the results will be presented in section 5.3.2.

5.2.2. Design of experiment (DOE):

Transient liquid phase sintering has been presented as a suitable alternative for solder attachment; however, complications exist in the ability to predict the progression of the system by analytical means. One such factor is the effect of particle size and shape distribution, which in most theoretical models is assumed as a monosized spherical powder. In practical applications, however, it involves a range of sizes that are often far from spherical in shape. Therefore, an empirical approach is presented in this section from which an estimation of the process kinetics will be obtained following a systematic design of experiments methodology. To develop an empirical kinetics model using the DSC data, as discussed in section 2.2.3, a response variable must be defined. The amount (mass) of indium diffused into silver during the isothermal solidification indicates the progression towards the completion of the in-situ alloying process. A remaining fraction of In-rich material (untransformed) will solidify as a persistent phase if the solidification time is not long enough, jeopardizing the ability of the newly formed system to survive high temperature environments. Thus, the kinetics of the system is to be modeled based on a response defined by the remaining In-rich phase(s) as function of isothermal holding time and base metal particle size. These two factors were selected as the main variables because the underlying diffusion mechanism is known to be sensitive to these parameters [12]. The processing temperature (T_p) was held constant at 250°C, the additive weight

percent was set to 25 Wt.% In, and the heating rate was held constant at 60°C/min, i.e. 1°C/s. The test was conducted using a full factorial experiment with two replicates for each time level. The input variable was the particle size (PS) in micrometers with three levels; this resulted in three treatment combinations (3^1) per holding time with a replicate at each time interval. The isothermal holding times (minutes) were defined as follows: $t_o = 0$, $t_1 = 0.5$, $t_2 = 1.0$, $t_3 = 2$, $t_4 = 5$, $t_5 = 10$, $t_6 = 15$, $t_7 = 25$, $t_8 = 40$, $t_9 = 60$, $t_{10} = 90$; for each of the three developed solder pastes (A, B, and C). A flow chart of the DOE is given in the figure below.

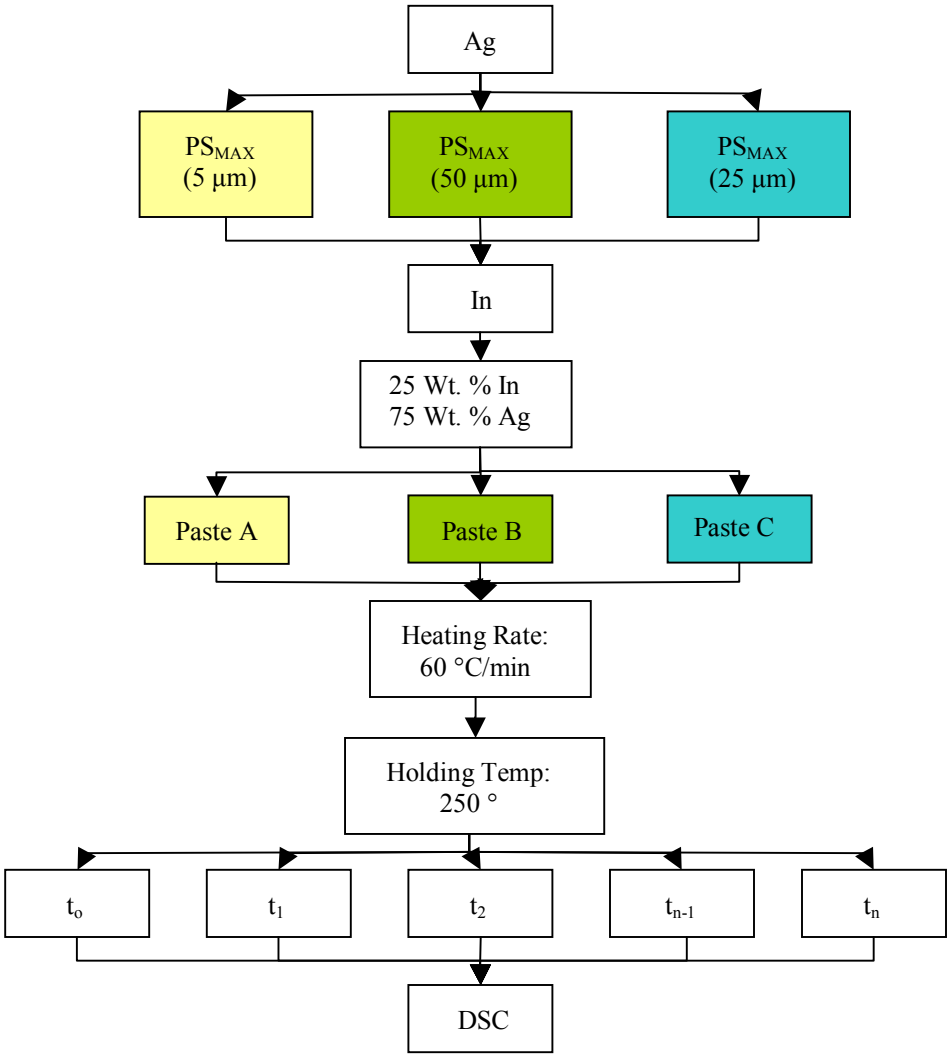

Figure 15. Experimental matrix for DOE.

5.2.3. Differential scanning calorimetry (DSC) thermal characterization:

In this investigation, we are interested in studying the transformation of the Ag-In mixture. This process is driven by the diffusion of the low melting In-rich phases into the high melting Ag-rich solid solution, for which a net mass flux exists from the high indium concentration in the liquid to the lower concentration in the solid as given by the liquid and solid compositions. The amount of solute mass (indium) that has diffused over time into the base metal (silver) defines the progression of this process. The problem of inaccurate measurement techniques for quantifying the kinetics of this isothermal solidification reaction during the transient process has been addressed by the development of a new technique using differential scanning calorimetry (DSC) [31][40]. This method has enabled the characterization of the process kinetics resulting in the advancement of the fundamental theoretical understanding of the mechanics of isothermal solidification, as is the case of the current investigation in which kinetics of the binary Ag-In system are analyzed by this technique. This method allows the determination of the amount of initial liquid formation as well as its duration, i.e. the kinetics of the isothermal solidification step. The DSC measures heat flow (mW) of a sample relative to a reference cell throughout a specified profile in which the temperature, heating/cooling rate, and isothermal holds can be controlled. Heat flow is measured using thermocouples that compare the temperature of the reference with the sample cell while keeping them balanced. The differential heat flow during the process is recorded as either an endotherm (energy input is required for balance) or an exothermic peak, the later being a release of energy by the sample under test. Based on this convention, the melting of a material consumes a

discrete amount of energy per unit mass (heat of fusion) that is plotted as an endotherm. The opposite happens during solidification, where the material releases energy to become more stable. Therefore, it is perceived as an exotherm during the DSC test. Information regarding the energy required for phase transformations in a particular material, as well as melting temperature and specific heat, can be directly obtained from this test. The progression of the TLPS process along its stages can be accurately calculated using this technique [40].

For this investigation, a Perkins Elmer DSC Pyris 1 was used in conjunction with the aluminum sample holder pan kit (PE Kit: 219-1073). Samples consisted of 30 – 80 mg of the solder paste deposited in the aluminum pan according to the standard operating procedure of the equipment; the exact weight of each sample was measured and recorded for further calculations. A baseline test using empty reference samples was conducted prior to the testing and subtracted from the final data. This accounted for any artifacts induced by the equipment itself. The equipment was calibrated using a standard indium sample as specified by the supplier. A nitrogen purge was used to avoid oxidation during the test.

5.2.4. Remaining fraction calculation by DSC:

In section 5.2.2, an experiment was designed to study the kinetics of the isothermal solidification process based on a response defined by the remaining In-rich phase as function of isothermal holding time and base metal particle size. In the previous

section, the fundamentals of the DSC were presented in which the formations of endothermic and exothermic peaks were defined as being proportional to a melting or solidification reaction, respectively. The ratio between the exotherm and the endotherm gives the fraction of liquid remaining [40]. A more comprehensive description of this method will follow.

Calculation of the remaining amount (mass fraction) of a phase requires the following ratio:

Equation 28

$$\text{Remaining of a Phase}\,(\%) = \left(\frac{\text{Remaining Amount}}{\text{Initial Amount}}\right)\cdot 100$$

where both, remaining and initial amounts of material are calculated as follows:

Equation 29

$$\text{Amount of Material}\,(\text{grams}) = \frac{\text{Endo or Exo Energy}\,[\text{J}]}{\text{Heat of Fusion}\,[\text{J/g}]}$$

The heat of fusion is available in literature; whereas the endothermic or exothermic energy is given by the area under the peak from the DSC trace, i.e. the integral of the heat flow (mW) over time. Since the heat of fusion is a constant property of the material, Equation 28 can be re-written as:

Equation 30

$$\text{Remaining of a Phase}\,(\%) = \left(\frac{\text{Exothemic Energy}}{\text{Endothermic Energy}}\right)\cdot 100$$

where the endothermic energy corresponds to the initial amount of liquid material located in the system and the exothermic energy to that left after the heating cycle. From a conservation of mass argument for a reversible transformation, the amount of material melting (endothermic energy) should equal the amount solidifying (exothermic energy) when no diffusional reaction occurs during the process (heating to T_p, hold, and cool down). In that case, the ratio of exothermic energy to endothermic energy would be close to unity (some small deviation might be observed due to errors in calculating the area under the curve), whereas ratios significantly less than one imply that a fraction of the material, originally present during the melting, is no longer solidifying (i.e. it has transformed into a new phase with a different melting point, Figure 20). This technique for calculating the remaining fraction of a material using Equation 30 was validated during this investigation. Figure 16 depicts the DSC trace of a pure indium sample that was heated to 170°C, held isothermally for five minutes, and cooled down to room temperature.

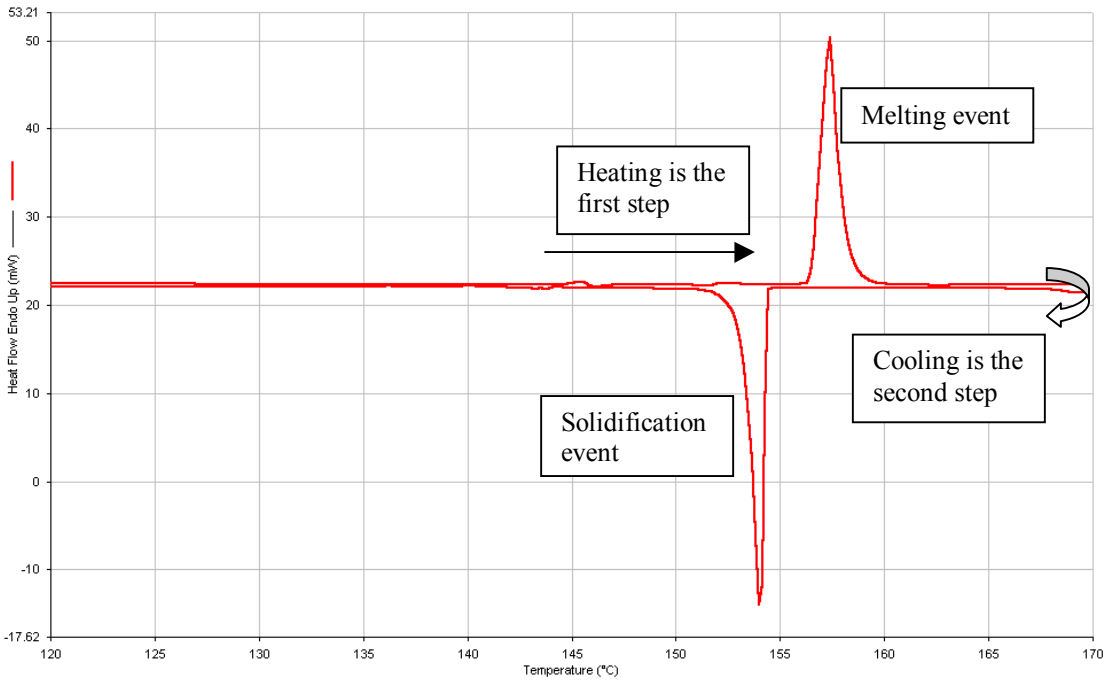

Figure 16. DSC trace of a pure indium sample heated to 170°C and cooled down, melting endotherm (upward) and solidification exotherm (downward) are shown.

An endothermic peak (upward) was recorded at 156°C. This corresponds to pure indium's melting temperature after the isothermal hold; an exothermic (downward) peak was recorded during the cool down. Note that the exotherm was recorded at around 154°C, which corresponds to a small undercooling effect during solidification. The area under both peaks was calculated by integration in the time scale using the equipment software as given in Figure 17.

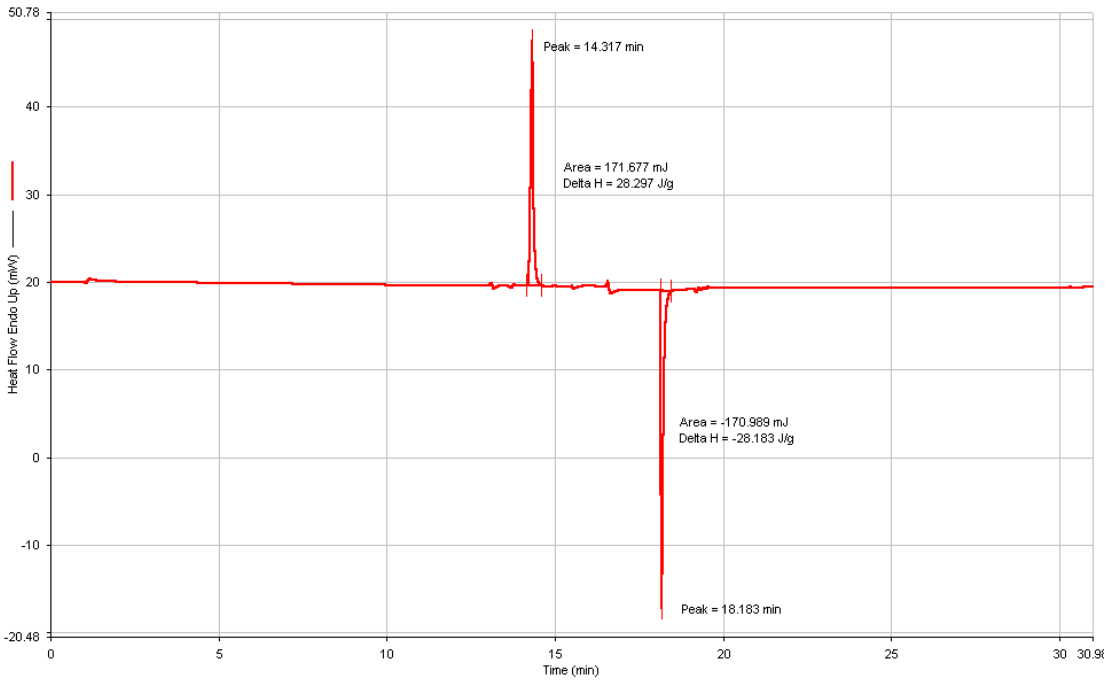

Figure 17. DSC trace in the time domain showing the calculation of the endothermic and exothermic energies by integrating the area under the peaks.

Substitution of these energies into Equation 30 confirmed that the DSC technique is an accurate and valuable tool for studying the transformation kinetics of the process. This concept provided the empirical approach in our calculation of remaining low melting point In-rich phase.

5.2.5. Metallography:

To assist in the interpretation of the results from the DSC, samples treated under the specified experimental conditions were cross-sectioned, etched (1 HNO_3 : 7 HCl : 8 Ethanol), and analyzed using scanning electron microscopy (SEM) and energy dispersive spectroscopy (EDS). A FEI Quanta 200 ESEM was used throughout this investigation. The metallographic techniques provided qualitative information in terms of the extent of liquid spreading through the compact, as well as morphological

information. This descriptive data assisted in defining the phenomenological aspects of the TLPS through the different stages of the process, by documenting the microstructural evolution of samples. Quantitative information on the extent of the diffusion at different stages was provided by spectral analysis in terms of atomic percent of the constituents. An example of this qualitative description of the TLPS by metallographic methods is given in Figure 18. In this figure, a sample of Paste A is depicted after processing for 60 minutes at 250°C. When compared to the dot maps in Figure 14, it is evident that the interdiffusion process has yielded the intended result. From this analysis, it can be seen that the system is now a well dispersed system of indium in silver, as opposed to the initial segregated paste depicted in Figure 13 and Figure 14.

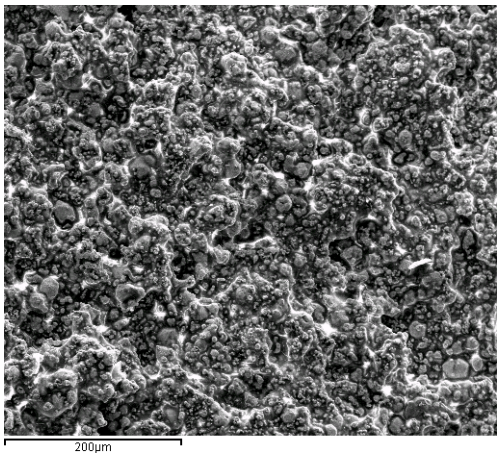

(a)

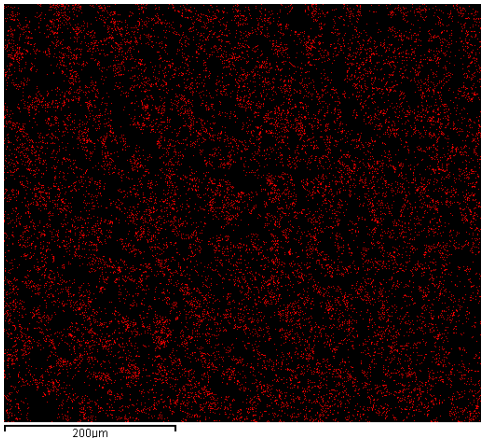

(b)

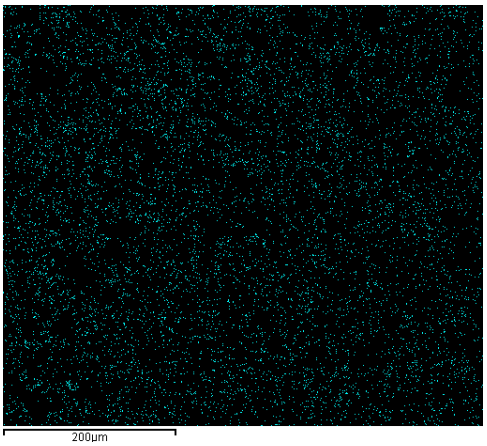

(c)

Figure 18. EDS dot map showing the elemental composition and distribution of a sample processed by TLPS. (a) SEM image of the region of interest, (b) Dot mapping showing the presence and distribution of silver, (c) Dot mapping showing the indium presence.

5.3 Results:

5.3.1. Interpretation of melting and solidification data from DSC

A typical DSC trace for the heating of a paste sample is given in Figure 19, which indicates the general melting behavior of the system:

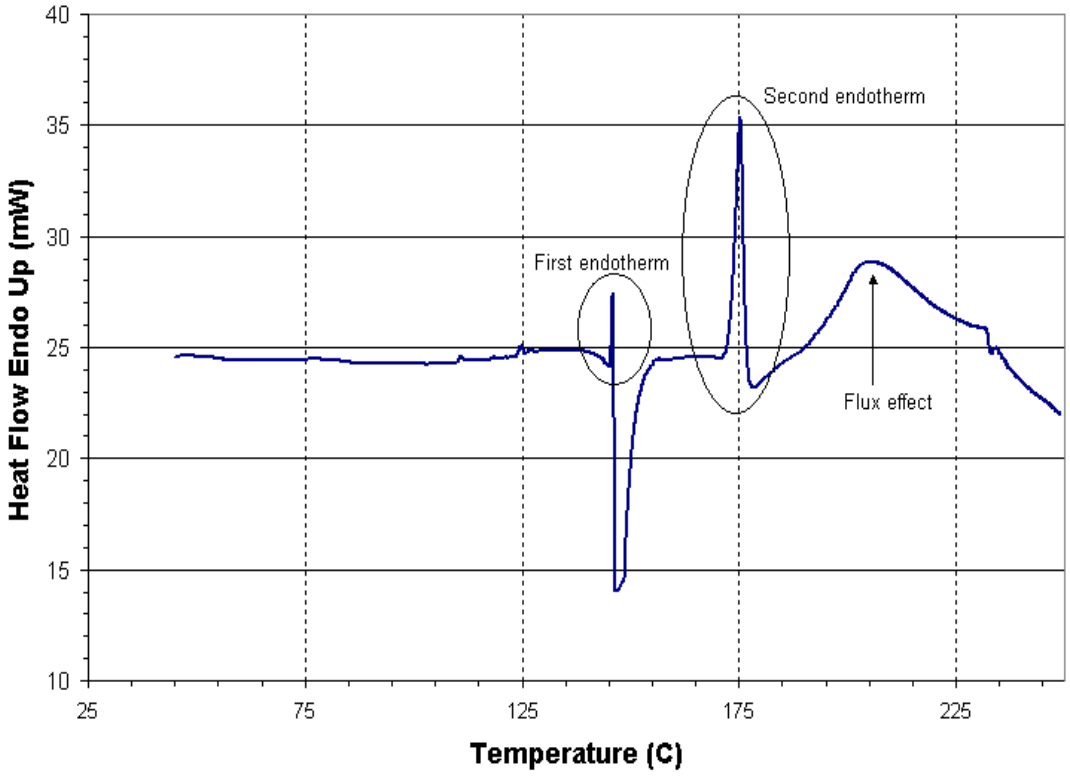

Figure 19. Typical DSC trace for a Ag-In paste sample heated to 250°C, endotherms are shown as upwards peaks.

During this heating cycle, two endothermic peaks that corresponded to phase changes were observed (these reactions were confirmed with the phase diagram). The polymerization of the flux vehicle was detected and labeled in the figure. The first endothermic peak corresponded to the eutectic reaction at 147°C [55], φ (66 at.% In) + In (100 at.% In) → L (97 at.% In); whereas the second endotherm occurred at ~ 170°C where a peritectic reaction [55] [φ (66 at.% In) → γ (33.5 at.% In) + L (96.2 at.% In)] takes place. The formation of the In-rich liquid via the eutectic reaction depends on the initial extent of material with the eutectic composition. It has been reported [54] that this eutectic could be formed at room temperature as silver and indium are mixed together; its formation is accelerated even further with temperature. The initial mass fraction of this phase is minimal and it its strongly dependent on the

heating rate used to reach the processing temperature [28]. Immediately after formation, the In-rich liquid infiltrates the silver powder compact by capillary action inducing an erosion effect as it comes into contact with the silver solid. At a temperature between ~147°C and ~170°C the newly formed liquid co-exists with φ, this φ phase is an In-rich material that is stable from room temperature up to ~170°C (Figure 6). This L + φ is a stable system in the temperature range between 147°C and 170°C, evidence of this stability can be seen in Figure 19 where energy was released (exotherm) following the eutectic reaction. Continuous heating towards the processing temperature results in the peritectic reaction at ~170°C, where φ melts resulting in more In-rich liquid. As can be observed, both of these reactions contributed to the formation of In-rich liquid during the heating stage. Upon cooling, after insufficient isothermal holding time at T_p, the fraction of material with the In-rich composition(s) underwent solidification reactions shown in Figure 20.

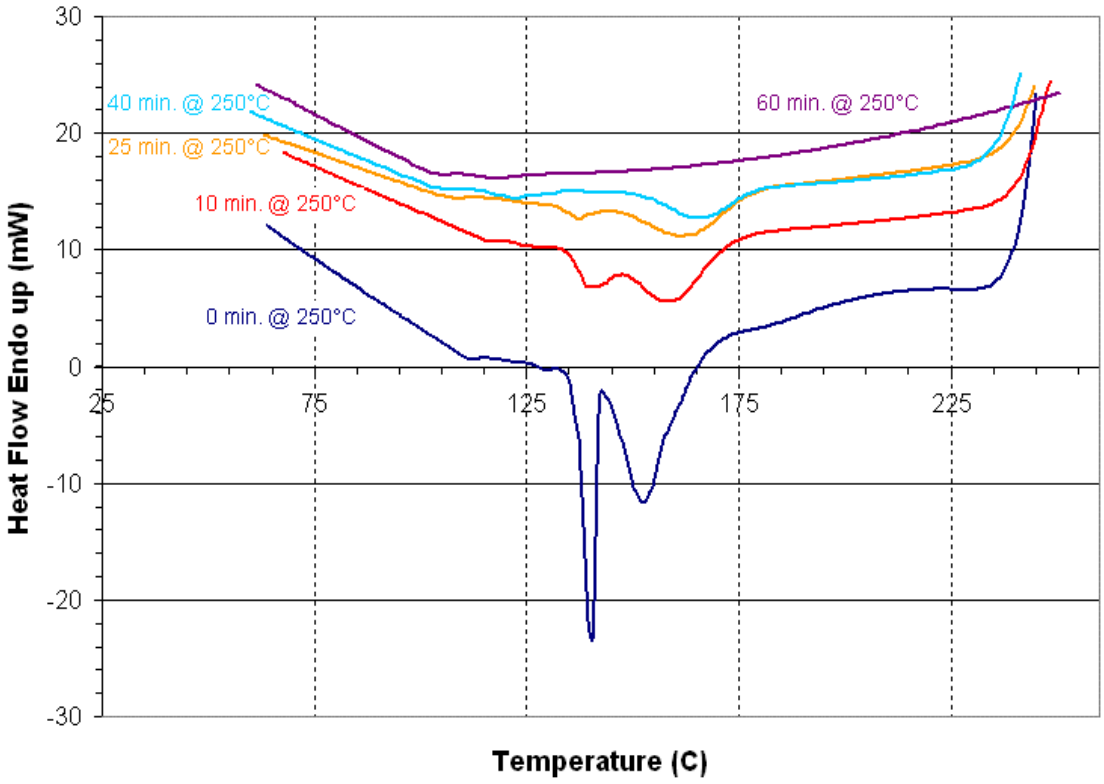

Figure 20. DSC traces for the cooling stage of samples treated at 250°C for various holding times. Exotherms are given by the downward peaks, it was observed that at 40 minutes the eutectic reaction at 147°C was not longer detected; whereas at 60 minutes no exotherms were recorded.

For short holding times, an exothermic reaction at ~ 170°C (Note: undercooling was observed on all samples) resulted in the precipitation of primary φ while the remaining fraction of eutectic liquid transformed into eutectic solid (φ + In). As the holding time increased, more diffusion of indium into silver occurred, resulting in the isothermal solidification of the In-rich liquid. From the DSC traces in Figure 20 it was observed that the magnitude of the eutectic exotherms decreased with holding time up to 40 minutes. At holding times larger than 40 minutes, the In-rich liquid solidified as φ with no eutectic transformation. When the holding time was even longer (≥ 60 minutes permitting complete isothermal solidification), all of the In-rich liquid transformed into the Ag-rich solid solution. No exotherms were observed

during the cool down. At this point, a newly formed in-situ alloying process had been accomplished with a resulting high melting temperature Ag-rich material, which based on the phase diagram, should exhibit a melting point above 650°C. To validate the thermal stability of this newly formed alloy, a sample was subjected to a second heating excursion that simulated an application condition of 400°C. In Figure 21, a DSC curve of a sample initially heated to a T_p of 250°C and then held for 60 minutes is given.

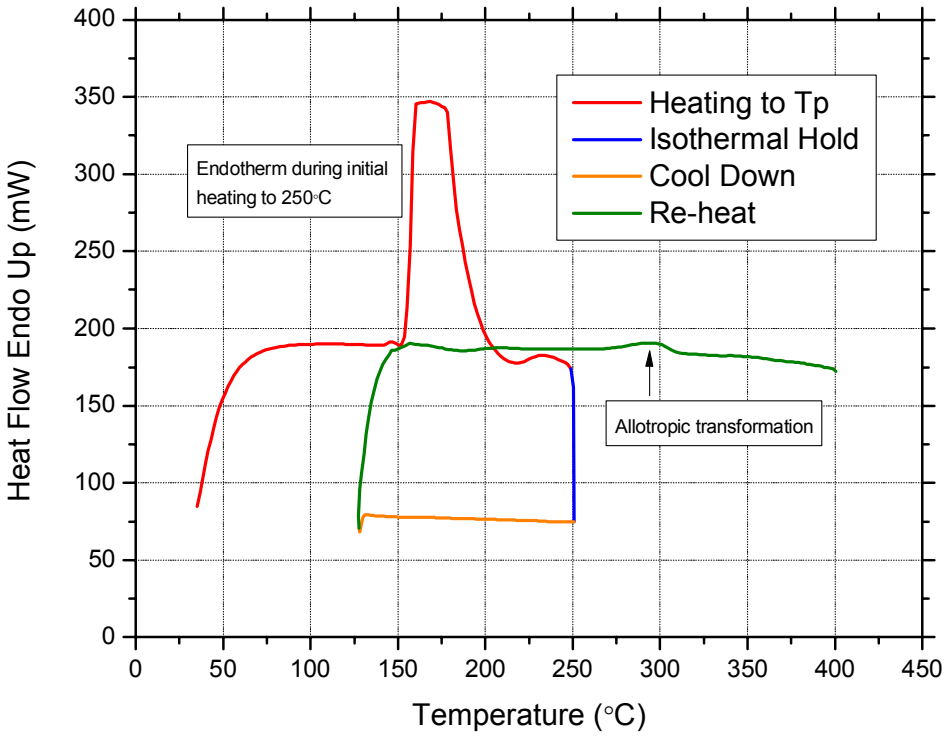

Figure 21. DSC trace for the heating – cooling – re-heat cycle used to demonstrate the thermal stability of the newly formed material.

During this first heating stage, the endotherm associated with the melting of the In-rich phases was observed. Upon cooling to 125°C, after a 60 minutes hold, no

exotherms were observed. This suggested that the diffusion controlled transformation had been successfully achieved. Heating the sample to 400°C resulted in no new endotherm, confirming that the material was stable up to such temperature. From the DSC trace, a small endotherm was observed at ~300°C corresponding to an allotropic transformation of the Ag-rich phase γ to the HCP ζ phase (this is a solid to solid transformation).

Two In-rich low melting phases were identified (Figure 19); thus, both need to be considered in order to provide an accurate description of the overall transformation. Based on the known reactions of the Ag – In system, Equation 30 takes the following form, where the response for this specific binary system is defined as:

Equation 31

$$\text{Remaining In - Rich Phase (\%)} = \left[\frac{\left(\text{Exo}_{\text{eutectic}} + \text{Exo}_{\varphi}\right)}{\left(\text{Endo}_{\text{eutectic}} + \text{Endo}_{\varphi}\right)} \right] \cdot \mathit{MixtureWt.\%In}$$

where *Mixture Wt.% In* is the actual indium weight fraction in the as-built paste as measured from sampling the batch of paste prior to the test (section 5.3.2). This is necessary to compensate for mixing errors induced during fabrication of the pastes in which the exact 75 Wt.% Ag – 25 Wt.% In may have not being obtained. Equation 31 provides a measurement of the response that can be later compared to metallographic observations as well as to results obtained from analytical solutions without being misleading since it considers the fact that the rest of the system is comprised of silver rich phase.

5.3.2. Empirical validation of paste composition:

In order to accurately obtain the remaining fraction of In-rich phase (Equation 31) for each paste, the indium mass fraction within the mixture was needed; a perfect 75 Ag : 25 In mass ratio should not be assumed. In order to obtain this initial as-built composition, empirical measurements of indium content on paste batches were required. A set of samples from each paste (A through C) was taken and individually weighed to record their bulk mass (mg). Each sample was subsequently tested on the DSC, from which the endothermic energy was obtained. This calculated energy (Joules) was divided by the heat of fusion, resulting in the empirical mass of indium present in the sample. Dividing this mass value of indium by the effective overall mass of the sample provided the empirical In Wt. %. A mean value of 23 Wt. % In was obtained for Paste A, 32 Wt.% In for Paste B, and 27 Wt.% In for Paste C [Appendix 1]. These values were incorporated in the calculations given in Appendix 1 and in Figure 22 and Figure 23.

5.3.3. Results from the design of experiment (DOE):

The remaining In-rich material was calculated using Equation 31 for all sixty six samples from the DOE [Appendix 1]. For each specimen, a particular heating / cooling DSC trace was obtained from which the exothermic and endothermic energies were calculated by the integration method using the Perkin Elmer software. Results from the whole experiment are presented in Figure 22 where the response variable was plotted as function of isothermal holding time for all three solder pastes. Note that the response variable has been normalized to the measured initial weight fraction of indium effectively present on each of the solder pastes undergoing testing.

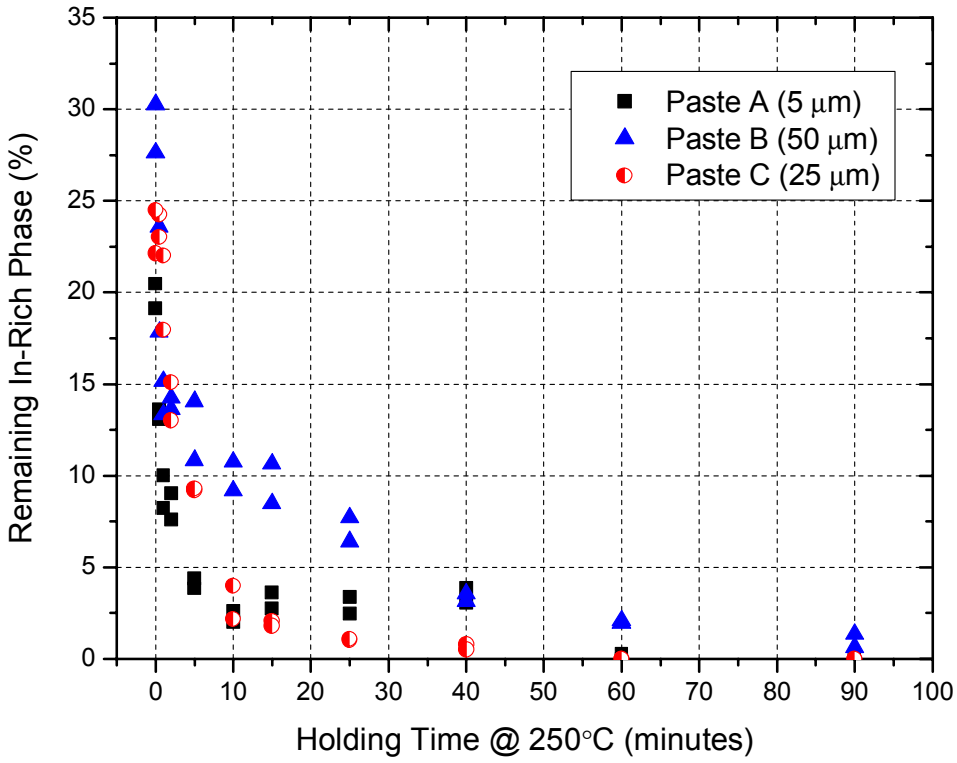

Figure 22. Experimental data showing the Remaining In-rich material as function of isothermal holding time. The chart shows the data obtained from the DOE for all three solders pastes.

The effect of particle size in the response is more clear from Figure 23, in which the mean value of the Remaining In-rich phase was used instead of all the experimental data as given above.

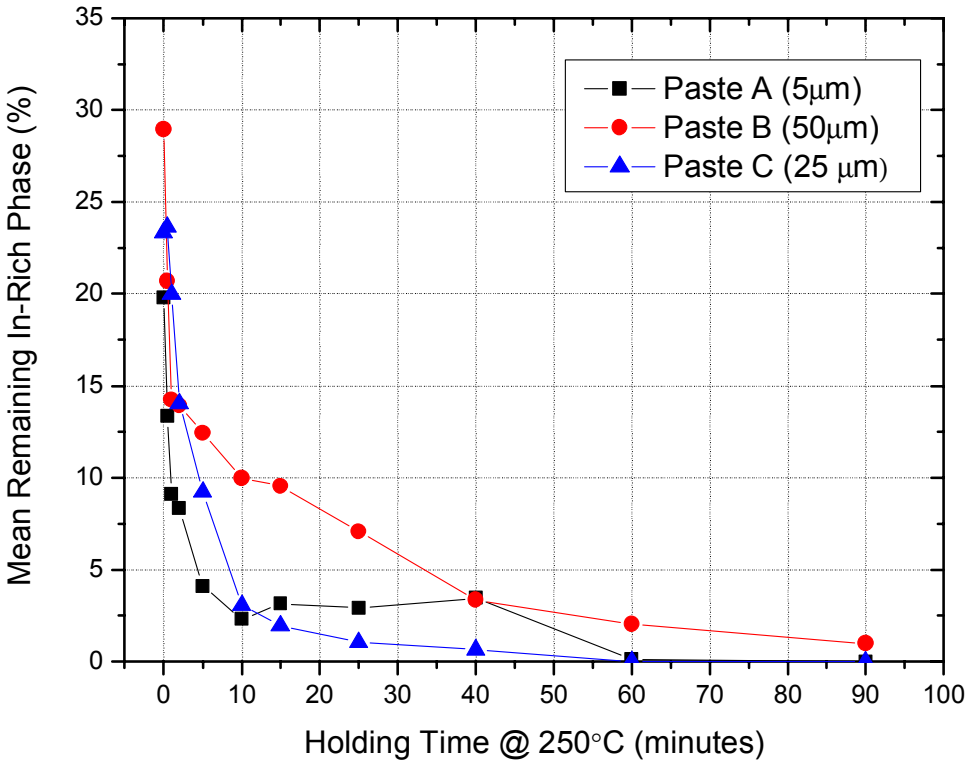

Figure 23. Experimental data showing the Remaining In-rich material (mean), as function of isothermal holding time and silver particle size.

From the above chart it is evident that silver particle size has an effect on the solidification rate. From inspection, it can be inferred that the smallest particle size (Paste A) exhibited the fastest transformation, in which the fraction of remaining In-rich material showed a steep decline in the first ten minutes, whereas the largest particle size (Paste B) required a much longer holding time to achieve an equivalent response (~60 minutes). Details of the effect of particle size on the kinetics of this reaction will be given in the following sections.

5.3.4. Empirical estimation of the reaction rate (k):

The effect of holding time on the isothermal solidification process was evidenced in the cooling traces in Figure 20. To obtain a kinetics model of this dynamic phenomenon, a reaction rate must be estimated. Silver particle size was chosen as the controllable variable for this first stage of the investigation whereas the remaining fraction of the low melting In-rich phases (i.e. φ with a T_m of 170°C and the eutectic solid with a T_m of 147°C) was defined as the response or dependent variable as expressed in Equation 31. The persistent presence of any of these two phases will result in a partial re-melt of the system when its melting temperature is exceeded during a future high temperature thermal excursion.

The rate constant (k) is an indicator of the solidification rate of the system. Increasing k results in a faster solid-liquid interface motion and a shorter duration of the isothermal solidification stage. The isothermal solidification stage is over when the remaining In-rich phase approaches zero; this suggests that all of the initial low melting point indium has diffused into the silver base metal. Experimental calculations of this rate constant were performed by fitting a modified Avrami [61] model to the DSC data. This exponential decaying model was used to fit the Remaining In-Rich Phase given in Figure 23 for each of the three particle sizes. The generalized model is given by Equation 32, in which "y" represents the fraction of untransformed material (%). In this investigation the progression of the process was analyzed from the unreacted material perspective, i.e. the remaining fraction as previously defined:

Equation 32

$$y = A_1 \cdot \exp\left(\frac{-t}{\tau}\right) + y_o$$

where A_1, y_o, and τ (time constant) are empirical constants, and t is the isothermal holding time in minutes. The rate constant, k (1/min.), is defined as:

Equation 33

$$\text{Rate Constant (k)} = \frac{1}{\tau}$$

Results from model fitting are given in Table 6.

Table 6. Empirical constants from model fitting.

Solder Paste	A_1	95% CI	y_o	95% CI	τ (min.)	95% CI	R^2
A (PS_{max}: 5 μm)	16.34	14.88 17.80	2.66	2.04 3.28	1.38	1.08 1.68	0.95
C (PS_{max}: 25 μm)	23.6	22.67 24.53	0.64	0.04 1.24	4.5	3.95 5.05	0.99
B (PS_{max}: 50 μm)	18.28	15.26 21.3	3.14	0.88 5.4	9.31	4.7 13.93	0.82

Figure 24 illustrates both the predicted Remaining In-Rich Phase for a particle size of 25 μm (Paste C) and the data obtained from the DSC tests. Similar plots were obtained for the other two pastes using the data from Table 6 and DSC [Appendix 2]. It is evident that particle size (PS) was isolated for each case, resulting in discrete prediction models with parameters specifically estimated for each particle size value. To obtain a generalized kinetics model, with particle size as one of the independent variables along with holding time, a correlation analysis was required. Dependency among the obtained constants (A_1, y_o, and τ) and PS (μm) was determined by inspecting of their scatter plots and their corresponding regression coefficients (R^2) [Appendix 3]. As evidenced by a R^2 value of 0.059, the y_o was demonstrated to be uncorrelated with particle size. A similar inspection and analysis of A_1 resulted in a

similar conclusion, where only 3.8% ($R^2 = 0.038$) of its variability was described by PS. A strong correlation between τ and particle size (μm) was obtained; their linear relationship is given by the following expression ($R^2 = 0.996$):

Equation 34

$$\tau(PS) = 0.1769 \cdot (PS) + 0.3458$$

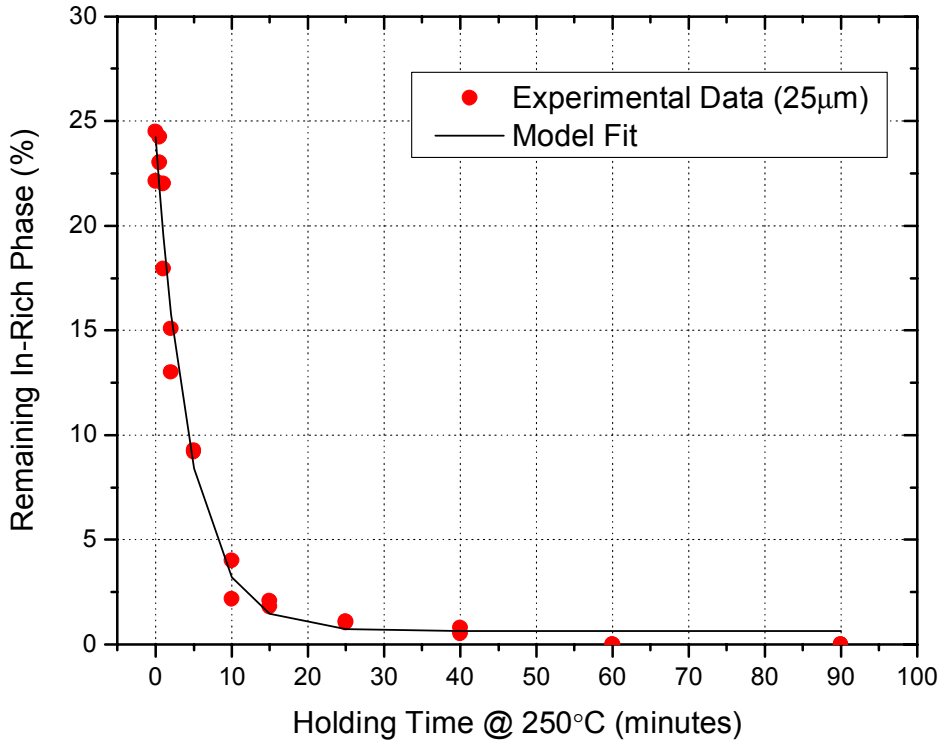

Figure 24. Prediction of the Remaining In-rich material by model fitting the experimental data from Paste C (25 μm silver particle size). Markers denote complete Paste C DSC data from the experiment, the solid line is the prediction from the model.

The rate constant (k) was previously defined as 1 / τ. Using this definition, the empirical rate constant for the Ag-In system as function of particle size was obtained for each paste. Measured rate constant values are given in Figure 25 together with predicted values from the model given in Equation 34. Fro the chart the highest

measured value of 0.73 corresponded to the smallest particle size. Data from this figure agreed with the theoretical principle of the governing diffusion mechanism, where as particle size decreases, the effective surface area increases, resulting in faster rates.

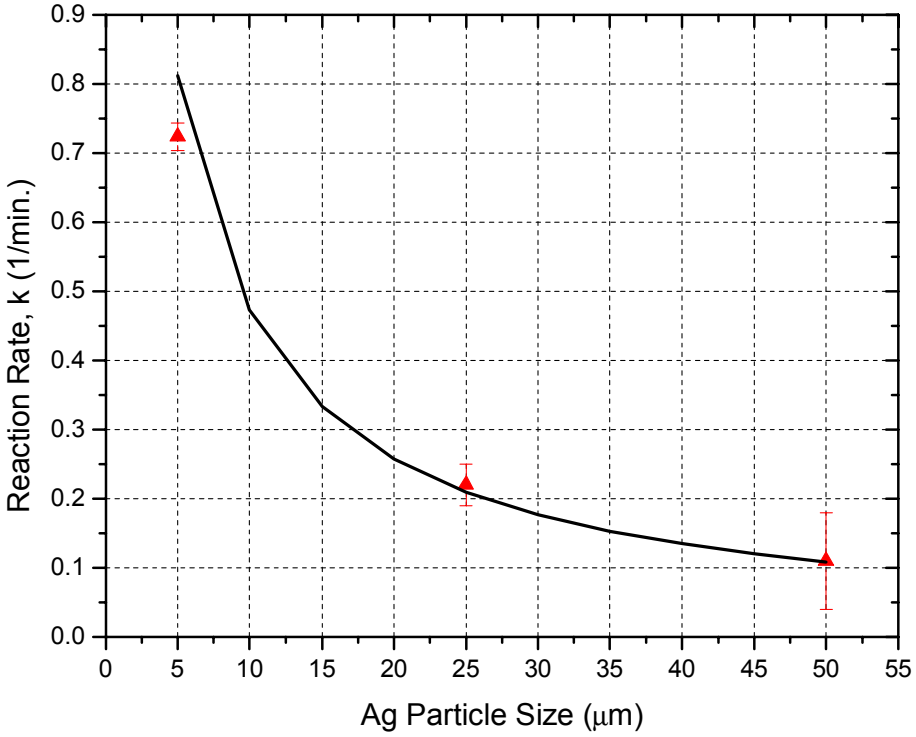

Figure 25. Correlation of the experimental reaction rate, k (1/min.) with the silver particle size (μm). Error bars denote the 95% confidence interval of the estimated value.

The independency of both A_1 and y_o with PS was used as the basis to obtain its best approximation by means of the arithmetic average. Nominal values for the three cases were taken from Table 6, and their averages were calculated. A generalized kinetics model for Remaining In-Rich Phase (%) as function of isothermal holding time and particle size was obtained:

Equation 35

$$\text{Remaining In - Rich Phase}\,(\%) = 19.41 \cdot \exp\left(\frac{-t}{\tau}\right) + 2.15$$

where τ (PS) = 0.1769·(PS) + 0.3458, A_{1avg} = (16.34+18.28+23.6)/3, and y_{oavg} = (2.66+3.14+0.64)/3. This model provides a good approximation for the progression of the Ag-In TLPS process, where the effect of particle size on reaction rate was established. Nevertheless, an inspection of Equation 35 suggests that at holding times approaching zero the prediction is independent of PS, therefore resulting in a constant value of 21.56% In-Rich Phase. This value results from an initial condition that depends on the as-built composition of the paste mixture, a variable that was set constant during this experiment. In chapter 6, a response surface methodology (RSM) will be used to study the progression of the Ag-In TLPS process. This RSM technique will consider the combined effects of the independent variables, some of which were fixed during this initial stage of the investigation.

5.3.5. Microstructural evolution and phase transformations:

To further elucidate the metallurgical reactions taking place during TLPS, samples of the 75 Wt.% Ag – 25 Wt.% In formulation treated for varying holding times (i.e. 0 min., 10 min., 40 min., and 60 min.) were epoxy mounted, polished, and etched. The microstructure developed in these samples was observed using backscattered electron (BSE) imaging in the ESEM. An EDS analysis was also performed to identify the phases present by their elemental composition. It should be noted that the microstructures in the following images represent the morphology of the phases as they solidified after cooling from 250°C to room temperature at 1°C/s. Figure 26

shows a BSE of the microstructure of a sample heated to 250°C at 60°C/min. with no isothermal holding time.

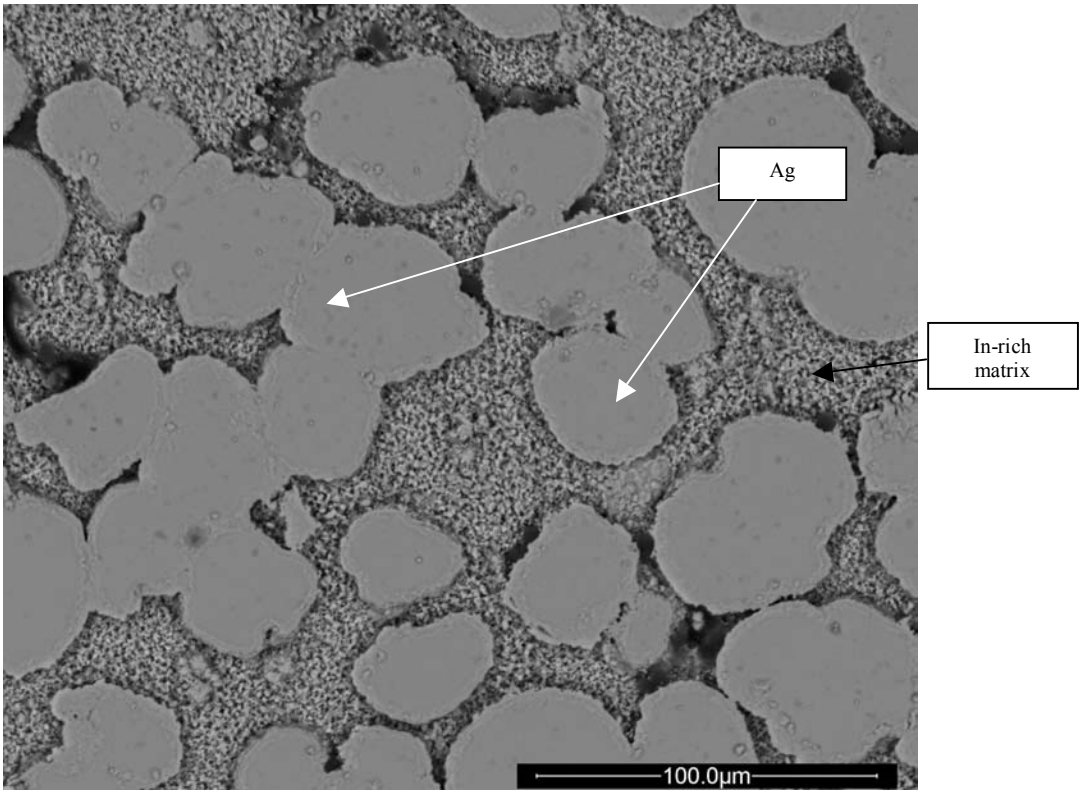

Figure 26. BSE image of a 75 Wt.% Ag – 25 Wt.% In specimen heated to 250°C and cooled to room temperature with no isothermal holding.

The presence of the low melting lamellar structure of the eutectic solid is evident. It is observed that this phase constitutes the continuous matrix where the silver particles are embedded. A DSC trace for such a holding period is given in Figure 20, where a considerable amount of In-rich phase is evident from the magnitude of the two exothermic peaks. Figure 27 shows a higher magnification of the sample in Figure 26. EDS analysis revealed that the matrix is composed of eutectic material and φ (~67 at.% In).

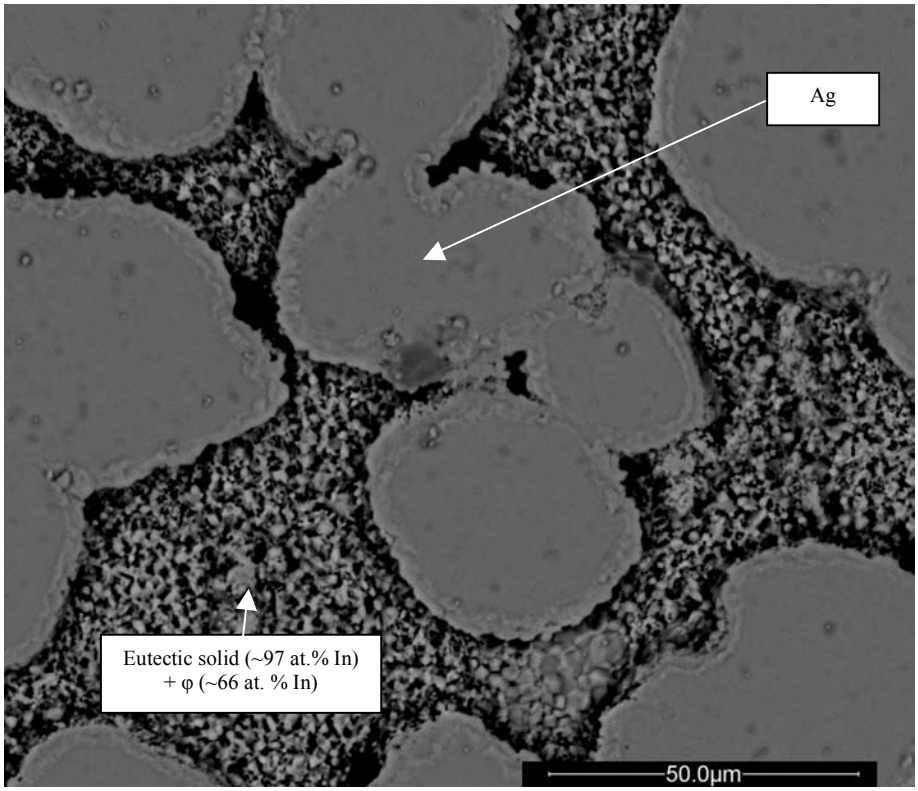

Figure 27. Zoom of the BSE image of a 75 Wt.% Ag – 25 Wt.% In specimen heated to 250°C and cooled to room temperature with no isothermal holding.

Figure 28 depicts the microstructure of a sample treated to 250°C and held for 10 minutes. From this micrograph, the growth and coagulation of the Ag-rich particles is evident. Necking formation between adjacent particles was observed as evidence of the sintering mechanism. After 10 minutes at 250°C, the In-rich phase is no longer a continuous matrix, suggesting its consumption by the isothermal solidification process. This observation agrees well with the corresponding DSC trace in Figure 20 (10 minutes), where a significant shrinkage in magnitude of the exothermic peaks was recorded. The In-rich liquid is now confined to discontinuous areas within the system and is no longer able to completely surround the silver particles.

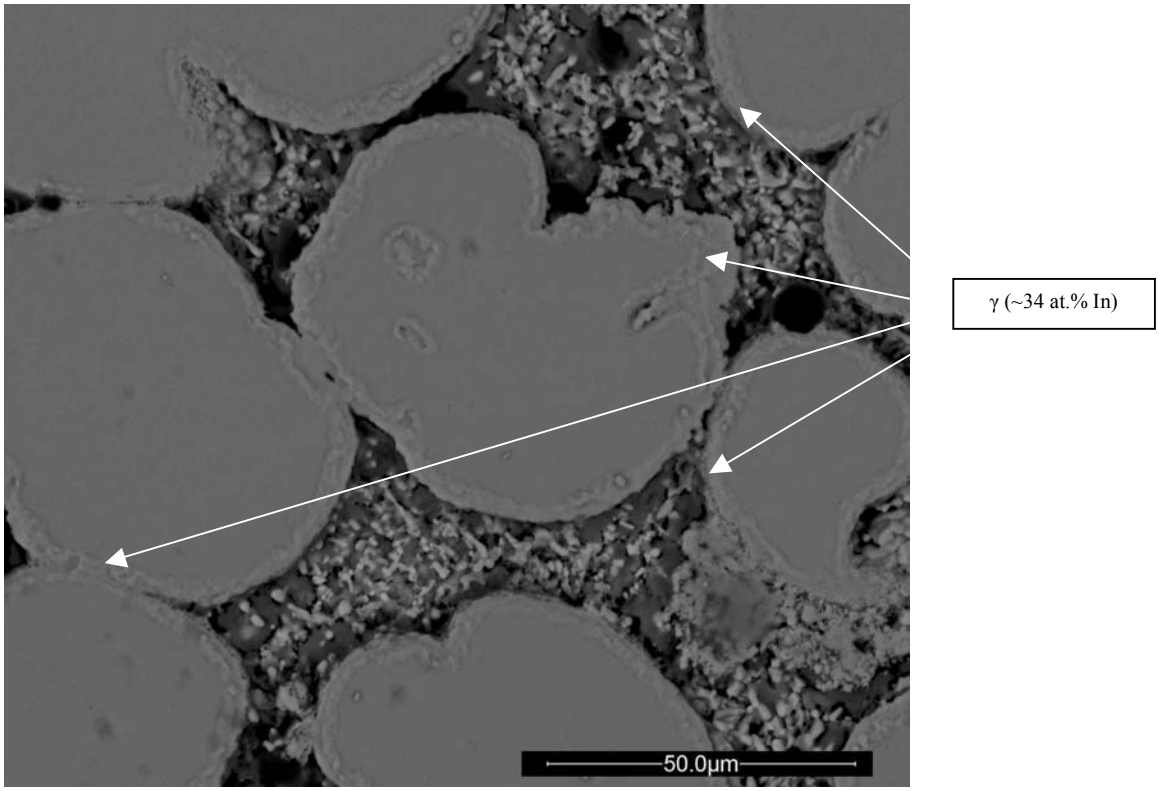

Figure 28. BSE image of a 75 Wt.% Ag – 25 Wt.% In specimen heated to 250°C, held isothermally for 10 minutes, and cooled to room temperature.

Figure 28 illustrates the precipitation of the Ag-rich γ (34 at.% In) phase at the solid / liquid interfaces and the forming of rings along the borders of the silver particles. Figure 29 illustrates that, after holding for 40 minutes at 250°C, the microstructure is now dominated by an Ag solid solution (α) matrix as measured by the EDS analysis. A network of γ decorates the silver (α) matrix. At this point, the remaining In-rich material is minimal and limited to isolated sites within the Ag-rich matrix. The composition of this fraction of remaining In-rich material was confirmed by EDS as having ~ 66 - 70 at.% In, i.e. φ. This data correlates with the DSC trace for a 40 minutes hold (Figure 20), where the eutectic peak was no longer detected and only a small exotherm was recorded at ~ 170° C, corresponding to the solidification of φ.

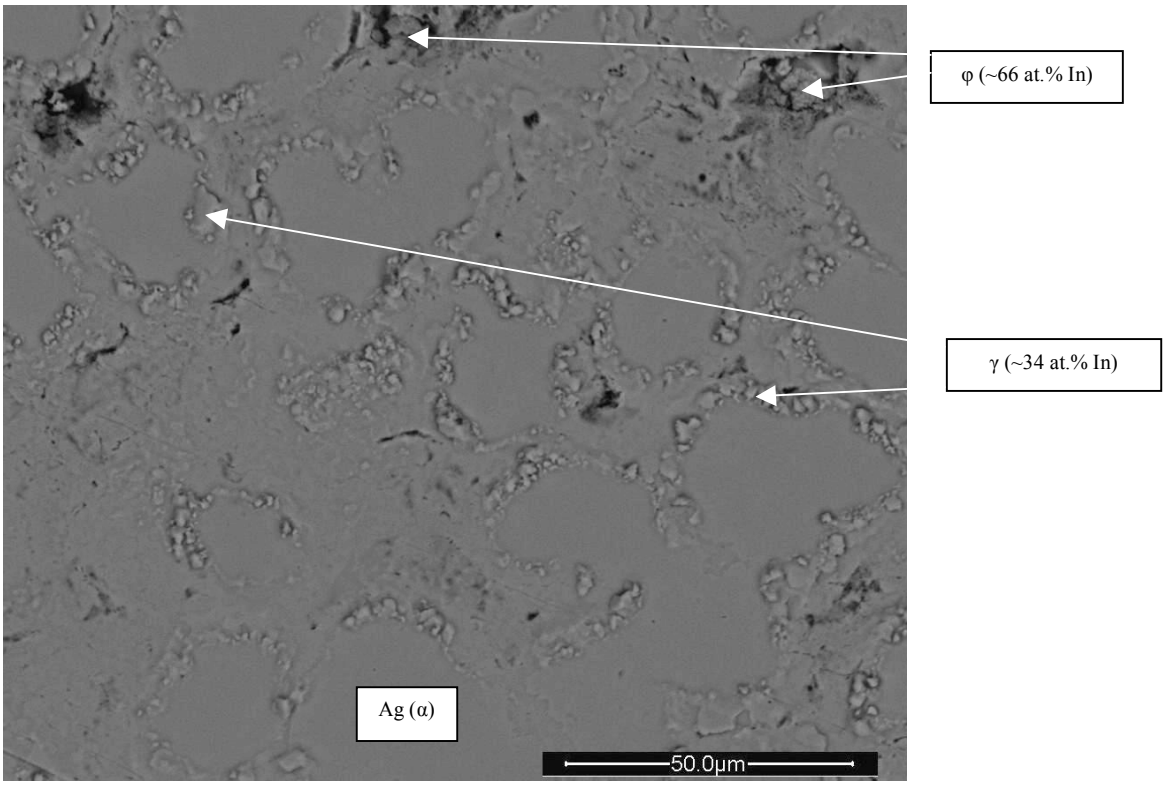

Figure 29. BSE image of a 75 Wt.% Ag – 25 Wt.% In specimen heated to 250°C, held isothermally for 40 minutes, and cooled to room temperature.

Figure 30 depicts the microstructure of a sample treated at 250°C for 60 minutes. In this case, the γ phase is evenly dispersed through the matrix. This represents the homogenization stage that tends to the final equilibrium composition. At this stage of the process, all the indium is present in the form of a high melting α + γ structure. This was confirmed (Figure 20) by the absence of exothermic peaks during the cool down.

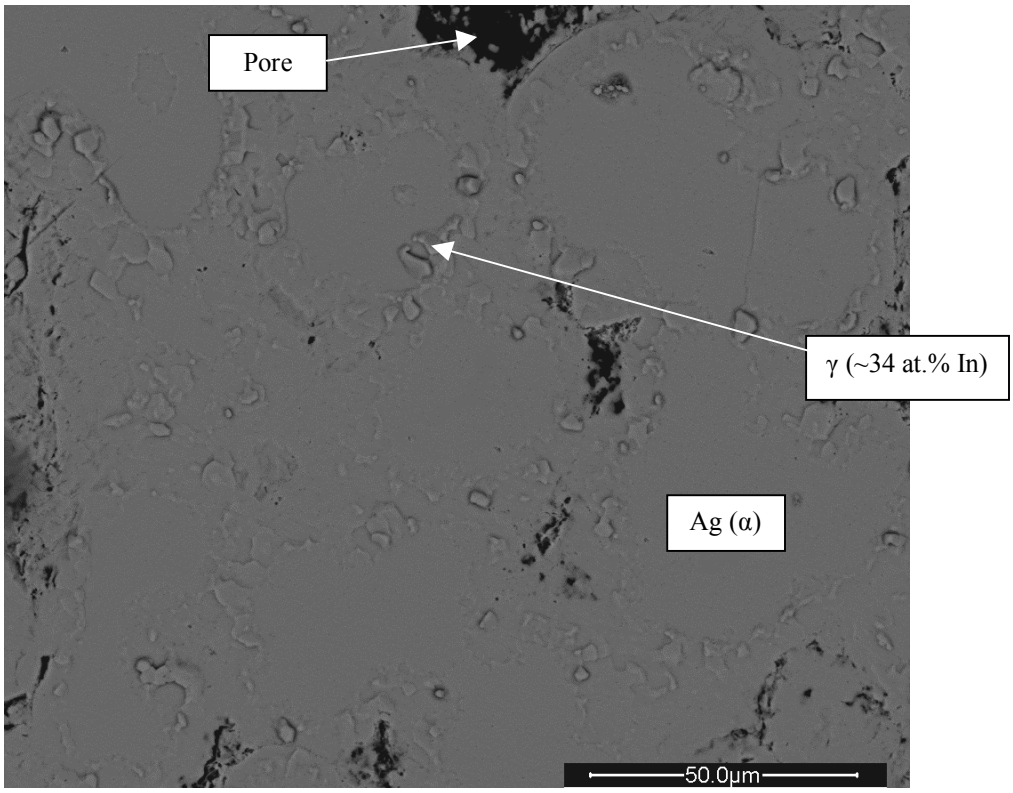

Figure 30. BSE image of a 75 Wt.% Ag – 25 Wt.% In specimen heated to 250°C, held isothermally for 60 minutes, and cooled to room temperature.

5.4 Discussion:

The achievement of a variable melting point material is the key enabler for a breakout from in the processing temperature hierarchy. This shift in melting temperature results from the in-situ alloying reaction between the silver base metal and the In-rich liquid at the processing temperature provided there is a sufficiently long isothermal hold. Determination of this time is crucial for any future development of this technology because it limits the economical viability of the process. In the previous section, the rate constant for the isothermal solidification stage was calculated as a function of silver particle size, a variable that can be controlled by the practitioner. The estimation of the solidification rate was accomplished by fitting the experimental

data obtained from the DSC analysis to an Avrami model. This information provided the remaining fraction of In-rich material as a function of the isothermal holding time for all three particle sizes. Results confirmed the existence of an inverse relationship between base metal particle size and the reaction rate; the highest rate (0.72) being obtained for the smallest particle size (5 μm). These results agreed with the expected theoretical outcome. It is well known [24][25][27] that TLPS is a diffusion driven process, and as particle size decreases, the effective surface area-to- volume ratio increases, resulting in faster mass transport rates.

The isothermal solidification process is the rate controlling stage in which the amount of indium that diffuses into the silver is the critical variable. From the DSC analysis it was possible to calculate the remaining fraction of indium using the ratio of the solidification and melting energies resulting from varying isothermal holds. From a mass conservation argument, the difference between the initial amount of indium in the system and the remaining quantity of indium represents the amount of indium that had been diffused into the silver. Thus, when remaining In-rich material approaches zero (as given by the absence of exothermic peaks in the DSC trace after 60 minutes) the completion of the solidification process and the subsequent accomplishment of the variable melting point can be suggested. This was confirmed in Figure 21, where no re-melts were detected during the re-heat to 400°C after a 60 minutes hold at 250°C.

In this investigation, the microstructural evolution of the process provided valuable information on the morphology and dispersion of the phases. Previous attempts to describe the progression of the TLPS process had focused on a phenomenological description, but physical evidence to correlate the modeling of its stages was missing [36]. DSC data provided quantitative information about phase changes and their corresponding temperatures, but qualitative information about these features is crucial for a better understanding of the TLPS underlying mechanism. Confirmed by the micrographs, there exists a transition from an In-rich continuous matrix where the silver particles are present as a discrete phase to an Ag-rich matrix where the remaining In-rich areas are isolated and disconnected. The growth of the Ag-rich matrix, driven by the increasing diffusion of indium atoms into the silver particles, resulted in the formation of a new microstructure where the intersection of the growing particles is evident by the ridges of the γ network (Figure 29). Upon completion of this transformation, a new alloy has been formed with the microstructure shown in Figure 30. Longer heat treatments should result in full dispersion of γ leading to a homogeneous structure with an equilibrium composition of 75 Wt.% Ag – 25Wt.% In and a solidus temperature of 693°C. This final stage (homogenization) is not critical in achieving high temperature stability because it involves a solid state reaction; at this stage, all of the low melting In-rich material had already been completely transformed into a Ag(α) + γ structure that is stable at high temperatures. Homogenization results as part of the TLPS process when enough time is provided, but it can be completed with additional heat treatment or during the high temperature operation.

To provide physical insight into the DSC results and the estimated solidification rates, a physics based approach was used. The physical description of TLPS as a diffusion controlled phase change is well established [11][24][25][27][30] and there is general agreement on the nature of the underlying physical phenomenon. The process may be understood by breaking it down into a succession of discrete steps [25][30], where it progresses into two distinct regimes. At short times (~ 2 minutes or less), rapid solute transport in the liquid means that atomic fluxes in that phase dominate the rate at which dissolution of the base metal occurs, i.e. an erosion process in which silver atoms are dissolved into the liquid indium. Once the liquid has become homogeneous (equilibrium composition at T_p), solidification takes place at a rate determined by the rate of solute diffusion within the solid phase. This step takes much longer to complete than the initial dissolution stage since it is dominated by diffusion of indium into the solid silver. For this reason, the attention has been restricted to the kinetics of the isothermal solidification stage. Fick's second law for the one dimensional case was given by Equation 2. When D (diffusion coefficient) is assumed constant and appropriate initial and boundary conditions are established, an analytical solution can be obtained [27]. Assuming local equilibrium at the interface, the concentrations of both phases are therefore constant and equal to the values of the liquidus (C_L) and solidus (C_s) compositions at T_p. To maintain equilibrium while conserving solute, any atomic fluxes present will lead to the movement of the interface (moving boundary problem). It has been shown [36] that the governing equations for this process can be written as function of only two dimensionless parameters: a geometric

factor "P" and a thermodynamic factor (saturation parameter) Ω that has been defined as $(C_s - C_o) / (C_L - C_s)$, where C_o is the initial solute concentration in the base metal. A complete derivation of the method was presented in section 2.2.2.5. Exact solutions to moving boundary problems are very limited; Crank provided an analytical solution for the semi-infinite solid case. Using this approach, an expression for the rate at which the interface moves (K) was derived in section 2.2.2.5 and given in Equation 25. This expression is independent of the geometric factor "P", implying that the solidification rate depends only on the saturation parameter Ω (which can be interpreted as the driving force for the movement of the interface, i.e. solidification). A graphical solution to Equation 25 has been given by Illingworth et al. [36]. In order to obtain a reaction rate for our system, Ω must be calculated first. From the phase diagram [46] at a processing temperature of 250°C, C_L = 90 Wt.% In, and C_s = 34 Wt.% In, C_o is zero in our case, assuming that at t = 0 the silver particles contain no indium. With these values the saturation parameter Ω was calculated to be 0.6, which corresponds to a solidification rate constant (K) of 0.25, obtained from the graphical solution [36] and confirmed with the tabulated data by Lesoult [32]. This value, obtained from a theoretical approach, agreed well with the 0.22 value obtained experimentally for the 25 μm particle size, but not with smallest particle size. This discrepancy, for very small particle size, has been attributed to the assumption of a semi-infinite media. Nevertheless, this exercise provided insights into the progression of the transformation process as described by a diffusion mechanism. The rate constant calculated from the theoretical solution of a moving boundary problem agreed with the value obtained from the DSC technique, therefore supporting

the capability of the experimental method to measure the kinetics of the underlying reaction.

5.5 Conclusion:

The development of a shifting melting point Ag-In paste via a transient liquid phase sintering process has been demonstrated during this stage of the investigation. Its formulation as a paste provided two critical advantages over previous planar thin film approaches. First, when powders are used, shorter processing times are required due to their enhanced surface area available for diffusion. Second, the assembly process requires standard stencil printing and reflow techniques, making it a less expensive and more flexible method. The kinetics of the isothermal solidification reaction were experimentally studied by means of DSC analysis and correlated with the microstructural evolution of the system. The solidification rate was estimated from empirical data and its dependency on base metal particle size was established. An analytical diffusion based model was used to evaluate the physical significance experimentally obtained solidification rate. Results from this approach agreed well with the medium particle size, thus confirming the DSC as a tool for studying reaction kinetics. The analytical model could not be used for comparison for the small particle sizes where it is not appropriate. The metallographic analysis revealed the morphology of the transient system and provided microstructural evidence to support the reactions detected by the DSC traces. Results from this initial stage of the investigation, in which critical parameters were deliberately fixed to set values, provided the basis for the next phase of this research. A more rigorous study of the transformation kinetics of this system is still needed. In this study, the effect of other

controllable processing variables must be evaluated so that a full response model can be built. The following chapter will deal with the development of an empirical model using a response surface methodology approach.

Chapter 6: Kinetics Model for Ag-In TLPS Process by Response Surface Methodology

6.1 Introduction:

When two different phases in a binary alloy system are brought in contact and held isothermally, a compositional gradient across the interface is produced. This gradient is associated with a difference in the chemical potential of the individual atoms, which is known to be the driving force for atomic flux. The fluxes on either side of the interface are not necessarily equal, thus to prevent accumulation or depletion of matter (conservation of mass principle), the interface must move [34]. An application of the above phenomenon that deals with the case in which one of the phases is a liquid is known as liquid phase sintering [11]. When there is a transient growth and subsequent solidification of the liquid, caused by isothermal diffusion of the melting point depressant (MPD), the process is referred as transient liquid phase sintering (TLPS) [11][24][36]. Numerous advantages have been given [11] for the usage of this technique, of which the most critical for the microelectronic industry comes from the ability to form a joint at a relatively low temperature which then yields a higher melting point alloy. This in-situ reaction occurs isothermally at the processing temperature and is driven by the solute (MPD) concentration gradient at the solid / liquid interface. Knowledge of the kinetics of this transformation is crucial for a better understanding of the phenomenon as well as for its control and optimization. The ability to predict the progression of this transient process will enable the

dissemination of this technique as a viable alternative to the industrial community. Currently, there is a lack of quantitative knowledge of the governing underlying physical mechanisms [11] [22][23][36]. However, its phenomenological physical description [25][30], defined by a diffusion mechanism that occurs through a series of stages, has been established. The complexity of the modeling task resides in the fact that the stages often occur simultaneously rather than the serialized discrete steps assumed for the analytical solutions. In addition, the sensitivity to multiple processing variables, such as mixture composition, base metal particle size, heating rate, isothermal holding time, and processing temperature; increases complexity as well.

During the TLPS process a layer of liquid forms, wets the contacting base metal, and then solidifies isothermally [25]. Liquid film formation during the process depends on the availability of a low melting point material within the mixture, which flows by capillary action resulting in particle re-arrangement and densification. This liquid film then solidifies at the processing temperature by reacting with the base metal, leading to the formation of a new alloy with an equilibrium composition given by the initial mixing ratio of its main constituents. This newly formed material is then homogenized during the process or by a later heat treatment. All three stages of TLPS (liquid formation and dissolution, isothermal solidification, and homogenization) depend on solute (MPD) diffusion from the high concentration phase to the lower concentration on the base metal. The first stage is a dissolution step, in which the base metal dissolves into the liquid as the temperature is raised

from the melting point of the MPD to the processing temperature (T_p). The composition of the liquid follows the liquidus line up until the equilibrium composition (C_L) is reached at T_p. The formation of the liquid and its subsequent capillary flow through the solid skeleton has been accounted for the densification of the compact. The duration of this stage has been reported to be very short (can be assumed to be instantaneous) [25][27], in which only a small fraction of solute is consumed by diffusion into the base metal [27]. The heating rate is critical during this stage since it controls the amount of liquid formed during the process. Values of 20 °C/min or less had resulted in the formation of no liquid due to the consumption of the MPD by solid state diffusion during heating [28][30]. During the second stage, isothermal solidification, there exists a local equilibrium condition at the solid / liquid interface in which C_L (solute composition of the liquid phase at T_p) and C_s (solute composition of the solid at T_p) are unchanged. Driven by diffusion of solute atoms from the liquid to the solid the liquid zone decreases continuously (moving boundary) until the liquid completely solidifies. This stage is considered to be the most important since the completion time required for the entire TLPS is largely determined by the time required for the completion of the isothermal solidification [30]. The last stage, homogenization, is where solid state solute redistribution occurs. This is not a critical step in achieving high temperature stability, because the formation of an Ag-rich solid has already been accomplished, yielding the desired shift in melting point of the alloy. However, it may affect the solidification rate during the late period of the previous stage. The homogenization process is finished

when an equilibrium condition is attained at a composition corresponding to the pre-selected value from the initial mixing.

Most modeling efforts to date have focused on analytical methods [25][27][30] to describe the progression of the TLPS process. However, this approach treats the process as a number of independent steps which is not what actually occurs during TLPS. Analytical solutions for each stage depend on error function, parabolic law assumptions, and semi-infinite media; which are all approximations. Attempts to provide an analytical solution to the first stage (heating and dissolution) have failed. This failure has been attributed to the fact that during this period, the solute concentrations of the solid and liquid phases, as well as the diffusion coefficient (D) are changing with increasing temperature [30]. Limited effort has been devoted to this problem since it has been demonstrated to be a near instantaneous reaction in which solute diffusion into the base metal is negligible [27]. The isothermal solidification has been successfully modeled using analytical solutions derived for moving boundary diffusion problems [25][27]. In their treatment, the problem was simplified to a planar semi-infinite base metal with a constant solute surface concentration C_s, as given by Figure 5 in section 2.2.2.5. Based on this assumption, an error function solution was obtained for the solute concentration profile within the base metal as function of position and time. An expression for the solute amount that has diffused into the base metal as function of time was also analytically derived [29]. Using this mathematical formulation, the time to complete the isothermal solidification can be estimated for the particular binary system. It needs to be

mentioned that this approach assumes a parabolic relation, i.e. the process is proportional to $\sqrt{t}$ for its duration, which may not be real for finite base metal samples. This analytical solution provides a tool to predict the response of the system during the time regime governed by the isothermal solidification mechanism, but fails to describe the true response of the system during the initial dissolution stage, and does not account for the delaying effects of the slower homogenization stage. As a result of these inadequacies, a more comprehensive approach for modeling the TLPS is needed. The new model should address the base metal dissolution, isothermal solidification, and solute homogenization as interdependent sequential processes. In addition, this model should be a function of controllable parameters so that the practitioner can use it in real engineering applications.

In this chapter, an approach for modeling the TLPS process using response surface methodology (RSM) will be presented. This technique has been developed for an Ag – In binary system in which elemental particles were mixed to form a paste. The prediction model will use data from all the stages, and should provide an estimate of the response as function of critical controllable process variables. This experimental approach can be used for process control as well as tailoring for specific application or fabrication conditions. The kinetics of this system will be studied by analyzing the response (remaining In-rich phase) as function of holding time, processing temperature, base metal particle size, indium weight fraction in the mixture (Wt.% In), and heating rate. Results will be provided in three dimensional charts and contour plots for ease of interpretation. An analytical solution of the transformation

will be presented for comparison to the empirical results. A microstructural analysis will provide further information useful for the discussion and explanation of the Ag-In system.

6.2 Methodology:

6.2.1. Response surface methodology (RSM):

The exploration of the response of a process is a common problem faced by the scientific community. In general, there is a response variable of interest "y"; and a set of predictor or independent variables x_1, x_2,…., x_k. For some systems the nature of the relationship between the "y" and the "x's" might be known exactly based on the underlying physical mechanism. For these cases a mechanistic model may be developed, but often requiring a series of assumptions that can deviate from the true response. Response surface methodology (RSM) consists of the experimental strategy for exploring the space of the independent variables and statistical modeling to develop an appropriate approximating relationship between the response and the regressors.

In general, the response variable "y" may be related to "k" regressor variables by a first order polynomial of the form

$$y = \beta_o + \beta_1 \cdot \zeta_1 + \beta_2 \cdot \zeta_2 + \ldots. + \beta_k \cdot \zeta_k + \varepsilon$$

where ε is a term that represents other sources of variability not accounted for in the function. This statistical error is assumed to have a normal distribution with zero

mean and unit variance. The variables $\zeta_1, \zeta_2, \ldots, \zeta_k$ are referred to as the natural variables because they are expressed in the natural units of measurement. In RSM it is common to transform these to coded variables $x_1, x_2, \ldots, x_k$, which are defined to be dimensionless. Making the substitution to the coded variables and assuming a zero mean ε, yielded the model in the following form:

Equation 36

$$y = \beta_o + \beta_1 \cdot x_1 + \beta_2 \cdot x_2 + \ldots + \beta_k \cdot x_k$$

This is called a multiple linear regression model with "k" regressor variables. The term linear is used because Equation 36 is a linear function of the unknown parameters $\beta_o, \beta_1, \ldots, \beta_k$ regardless of the shape of the response surface that it generates. The parameters β_j , j = 0, 1, 2, …, k are known as the regression coefficients. The above model (Equation 36) describes a hyperplane in the k-dimensional space of the regressor variables $\{x_j\}$. The parameter β_j represents the expected change in the response per unit change in x_j when all the remaining independent variables x_i ($i \neq j$) are held constant. The addition of an interaction term, $\beta_{12} \cdot x_1 \cdot x_2$, can still be analyzed by multiple linear regression techniques by introducing a simple substitution. Letting $x_3 = x_1 \cdot x_2$ and $\beta_3 = \beta_{12}$, Equation 36 will still be a linear function of β's. Adding interaction terms to the model introduces curvature into the response function. A RSM would be incomplete without discussing the method for estimating the regression coefficients, checking for their significance on the response, and lastly checking the adequacy of the model fit.

The method of least squares will be used to estimate the regression coefficients for the multiple linear regression model. Suppose that from an experiment n > k

observations of the response variable are available, say y_1, y_2, …, y_n. Along with each observed response y_i, there will be an observation on each regressor variable. Letting x_{ij} denote the i^{th} observation (setting) of variable x_j; we may write the model (Equation 36) in matrix notation:

Equation 37

$$y = X \cdot \beta + \varepsilon$$

where:

$$y = \begin{bmatrix} y_1 \\ y_2 \\ \downarrow \\ y_n \end{bmatrix}, \qquad X = \begin{bmatrix} 1 & x_{11} & x_{12} & x_{1k} \\ 1 & x_{21} & x_{22} & x_{2k} \\ 1 & x_{n1} & x_{n2} & x_{nk} \end{bmatrix}, \qquad \beta = \begin{bmatrix} \beta_o \\ \beta_1 \\ \beta_k \end{bmatrix}, \qquad \varepsilon = \begin{bmatrix} \varepsilon_1 \\ \varepsilon_2 \\ \varepsilon_n \end{bmatrix}$$

The method of least squares chooses the β's so that the sum of squares of the residual errors, ε_i, are minimized. The fitted model in scalar notation is given by:

Equation 38

$$y_i = \beta_o + \beta_1 \cdot x_{i1} + \beta_2 \cdot x_{i2} + \ldots + \beta_k \cdot x_{ik} + \varepsilon_i$$

or:

Equation 39

$$y_i = \beta_o + \sum_{j=1}^{k} \beta_j \cdot x_{ij} + \varepsilon_i \qquad \text{i = 1, 2, 3,…, n}$$

where the β's are obtained from [63]:

Equation 40

$$\beta = (X'X)^{-1} X'y$$

A test for significance of regression is needed to determine the contribution of the independent variables on the response. This task is done by using hypothesis testing, in which:

H_o (null hypothesis): $\beta_1 = \beta_2 = \ldots = \beta_k = 0$

H_1 (alternative): $\beta_j \neq 0$ for at least one j

Rejection of H_o implies that at least one of the regressor variables (x_1, x_2, …, x_k) contributes significantly to the model. The approach of hypothesis testing is called analysis of variance (ANOVA) because it is based on a decomposition of the total variability of the response variable "y". When using this method, H_o is rejected (which means that there is statistical evidence showing that the particular effect is significant) if the p-value for the F_o statistic is less than α. The p-value is the probability value for the given test, whereas α is a predetermined level of significance. F_o is given by:

Equation 41

$$F_o = \frac{(SS_R / k)}{(SS_E / n-k-1)}$$

SS_R is the sum of squares of errors attributed to the regression model and SS_E is the sum of squares of the residual errors [62]. The α value has been fixed as 0.05. All these values are calculated and tabulated for the experimental data in the form of an ANOVA table by the statistical software Minitab™. After the elimination of non-significant parameters, a reduced model can be obtained in terms of critical parameters. A good indicator of the ability of the proposed model to predict the response of the system for future conditions is given by the R^2_{pred}. This statistic gives an indication of the predictive capability of the regression model. Therefore, maximizing this parameter will lead to the best fit.

The mathematical definition of the R^2_{pred} is given by [62]:

Equation 42

$$R^2_{pred} = 1 - \left(\frac{PRESS}{SS_T} \right)$$

where PRESS (prediction error sum of squares) is defined as:

Equation 43

$$PRESS = \sum_{i=1}^{n} (y_i - y_{(i)})^2$$

y_i is the experimental observation and $y_{(i)}$ is the predicted response from a model in which the corresponding observation y_i was not considered during the fitting. The SS_T value is the total sum of squares of the error, i.e. $SS_E + SS_R$. Model adequacy checking is always necessary to ensure an appropriate approximation of the true system and to verify that none of the least squares regression assumption are violated. Statistical checking can be accomplished by verifying the normality assumption, which requires that the normal probability plot of the residuals fits a line. To verify the ability of the approximated function to describe the true response it is important to compare the RSM model to a mechanistic model of the underlying mechanism.

6.2.2. Design of experiment (DOE):

It has been hypothesized that the progression of the TLPS process depends on multiple variables such as isothermal holding time, processing temperature, heating rate, base metal size, and solute composition of the mixture [11][30]. In this second phase of the investigation all of the above parameters have been identified as the independent variables whereas the remaining In-rich phase has been defined as the response. The response will be measured experimentally using the thermal analysis from the DSC as defined by Equation 31 in section 5.3.1. A DOE was designed to investigate the joint effects of these factors on the solidification kinetics of the Ag – In system. Joint factor effects refer to main effects and all possible interactions. In this case, a two level full factorial experiment will be used to develop the prediction

model in terms of four input variables at each holding time. The design of the experiment is summarized in Table 7 below.

Table 7. Experimental factors and their levels for second phase DOE.

Factor	High Level	Low Level
Particle Size (PS)	50 μm (spherical) [Max]	25 μm (spherical) [Max]
Heating Rate (HR)	60 °C/min	30 °C/min
Processing Temperature (T_p)	300 °C	250°C
Additive Weight Fraction (Wt. %)	30 Wt. % In	15 Wt. % In

All of the factors but holding time have two levels. Therefore, a 2^k random experiment with a replicate will be performed at each holding time. Considering that k = 4 (for each holding time setting), the complete model will contain as many as 15 possible effects (2^k-1). The isothermal holding time is the fifth input variable, which requires multiple levels in order to obtain an accurate estimation of the true response. This is necessary because in studying the kinetics of a diffusion controlled process time is critical, so a finer resolution of this variable is required. When the holding time variable is introduced to the model, a complete description of the kinetics can be obtained in which up to 31 possible effects (5 main effects, 10 two-way, 10 three-way, 5 four-way, and 1 five-way interactions) will have to be considered. Diffusion controlled mechanisms are known to have a parabolic correlation with time [34], i.e. the process is proportional to the $\sqrt{t}$. Based on this assumption, the holding time variable will be transformed accordingly. The natural values of the isothermal holding times (in minutes) are as follows: 0, 0.5, 1, 5, 10, 25, 40, and 60; resulting in eight levels. To summarize, the entire DOE for this second phase will require 2^4 runs per replicate, i.e. 32 trials per holding time which will result in 256 test runs.

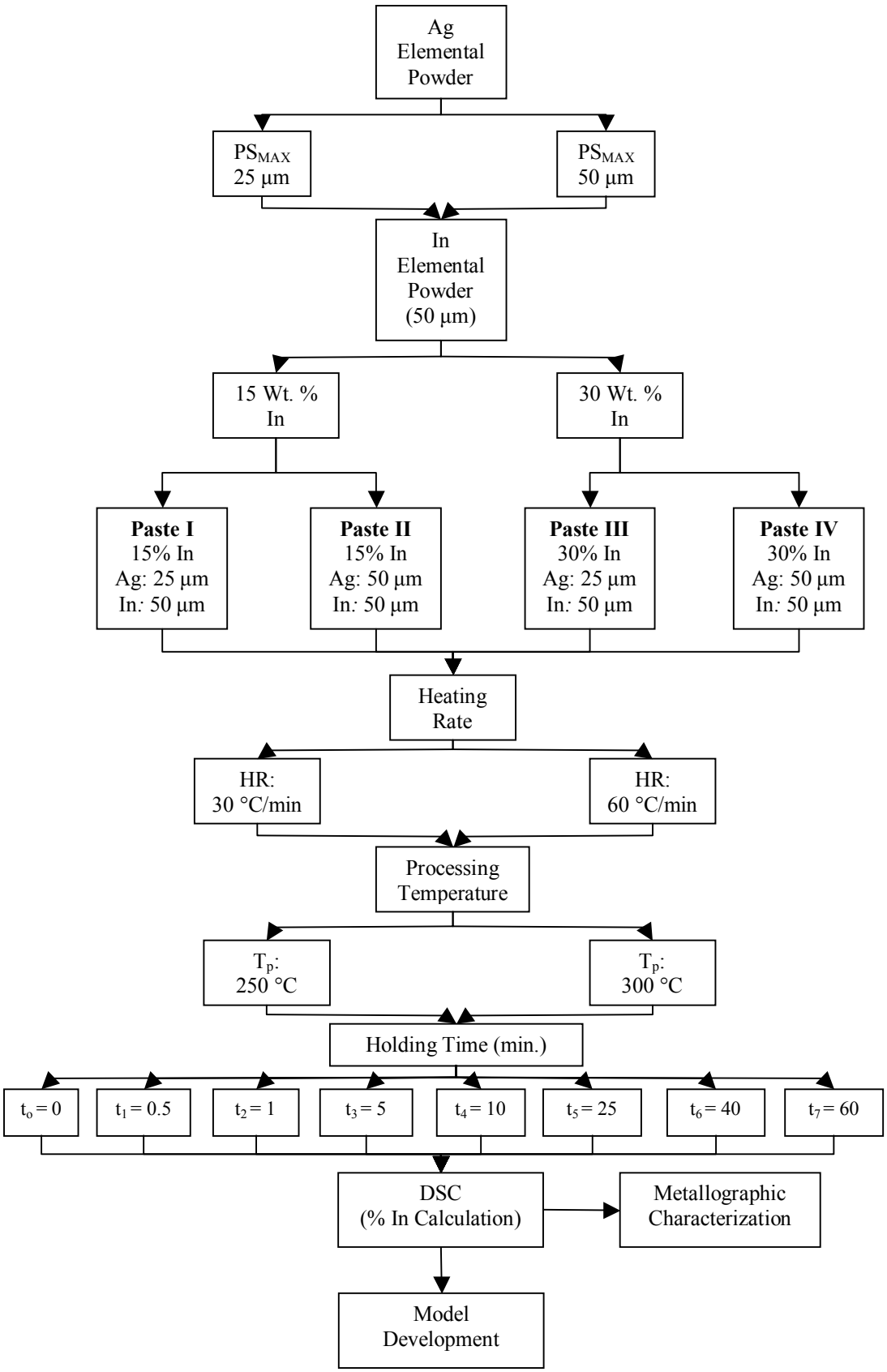
Ag Elemental Powder
PSMAX 25 µm
PSMAX 50 µm
In Elemental Powder (50 µm)
15 Wt. % In
30 Wt. % In
Paste I 15% In Ag: 25 µm In: 50 µm
Paste II 15% In Ag: 50 µm In: 50 µm
Paste III 30% In Ag: 25 µm In: 50 µm
Paste IV 30% In Ag: 50 µm In: 50 µm
Heating Rate
HR: 30 °C/min
HR: 60 °C/min
Processing Temperature
Tp: 250 °C
Tp: 300 °C
Holding Time (min.)
to = 0
t1 = 0.5
t2 = 1
t3 = 5
t4 = 10
t5 = 25
t6 = 40
t7 = 60
DSC (% In Calculation)
Metallographic Characterization
Model Development

Figure 31. Experimental Matrix for Phase II DOE

A flow chart of this experimental matrix is given in Figure 31. During this investigation the natural variables were coded for the development of a regression model.

Experimental data from all runs was analyzed using commercial statistical analysis software (Minitab) which provided the ANOVA and goodness of fit statistics for all of the models. Estimation of all parameters was done using coded variables, which allows to directly compare the various effects based on their absolute magnitudes.

6.2.3. Metallography:

To assist in the interpretation of the results from the DSC, samples treated under the specified experimental conditions were cross-sectioned and analyzed by scanning electron microscopy (SEM) and energy dispersive spectroscopy (EDS). A FEI Quanta 200 ESEM was used throughout this investigation. Elemental, as-received powders were characterized in terms of particle shape and size using the SEM equipment. These metallographic techniques provided qualitative information in terms of the extent of liquid spreading through the compact, as well as morphological information. This information assisted in describing the phenomenological aspects of TLPS at the different stages of the process. The atomic percents of the main constituents were also determined by spectral analysis to demonstrate the extent of the diffusion.

The DOE presented in the previous section suggested the formulation of four pastes:

Paste I with an 85 Wt. % Ag – 15 Wt. % In composition and Ag maximum particle size of 25 μm.

Paste II with an 85 Wt. % Ag – 15 Wt. % In composition and Ag maximum particle size of 50 μm.

Paste III with an 70 Wt. % Ag – 30 Wt. % In composition and Ag maximum particle size of 25 μm.

Paste IV with an 70 Wt. % Ag – 30 Wt. % In composition and Ag maximum particle size of 50 μm.

These four pastes were fabricated according to the above specifications and analyzed using the ESEM and EDS. From the morphological analysis it was evident that these powders were far from been mono-sized, but for standardization purposes, the maximum particle diameter for the specific mesh designation (per ASTM-B214) will be used during this investigation. This information will be used for the analytical model, whereas the true effect of the particle distribution will be recorded during the experimental tests. Figure 32 through Figure 35 show the morphology of the mixed powders (silver and indium), whereas the EDS dot maps provide the elemental analysis together with a qualitative impression of the elemental distribution.

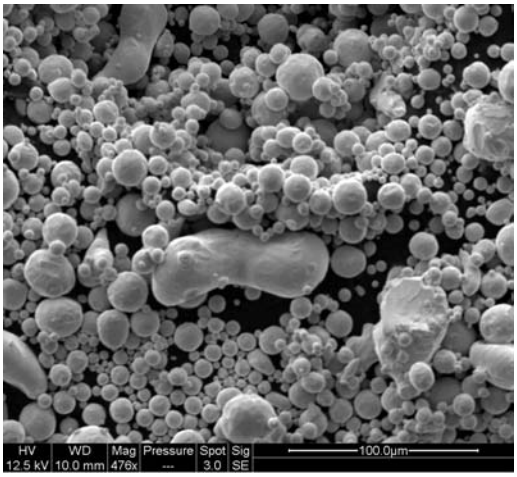

(a)

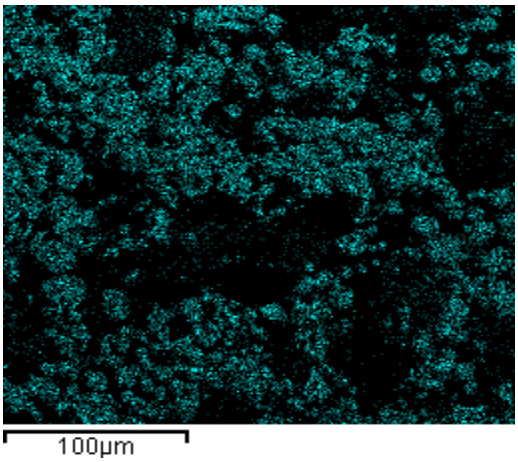

(b)

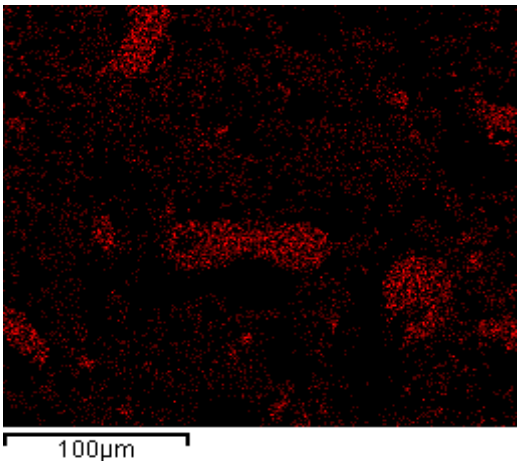

(c)

Figure 32. Micrographs for Paste I analysis, (a) SEM image of powder mixture showing the ligamental shape of the indium particles and the spherical nature of silver (25 µm). (b) EDS dot map showing the dispersion of silver within the mixture (c) EDS dot map showing the presence of indium.

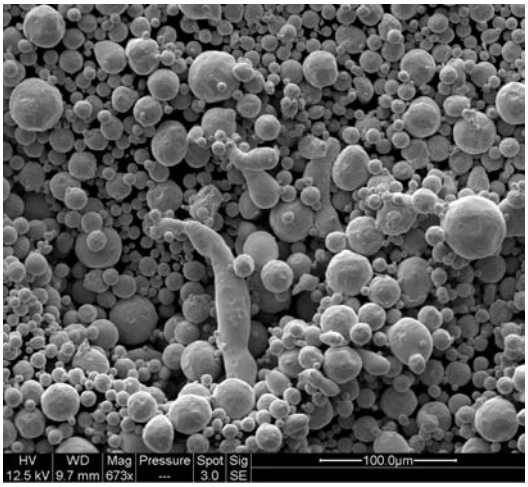

(a)

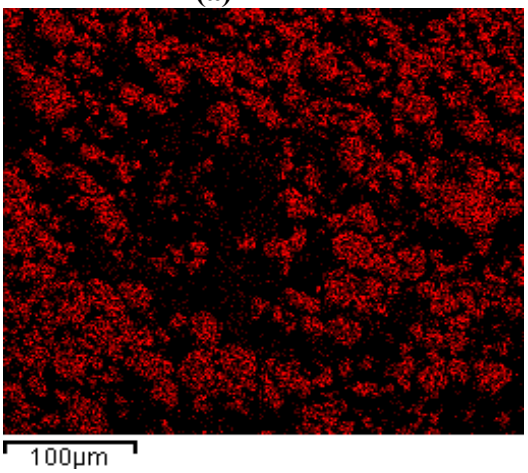

(b)

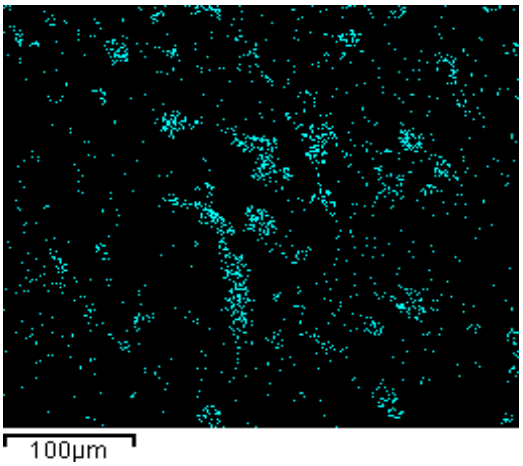

(c)

Figure 33. Micrographs for Paste II analysis, (a) SEM image of powder mixture showing the ligamental shape of the indium particles and the spherical nature of silver (50 µm). (b) EDS dot map showing the dispersion of silver within the mixture (c) EDS dot map showing the presence of indium.

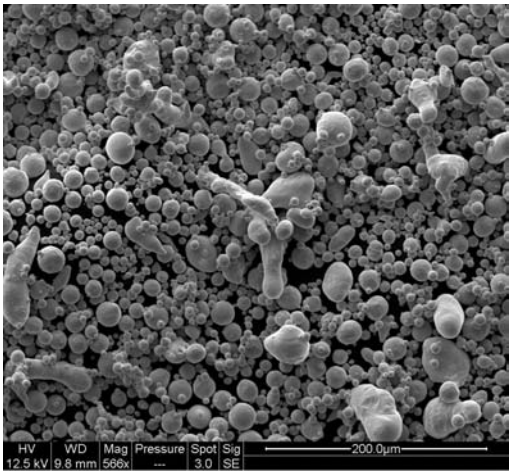

(a)

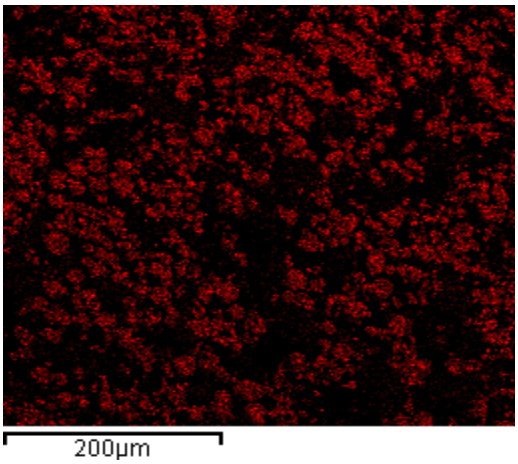

(b)

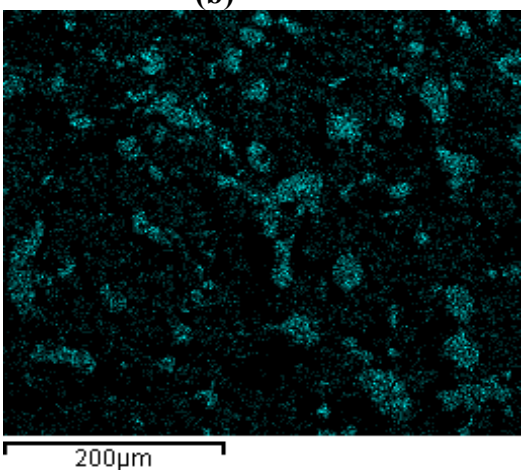

(c)

Figure 34. Micrographs for Paste III analysis, (a) SEM image of powder mixture showing the ligamental shape of the indium particles and the spherical nature of silver (25 µm). (b) EDS dot map showing the dispersion of silver within the mixture (c) EDS dot map showing the presence of indium.

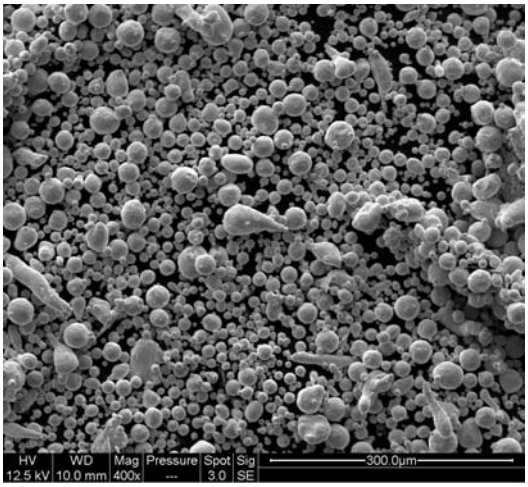

(a)

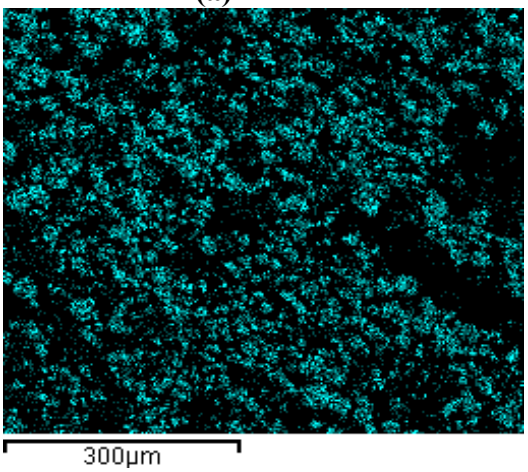

(b)

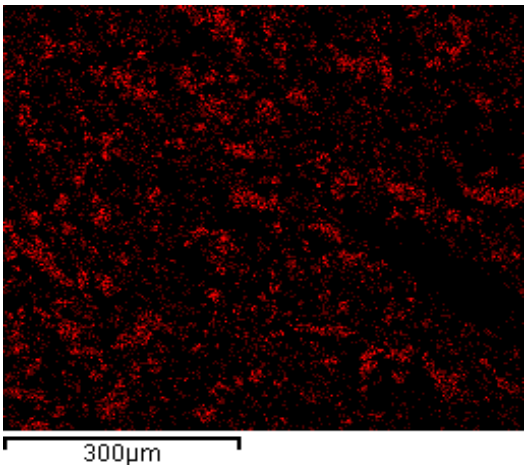

(c)

Figure 35. Micrographs for Paste IV analysis, (a) SEM image of powder mixture showing the ligamental shape of the indium particles and the spherical nature of silver (50 µm). (b) EDS dot map showing the dispersion of silver within the mixture (70% by Wt.) (c) EDS dot map showing the presence of indium (30% by Wt.)

6.3 Results:

6.3.1. Empirical kinetics model for the TLPS process of an Ag-In paste mixture:

A full factorial, randomized experiment, with five independent variables and one replicate was defined in section 6.2.2. The levels of all variables were pre-defined based on previous knowledge of the system and specific processing requirements and/or limitations. The development of an empirical model consisted of fitting the experimental observations [Appendix 4] from the DOE into a multiple linear regression function of the form given by Equation 36. The estimation of the regression coefficients (β's) was obtained by the least squares method as defined previously. A response model for this experiment could have up to 31 possible effects, so the estimation of the parameters becomes a mathematically intensive operation. A commercially available software (Minitab) was used for all of the analysis. Model simplification was accomplished through hypothesis testing using ANOVA (p-value approach), by which statistically significant effects were identified and a new reduced model was obtained. The goodness of fit of the proposed model was assessed by maximizing the predictive R^2_{pred} value and by residual analysis [62].

The first fit attempted to obtain a global model for the Ag – In TLPS process for the entire time regime. From this initial exercise it was obtained that the best fitted model resulted in an R^2_{pred} of 70.07%. This result suggested that a global model is not appropriate because it may be trying to accommodate distinct mechanisms driven by different parameters. During this first assessment, a main effects model was also

tried with a resulting R^2_{pred} of 51.43%. This result confirmed the fact that TLPS is a complex process which is controlled by interactions of its independent variables, therefore a main effect approximation yields a poor prediction of the response. A new approach was designed using the rationale from the phenomenological description of the TLPS process [30] in which its progression is explained as a series of steps along the time regime. With this knowledge about the expected response of the system with time, the time scale of the model needed to be divided into a series of steps as well. Defining the number of time divisions and their boundaries is a critical task that was performed by statistical analysis of the possible combinations. This exercise was performed with the assistance of the software, in which the success indicator was based on statistics from the model fitting. In this instance, the maximization of the R^2_{pred} statistic along with the residual analysis was used to define the best fit. After performing this analysis, it was obtained that the best strategy was to use a piecewise empirical model in which the time domain was divided into three regimes. For each time step, a model was obtained, each dominated by distinct effects as given by the ANOVA analysis [Appendix 5]. The results with the regression coefficients reported to one decimal place (for coded variables) are summarized in Table 8 below:

Table 8. Estimated regression coefficients for the empirical piecewise model for the Ag-In TLPS

Term	$0 \leq t < 1$ (minutes)	$1 \leq t < 10$ (minutes)	$10 \leq t \leq 60$ (minutes)
Constant	11.9	4.5	1.0
Wt. % In	8.6	3.8	1.0
Ag PS	3.3	1.6	0.4
T_p	-2.4	-1.4	-1.0
HR	2.1	0.5	-------
t (holding time)	-3.0	-3.7	-0.5
Wt. % In· Ag PS	2.3	1.2	0.3
Wt. % In· HR	1.7	-------	-------
Wt. % In· t	-1.4	-3.0	-0.4
Wt. % In· T_p	-------	-0.7	-1.0
Ag PS· T_p	-2.0	-0.7	-0.4
Ag PS· HR	0.8	-------	-------
Ag PS· t	-------	-1.5	-------
t· T_p	1.7	-------	0.5
HR·t	-1.0	-------	-------
Wt. % In· Ag PS· t	-------	-1.1	-------
Wt. % In· Ag PS· T_p	-1.6	-------	-0.3
Wt. % In· Ag PS· HR	0.6	-------	-------
Wt. % In· T_p· t	0.8	-0.9	0.4
Wt. % In· HR· t	-0.7	-------	-------
Wt. % In· AgPS· T_p · t	0.6	-------	-------
Wt. % In· AgPS· HR · t	-0.8	-------	-------
AgPS·T_p·t	-------	0.7	-------
R^2	**96.04%**	**91.40%**	**93.47%**
R^2_{pred}	**93.54%**	**88.40%**	**91.92%**

Key: ***Wt.% In*** = mass fraction of indium in the mixture, ***Ag PS*** = silver particle size, ***t*** = isothermal holding time, ***HR*** = heating rate, $\boldsymbol{T_p}$ = processing temperature

From the tabulated results, it can be seen that for all three models, a significant reduction in the number of regression coefficients was achieved when compared to the possible 31 effects. For the first regime of times, two four-way interactions are necessary for the model; whereas for the remaining two regimes of time none of these higher order interactions were significant. This information is encouraging from a practical perspective because control of the system is a more feasible when higher order interactions are not dominant effects. From these results it is clear that heating rate is a significant parameter during the initial dissolution stage, as suggested by the theoretical work. It is during later stages that its effect begins to be less definitive, as

given by its decrease in regression coefficient from 2.1 to 0.5. During the last stage of the process, the heating rate becomes a negligible parameter altogether. This information demonstrated that the suggested empirical approach is capable of describing the true physical response of the system in a quantitative fashion.

The definition of the three time regimes, along with their boundaries, was based purely on statistical analysis from the experimental observations. The response as a function of holding time, averaged over all other parameters, is depicted in Figure 36. This main effect plot of holding time on remaining In-rich phase shows a "knee" at approximately 10 minutes, which suggests a possible shift in the dominant mechanism after this point. This observation was successfully captured by the statistical analysis used for the selection of the models, as evidenced by the information in Table 8.

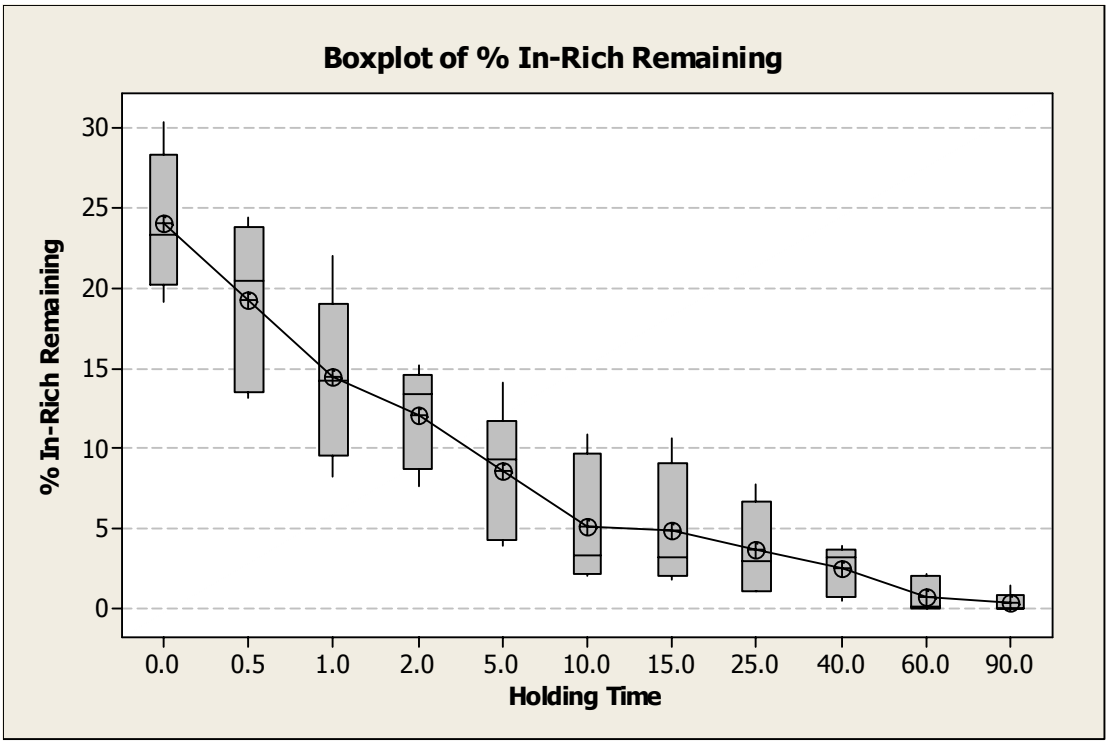

Figure 36. Boxplot showing the main effect of Holding Time on the Remaining In-Rich Phase (%).

The piecewise model provided a better description of the kinetics of transformation for the Ag – In system as function of practical controllable variables across the entire time range. The complexity of this model is evidenced by the data in Table 8, in which the response is given by a function of multiple effects including up to four-way interactions. To visualize the usefulness of this type of model, a graphical representation can be used. For instance may one take the case where the solute composition was set to 15 Wt.% In, the heating rate to 30 °C/min, and the silver particle size to 25 μm (-500 Mesh or Type V ASTM-B214). These parameters were fixed to the above values based on the fact that they will likely be chosen prior to the processing and thus, be constant during TLPS. Then, processing temperature and holding time, which compose the thermal profile, are what the practitioner will be

able to change during the actual process. Because these parameters can be changed, they will be treated as variable vectors for the graphical solution. Values for these two parameters are typically defined by the materials to be joined, the available time, and the equipment limitations. A response of the system in terms of these two variables yield prediction graphs than can be used to define the process. Solutions from the prediction piecewise model, for the above conditions, are given as 3-D surfaces and contour plots in Figure 37, Figure 38, Figure 40, Figure 41, Figure 42, and Figure 43.

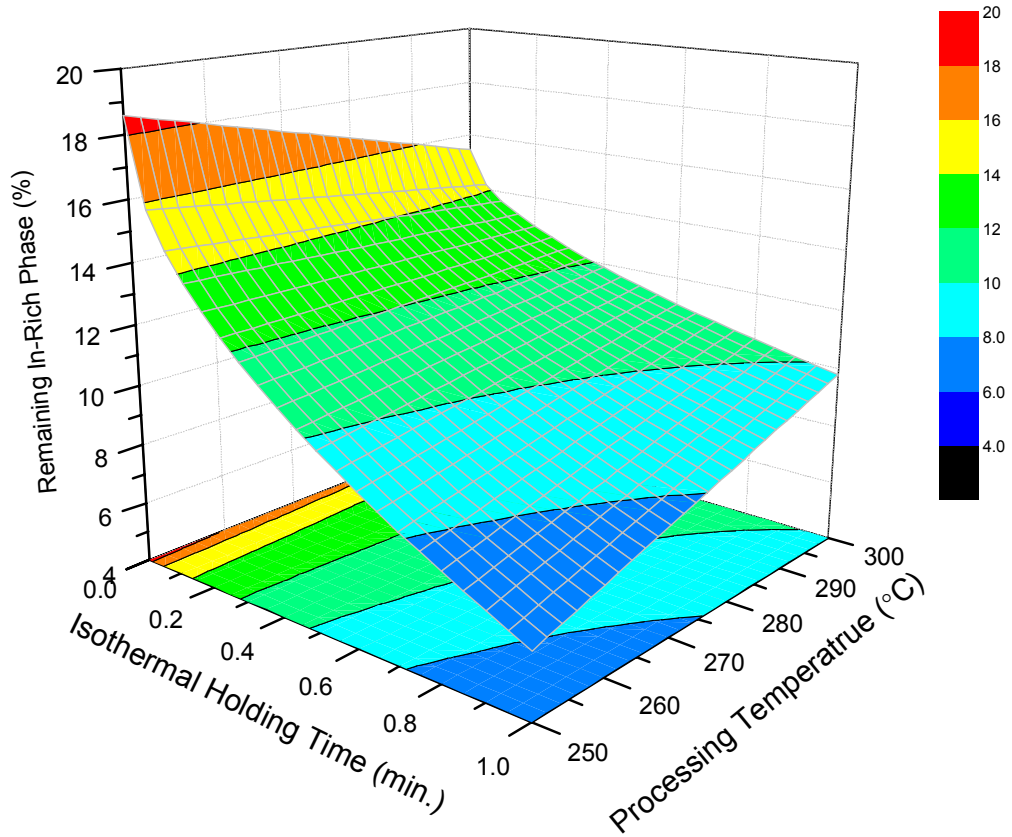

Figure 37. Response surface of the predicted Remaining In-rich Phase Remaining as function of Isothermal Holding Time and Processing Temperature for the first time step (0 ≤t <1).

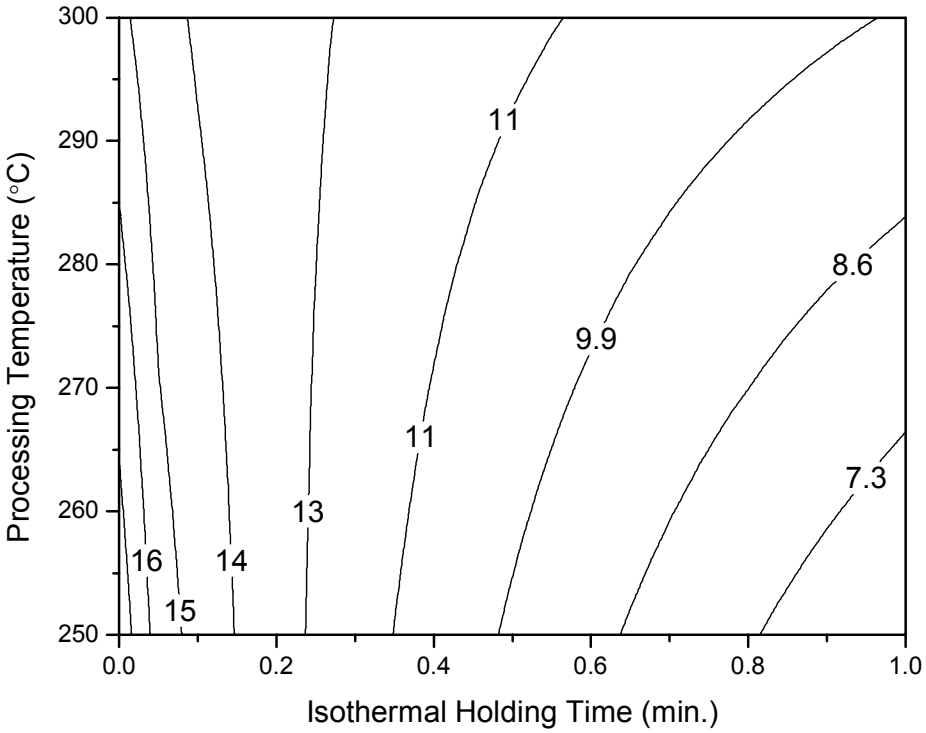

Figure 38. Contour plot for the predicted response ($0 \leq t < 1$) as function of Processing Temperature and Isothermal Holding Time. The plot shows line of constant Remaining In-rich Phase (%).

During the first time step ($0 \leq t < 1$ min.), which corresponds to the dissolution stage of the TLPS process, it was observed that at very short holding times (less than 0.3 min.), the amount of Remaining In-rich Phase decreased with increasing processing temperature. This behavior was expected based on the fact that it takes longer to achieve a higher processing temperature at a constant heating rate, thus providing more time for interdiffusion to occur; resulting in a lost of solute (In) into the silver base metal. An interesting reversal was observed in Figure 38 as the isothermal holding time approached 1 minute. In this case, the Remaining In-rich Phase was

larger at higher processing temperatures. This behavior can be explained by inspection of the Ag – In equilibrium phase diagram given in Figure 39.

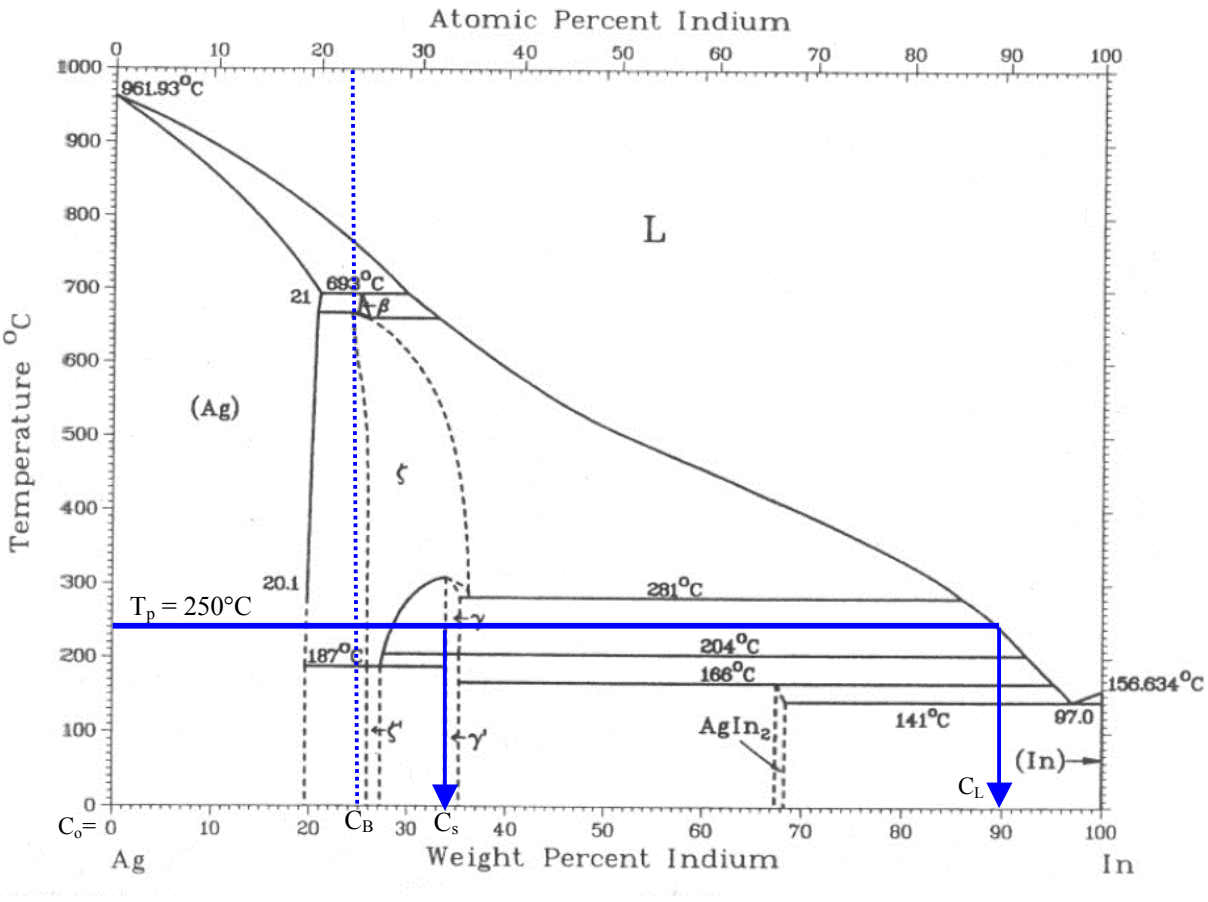

Figure 39. Equilibrium phase diagram for the Ag-In binary system. The horizontal line shows a particular condition of a processing temperature of 250°C, the equilibrium composition of both the solid (Cs) and the liquid (CL) for that Tp are given by the vertical downward arrows. The bulk composition of the mixture is given by CB, which is set constant by design. Initially, at t = 0, the solute composition of the solid is given by Co which is zero, i.e. pure base metal.

At a lower processing temperature (250°C) the equilibrium composition of the liquid is ~90 Wt. % In, which means that 10 Wt.% Ag needs to be dissolved by the In-rich liquid before the isothermal solidification (stage 2) can begin. A similar analysis at a processing temperature of 300°C will yield a liquid equilibrium composition of ~82 Wt. % In, which is equivalent to a dissolution of 18 Wt.% Ag into the In-rich liquid to

reach equilibrium. Based on the fact that the isothermal solidification process starts after equilibrium had been reached, the extra 8 Wt.% Ag at 300°C imposed a delaying effect for the initiation of this second stage. The consumption of the In-rich liquid happens by an isothermal solidification mechanism driven by the atomic flux from the liquid to the solid phase. Therefore, it is not until this stage is underway that a reduction in the response can be observed. Based on this analysis, at a processing temperature of 250°C, a one minute hold seemed to be enough for achieving the equilibrium composition and the start of the In-rich phase consumption, thus resulting in a reduction of the response variable. For a processing temperature of 300°C, a one minute hold may not have provided sufficient time to get to the equilibrium composition, and initiate isothermal solidification. The delay of the initiation of the isothermal solidification resulted in no consumption of the In-rich phase, thus explaining the observation that for short holding times a higher processing temperature may result in a larger fraction of the In-rich phase. The achievement of the equilibrium condition for any particular processing temperature has been suggested to be instantaneous for modeling purposes [25] [27] [30], so the aforementioned phenomenon has not been considered in earlier investigations. When higher heating rates were used, such as 60°C/min., the loss of solute before melting was not observed; suggesting that the assumption of minimal solute lost during the initial stages of the process may be valid. A similar conclusion about the sensitivity of the response to heating rate was reported by Turriff [28] for a Ni – Cu binary system. Based on these results from the empirical model, it has been shown that the analytical approaches may be accurate only for fast heating rates, whereas the

consumption of MPD during the dissolution stage at low heating rates may be critical for the TLPS kinetics. Simulation results with a 60 °C/min. heating rate showed negligible consumption of MPD, further discussion about this simulation will be presented later.

For the second time step ($1 \leq t < 10$ min.), the prediction model showed that the equilibrium condition was reached for all the processing temperature range studied (250°C - 300°C), at ~2 minutes or less. This can be observed in Figure 40 in which the response was predicted to be approximately constant over the entire temperature range during the initial holding times of 1 – 2 minutes.

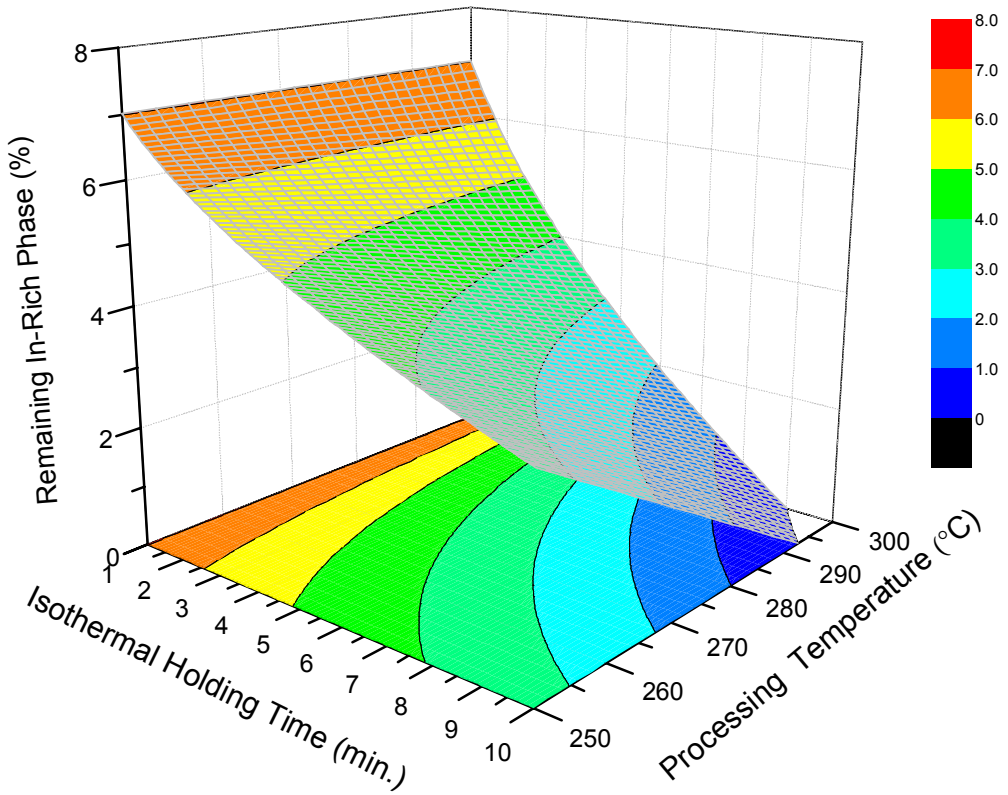

Figure 40. Response surface of the predicted Remaining In-rich Phase Remaining as function of Isothermal Holding Time and Processing Temperature for the second time step ($1 \leq t < 10$).

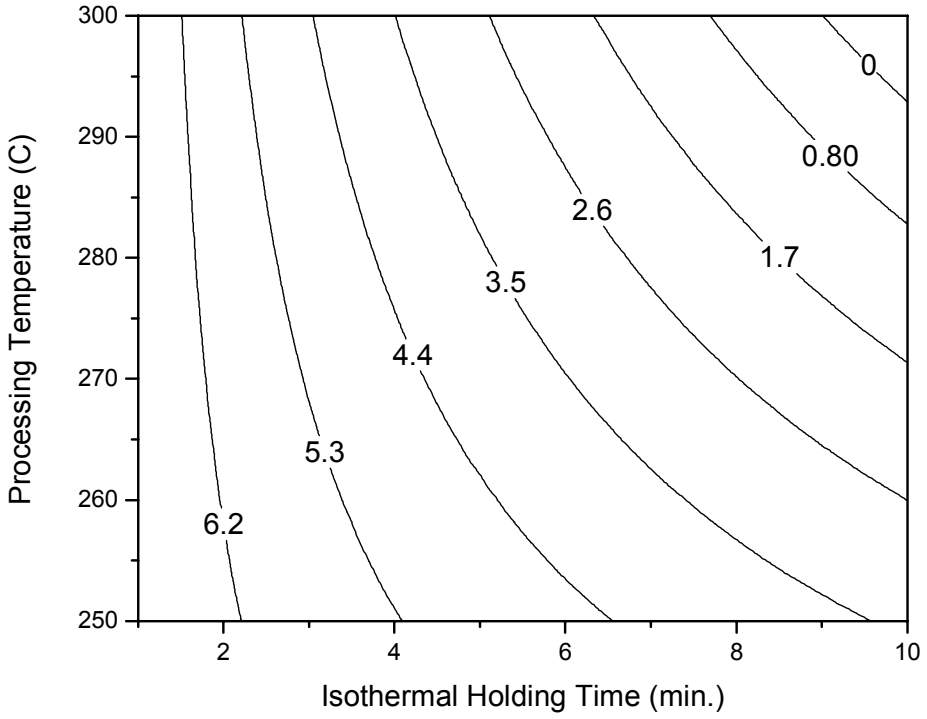

Figure 41. Contour plot for the predicted response (1 ≤t <10) as function of Processing Temperature and Isothermal Holding Time. The plot shows line of constant Remaining In-rich Phase (%).

After no more than two minutes, the TLPS process is governed by the isothermal solidification stage in which both temperature and time become critical parameters. This effect is shown graphically in Figure 40 and Figure 41. The contour plot in Figure 41 can be used as a prediction map to define a custom process for any particular desired response. From this chart it is shown that the solution can be tailored depending on specific limitations, i.e. when the temperature stability of a material is a critical factor, the isothermal holding time becomes the variable to control. The opposite is true for a process that is limited by throughput or cycle time, in which minimizing the time requires an increase in processing temperature. In fact,

the formation of these maps becomes a key contribution from this study. Through which the transformation kinetics of the Ag-In TLPS process is given as a function of controllable parameters.

The third time step ($10 \leq t \leq 60$ min.), is illustrated in Figure 42 and Figure 43.

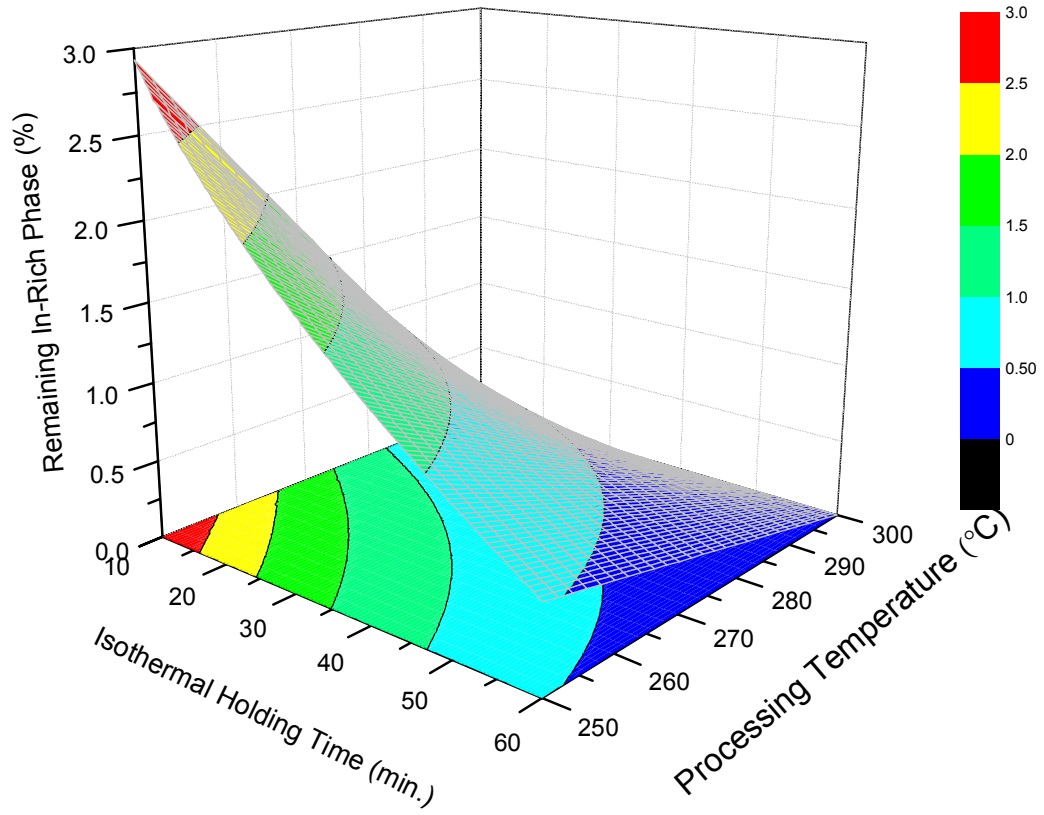

Figure 42. Response surface of the predicted Remaining In-rich Phase Remaining as function of Isothermal Holding Time and Processing Temperature for the third time step ($10 \leq t \leq 60$).

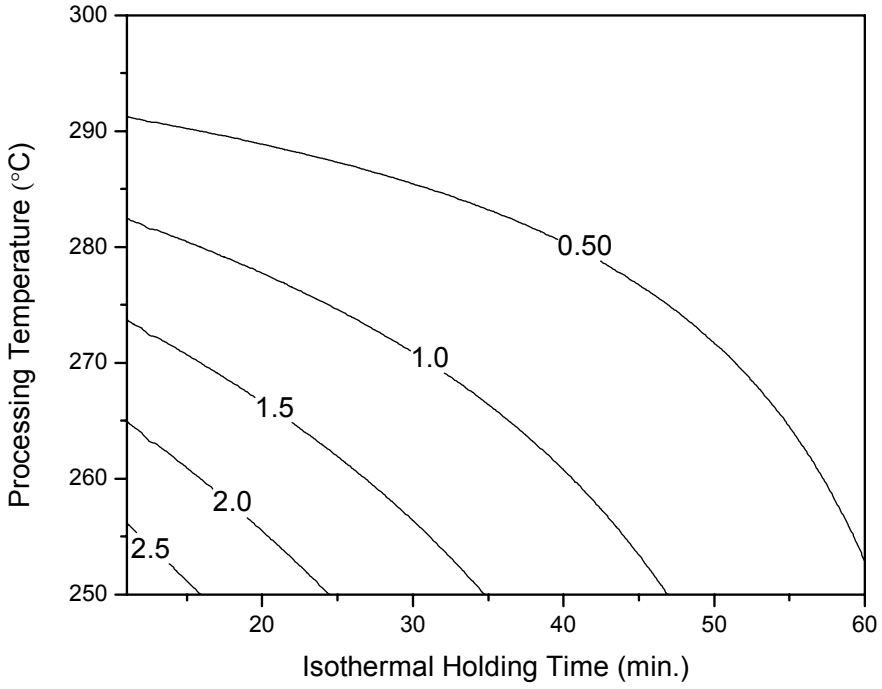

Figure 43. Contour plot for the predicted response ($10 \leq t \leq 60$) as function of Processing Temperature and Isothermal Holding Time. The plot shows line of constant Remaining In-rich Phase (%).

From these maps, it is evident that the response is sensitive to both processing temperature and holding time, with the temperature effect being dominant during this stage as suggested from the steep descent of the response at temperatures close to 300°C. In fact, from this prediction, it is possible to obtain zero Remaining In-rich material in 10 minutes when a 300°C processing temperature is employed, whereas at 250°C a minimal fraction In-rich phase was still present after 60 minutes.

6.4 Mechanistic diffusion based model for the Ag-In paste mixture:

Up to this point the model adequacy analysis had been based completely on statistical techniques of model fitting. Based on that statistical information it was demonstrated that the piecewise model effectively predicts the response of the system, as given by

the R^2_{pred} index. To validate the adequacy of this proposed model in predicting the true response in terms of transformation kinetics, some information on the underlying physical mechanisms is needed. It is known that the TLPS reaction is driven by a diffusion mechanism, so an analytical approach may be derived. What follows is the development of a mechanistic diffusion based kinetics model for a powder mixture. This model provides an analytical tool for describing the solidification kinetics of the In-rich liquid towards its transformation to a final Ag-rich solid solution. The progression of this transformation with time will be compared to the predicted response from the piecewise empirical model as well as to the direct measurements from the DSC. Metallographic information will assist in the physical description of the governing mechanism. This exercise will serve as a model adequacy check in terms of RSM model ability to predict a true response of this system, and depending upon the results, it may provide some insights into the caveats of the analytical approach.

The proposed model has been restricted to a TLPS mixture consisting of an array of powders from an Ag – In binary system with a phase diagram depicted in Figure 39. The TLPS system has been defined as a mixture of silver powder and indium powder, such that a particular bulk composition (C_B) is achieved by design (C refers to the compositional weight fraction of solute, indium, for the current case, in a phase). The processing temperature (T_p) has been defined as $T_p > T_m$, such that all low melting In-rich phases are melted during the process. This model assumes [11][28][63] that solid-state interdiffusion prior to melting is negligible, and that the melting, particle

rearrangement, and capillary flow instantaneously produces the structure depicted in Figure 44, in which an array of solid silver particles are covered by a layer of In-rich liquid of constant thickness (dr).

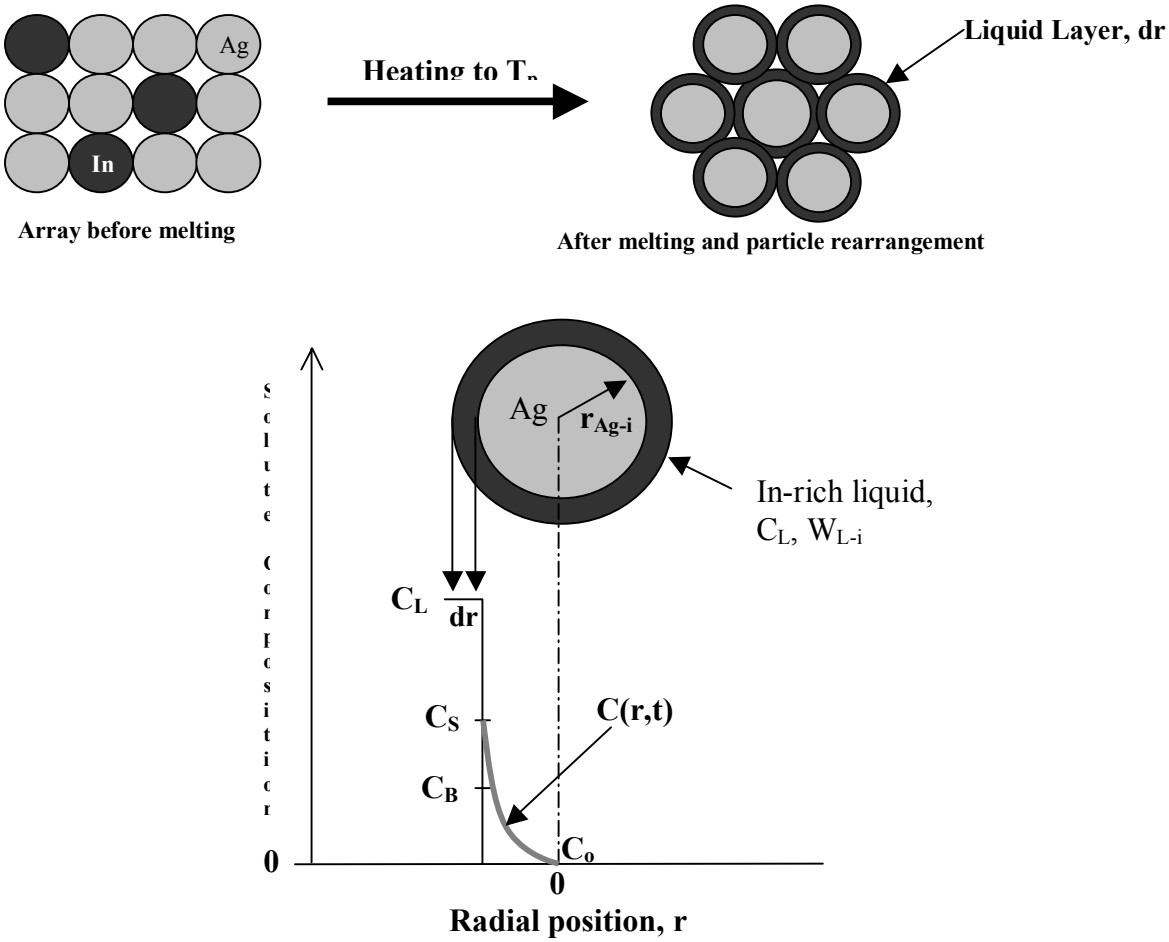

Figure 44. Schematic representation of the system showing the conditions considered for the model. Lower image represents the unit cell for the isothermal solidification model, in which the initial particle size is given along with the solute compositions of each phase.

The effect of the dissolution stage, in which the liquid dissolves some amount of base metal, will be indirectly considered in this model. Assuming that the re-arranged structure in Figure 44 repeats throughout the volume of the mixture, a representative

unit cell for the model is given in the lower schematic in Figure 44. A set of parameters together with initial and boundary conditions were defined for the development of the model. It is worthwhile noting that the initial conditions, i.e. t =0, refers to the start of the isothermal solidification process, thus base metal uptake by the liquid during the dissolution stage was considered within the initial conditions. Isothermal solidification starts once the equilibrium composition of the liquid reaches C_L, a composition that will reflect the absorption of some base metal, in other words at t = 0 the composition of the liquid will be less than one. At t =0 it was assumed that the silver particles were pure, i.e. $C_o = C_{Ag\text{-}i} = 0$ %In ("i" denotes initial conditions at t = 0); and an initial particle size (radius) given by $r_{Ag\text{-}i}$, which is specified as a distribution for the mesh size or powder type according to the standard ASTM-B214. Assuming that the distribution is represented by the maximum diameter may result in an overestimation of the time to solidification, which will lead to a conservative prediction, whereas a more realistic representation of the system can be obtained using the lower bound of the 80% confidence interval as given by the specification. Particle distributions are not normally distributed; therefore the standard specifies a maximum size and a lower bound, which groups 80% of the population with the remaining 20% being smaller than the lower bound. This information was confirmed by stereological techniques in which a sample of the powder was measured. The distribution was affected by the effect of small particles that tend to agglomerate with larger particles, a phenomenon known as satellite effect [60]. The diffusivity within the liquid was assumed to be fast enough so that no concentration gradient exists in this phase [34][63], thus its composition remains

constant at C_L (Figure 39) provided the process temperature is held constant. A set of boundary conditions were required for the complete description of the system. Assuming local equilibrium at the solid/liquid interface during the isothermal hold, the solute composition at the solid surface, i.e. $r = r_{Ag(t)}$ for $t > 0$, is given by C_s at T_p (Figure 39). Analytical solutions to diffusion problems are only valid for semi-infinite media, which requires a boundary condition at the center of the silver particle given by $\partial C/\partial r = 0$ or that C_{Ag} at $r = 0$ is zero. This boundary condition implies that the silver particle is large enough that at a distance far from the interface the diffusing solute has no effect on the composition of the base metal. This assumption is acceptable for processes used in forming large scale bulk materials, but it may induce considerable errors when dealing with a smaller scale, as in the case of the proposed paste for microelectronic attachment in which the formation of μ-joints is desired.

With the unit cell from Figure 44 and initial and boundary conditions defined, a model has been defined [28][63] based on mass balance arguments and Crank's [29] solutions to Fick's second law of diffusion. The process starts ($t = 0$) once the equilibrium conditions are reached, i.e. formation of a liquid layer with constant composition C_L at T_p. Under this condition, diffusion of indium into the silver particles causes a reduction in the amount of In-rich liquid remaining (isothermal solidification), and due to mass conservation, a concomitant growth of the silver alloy particles must occur.

6.4.1. Derivation of the mechanistic model:

The derivation of this model was based on a mass balance of solute (In) between the amount in the mixture as a whole, and its sum in the two separate phases (liquid and solid) [42][63]. By definition [42] the solute content or mass of indium (M_{In}) present in any phase (x) is given by:

Equation 44

$$M_{In(x)} = C_x \cdot W_x$$

where "x" can be the liquid (L) phase, the solid (s), or the mixture as a unit. In Equation 44, "C" is the composition of the phase in terms of solute content, i.e. Wt. % In from the phase diagram, whereas "W" is the weight or mass fraction of the particular phase in the mixture. The amount of indium in the mixture is selected by design, so that the bulk or average indium composition in the paste mixture (C_B) is fixed. This known composition (C_B) is equivalent to the total mass of indium added to the mix, which means that $M_{In(mix)} = C_B$ since the mixture represents the whole ($W_{mix} = 1$). From a mass balance perspective, at any time during the process:

Equation 45

$$M_{In(mix)} = M_{In(S)} + M_{In(L)}$$

or, from Equation 44:

Equation 46

$$C_B = W_S \cdot C_S + W_L \cdot C_L$$

Rearranging Equation 46, the mass fraction of liquid in the system at any time (t) is given by:

Equation 47

$$W_{L(t)} = \frac{[C_B - (W_{S(t)} \cdot C_{S(t)})]}{C_L}$$

The expression in Equation 47 provides an equation to calculate the remaining fraction of In-rich material present in the mixture at any time, which in fact is the response variable measured by the DSC experimental technique. Therefore, a solution to the above expression will allow a comparison between the RSM and the analytical model. Inspection of Equation 47 suggests that a solution to ($W_{S(t)} \cdot C_{S(t)}$) is needed as this term represents the indium content in the solid at any time. It is known that the solidification of the liquid takes place isothermally due to a diffusion controlled mechanism of indium atoms going into the silver solid. By definition the indium content in the solid is $M_{In(s),t} = W_{S(t)} \cdot C_{S(t)}$. For the kinetics model it is necessary to calculate the fractional uptake of solute (In) into the solid (Ag) which is given by:

Equation 48

$$\frac{M_{In(S),t}}{M_{In(S),f}} = \frac{(W_{S(t)} \cdot C_{S(t)})}{(W_{S(f)} \cdot C_{S(f)})}$$

where $M_{In(s),f}$ is the final solute content in the solid phase at the end of the isothermal solidification stage. At the end of the solidification process and in-situ alloying, the mixture should be completely solid, thus $W_{s(f)} = 1$ and $C_{s(f)}$ should correspond to the final equilibrium composition (C_s) at T_p. Making these substitutions into Equation 48, an expression for the indium fractional uptake into silver was obtained:

Equation 49

$$\frac{M_{In(S),t}}{M_{In(S),f}} = \frac{(W_{S(t)} \cdot C_{S(t)})}{C_S}$$

Rearrangement of Equation 49 yields a formula for obtaining the desired $W_{S(t)} \cdot C_{S(t)}$, so that $W_{L(t)}$ can be calculated:

Equation 50

$$W_{S(t)} \cdot C_{S(t)} = \left[\frac{M_{In(S),t}}{M_{In(S),f}} \right] \cdot C_S$$

In his work on the mathematics of diffusion, Crank [29] developed a solution for the fractional solute uptake [M_t/M_f] entering a spherical particle. His solution is valid for semi-infinite large particles and constant diffusivity. In this analytical solution, $t = \infty$ corresponds to the time when the spherical particle is completely saturated with solute so that the composition of the solid is given by the maximum solid solubility at T_p, i.e. $C_{s(f)} = C_s$. This condition is a result of the mathematical formulation of the problem, which is known to be an approximation since it does not consider the impact of later stages. The homogenization stage, not considered by the analytical model, is responsible for the final equilibrium transformation from C_s to C_B; these discrepancies will be discussed in a later section. The solution provided by Crank is given by:

Equation 51

$$\frac{M_t}{M_f} = 1 - \frac{6}{\pi^2} \sum_{n=1}^{\infty} \left(\frac{1}{n^2} \right) \exp(-Dn^2 \pi^2 t / r_t^{\,2})$$

Where t is the isothermal holding time, D is the diffusivity of indium into silver which is given by $D=D_o\exp(-Q/RT)$, and r_t is the silver particle radius at any particular time. Diffusivity calculation requires knowledge of the D_o and the activation energy (Q) for the diffusion of indium atoms into silver. These values are available in literature from diffusion couple experiments [48]. Substitution of

Equation 51 into Equation 50 and then into Equation 47 resulted in the final expression for $W_{L(t)}$:

Equation 52

$$W_{L(t)} = \frac{\left[C_B - \left(\left[\frac{M_t}{M_f} \right] \cdot C_S \right) \right]}{C_L}$$

For a selected constant processing temperature, and known values for D_o and Q; parameters D, C_B, C_s and C_L can be obtained. An expression for the incremental growth of the silver particle with time (r_t) is still needed before a final stepwise solution algorithm can be employed. One of the critical consequences of TLPS is that the solid/liquid boundary moves into the liquid (solidification) over time, decreasing the liquid layer and increasing the size of the alloyed particle. At a particular point in time (t), the ratio between the current volume and initial (i) volume of the sphere is given by [63]:

Equation 53

$$\frac{V_{S(t)}}{V_{S(i)}} = \frac{\left(W_{S(t)} \middle/ \rho_{S(t)} \right)}{\left(W_{S(i)} \middle/ \rho_{S(i)} \right)}$$

where W refers to the mass fraction and ρ to the density of the solid. If the density is assumed constant [63] during the process, using the volume of a sphere, it can be stated that:

Equation 54

$$r_{S(t)} = r_{S(i)} \cdot \left(W_{S(t)} \middle/ W_{S(i)} \right)^{1/3} = r_{S(i)} \cdot \left[(1 - W_{L(t)}) \middle/ (1 - W_{L(i)}) \right]^{1/3}$$

$W_{L(i)}$ is the initial mass fraction of In-rich liquid at the beginning of the isothermal solidification stage. This value was obtained from Equation 47 after consideration of the initial conditions. $W_{L(t)}$ is the fraction of In-rich liquid present at the previous time step, a value that is given by the solution of Equation 52. From this analytical formulation of the TLPS process during the isothermal solidification stage, a stepwise algorithm was programmed and the results from a particular example will be presented. The algorithm works as follows: {1} At t = 0, $r_{s(t)}$ = initial particle size from mesh designation , {2}Obtain (M_t / M_f) from Equation 51 with the initial conditions from step {1}, {3} Calculate $W_{L(t)}$ from Equation 52 using the result from step {2}, {4} Obtain the new value of the solid particle from Equation 54 by substituting the $W_{L(t)}$ from step {3} and the corresponding initial conditions, {5} Get back to step {1} and increment the time by one step and use the new particle size from step {4}. This solution is repeated for the entire time range up until complete solidification is achieved, i.e. $W_{L(t)}$ reaches zero.

6.4.2. Simulation results:

The derivation of the mechanistic kinetics model for the isothermal solidification stage of the TLPS process was introduced as a tool for evaluating RSM model adequacy. The physical meaning of the experimental data is to be assessed by comparing simulation results from both models and analyzing their predictions based on the expected phenomenological response. In order to obtain the desired predictions from both the empirical (RSM) and the mechanistic models, a set of conditions were defined as follows:

Mechanistic model parameters:

T_p = 250°C = 524.15 K, D_o = 2.79 X 10^{-14} m^2/s [48], Q = 41, 489 J/mol [48], R = 8.314 J/mol·K, C_S @ 250°C = 33 Wt.% In [46] (Figure 39), C_L @ 250°C = 90 Wt.% In [46] (Figure 39), C_B = 25 Wt.% In, silver particle size for -500 Mesh = 25 μm (maximum) and 15μm, $D=D_o\exp(-Q/RT)$ = 2.05 X 10^{-18} m^2/s.

Response surface model input variables:

Bulk composition of the paste (C_B) = 25 Wt.% In, silver particle size for -500 Mesh (Type V), Heating rate = 60°C/min., T_p = 250°C

The RSM considers the effect of the heating rate, which has been demonstrated to be critical in defining the initial consumption of solute during the early stages of the process, as evidenced by the contour plot in Figure 41 and previous work by Turriff [28]. That is not the case for the mechanistic model, which is independent of heating rate and assumes no solute consumption prior to the isothermal solidification stage. In order to get a valid comparison of both models the heating rate for the empirical simulation was set to 60°C/min. This would result in an acceptable approximation of the assumption of no solute loss during the initial heating. After the necessary substitutions and solution of the stepwise algorithm, the results from the mechanistic model together with the empirical model (RSM) are given in Figure 45. Experimental observations from DSC at different holding times were plotted as well.

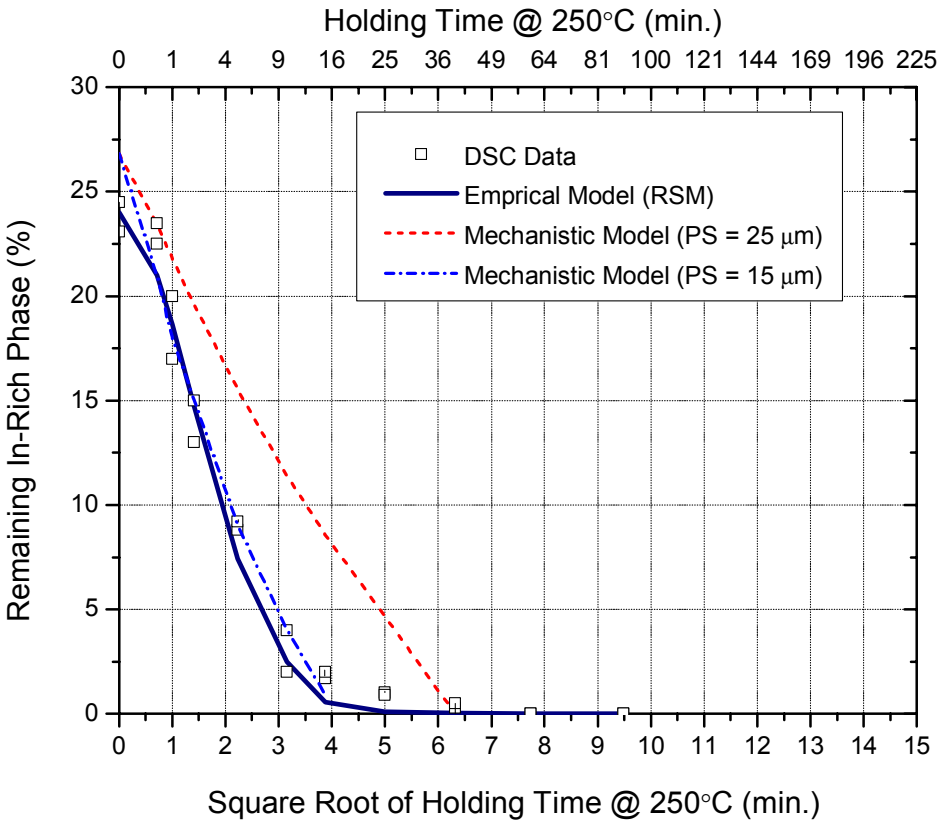

Figure 45. Simulation results from both the mechanistic and the RSM model, for a paste mixture containing 25 Wt. %In, -500 Mesh silver particle size, processed at 250°C with a heating rate of 60°C/min, and isothermally held for different times.

6.5 Discussion:

From Figure 45 it was observed that the solution from the mechanistic model exhibited a constant progression towards complete solidification. This behavior in which the consumption of the In-rich liquid phase follows a parabolic relation with time (linearly proportional to $\sqrt{t}$) is the result of the mathematical formulation given by the analytical solution by Crank. The model assumes that the entire initial mass fraction of indium is transformed into liquid, which means that no solute is lost prior to the start of the isothermal solidification stage. This assumption is valid for fast heating rates only [28]. Although the analytical formulation considers only the

isothermal solidification step, it indirectly treats the dissolution stage (Stage 1). Initial conditions for this model assumed that the system was instantaneously brought to the processing temperature, therefore no interdiffusion during heating was considered. However, the composition of the liquid at the processing temperature was taken at equilibrium (C_L), which is no longer pure indium but a value less than one (Figure 39). Calculation of the initial mass fraction of In-rich liquid ($W_{L(i)}$) was performed from the mass balance given by Equation 46. At t = 0, the amount of indium in the solid is zero (assumption of no prior interdiffusion) therefore the C_S term in Equation 46 has to be equal to zero. Solving this equation for the initial mass fraction of In-rich liquid, considering $C_S = 0$ and $C_L < 1$, resulted in a value slightly larger than 25% as seen in Figure 45. This is an artifact of the assumptions required for obtaining an analytical solution to the problem. During the time frame governed by the isothermal solidification mechanism, i.e. up to ~10 minutes, it was observed that both the RSM and the mechanistic model behaved similarly. In both models during this time period it is clear that the solidification kinetics follows a linear relationship with the $\sqrt{t}$. As Figure 45 shows, the analytical model provided an overestimation of the time to solidification when the maximum particle size of 25 μm was used, as demonstrated by the curve location to the right of the DSC data. Several factors will be discussed to explain this behavior. For this analytical solution, the silver particle shape and size were assumed to be perfectly spherical and monosized as given by the maximum diameter from the mesh designation. This resulted in a conservative estimation since these powders are far from being perfectly shaped and sized. In fact, the size randomness is evident in Figure 32 through Figure 35. A

better representation of the particle size should consider the distribution associated with the population, in this way the model will be able to predict a behavior that is in accordance with the real condition in the paste. From the specification (ASTM-B214), a Type V powder will have particles ranging from 5 μm to 25 μm, with 20% of the population below 15 μm. A mean particle size is not typically given due to agglomeration and "satellite" effects that result in a bi-modal distribution. For this simulation, a 15 μm particle size was used based on the standard as well as on stereological quantitative analysis of samples taken from the silver powder. Smaller particles, represented by the case in which the model was solved for 15 μm, have a larger surface area- to- volume ratio that increases the diffusion rate. This effect was observed by the predicted response given by the 15μm solution, in which a better agreement with the experimental data was obtained. Albeit the errors associated with representing the powder by monosized particles, the bounded solution considering the particle size distribution provided a good approximation of the response when compared to the experimental data. The critical outcome of this analysis was that both of the analytical and empirical models agreed on the behavior of the system during this stage, the analytical being a more conservative approach when larger particles were considered. Another factor affecting the difference between the models was the initial amount of In-rich liquid available. The mechanistic model assumed that all the In-rich phase was transformed into liquid, whereas the RSM accounted for some consumption during the heating stage. The larger the amount of In-rich material, the longer it takes for its complete solidification.

An interesting behavior was observed after the 10^{th} minute in that the RSM no longer exhibited a linear relation of the In-rich remaining with $\sqrt{t}$. This change in reaction rate is a critical factor in the kinetics of the TLPS process because it defines the true response of the system at longer holding times. The mechanistic model failed to predict this behavior due to the nature of its mathematical formulation. Crank solutions are only valid for semi-infinite media, which means that the solid is large enough so that its solute distribution in the bulk does not affect the diffusion reaction at the interface. Based on this fact, the diffusion of solute into the solid can continue to be linearly proportional to $\sqrt{t}$ until the completion of the solidification process. This can be observed by the mechanistic simulation in Figure 45. The solution provided by Crank also assumed that at the end of the process ($t\rightarrow\infty$) the solid would have absorbed all the solute until the maximum solid solubility at T_p is reached, i.e. at $t\rightarrow\infty$ $C_B = C_{max} = C_s$. All of these conditions are necessary for the derivation of the analytical solution, but they may not form an accurate representation of the real system because they do not account for the interdependency of later stages. Another factor affecting the mechanistic model at longer holding times is related to geometrical considerations. The cell given in Figure 44 depicts the fundamental unit for model development. This system assumed that with time the liquid ring (dr) shrinks as the silver particle grows, this being a perfect radial movement of the boundary. This assumption estimates that at any time, the surface area available for diffusion is given by that of the sphere at any instant. From the metallographic analysis it was observed that before 10 minutes the silver particles were surrounded by the In-rich matrix (Figure 46) validating the assumption from Figure 44. This

explains the similarity in the kinetics of transformation from both models during this initial time frame.

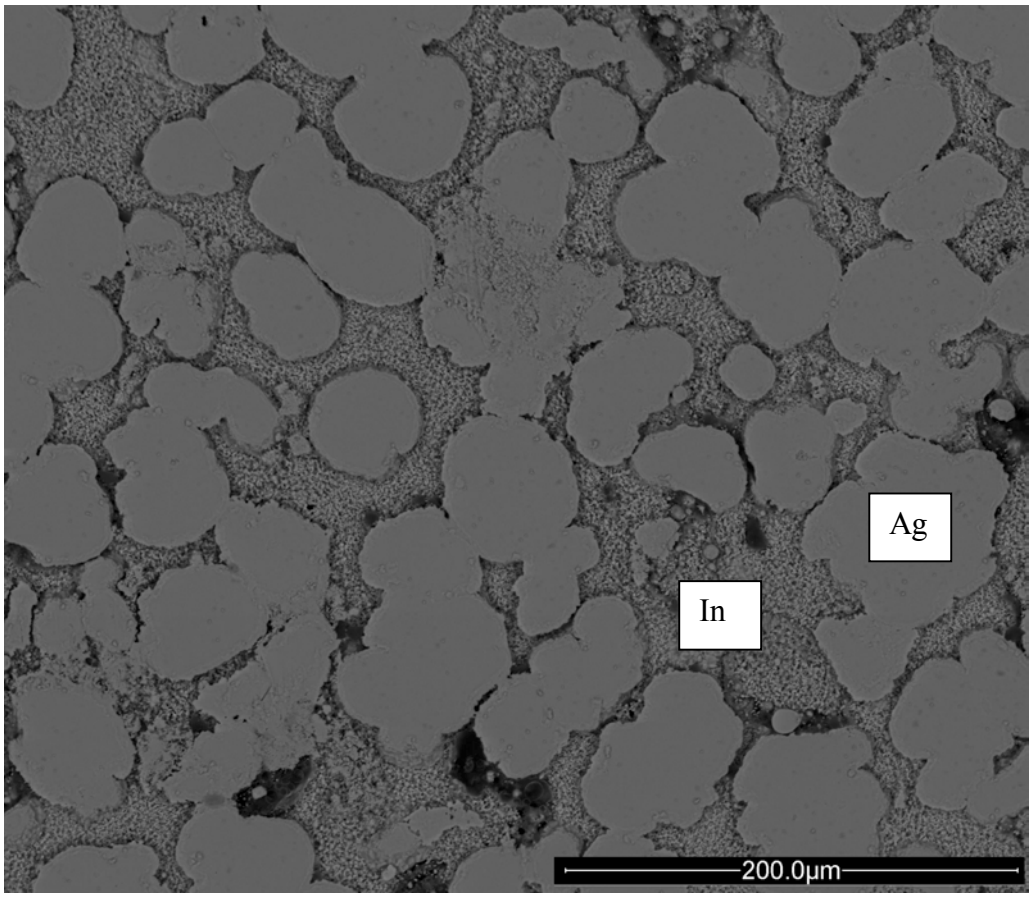

Figure 46. SEM micrograph (BSE) of a 30 Wt.% In sample heated to 250°C and cooled down after an isothermal hold of 1 minute. Silver particles are embedded into the In-rich matrix.

At longer holding times, (Figure 47 depicts the case of 10 minutes) it was observed from the micrographs that the coagulation and growth of the silver rich particles had started to result in a structure that was no longer characterized by a continuous In-rich matrix. The condition of an In-rich matrix is not longer valid for the entire area, save for a few specific sites. In general, the system is starting to show a shift to a more Ag-rich dominated microstructure.

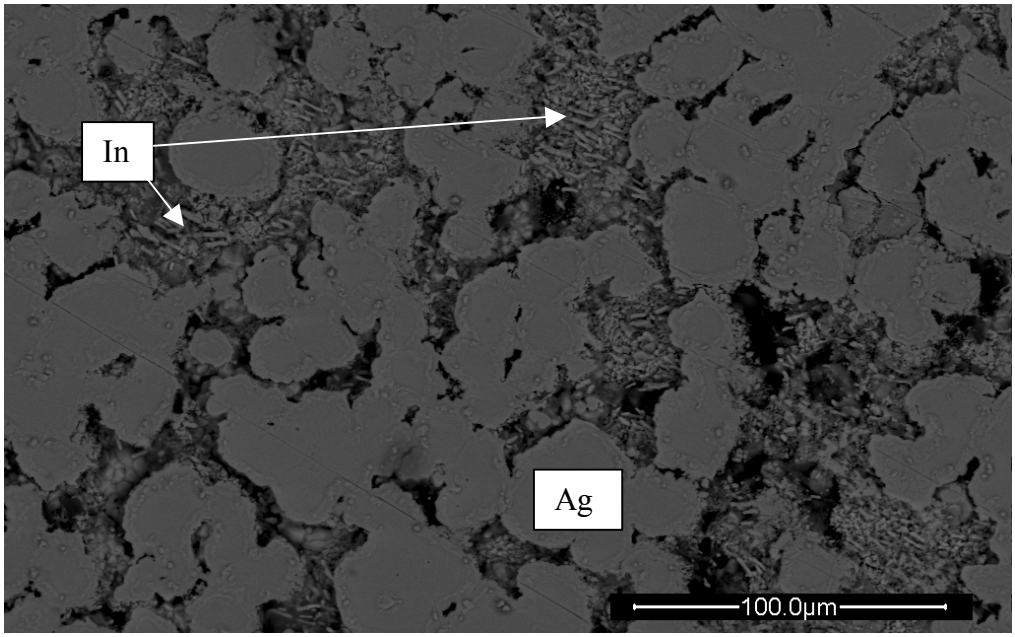

Figure 47. SEM micrograph (BSE) of a 30 Wt.% In sample heated to 250°C and cooled down after an isothermal hold of 10 minutes. Silver-rich particles are now present as agglomerated clusters in which the presence of the In-rich matrix is not longer as evident as for the shorter holding time.

After holding for 25 minutes at 250°C, the In-rich liquid appeared to be constrained to localized areas with minimal contact to the dominant Ag-rich skeleton (Figure 48). This greatly reduces the surface area for diffusion, leading to a decrease in the solidification rate. This physical phenomenon explains the behavior of the prediction from the empirical model (solid RSM line in Figure 45) which tended to a slower solidification rate after the 10^{th} minute. The mechanistic model did not account for this condition. An important factor affecting the behavior of the two models at longer holding times is the fact that homogenization was not considered for the mechanistic approach. As discussed already, Crank provided a solution up to $t \rightarrow \infty$ assuming full saturation of the solid, i.e. the process stops at $C_B = C_{max} = C_s$. It is known that there is a final stage during the TLPS process by which the real equilibrium condition is attained. During this last stage, diffusion occurs at a slower rate dominated by a

solid-solid interdiffusion mechanism driven by a smaller concentration gradient given by ($C_S - C_B$). At this point in time indium atoms from the newly formed solid with composition C_S slowly diffuse into the Ag-rich core until final equilibrium is reached. A stable microstructure consisting of Ag(α) + γ will result. The RSM accounts for this step, which imposes a delaying effect during the late isothermal solidification stage.

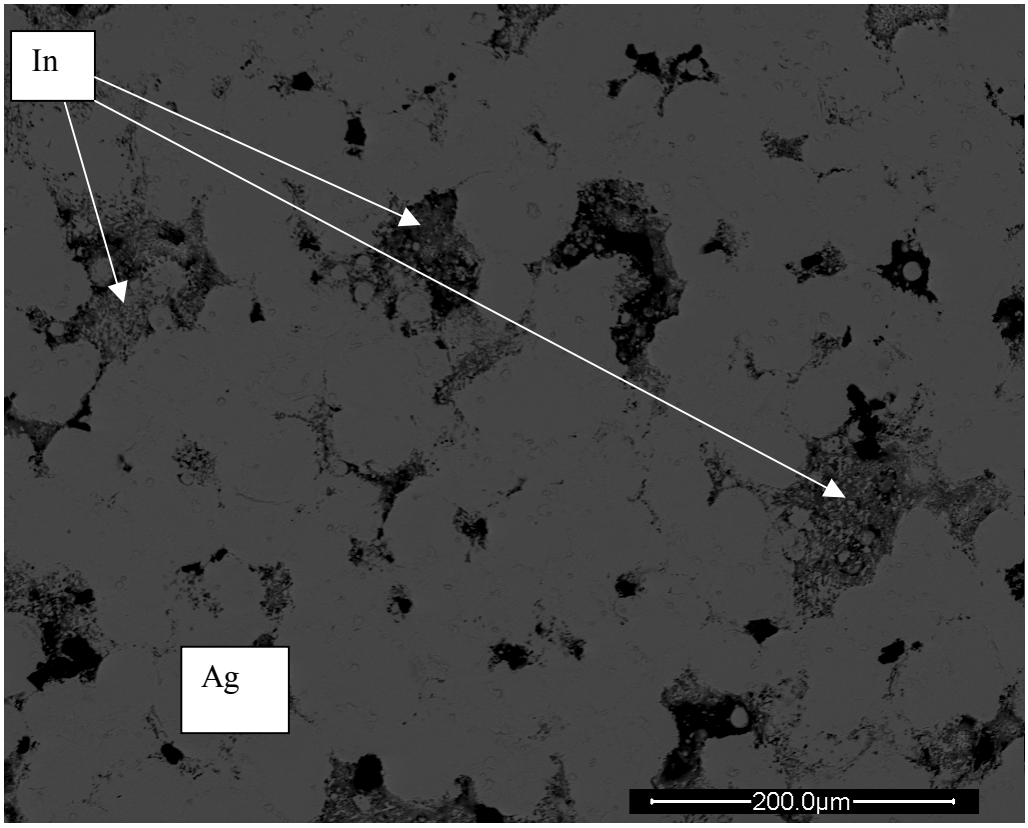

Figure 48. SEM micrograph (BSE) of a 30 Wt.% In sample heated to 250°C and cooled down after an isothermal hold of 25 minutes. Silver solid skeleton is now dominant with the remaining In-rich phase constraint to discrete portions of the system.

The interaction between stages in TLPS is a known problem [30] that analytical solutions cannot treat due to their sequential approach to the solution. The truth is that the stages are inter-dependent and they do affect the kinetics of one another.

All of the factors discussed regarding assumptions of the analytical solution and the microstructural evolution with time have explained the behavior of the two models across the entire time regime. During the early period ($0 \leq t < 10$) dominated by the isothermal solidification mechanism, both models were able to predict a similar response whereby the solidification rate exhibited a linear correlation with $\sqrt{t}$. At longer holding times, the mechanistic model projected a constant reaction rate up until the completion of the solidification process, a prediction that was showed to be inaccurate. The RSM was capable of predicting a shift in the solidification mechanism that was driven by the slower homogenization stage and microstructural changes. This prediction from the RSM at longer holding times was crucial for process definition. Without this consideration, the model would have failed in the prediction of the final constitution of the system as well as in the estimate of the time to completion. The assumption of a continuous solidification rate by the mechanistic model would have yielded a premature prediction of the time to complete solidification. This miscalculation could have resulted in failure if the application temperature was to exceed the melting point of the remaining fraction of the In-rich phase. The RSM model provided a more accurate tool for the prediction of the time needed to complete solidification since it considered all stages of the TLPS process. As a result, tailoring of the proposed Ag-In paste process should be based on simulations from the more comprehensive RSM.

6.6 Conclusion:

A piecewise empirical kinetics model for TLPS of an Ag – In paste mixture was developed using response surface methodology (RSM). This model estimates the solidification of the low melting In-rich phase as a function of controllable variables available to the practitioner. The experimental outcome of this investigation demonstrated the existence of three stages during the process as previously suggested by theorists in this field. This piecewise technique provided specific response functions for each time regime which proved to be sensitive to specific critical parameters and interactions, as defined by the analysis of variance. The physical significance of the obtained experimental data was accomplished via a metallographic study in conjunction with a comparative analysis of the results obtained from a diffusion based mechanistic model. Results from both prediction models were compared, and the adequacy of the experimental technique was confirmed. The mechanistic model, when compared to the empirical approach, provided a similar behavior of the response during the period governed by isothermal solidification. A change late in the solidification process, during which the reaction rate decreased, was observed from the RSM prediction. This phenomenon was explained by the microstructural changes observed in the samples in which a transition from an In-rich matrix to a Ag-rich solid solution skeleton occurred. This new morphology imposed limitations to the governing diffusion mechanism, thus delaying the solidification reaction. The effect of the last stage of the TLPS process, solid sate homogenization, was also identified as a delaying agent in which the slower diffusion of indium into the solid (Ag) α phase imposed a bottleneck effect to the solidification process. This

interdependency among the different stages of the TLPS process had been suggested in previous investigations as a critical aspect for this powder metallurgy technique. The conditions established for the derivation of the mechanistic model (semi-infinite medium and parabolic law) made it unresponsive to these effects, thus limiting its ability to predict the true behavior at longer holding times. Contour maps from the RSM simulation provided an accurate estimation of the kinetics of transformation for the Ag-In paste as function of critical variables, making it possible to tailor the process to specific applications or limitations so that the desired results can be accomplished.

Chapter 7: Characterization of the Ag-In Transient Liquid Sintered Material

7.1 Introduction:

A common characteristic of all forms of sintering is a reduction in surface area with an accompanying compact strengthening. This occurs by the formation of interparticle bonds facilitated by atomic motion at the sintering temperature. During TLPS, liquid coexists with the solid particles at the processing temperature (T_p). This liquid phase enhances interparticle bonding, which results in significant changes in the pore structure and compact properties. From a processing standpoint, the major advantage of liquid phase sintering is a faster process without the need for external pressures. The liquid phase provides sufficient internal force on the particulate solid through capillary action that external forces are not required. The magnitude of these capillary (wetting) forces are equivalent to external pressures [11]. The liquid also reduces the interparticle friction, thereby aiding rapid rearrangement of the solid particles. The liquid wetting present at T_p acts on the solid particles to eliminate porosity and reduce interfacial energy. With liquid formation there is a rapid (almost instantaneous) densification due to the capillary force exerted by the wetting liquid on the solid particles. The elimination of porosity occurs as the system minimizes its surface energy. The amount of densification attained by rearrangement is dependent on the amount of liquid and the particle size [11], (i.e. finer additive particles tend to give better densification). Maximization of the density (reduction of porosity to a minimum) is possible when an estimated 35 volume percent liquid is available [11] a

phenomenon that occurs during the early stages of TLPS. During the later stages of TLPS, densification is slower due to the existence of a solid skeleton. The rigidity of this solid structure inhibits further rearrangement.

When a liquid forms during liquid phase sintering the microstructure consists of three phases: solid, liquid, and vapor. Wetting describes the equilibrium between these three phases. For a liquid to wet a solid, the total free energy must be decreased. The wetting is characterized by the contact angle, the magnitude of which depends on the balance of the surface energies. In typical powder systems, there is a range of particle sizes, pore sizes, pore shapes, and particle shapes which result in a range of capillary conditions. A wetting liquid will attempt to occupy the lower free energy position, therefore it preferentially flows to the smaller capillaries which have the highest energy per unit volume. When there is insufficient liquid to fill all the pores, the liquid will attempt to pull the particles together to minimize the total free energy of the system. This effect explains the rearrangement and rapid initial densification during the beginning of the TLPS process.

Pores are an inherent part of liquid phase sintering. Pores are present in powder compacts as interparticle voids (packing), and can also result from uneven liquid distribution, unbalanced diffusion events (Kirkendall effect), reactions with gases, and capillary spreading. Porosity is characterized by its amount, size, shape, and distribution of pores throughout the compact. By definition, the fractional density plus the fractional porosity must equal unity. Generally the objective during TLPS is

for the fractional porosity to approach zero. In this way the mechanical, electrical, and thermal properties of the resulting material are optimized. Pores are typically detrimental to the properties of liquid phase sintered materials. Microstructural analysis can be used for analyzing the fractional porosity of a material processed by TLPS. The most typical technique for measuring the volume fraction of pores in the structure is to apply point-count analysis to the specimen [11][12][64]. Densification to near zero porosity is energetically favorable, but trapped gas in the pores inhibits final densification. The formation of the rigid solid skeleton in the final stages of TLPS will also hinder pore elimination. It has been demonstrated [65] that capillary attraction for a liquid resulting from the surrounding pore structure generates a pore at the particle site where the liquid forms. Since the subsequent pore size is roughly the same as the additive particle, it is desirable to have small additive particle sizes. The amount of additive directly influences the volume fraction of liquid, which, in fact, dictates the densification of the structure leading to the final compact properties. As a consequence, the amount of additive is a critical processing parameter which influences the final microstructure and sintered properties.

In this chapter the densification of the Ag-In paste will be analyzed in terms of controlling parameters. The effect of fractional density on the mechanical strength and the thermal and electrical conductivities will be studied. An optimal formulation, based on the obtained results, will be used for the fabrication of test specimens for a reliability assessment of the proposed Ag-In attach material.

7.2 Porous nature of TLPS material:

Transient liquid phase sintering is a special powder metallurgy technique in which the presence of a liquid phase results in densification of the compact. The properties of these sintered materials depend on pore morphology (size, shape, interconnectivity) and total porosity [66]. The concept of microstructure has to be defined with care for this type of material, since it not only refers to the grain scale within the solid phases but to the size, volume fraction, and distribution of the pores as well [11][66]. TLPS is a complex processing technique sensitive to a myriad of variables in which the amount of liquid has been suggested as a dominant parameter for the densification mechanism [11]. Bulk physical properties of these porous materials are a function of not only the intrinsic properties of its main constituents but of its porosity characteristics as well. There have been a series of expressions for modeling the effective properties of porous structures; a summary has been presented by Montes [67]. The most widely used model was presented by Schulz [68] in which the effective property of the porous material (g_E) is given by:

Equation 55

$$g_E = g_o \cdot (1 - \Theta)^x$$

where g_o is the property of the solid material (theoretical), Θ is the fractional porosity (i.e. the ratio of void volume to the total volume of the specimen), and x is the pore scaling exponent. This scaling exponent has been reported to range from 1.6 – 5.0 [67][68] depending on pore geometry and interconnectivity. Special interest in transport properties such as thermal and electrical conductivity has lead to recent research efforts [20][67]. This investigation will focus on the effect of fractional density on mechanical, electrical, and thermal properties of the transient liquid phase

sintered material. Particular attention will go into studying the effect of solute addition (volume fraction of indium) on the densification of the compact and its subsequent effect on the above properties.

7.2.1. Densification analysis:

In previous sections it was discussed that the physical properties of porous materials depend upon their fractional density. Attaining full densification of a sintered compact requires large amounts of energy in the form of heat and hydrostatic pressure. The suggested method during this investigation is a TLPS process in which the external pressure is substituted by an internal capillary force that shall result in the required densification. The fractional porosity (Θ) has been defined as the ratio of void volume to the total volume of the specimen, a ratio that can be measured by stereological techniques [64][70]. Stereology deals with a body of methods for the exploration of three dimensional space when only two dimensional sections through solid bodies are available. Therefore, stereology can be viewed as an extrapolation from two - to - three dimensional spaces. Quantitative stereology attempts to numerically characterize specific features in the microstructure. For the present investigation, pores obtained in the samples fabricated via the TLPS process will be the feature of interest. Calculation of volume fraction of these pores will result in a quantitative estimation of the fractional porosity or fractional density ($1 - \Theta$).

Determination of the volume fraction of a particular feature (pores in this case) is one of the most important and most common stereological measurements. The point-count method detailed in ASTM Specification E562 is the most accurate procedure to estimate volume fraction from two-dimensional section planes [64]. In this method a test grid is overlaid on a micrograph. The magnification should be high enough so that the location of the test points (crosses of the grid) with respect to the structural features can be clearly discerned. Magnification should always be the lowest possible, where in general, no more than one grid point falls on any given feature of interest. Calculation of the volume fraction of voids (V_v) results from counting the number of pores (voids) "hit" by the intersection of the grid when applied to a field selected at random. The number of hits in the pores (P_v) are counted as unity, whereas tangential hits are counted as 0.5. Generally 10 or more fields are measured, and the point fraction (P_p) is calculated as follows:

Equation 56

$$P_p = \sum P_v / P_T = \sum P_v / n \cdot P_o$$

where n is the number of fields and P_o is the number of grid points. Alternatively, the value of P_p can be determined for each field and then averaged for *n* fields as an estimate of the volume fraction. This method produces data ready for statistical analysis while providing the exact same value as the one obtained from Equation 56. In the current investigation this alternative method will be followed. It has been demonstrated [70] that $V_v = P_p$, so the volume fraction of voids (fractional porosity) can be estimated with this stereological technique.

All stereological measurements are estimates rather than absolute measurements, so a basic statistical analysis for uncertainty is required if microstructural parameters are to be estimated from this approach. In the current case, a 20 point grid ($P_o = 20$) was used with a total of 20 fields per condition (n = 20). The mean value of P_p ($P_{p,avg}$) is given by $\sum P_v / nP_o$, whereas the standard deviation (s) of the data is given by:

Equation 57

$$s = [\sum (P_{p,i} - P_{p,avg})^2 / (n-1)]^{0.5}$$

The 95% confidence limit of the calculated fractional porosity (i.e. $V_{v,avg} = P_{p,avg}$) is given by:

Equation 58

$$95\%CL = t \cdot s / (n-1)^{0.5}$$

where *t* varies with the number of measurements *n* and is tabulated; a t value of 2.086 was used for n = 20 [64]. An estimated fractional density was obtained using these statistics for all measurements performed during this investigation.

7.2.2. Specimen fabrication:

All samples used for the point-count analysis were fabricated into "pill" shaped specimens as depicted in Figure 49. Dimensions of the test specimens were as follows: diameter (D) = 6.7 mm, thickness (t) = 0.7 mm, yielding a D/t ratio of 9.6.

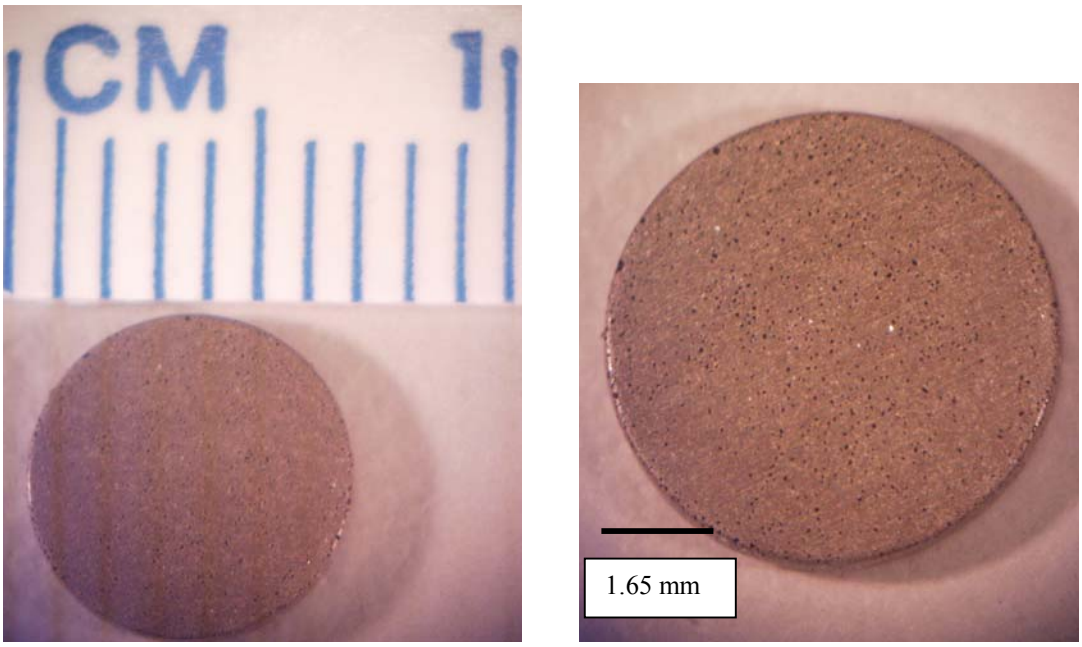

Figure 49. Typical "Pill" shaped specimen for point count analysis. Diameter of the sample is 6.7 mm with a thickness (t) of 0.7 mm.

Morphological details of a typical sample are given in Figure 50 which shows a typical scanning electron micrograph of a sample fabricated by TLPS of the Ag-In paste.

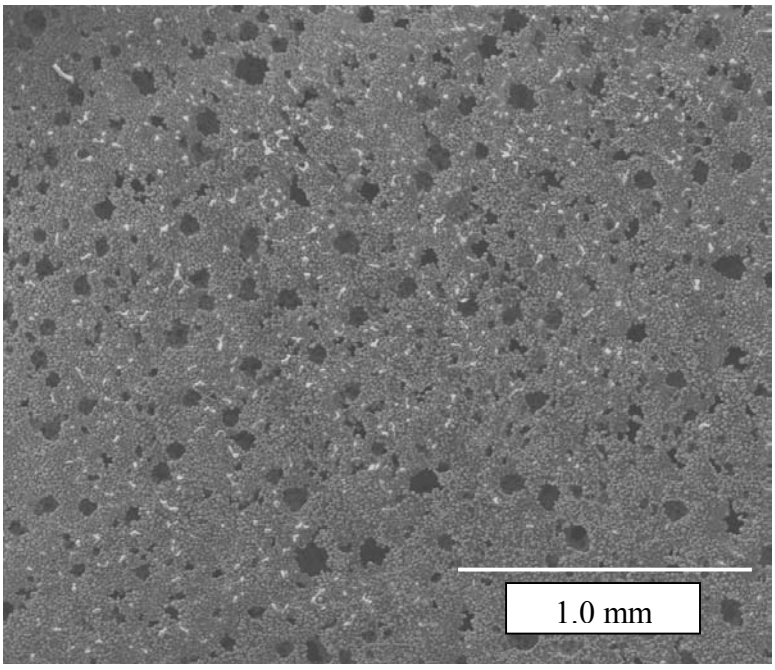

(a)

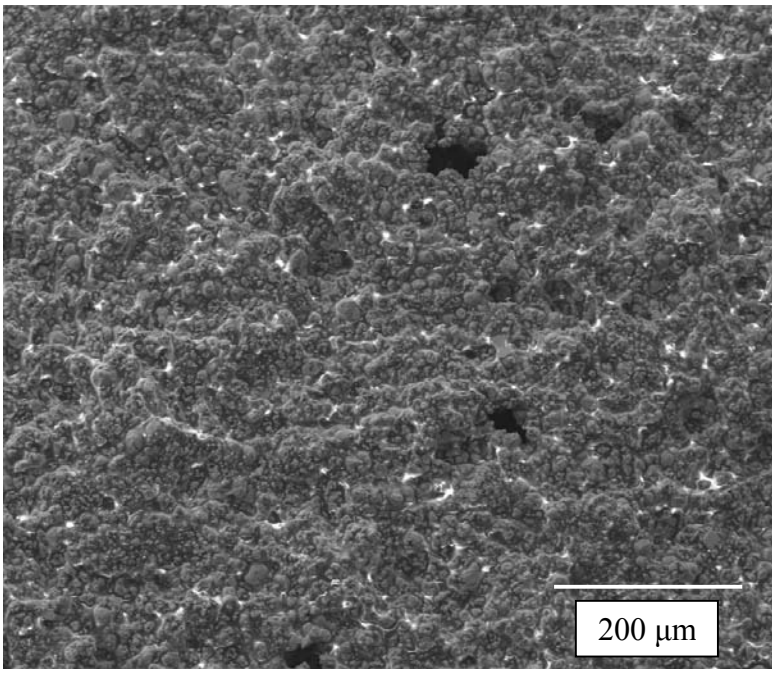

(b)

Figure 50. Typical SEM image of the sintered Ag-In "pill" sample showing a uniform distribution of micro-pores. (a) SEM at a low magnification (50X) showing the obtained porosity, (b) higher magnification (160X) showing the morphological details of the solid portion and a few pores of ~ 30-50 μm diameter.

From these images the pores appeared to be dispersed through the matrix with an average measured diameter of 52 μm, which correlates to the additive (indium) particle size used for the mixture. Based on this pore size and the morphological details revealed during this initial characterization, a magnification of 40X was selected for the stereological analysis.

7.2.3. DOE for densification study:

TLPS is a complex processing technique that depends on multiple input variables as presented in previous chapters. Densification is primarily driven by the spreading of a wetting liquid through a solid skeleton, but the effect of other variables such as heating rate, particle size, and processing temperature need to be determined. In

theory-based works [11] it has been suggested that the volume fraction of liquid formed during the process, which is proportional to the mass fraction of MPD additive in the mixture, drives the densification of the system. In this investigation a screening 2-level factorial experiment was designed to study the effects of input variables on fractional density. Table 9 illustrates the input variables and their pre-defined levels.

Table 9. Input variables and their levels used for the densification DOE.

Factor	High Level	Low Level
Silver Particle Size (PS)	50 μm (spherical) [Max]	25 μm (spherical) [Max]
Heating Rate (HR)	60 °C/min	30 °C/min
Processing Temperature (T_p)	300 °C	250°C
Additive Weight Fraction (Wt. %)	30 Wt. % In	15 Wt. % In

The response variable for this experiment is the fractional density ($1 - \Theta$) which was measured by the point-count technique previously defined. During this DOE the holding time was deliberately fixed because liquid induced densification is an instantaneous phenomenon [11]. Samples for the randomized DOE were fabricated into "pill" shaped specimens, and analyzed using an optical stereo microscope. A 20 point grid overlay was used for the point-count analysis. A hypothesis test (ANOVA) was used for studying the statistical significance of the data from which a reduced multiple linear regression model for coded variables was developed [Appendix 7]. From the statistical analysis it was determined that the most significant effect on the response was the additive weight fraction (Wt.% In). This significance is evidenced by the magnitude of the estimated regression coefficient when compared to the other main effects. Results for the empirical model with coded variables are given in Table 10.

Table 10. Estimated regression coefficients for the fractional density model (coded variables).

Term	Regression Coefficient
Constant	63.6
Additive Weight Fraction (Wt. % In)	10.2
Silver Particle Size	-1.7
Processing Temperature	3.4
Heating Rate	0.6

An empirical estimation for the fractional density of the Ag-In sintered material is given by the following model (R^2_{pred} = 91.5%):

Equation 59

$$FractionalDensity = 63.6 + 10.2 \cdot (Wt.\%In) - 1.7 \cdot (AgPS) + 3.4 \cdot (T_p) + 0.6 \cdot (HR)$$

From the analysis of variance it was obtained that the interactions had no statistical effect on the response, as given by their p-values. The model given by Equation 59 is only valid for coded input variables [Appendix 7].

From these results it was confirmed that the densification of this system is dictated by the volume of liquid present, given by the solute composition of the mixture, i.e. Wt.% In. From a practical standpoint, the formulation of a paste mixture is controlled by the weight fraction of its constituents which has been the input variable throughout this investigation. Physically, it is the volume fraction of the main constituents of the mixture that is critical for the densification mechanism and other transport properties; this volume fraction is proportional to the weight fraction. By knowing the densities of the constituents in the mixture, the volume can be calculated. In this instance all volume calculations were obtained using the density of silver: 10.49 g/cm^3 and

indium: 7.31 g/cm^3 [45]. To obtain a more accurate estimation of the effect of volume fraction of indium on the fractional density, a refined experiment was needed. The initial two level experiment provided a good screening tool from which the main effect of indium weight fraction was revealed, but a higher resolution of this variable is required for a better understanding of its effect on the response. For this refined experiment, the remaining input variables were set to fixed values obtained by the optimization of the time to zero percent remaining In-rich phase. From this optimization exercise the values were set as follows: HR = 60 °C/min., T_p = 300°C, silver PS (Type V or -500 Mesh) = 25 μm, and Holding Time = 60 minutes. A total of five new pastes were formulated in which the solute weight fraction was the only changing variable, details of these pastes are given in Table 11 below.

Table 11. Specifications for the pastes used for the refined densification experiment.

Paste	Wt. % In	Vol. % In	Ag PS_{max} (μm)	In PS_{max} (μm)	Solid content (%)
1	10	13.8	25	50	91
2	20	26.4	25	50	91
3	30	38.1	25	50	91
4	40	48.8	25	50	91
5	70	77.0	25	50	91

Two samples from the each of the above solder pastes were fabricated into the pill shaped specimens described in Figure 49. The specimens were analyzed using the point-count technique; results from all fields are given in Appendix 6. Figure 51 shows a typical optical micrograph used for the quantification of the fractional density, in which a 20-point grid was used per inspection field; a total of twenty fields per sample were measured.

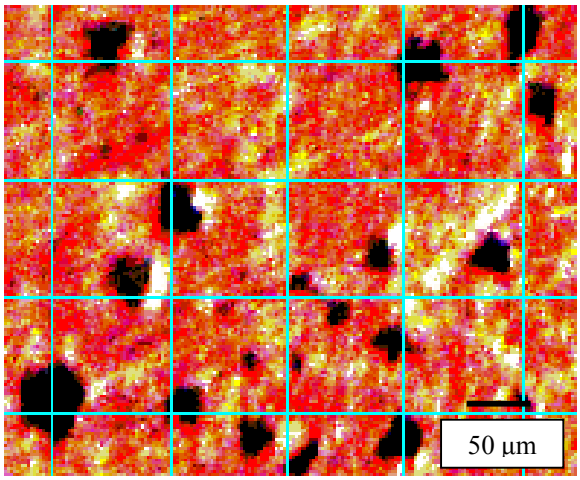

Figure 51. Typical optical micrograph with the 20-point grid overlay used for the point-count analysis. Fractional density, 1 – Θ, was estimated from the calculation of the pore volume fraction (Θ) given by P_v / P_o. In this example a $P_v = 5$ was counted, a given $P_o = 20$, resulting in a porosity of 0.25 or a fractional density of 75%.

The correlation between the indium weight fraction and the measured fractional density is given in Figure 52, in which the effect of increasing indium fraction on the densification of the system is evident.

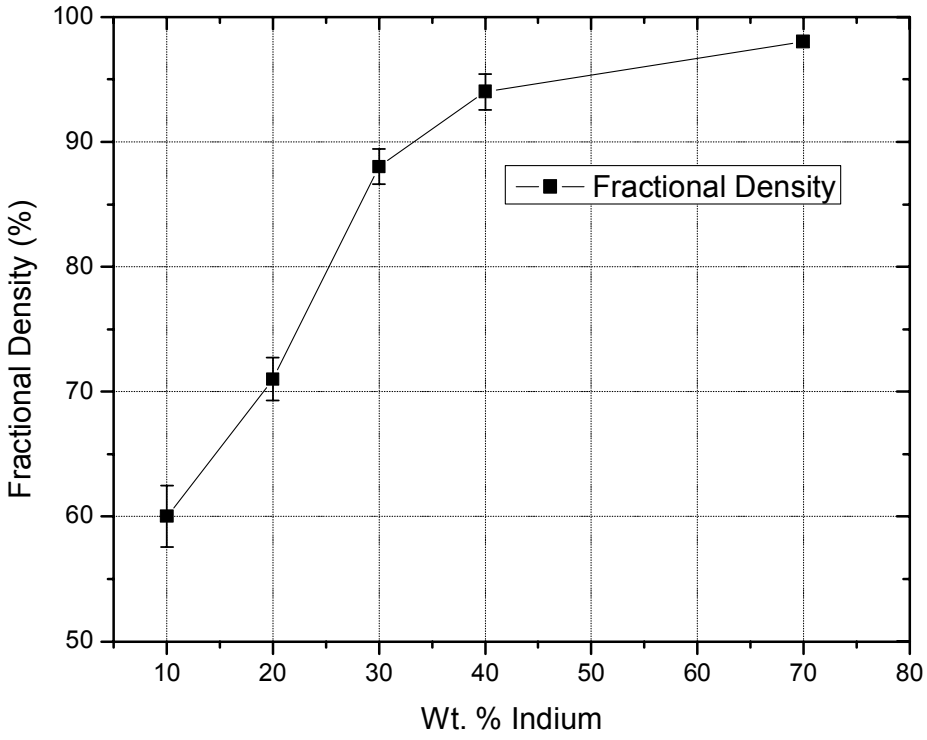

Figure 52. Measured fractional density as function of indium weight fraction, error bars represent the 95% confidence interval.

In this figure the data from the 70 Wt. % In paste showed that a liquid volume fraction of 77% produced a near-fully dense solid, but the presence of such a high amount of indium would have resulted in a persistent low melting In-rich phase. The presence of this phase would have limited the maximum application temperature of the system, thus defeating the objective of this investigation. Data from this In-rich paste was only used for fundamental studies on the physical properties of this material.

Within the compositional range valid for the transient solidification and subsequent achievement of a variable melting point alloy, which is limited by the maximum solid

solubility of indium in the Ag-rich phase (i.e. ~ 40 Wt.% In), the fractional density went from 60% to 94%. The upper bound for indium composition is given by the solubility limit, but a lower bound has yet to be defined. Defining a feasible indium compositional range depends not only on the achievement of the highest density (which was given by the upper bound), but on the optimization of the resulting mechanical, electrical, and thermal properties as well. From a practical standpoint, minimizing the time required for complete diffusional solidification is also desired. Such a goal is achievable by simply minimizing the indium addition in the mixture. However, minimal indium content could result in a highly porous structure that may not provide acceptable properties; thus, a method to assess this lower limit will be presented. In the following sections, the optimal compositional range of indium will be assessed in terms of resulting fractional density, electrical conductivity, and mechanical strength.

7.3 Characterization of the TLPS Ag-In system:

7.3.1. Electrical and thermal properties:

The motivation behind the development of this Ag-In paste using a TLPS process was to provide a high temperature resistant attachment using a low temperature process. Electronic packaging deals with providing a mechanical, electrical, and thermal connection of an integrated circuit with subsequent packaging levels. In such a quest, the mechanical, electrical, and thermal properties of interconnect materials become critical factors. Signal processing is critical for the operation of electronic systems in which the materials involved play an important role in the propagation of these

signals. One of the most important electrical properties of materials is volumetric resistivity. Resistivity is the characteristic of a material that resists the passage of electric current. In this case, volumetric resistivity is the electrical resistance between opposite faces of a given volume when a current flow is confined to the specimen [71]. Volumetric resistivity (ρ_v) is a bulk material property and is given by:

Equation 60

$$\rho_v = \frac{(R \cdot A)}{L}$$

where R is the measured electrical resistance, A is the cross sectional area, and L is the length of the test pattern. The inverse of volumetric resistivity is known as electrical conductivity (σ).

It has been demonstrated that the porosity of the proposed Ag-In material is related to the solute composition of the mixture (Figure 52). The effect of porosity on the electrical conductivity of the material is an important factor in determining the best level of solute addition. This optimal quantity should ensure the maximum electrical conductivity possible. It is well known that the bulk transport properties of porous materials are not only a function of their main constituents, but of their fractional porosity (or density) as well. A number of expressions for modeling thermal and electrical conductivities have been reported [67]. An expression developed by Schulz [68] provides the effective electrical conductivity (σ_e) of a porous material:

Equation 61

$$\sigma_e = \sigma_o \cdot (1 - \Theta)^x$$

in which σ_o is the theoretical conductivity of the solid material that can be obtained for most pure metals in the literature, Θ is the fractional porosity, and "*x*" is the pore

scaling exponent. In this instance, the electrical resistivities of the materials of interest are as follows [44]: $\rho_{Ag} = 1.55 \text{ X } 10^{-6}\ \Omega - \text{cm}$, $\rho_{In} = 9.0 \text{ X } 10^{-6}\ \Omega - \text{cm}$. Note that $\sigma_o = 1 / \rho_o$. The conductivity of an alloy, however, is often lower than the pure metals of which it is comprised, owing to impurity scattering in solid solutions, and to the lower conductivity of some intermediate phases. This effect must also be considered in determining the optimum indium addition in the paste mixture.

7.3.1.1. Experimental set-up:

In order to measure the effective electrical resistivity of the sintered material, a standard test is required. For this experiment, solder pastes described in Table 11 (except 5) were used for the fabrication of test traces. The trace pattern was obtained by printing the paste through a custom laser cut stencil onto a bare alumina (Al_2O_3) substrate. Figure 53 depicts the artwork of the stencil used for trace fabrication; a foil thickness of 0.008" (8 mil) was used.

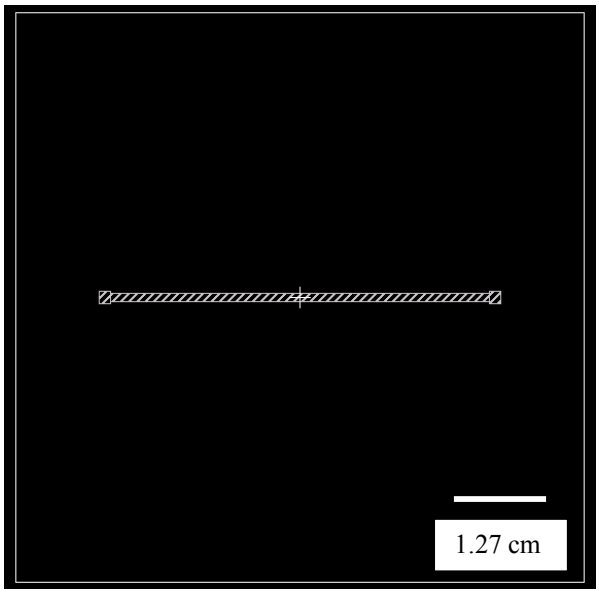

Figure 53. Laser cut stencil with the electrical test trace pattern.

The deposited patterns from each paste were processed by the TLPS technique using the optimized profile from the kinetics study, i.e. HR = 60 °C/min., T_p = 300°C, and a Holding Time of 60 minutes. These same conditions were used for the fabrication of pills during the fractional density experiment. Fractional densities (1 - Θ) for each of these pastes are given in Figure 52. After sintering, traces were measured to obtain the length (L) and cross-sectional area (A), values that were required for electrical resistivity calculations. Figure 54 depicts a typical as-built trace pattern after the TLPS process.

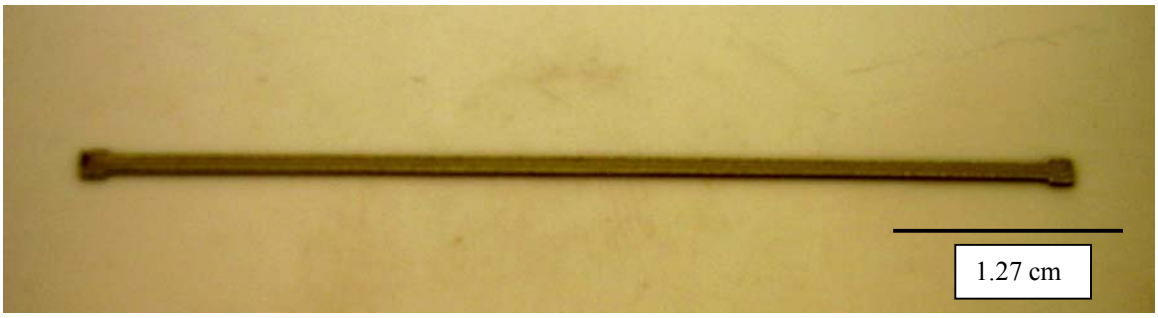

Figure 54. Typical as-built image of the test trace obtained by stencil printing and subsequent TLPS processing of the Ag-In paste.

The electrical resistance (R) of the test patterns was measured by a four-point probe test using an Agilent milliohm meter 4338B with a 1mA test current at room temperature. Four point testing eliminates the error induced by the added resistance of the probing tips. This is accomplished by supplying the test current independently of the probes used to measure the voltage drop across the specimen. The contact resistance inherent in the probing action is accounted for by the short correction that is performed before each test. The resulting resistance value from this type of test is then an accurate measurement of the material under test. A total of 20 readings per

test condition were used during this investigation; the mean values along with the measurement errors were documented. Mean resistance values for each of the five pastes were used for the calculation of the effective resistivity of the material, in which the length and cross-sectional area were measured to be 5.08 cm and 0.001 cm^2, respectively. Volumetric resistivity was then obtained by substitution of these values into Equation 60, from which the measured effective electrical conductivity was calculated ($\sigma_e = 1/\rho_e$).

7.3.1.2. Results:

Figure 55 shows the measured electrical conductivity obtained from the four-point testing on the fabricated traces.

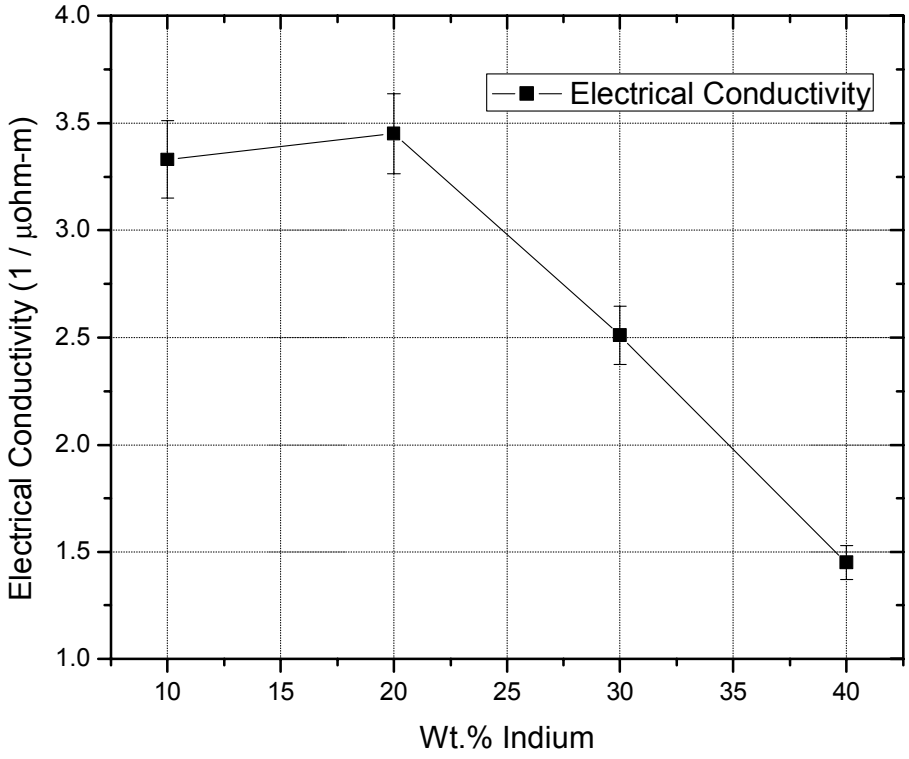

Figure 55. Measured electrical conductivity of sintered Ag-In pastes with various indium compositions. Markers represent the mean whereas the error bars depict the +/- 5.4% measurement error from the equipment.

Results from pastes up to 40 Wt.% In were used for this plot because this is the upper bound for the achievement of a variable melting point alloy without the precipitation of any persistent phases. From this chart, it was observed that the electrical conductivity reached its maximum value at around 20 Wt.% In and then began to decrease with further addition of indium. A more comprehensive analysis is obtained by inspection of Figure 56, in which the effect of indium addition on both the fractional density and electrical conductivity is given.

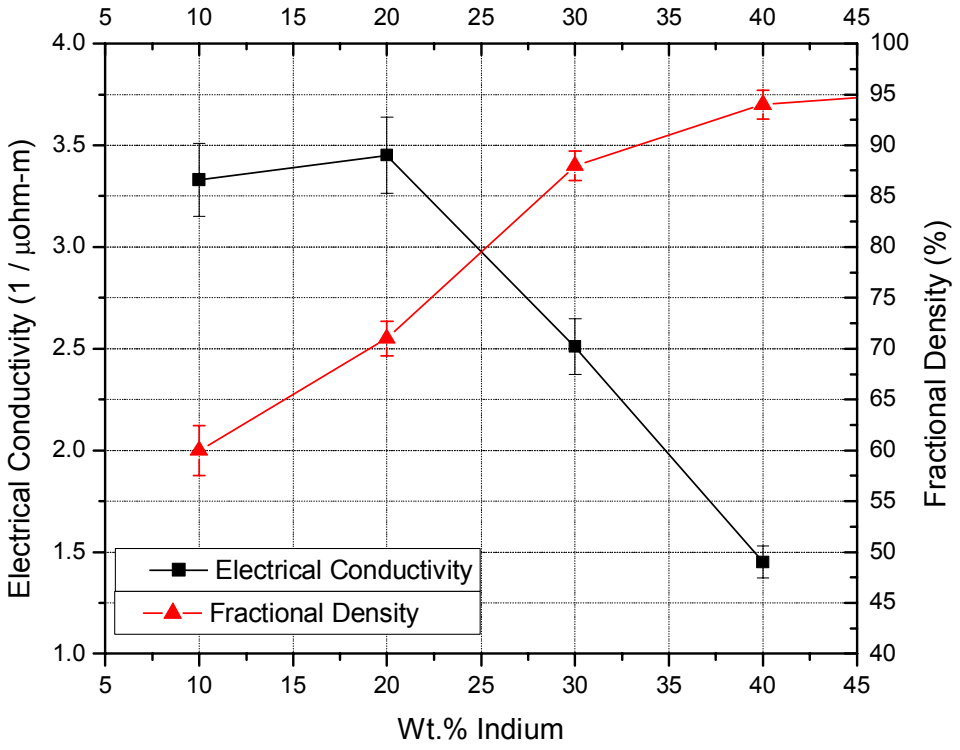

Figure 56. Combined plot showing the relationship between indium weight fraction with both the electrical conductivity and fractional density.

From this chart it can be seen that the maximum electrical conductivity was obtained at a fractional density of approximately 71%, or an indium weight fraction 20%. Using this information a lower bound may be apparent at 20 Wt.% In in which maximum electrical performance is possible with an acceptable fractional density. Nevertheless, there is concern that such fractional density values may affect other physical properties of the system. In terms of bounding, however, the composition of 20 Wt.% In still seems to be reasonable. The mechanical strength of this material is another important factor that has must be considered in order to make a final recommendation of a lower bound. It is evident that a decision based on fractional density alone would have yielded an erroneous conclusion, as evidenced by a

noticeable degradation of the electrical conductivity even though the densification showed an excellent response. Results from the electrical characterization are summarized in Table 12.

Table 12. Electrical conductivity characterization for the TLPS Ag-In material*

Paste	Wt. % In	Vol. % In	Vol. % Ag	Fractional Density [1-Θ]	σ_{Ag} [Porous Ag] (1 / μΩ·m)	σ_e (1 / μΩ·m) [measured]
1	10	13.8	86.2	0.60	5.0	3.33
2	20	26.4	73.6	0.71	11.6	3.45
3	30	38.1	61.9	0.88	34.0	2.51
4	40	48.8	51.2	0.94	47.3	1.45

* All properties and measurements were taken at room temperature (25°C)

7.3.1.3. Analysis:

The effective measured electrical conductivity of the Ag-In sintered material exhibited a peak value at 20 Wt.% In and then started to degrade with further indium addition, the reason for this behavior can be explain as follows. If the material were a pure silver compact then the effect of fractional density on electrical conductivity would be given by Equation 61, where σ_o would be the electrical conductivity of pure silver [64.5 $(\mu\Omega\text{-m})^{-1}$] [44] and *x* would be 5 [68] for the maximum porosity effect. In such a situation; the compact would have the theoretical conductivities shown in the sixth column of Table 12. For this case a compact with a fractional density of 60% would have a conductivity of 5.0 $(\mu\Omega\text{-m})^{-1}$ whereas a 71% dense compact would have a conductivity of 11.6 $(\mu\Omega\text{-m})^{-1}$. This is a significant increase in electrical conductivity with increase in fractional density. However, the measured conductivity shows a much smaller increase from the 60% dense compact to the 71% dense compact owing to the fact that the increased indium concentration will also create

increased scattering in the silver solution. Nevertheless for this range of indium the densification effect is larger than the indium impurity effect so the conductivity shows a slight increase. Above 20% In the γ-phase is created and, while there is no published value for the conductivity of γ in the literature, it can be assumed that it is quite poor because as the amounts of this γ phase increases, with increasing indium concentration, the conductivity decreases even further. This impurity effect is much stronger than the enhanced densification resulting from the increasing indium in the mixture; this can be observed in Figure 56 from the behavior of the curves at values above 20% In. To summarize, increased density (positive effect of indium addition) means reduced porosity, but the presence of a larger volume fraction of indium, as an impurity, was demonstrated to produce an adverse effect in the electrical conductivity (negative effect of indium addition). This situation becomes critical because a compromise between these competing effects will be required.

Based on this analysis, the indium composition of the mixture should be high enough to produce an acceptable densification but without causing a significant degradation of the electrical conductivity. From Figure 56 it can be suggested that for optimal electrical conductivity the composition of the Ag-In material should be kept around 20 Wt.% In. A compositional range of 20 to 25 Wt.% In can be suggested from this analysis over which the improvement in the density from 70% to 80% comes with a slight decrease in electrical conductivity from 3.45 to 3.0 $(\mu\Omega \cdot m)^{-1}$.

7.3.1.4. Thermal conductivity:

In electronic packaging, thermal management is crucial, especially in high power and/or high temperature applications. Increasing internal temperatures in semiconductor devices have been related to reliability problems induced by thermally activated failure mechanisms. It is also known that as temperature rises, the semi-conducting capability of the materials starts to degrade, which may result in poor performance or malfunctions. Removing heat is, therefore, an essential task of the electronic packaging. In addition to providing a mechanical bond to the substrate and an electrical path for the signal (in vertical channel devices), metallic attaches must also aid in the removal of heat from the chip. Heat transfer through a metal obeys the same physical laws as electrical conductance when only conduction through the solid is considered; thus, thermal conductivity parallels the electrical conductivity [11]. The relationship between these two transport phenomena is given by the Wiedemann-Franz law [20][72] in which the electrical conductivity (σ) of a metal and its thermal conductivity (K) are proportional:

Equation 62

$$K/\sigma = L \cdot T$$

where L is known as the Lorenz number and represents the proportionality constant between the two conductivities provided that both are measured at the same temperature. The value of this parameter is constant for metals and is equal to 2.44 X 10^{-8} ($W \cdot \Omega / K^2$), and T is the temperature in Kelvin. For each case in Table 12 a thermal conductivity value (K) was estimated from Equation 62. The measured electrical conductivity (σ_e) and a temperature of 300 K were used for the calculations. Results are given in Table 13 below.

Table 13. Thermal conductivity for the TLPS Ag-In material*

Paste	Wt. % In	Vol. % In	Vol. % Ag	Fractional Density [1-Θ]	Thermal Conductivity (W /m·K)
1	10	13.8	86.2	0.60	24.1
2	20	26.4	73.6	0.71	25.1
3	30	38.1	61.9	0.88	18.2
4	40	48.8	51.2	0.94	10.5

* All properties and measurements were taken at room temperature (27°C)

As evidenced by Equation 62, estimation of the thermal conductivity of the Ag-In sintered material depends on the electrical conductivity. Based on the direct relationship between these two properties, the compositional range established from the optimization of the electrical conductivity is still valid.

7.3.1.5. Discussion:

So far the kinetics of the TLPS process for the Ag-In paste have been presented in terms of the remaining In-rich phase. This analysis of the system provided a prediction model for the solidification reaction as function of controllable parameters. By virtue of this diffusional solidification process, a shift in the melting point of the system was achieved, providing the basis for the high temperature tolerance of this material. The feasibility of this material as an attach alternative required further characterization beyond the modeling of the in-situ alloying reaction kinetics. The electrical and thermal conductivity of the resulting porous structure yielded interesting results in which the effect of fractional density, controlled by the composition of the mixture, proved to be critical. A summary of the results from the characterization of the optimal Ag-In material are given in Table 14 together with a series of alternative materials commonly used in the electronic industry for similar applications.

Table 14. Properties for the Ag-In TLPS material compared to commonly used alternatives [59][73].

Metallurgical System (by weight)	Melting Temp., T_m (°C)	Processing Temp., T_p (°C)	Maximum Application Temperature, T_a (°C)	T_m / T_p	Electrical Conductivity $(\mu\Omega \cdot m)^{-1}$	Thermal Conductivity (W / m·K)
63Sn / 37Pb	183	> 213	< 183	0.86	6.7	50
96.5Sn / 3.0Ag / 0.5Cu	217	> 247	< 217	0.88	9.3	33
81Pb / 19In	260	> 290	< 260	0.90	2.61	17
80Au / 20Sn	280	> 320	< 280	0.90	6.3	57
92.5Pb / 5.0 Sn / 2.5 Ag	287	> 317	< 287	0.91	5.0	25
90 Pb / 10 Sn	275	> 305	< 275	0.90	5.2	25
96.8Au / 3.2Si	363	> 393	< 363	0.92	-	27
94.5Pb / 5.5Ag	304	> 334	< 304	0.91	3.5	23
80Ag / 20In (TLPS)	**690**	**> 200**	**< 690**	**3.45**	**3.5**	**25**

Data from the above table shows that the material developed during this investigation exhibited electrical and thermal conductivity comparable to other available alloys. Even though these are encouraging findings, the measured electrical conductivity exhibited a decrease of about one order of magnitude below the theoretical value for silver. A similar behavior has been reported for thick film conductors which normally exhibit an order of magnitude reduction in their electrical conductivity as compared to the pure metal [59]. Much of the measured drop in conductivity has been linked to the inherent porosity of sintered materials. From the tabulated data it can be observed that if an application temperature above 300°C is desired, only a few alternatives are available. These alternatives include 94.5Pb / 5.5Ag and 96.8Au / 3.2Si, both of which will require extreme processing temperatures. In the case of the Ag-In material processed by the TLPS technique, a maximum application temperature of 690°C is achievable while utilizing processing temperatures as low as 200°C. The breakthrough of this proposed technology is evident from the T_m / T_p

column. Note that for all of the traditional technologies this ratio is, by definition of reflow, less than 1, whereas for the Ag-In TLPS system it is as high as 3.45. This proposed material and manufacturing process required lengthy holding times, as long as 90 minutes in some instances, whereas standard reflow is usually accomplished in less than 7 minutes. This difference in processing time is a tradeoff that needs to be considered for high volume production. The advantage provided by this technology in terms of maximum application temperatures ($T_m / T_p > 1$) in conjunction with competitive electrical and thermal conductivities makes it a promising alternative for high temperature attach applications.

7.3.2. Mechanical assessment:

In order to define a suitable process for fabricating mechanical samples of the Ag-In material, the kinetics model developed earlier in this investigation will be used. This model is capable of predicting the time for complete transformation of the material into a high melting point system for any specific set of controllable parameters. In addition to this fundamental study, a characterization of the material in terms of its feasibility as an attach for electronic packaging was presented. In previous sections the electrical and thermal properties of the sintered material were analyzed and the results were discussed. From that assessment it was demonstrated that the optimal compositional range for the proposed system is from 20 – 25 Wt.% In, based on maximization of the fractional density and its electrical conductivity. In electronic packaging securing the semiconductor chip to the substrate is also crucial; thus, the mechanical integrity of the attachment becomes critical. For the complete characterization of the proposed Ag-In TLPS technology a mechanical assessment is

required. In this section the effect of porosity (fractional density) on the attach strength will be studied by means of die shear. These results will be used to complement the information from the kinetics model (time-to-solidification) and electrical/thermal characterization, so that a final recommendation can be made.

Sintered materials are porous structures by the nature of their fabrication process, featuring microstructures dominated by solid phases and a network of pores throughout their volumes (Figure 50). Mechanical behavior of these materials is affected by their fractional density and the morphology of their internal structure (pore size, interconnectivity, distribution) [11]. In previous sections it was demonstrated that the fractional density of this material is controlled by the amount of indium in the mixture, which is limited by its solid solubility in the silver-rich phases. Obeying this solid solubility limit is critical to achieving a shift in melting temperature. Therefore, an addition of more than ~40 Wt.% In is not tolerable by the system because the precipitation of a persistent In-rich phase will limit the maximum allowable application temperature. In order to assess the effect of solute loading on mechanical strength, fractional density will be controlled by varying the indium addition, the subsequent effect of varying fractional density on the mechanical strength (provided that failure occurs through the bulk) will be assessed by die shear of specimens fabricated with each of the pastes. Results from this analysis should provide quantitative information to establish the best indium compositional range for mechanical properties. This information in conjunction with the already obtained

optimal composition from the transport properties should give an overall optimal space for the composition of an Ag-In TLPS attach alternative.

7.3.2.1. Experimental set-up:

During this stage of the investigation the mechanical integrity of the material will be assessed by means of die shear as per MIL-STD-883G Method 2019.7 [74]. In order to perform this test, a set of test specimens was fabricated as described in the following section.

7.3.2.2. Fabrication sequence for mechanical samples:

Test samples consisted of back side metallized Si chips that were diced to specific dimensions. Electron beam evaporation was used to deposit a thin film layer of chromium that served as an adhesion layer, followed by a nickel barrier layer, on top of which a final silver layer was deposited. Die were to be attached to alumina (Al_2O_3) DBC substrates metallized by the same technique in which silver was deposited over nickel. A schematic diagram of both the die and substrate metallization sequence is given in Figure 57.

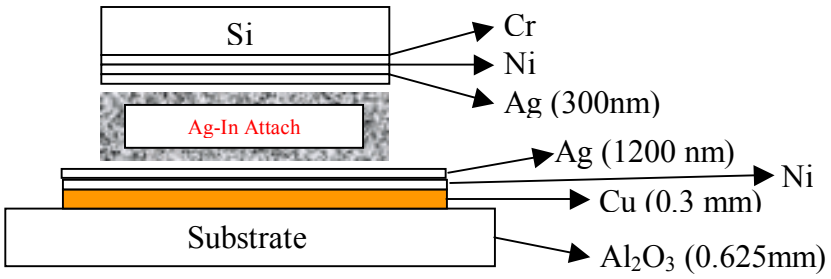

Figure 57. Schematic diagram of typical test specimen, back side metallization of Si die was performed by electron beam evaporation as well as the silver thin film on the ceramic substrate.

Prior to the attachment process, both the substrates and die were cleaned using acetone, methanol, and IPA.

Solder pastes from Table 11, except for paste #3 (30 Wt.% In), were used for fabrication of the test samples. The paste was deposited onto the substrate by a printing process using a laser cut stencil. Figure 58 depicts the stencil used for sample fabrication. After paste deposition, die were placed over the solder block and transferred to the furnace for the subsequent transient liquid phase sintering process.

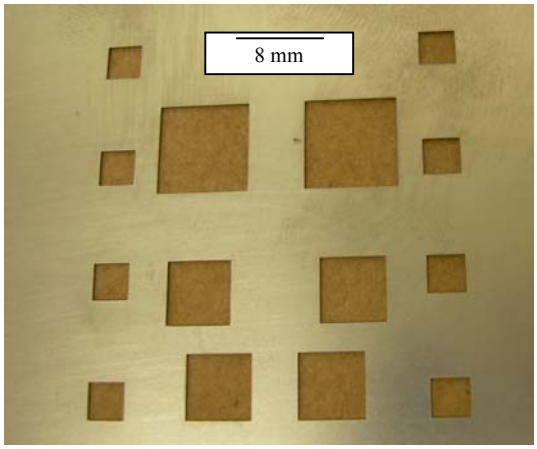

Figure 58. Laser cut stencil used for paste deposition. Apertures for the three die sizes, 8mm, 5mm, and 3mm, are evident.

The TLPS profile used for the fabrication of mechanical samples was similar to the one used during the densification study and for fabrication of the electrical test patterns. This profile was defined using the kinetics study to set the processing parameters so that no remaining In-rich phase condition was achieved. In this way, the final microstructure of all samples was similar, (i.e. dominated by an Ag-rich solid solution matrix with dispersed γ). The only expected difference between

samples should be their fractional density, which was already characterized in samples built under similar conditions. The profile used during the fabrication consists of processing temperature of 300°C, heating rate of 60°C/min., and an isothermal holding time of 60 minutes. A representative as-built sample is shown in Figure 59.

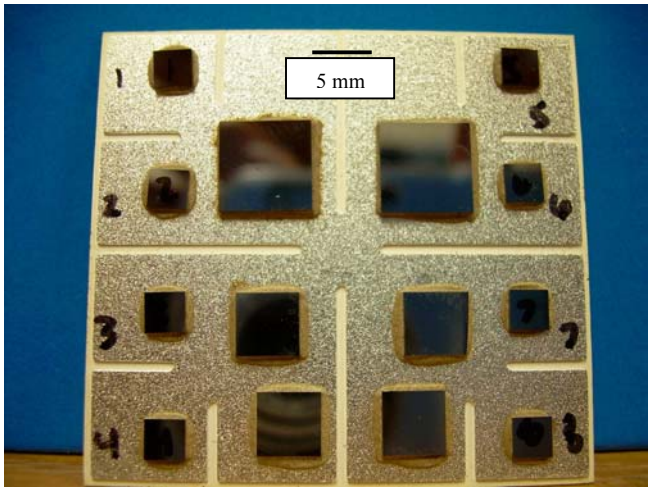

(a)

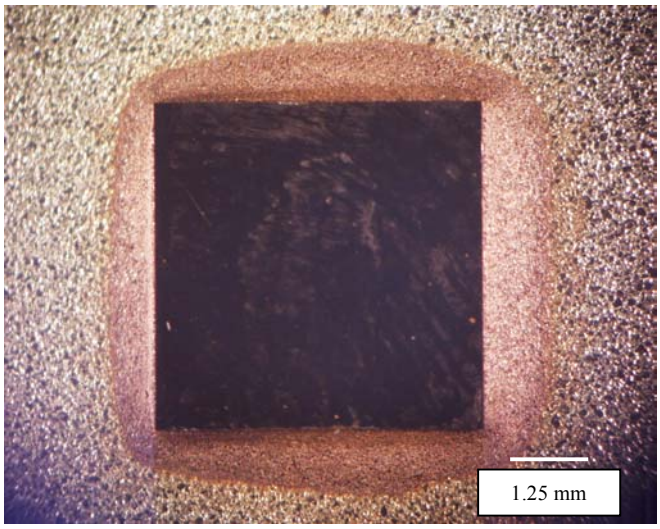

(b)

Figure 59. Typical fully populated DBC substrate fabricated with the TLPS process. (a) The three die sizes are illustrated. (b) Detail of a 5mm square die attached with the Ag-In paste using the TLPS process.

7.3.2.3. Die shear test:

The mechanical strength of the attach system was assessed by means of a standardized die shear test. This destructive method measures the maximum shear load to failure. The fractographic analysis of the surfaces provided insights into the fracture mode and possible failure mechanisms. The die shear test was performed according to the MIL-STD883G Method 2019.7 [74]. For this investigation, the equipment and test parameters were as follows: a Dage 2400 shear tester was used with a DS 20 Kg-F load cell, the test was set as destructive at a test velocity of 200 μm/s, and a test height of 200 μm. A total of eight (8) 3mm square dice per solder paste were tested. Failure was based on the measured force required to cause complete separation in conjunction with a qualitative description of the fracture surface. The shear strength of an attachment material is reported as the force required to shear the die from the substrate; values below the specified 2.5 Kg-F (Fig. 2019-4 in Ref. [74]) constitutes a failure. Results from this test must include force data together with the separation category, i.e. a description of the physical appearance of the specimen.

Shear strength data for revealed that the proposed attach material fulfilled the minimum requirements of the standard, with all samples testing above 4 Kg-F. Figure 60 shows a plot of the shear strength (MPa) as function of weight percent indium. From this chart it was observed that the strength of the material initially went up with increasing indium content, but reached a plateau at approximately 8 MPa. It is worthwhile noting that even though the strength did not show a considerable

improvement at higher indium compositions, less scattering occurred in the response as given by the 95% confidence interval (error bars). Experimental data proved that in fact, the improved fractional density had a positive influence on the mechanical strength.

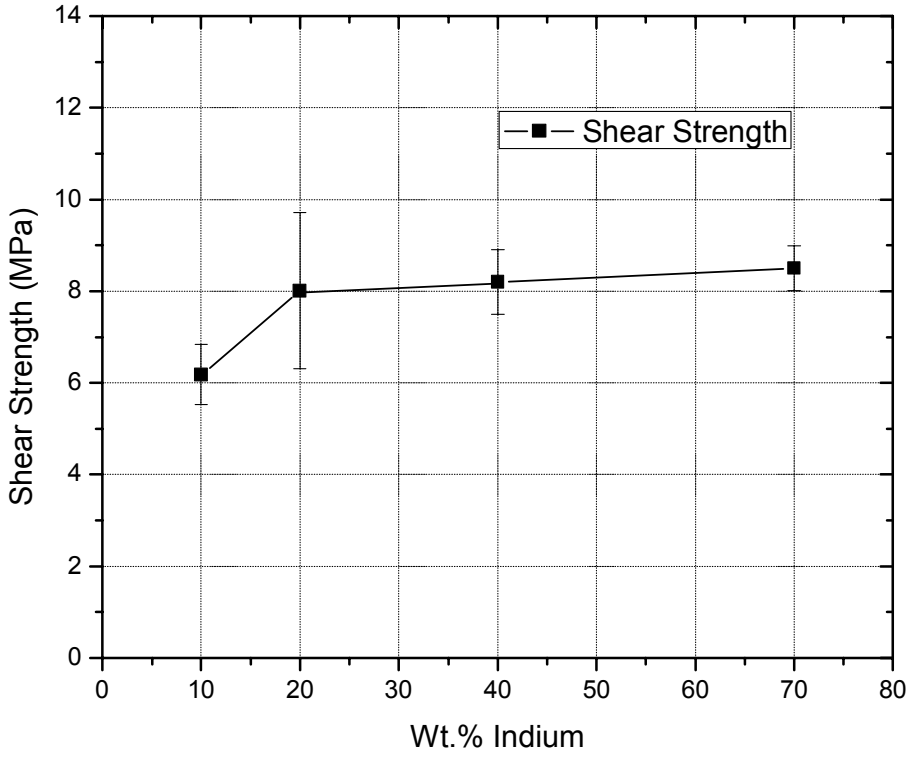

Figure 60 . Measured shear strength for Ag-In sintered material as function of indium composition in the mixture. Markers represent the mean value whereas the error bars depict the 95% confidence interval of the experimental data.

Figure 61 shows a combined plot from which the effect of indium addition on fractional density and strength is evident. From this chart it can be inferred that 8 MPa might be a limit to the shear strength of the material. The effect of fractional density on shear strength is dominant for indium concentrations below 25%, this is evident from the intersection of this two properties as shown in Figure 61. Further

indium addition has a very limited impact on shear strength although its effect on fractional density is evident. The TLPS Ag-In material reached stable shear strength of 8 – 8.2 MPa above 25 Wt. In, suggesting it as a mechanical property of the formed alloy.

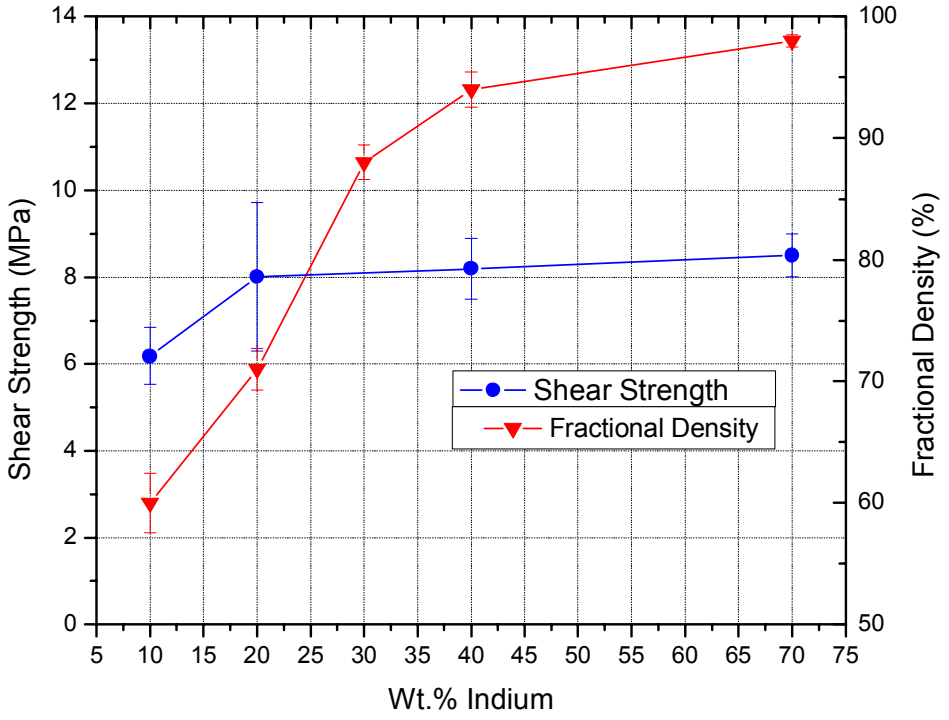

Figure 61. Shear strength of Ag-In TLPS material and fractional density as function of weight percent indium in the mixture.

In this section, the data from the die shear test has been attributed to the material's ability to withstand a shear load, and has been discussed as a bulk material property. This assumption was made valid based on the fractographic analysis performed on shear-tested samples. As given by the standard, die shearing not only provides mechanical strength information, but evidence of the dominant failure mechanism during fracture too. From the fractographic analysis it was revealed that all samples

failed cohesively through the attach material, suggesting acceptable adhesion to both the die and substrate. Evidence of this can be observed in Figure 62, in which the DBC substrate and matching die are illustrated.

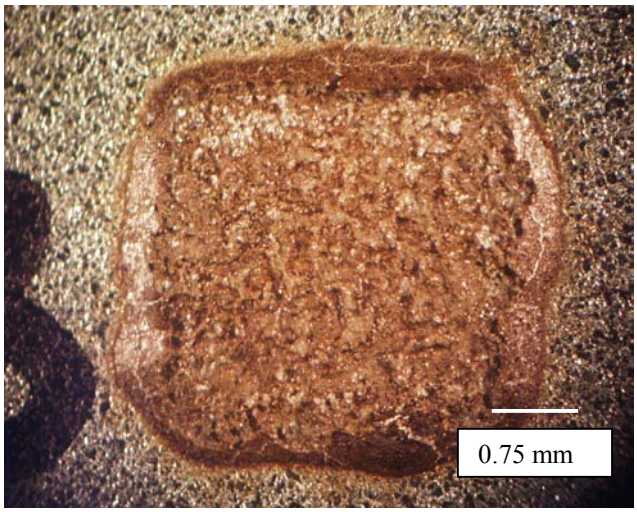

(a)

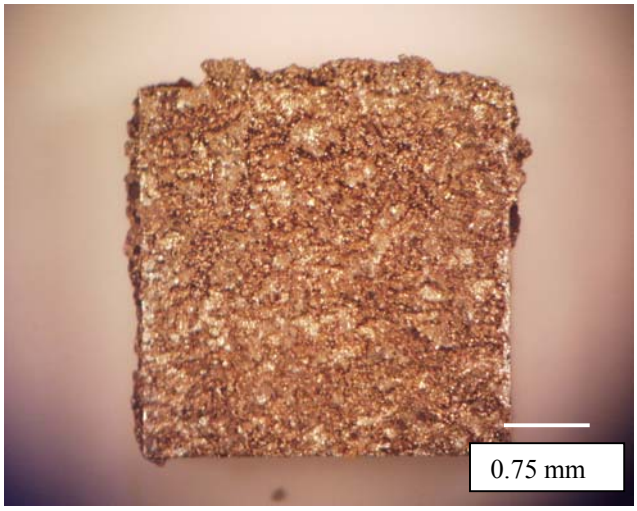

(b)

Figure 62. Fractograph of sample after die shear test. (a) Attach material on the DBC substrate showing evidence of good adhesion. (b) Matching die showing adhesion of the attach material on its surface confirming that failure occurred through the bulk.

The fracture surfaces revealed that the morphology of this material is quite unique. The Ag-solid solution matrix together with the γ precipitates may contribute to its

mechanical properties, but the ligament features of the cellular structure are also critical. Sintered materials consist of a network of pores interconnected by a solid; such a structure is naturally weaker than a continuous solid counterpart due to the reduction in material capable of withstanding the applied load. Figure 63 depicts a backscattered scanning electron image of the fracture surface after the die shear test.

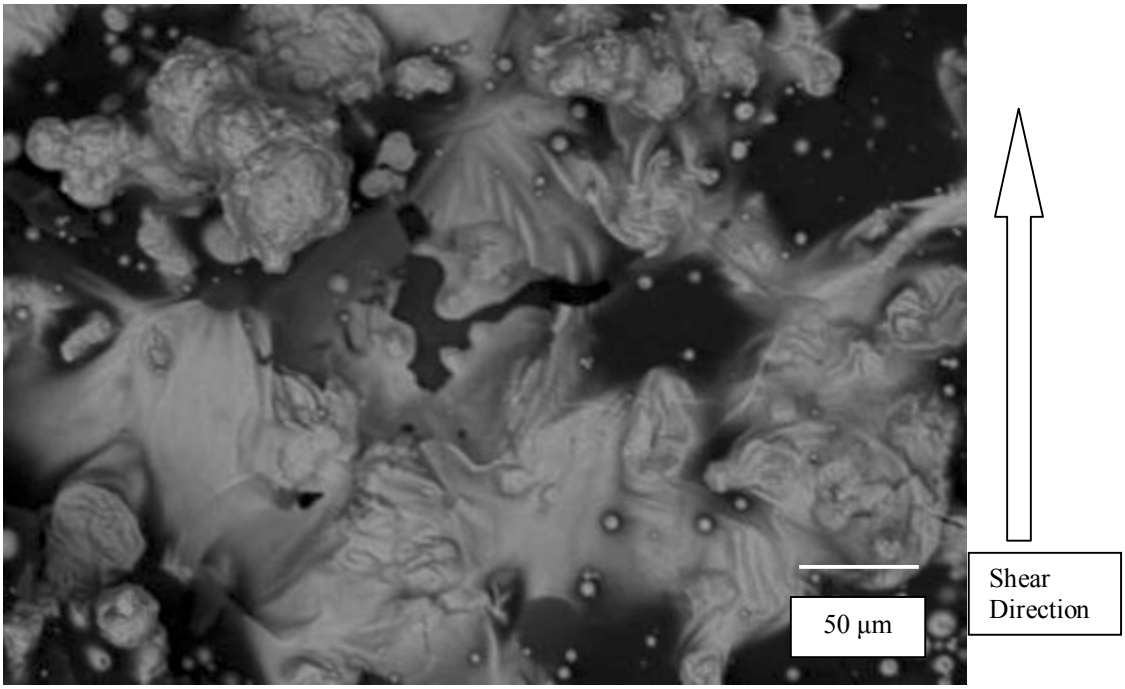

Figure 63. Backscattered image of the fracture surface after die shearing. Characteristic features of plastic fracture through the solid were observed. The arrow on the right indicates the shear direction during test.

In this image the porosity can be observed and the shearing effect on the solid portion is apparent, suggesting some plastic deformation occurred prior to rupture as evidenced by the tearing effect. This behavior is expected based on the known ductility of silver. Although this cellular structure constitutes a weaker system (reflowed metallic attachments typically exhibit shear strength values ranging from 15 – 35 MPa [20]), it provides a compliant morphology that might be capable of

absorbing higher strain energies. Materials such as this one have been used for impact absorption applications in what are known as metallic foams [66]. The ability of this material to absorb strain energy will be tested during the reliability assessment.

7.4 Analysis and Discussion:

In the mechanical testing, it was demonstrated that for all cases the fracture occurred cohesively through the material, an indication of good adhesion to both the substrate and die. The fractographic analysis revealed that the material failed in a ductile manner through the solid portions of the cellular structure, as evidenced by the plastically deformed regions in Figure 63. The porous nature of the material makes it a relatively weaker attach when compared to other metallic technologies, a reduction to about 1/3 of the shear strength (taking 25 MPa as the average [73]) of common metallic alloys was observed during this investigation. This might be a considerable difference, but in terms of acceptability, it surpasses the minimum requirements [74] in all cases. For higher fractional densities, i.e. higher indium additions, the material exhibited a more stable mechanical response, as given by a smaller scattering from the error bars (95%CI); but not a significant improvement in strength.

Among the objectives of this investigation, the development of a variable melting point Ag-In system by TLPS was the most important. The fundamental study of the in-situ alloying reaction and its kinetics modeling was the foundation for further exploration regarding a practical material/method for high temperature die attachment. The densification study proved that particle rearrangement and compaction were driven primarily by the amount of liquid formed during the process.

As expected from any porous structure, its physical properties were a function of not only the main elemental constituents but also of the morphology of its microstructure. Guided by this knowledge, an electrical, thermal, and mechanical characterization of the Ag-In material was performed with acceptable results presented in the previous sections. From a processing perspective, TLPS of pastes limited to ~ 40 Wt.% In and below provided a breakthrough in the soldering paradigm due to a shift to $T_m / T_p > 1$. It was also demonstrated, by the kinetics model, that higher processing temperatures resulted in faster times to the zero remaining In-rich phase condition, i.e. complete removal of the low melting point material and subsequent achievement of the shift in melting point. It was evident from this study that smaller amounts of indium corresponded to shorter the times to full solidification, so minimization of processing time would have resulted in a reduction of indium to zero; but obviously that would have defeated the entire purpose of the study. The indium is the MPD constituent that forms the liquid during the process, a phase necessary for the pressure-less densification during the sintering operation. Thus, the minimization of time proved to be part of the desired solution, but a method for calculating the necessary minimal addition of indium was needed. By using the trend in electrical conductivity, an optimal compositional range (indium Wt. fraction) was obtained. In this case, addition of 20 – 25 Wt.% In resulted in maximum conductivities and optimal fractional densities (~ 70 – 80%). Additional complementary information was obtained from the mechanical assessment, from which the best results were observed for indium additions above 20 Wt.% where the shear strength exhibited a more stable (less scattering) behavior. The shear strength of this material tended to stabilize at

around 8 MPa with a small improvement with incremental indium as shown in Figure 60. In order to provide an overall recommendation, an analysis of the combined properties was performed. Figure 64 shows a combined plot in which the measured shear strength and the electrical conductivity of the sintered Ag-In system are given as function of indium content (Wt. % In). In Figure 65 the same data is plotted as a function of the fractional density of the sintered structure.

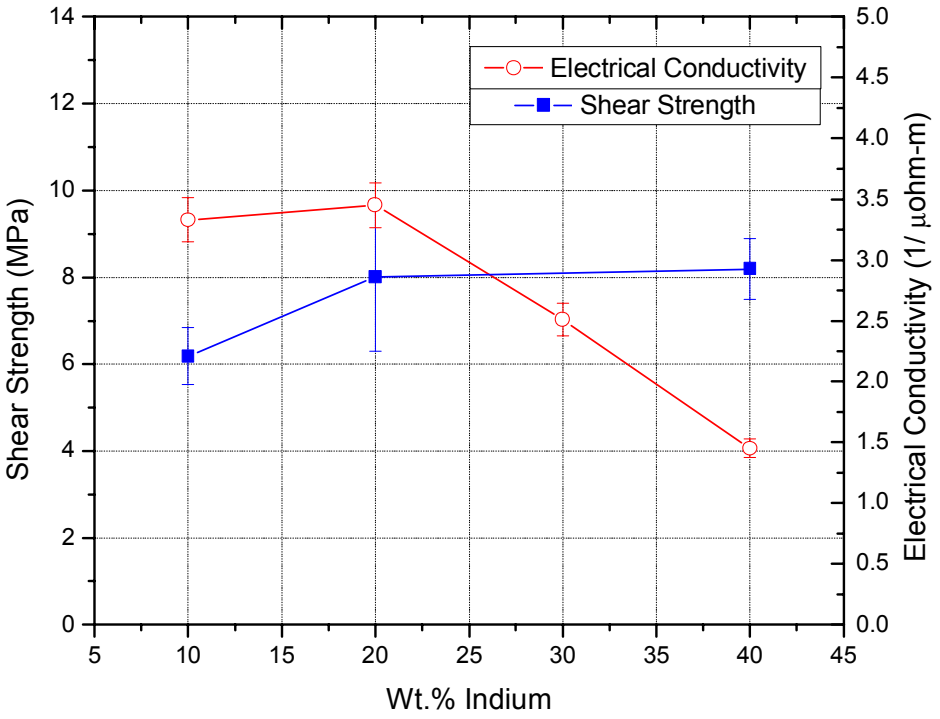

Figure 64. Combined plot showing the measured electrical conductivity and shear strength of the TLPS Ag-In system as function of indium content.

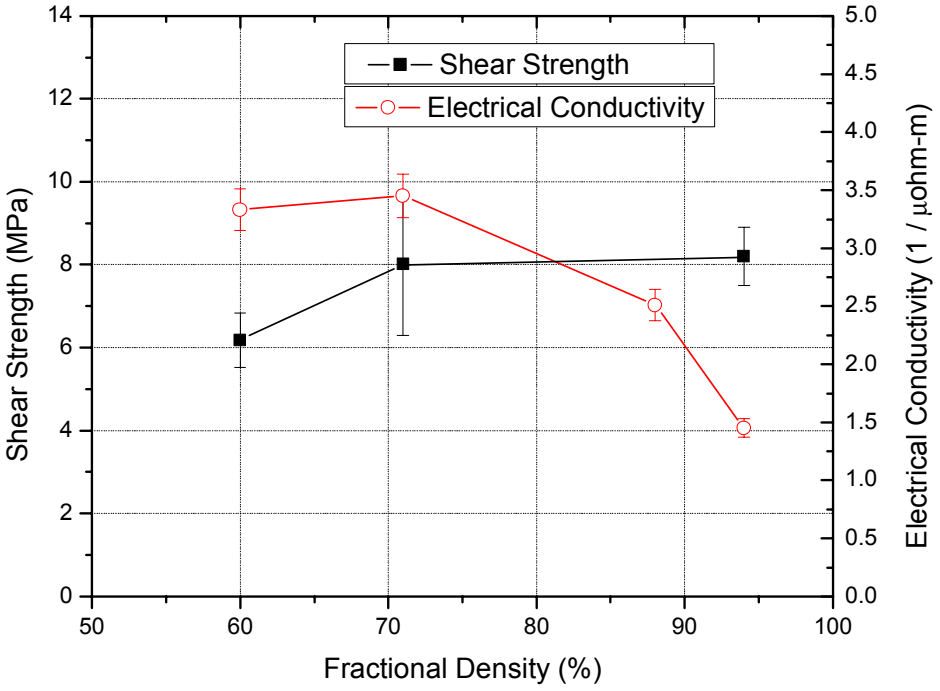

Figure 65. Combined plot showing the measured electrical conductivity and shear strength of the TLPS Ag-In system as function of fractional density.

From these two figures it can be observed that even though the mechanical strength shows a slight tendency to improve with increasing indium content, such an addition adversely affects the electrical (and thermal) conductivity. In order to have an optimal overall performance from this material, the indium addition should be controlled to values ranging from 20 to 26 Wt.%.

This compositional range provided encouraging results in terms of the feasibility of the proposed TLPS process for creating a suitable electronic packaging attach. From the kinetics model and the microstructural analysis, a paste with the suggested indium content can be processed at temperatures below 300°C and reach full transformation

in 60 minutes or less. Specific time-temperature responses can be obtained from the model developed as part of this investigation.

7.5 Reliability assessment:

Reliability refers to the probability that a system can perform its intended function under the specified life cycle operating environmental conditions for a specific period of time. During this investigation, a reliability test was performed on die-attached specimens using the Ag-In TLPS paste fabricated with the best known method. This best embodiment was defined by several characteristics, including composition, heating rate, processing temperature, and isothermal holding time. A mixture was considered first. A mixture consisting of 75 Wt. %Ag – 25 Wt. %In was selected based on a trade-off of its resulting fractional density, electrical/thermal conductivity, and mechanical strength. The processing profile was tailored using the kinetics model so that complete transformation of the In-rich phase together with its accompanying microstructural evolution was obtained. The settings for the sintering process were as follows: heating rate = 60°C/min., processing temperature = 300°C, and isothermal holding time = 60 minutes. Details of the test specimen fabrication using the solder paste together with the TLPS profile are described in the following section.

7.5.1. Fabrication:

Test samples were fabricated using the technique described in the fabrication sequence for mechanical samples in section 7.3.2.2. A laser cut stencil with apertures for three die sizes was used for printing the paste onto the metallized alumina DBC

substrates (Figure 58). Back side metallized Si chips were placed in position and the entire assembly was processed in the sintering furnace. A representative as-built sample is depicted in Figure 59. Table 15 summarizes the fabrication matrix and specifications for the reliability test.

Table 15. Specifications for test specimens used during the reliability test.

Die				
Material	**Size**	**Thickness**	**Metallization**	**Deposition**
Si	3.3mm X 3.3mm 5mm X 5mm 7.5mm X 7.5mm	500 μm	Cr – Adhesion Ni – Barrier Ag - Bonding	PVD (electron-beam evaporation)
Substrate				
Material	**Metallization**		**Deposition**	
Al_2O_3	DBC (Direct Bond Copper) Ni – Barrier Layer Ag – Bonding Layer		Ni: Electroless Plating Ag: e-beam evaporation	

7.5.2. Reliability test:

The ability of this material to render its intended function throughout its expected life cycle was studied by means of passive thermal cycling. When test specimens are subjected to thermal cycling, the global mismatch in coefficient of thermal expansion between the substrate and die will cause stresses to be placed on the attach material. By subjecting a statistically significant number of samples to different temperature cycles (given by ΔT), distinct strain values are developed. Two different accelerated thermal profiles were generated for this investigation (HT and LT), which were carried out in a SUN EC12 environmental chamber. The high temperature profile (HT) was designed to subject the samples to temperature cycling from -55°C to 185°C with a 5 minute dwell at -55°C and a 10 minute dwell at 185°C for a ΔT of 240°C at a T_{mean} of 65°C. The low temperature profile (LT) was designed to subject the samples to temperature cycling from -55°C to 150°C with a 5 minute dwell at

-55°C and a 10 minute dwell at 150°C for a ΔT of 205°C at a T_{mean} of 47.5°C. Specifications of the LT profile correspond to the test condition H and soak modes 2 and 3 as given by the JEDEC standard temperature cycling specification [75]. A schematic of both profiles is given in Figure 66. The combination of the three die sizes (Table 15) with the two thermal profiles (HT and LT) provided a total of six strain levels. Samples were removed from the temperature cycling chamber after every 50 cycles for inspection using X-ray imaging. Failure of the die attach was to be defined based on crack propagation through the bond area, as observed by X-ray. Joints were to be deemed as failures when the crack/delamination exceeded 20% of the bonding area. Initial characterization of the as-built samples was used as the base line for failure definition.

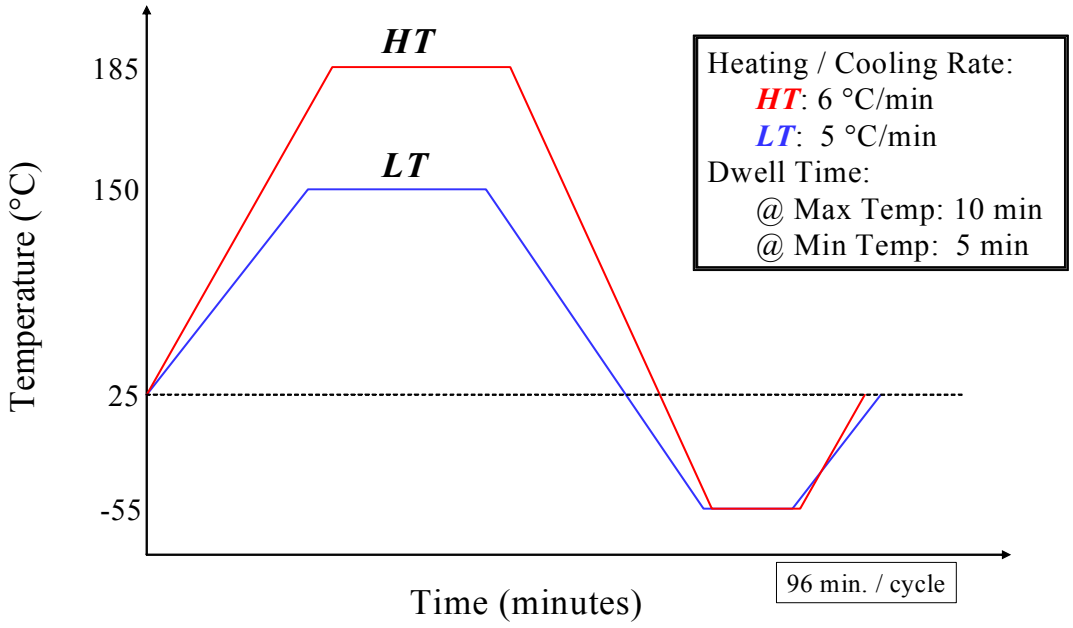

Figure 66. Schematic diagram of the two thermal cycling profiles used during the reliability assessment.

7.5.3. Results and Discussion:

A total of 2,200 LT cycles were completed for all three die sizes without observing discernible degradation of the attach material as revealed by X-ray and physical inspection. For the HT profile, no failures were observed after 1,000 cycles for all sizes, though extensive damage to the DBC substrates was observed. Separation of the copper from the ceramic material began at the corners of the substrate and fracture progressed as a crack through the ceramic. From these observations it was revealed that the proposed Ag-In TLPS attach material outperformed the DBC substrates during the thermal cycling test. Results obtained from life cycle data (cycles) were comparable to the observed performance of the Pb-rich solder; the most widely used material for high temperature electronic applications [9][10]. When compared to lead-free alternatives, it outperformed technologies such as sintered Ag-nano colloids as well sintered silver nano-particle pastes [9][10]. Both of these technologies resulted in complete separation of the die from the substrate. For the case of the LT test all samples, of the aforementioned two technologies, failed at or before 700 cycles, whereas for the HT condition all samples failed at or before 400 cycles. To avoid the uncertainties associated with the subjective characterization of damage from an X-ray image (from which no discernable change was observed after 2,200 cycles), the failure criterion for the relative reliability study was changed to cycles for complete separation [10]. For all attach materials tested under similar conditions, the data was recorded using this new failure definition. At the conclusion of the investigation, the Ag-In TLPS material had significantly outperformed all of the

tested lead-free alternatives, and proven that its reliability was competitive with Pb-rich attaches for high temperature applications.

7.6 Conclusion:

The resulting liquid phase sintered material exhibited a porous structure as expected from the TLPS powder metallurgy technique. The densification of this material was studied in terms of the fractional density, which was demonstrated to be influenced heavily by the indium fraction in the mixture. Transport and mechanical properties of porous materials are known to be sensitive to their fractional density (packing). From this investigation an order of magnitude (1/10) reduction of electrical conductivity was obtained when compared to a fully dense solid. The addition of indium proved to increase the densification of the system, but it also introduced an impurity effect on the final overall electrical performance. Optimization of the electrical conductivity of this material, while yielding an acceptable fractional density and not affecting its shifting melting point capability, resulted in a recommended indium addition of 20-25 % by weight.

The mechanical integrity of the system is a critical aspect of its feasibility as a die attach. During this investigation the mechanical strength was assessed by die shear. Indium additions had a dominant effect on fractional density, which indeed affected the mechanical response of the system. Increasing fractional density resulted in a stable shear strength of 8 – 8.2 MPa with failure by cohesive fracture through the bulk. Results suggested that a minimum indium addition of approximately 20 Wt.% should be used to optimize the strength of the Ag-In TLPS system. A combined

analysis, from which transport properties, mechanical strength, and fractional density were optimized, resulted in a final recommendation of 20 – 26 weight percent indium to provide the best embodiment. In this case, "best embodiment" is defined as an attach with competitive properties as compared to other metallic alternatives for high temperature environments, in addition to the superior advantage of a $T_m / T_p > 1$. From the kinetics model, achievement of a full transformation into a new melting point could be accomplished in a processing time of 60 minutes or less, depending on the processing temperature.

From the reliability assessment it was concluded that this material is capable of withstanding high temperature environments, outperforming other alternatives such as silver nano-colloids as well as silver nano-pastes. The cellular nature of this structure together with its new higher melting point, which inhibits creep damage, was theorized as the cause for the obtained reliability.

Chapter 8: Conclusions

Transient liquid phase sintering was presented as a method to obtain the desired shift in melting point of the Ag-In system. The successful accomplishment of this melting temperature transformation provided a breakout from the conventional soldering process temperature hierarchy in which a novel $T_m / T_p > 1$ ratio was demonstrated. The transient nature of this in-situ alloying process required a fundamental understanding of its reaction kinetics. A differential scanning calorimetry technique (DSC) was employed from which the progression of the process, in terms of the remaining fraction of In-rich phase, was studied. This experimental method provided an accurate tool for understanding the reaction kinetics, and served as the basis for the estimation of a reaction rate as a function of silver particle size. A diffusion based analytical model was used to provide the physical significance of the DSC method. Phase transformations from DSC traces were confirmed from the microstructural analysis where phase evolution, as a function of isothermal holding time, was revealed together with morphological aspects of the Ag-In system's internal structure.

A comprehensive kinetics model for the entire time regime during the TLPS process was developed using response surface methodology (RSM). This prediction model provided a tool for tailoring the process as function of controllable parameters such as heating rate, processing temperature, isothermal holding time, silver particle size, as well as mixture composition. Contour maps from this empirical prediction model proved useful in tailoring the process for particular application conditions. Model adequacy was confirmed using a mechanistic diffusion based model for powder

mixtures, which provided an estimation of the response for the isothermal solidification stage, but not for the later stages. The mechanistic model concurred with the empirical method during the time frame governed by the isothermal solidification stage, in which the fraction of remaining In-rich phase obeyed the square root law. Overestimation of solidification time from the mechanistic model was mainly attributed to geometrical factors, primarily to the assumption of mono-sized and perfectly shaped particles considered for the mathematical solution. The RSM proved to be a more accurate tool, and more importantly, it was capable of modeling the three stages of the TLPS process as inter-dependant steps. The metallographic analysis yielded crucial information about the progression of the TLPS process in terms of microstructural evolution as a function of holding time. It was confirmed that a transition exists, detected by the statistical analysis from the DSC experiment as well, at which the low melting In-rich phase matrix is overtaken by the growing Ag-rich solid solution network. After this point, the remaining In-rich phase was present as the discontinuous phase which subsequently delayed the diffusional solidification process; a condition that was not recognized by the mechanistic model. The combination of the experimental DSC method together with the mechanistic approach for studying the reaction kinetics, assisted by metallographic observations, resulted in a comprehensive fundamental characterization of the TLPS process kinetics for the Ag-In paste.

Fabrication of samples for the mechanical and electrical characterization was done following the best method as defined by the kinetics model. In all cases, specimens

were fabricated so that complete transformation of the In-rich phase was attained, which resulted in the desired final melting point shift. By standardizing the silver particle size (-500 Mesh - 25μm), heating rate (60°C/min.), processing temperature (300°C), and isothermal holding time (60 min.), a stable microstructure was obtained. The fractional density of the resulting porous material proved to be governed by the fraction of indium addition in the mixture. Excellent consolidation was observed with increasing indium content, but achievement of a transient low melting phase was limited to an upper bound defined by the maximum solid solubility of indium into a silver-rich phase. The effect of fractional density on the electrical conductivity of the sintered material was analyzed, from which an interesting competing effect was established between increasing density and declining conductivity as function of indium addition. The mechanical integrity of the material was assessed and its correlation with fractional density was established. A combined analysis, for which maximization of electrical conductivity together with improved mechanical strength was the goal, yielded a recommended indium addition range between 20 – 26 weight percent. This mixing ratio of (74 – 80)Wt.% Ag – (20 – 26)Wt.% In resulted in a shifting melting point system achievable in holding times of 60 minutes or less that exhibited competitive electrical, thermal, and mechanical properties.

The reliability of this material was assessed for a specific set of conditions by means of passive thermal cycling. Within the test conditions it was concluded that this material is capable of withstanding high temperature environments, outperforming other alternatives such as silver nano-colloids as well as silver nano-pastes. The

cellular nature of this structure together with its new higher melting point, which inhibits creep damage, was theorized as the cause for the obtained reliability.

Chapter 9: Contributions

The main objective of this investigation was to develop a shifting melting temperature solder paste by means of a TLPS method which could serve as an enabler for high temperature electronic packaging. The fundamental understanding of the underlying in-situ alloying reaction at the processing temperature was identified as critical for this investigation. A microstructural characterization of this novel material as well as an electrical and mechanical assessment was performed as part of the feasibility study. From this investigation the following contributions can be listed:

- Developed a formulation for an Ag-In paste that when processed using a TLPS technique, exhibited a shift in its melting temperature.
- Demonstrated a major advancement over the conventional soldering process temperature hierarchy, in which a novel $T_m / T_p > 1$ was established while using traditional, pressure-less assembly methods for a solder paste. Thermal stability of the newly formed alloy was confirmed to 500°C.
- Developed an empirical model for the reaction kinetics of the system as function of controllable parameters, which served as a tool for process control.
- Determined the stages of the Ag-In TLPS progression based on microstructural evolution studies.
- Established the effect of fractional density on shear strength and electrical conductivity as a function of indium weight fraction.

- Determined an optimal paste formulation in terms of compositional range together with optimum processing parameters as suggested from the kinetics model.
- Demonstrated a proof-of-concept using the material as a die attach for a high temperature package. The reliability of the system was confirmed by passive thermal cycling.

Appendices:

Appendix 1. DSC data for phase I DOE

Paste A:

Sample	HoldingTime (min)	Weight (mg)	Eu Melt.Temp (°C)	Eu Endo Start (mW)	Eu Endo End (mW)	φ Melt. Temp (°C)	φ Endo Start (mW)	φ Endo End (mW)	φ Exo Start (mW)	φ Exo End (mW)	Eu Exo Start (mW)	Eu Exo End (mW)	% Remaining In [(Integration ratio)*23]
22	0	45	146	57.4	63.6	174	57.4	89.8	0	-4.8	0.2	-2.9	20.5
23	0	62	147	69.5	77.6	172	70	109.5	-10	-15.2	-12.2	-16.1	19.1
24	0.5	73	147	77.2	84.7	172	74	130	-17.1	-22.1	-18.5	-21.8	13.1
25	0.5	77	147	82	90.8	173	77	135	-18.1	-23.6	-20	-23.6	13.6
5	1	44	146	53	57.3	172	53	87.6	-7.6	-9.1	-6	-7.7	8.2
7	1	69	146	70.7	78.6	173	70.7	129.7	-19.6	-23.2	-18.5	-21.6	10.0
8	2	58	146	64.5	68.7	174	64.5	99	-13	-14.9	-11.8	-13.4	9.0
9	2	80	146	80.9	89.6	174	80.9	139.2	-23.7	-26.7	-22.5	-24.6	7.6
10	5	89	146	64.8	70.7	174	64.8	104.6	-10.5	-11.7	-9.1	-9.9	4.4
11	5	72	147	77.2	84.6	174	77.2	124.3	-20.2	-21.5	-18.8	-19.6	3.9
12	10	73	147	78.7	84	175	78.7	118.4	-19.4	-20	-17.7	-18	2.0
13	10	56	146	65.5	69.6	174	65.5	99.6	-11.2	-11.8	-10.1	-10.5	2.6
14	15	64	148	69.4	73.2	175	69.4	98.6	-11.5	-12.1	-10.5	-10.8	2.7
15	15	57	148	62.9	66.9	174	62.9	92.3	-8.1	-9	-8.5	-8.8	3.6
16	25	48	148	58.5	61.9	174	58.5	84.8	-2.7	-3.4	-3.1	-3.4	3.4
17	25	66	148	75.4	79.1	174	75.4	108.1	-6.7	-7.4	-7	-7.2	2.5
18	40	65	148	71.9	75.3	174	71.9	101.2	-9.4	-10.1	9.8	10.1	3.1
19	40	67	149	79.7	83.3	174	79.7	109.8	-4.2	-5.2	-5.1	-5.4	3.9
20	60	70	149	82	86.1	174	82	116.1	0	0	-4.2	-4.3	0.3
21	60	64	149	79.4	84.3	173	79.4	114	0	0	0	0	0.0

Paste B:

Sample	Holding Time (min)	Weight (mg)	Eu Melt.Temp (°C)	Eu Endo Start (mW)	Eu Endo End (mW)	φ Melt. Temp (°C)	φ Endo Start (mW)	φ Endo End (mW)	φ Exo Start (mW)	φ Exo End (mW)	Eu Exo Start (mW)	Eu Exo End (mW)	% Remaining In [(Integration ratio)*32]
33	0	72	147	70	92.7	170	70	109.4	-14.5	-25.8	-19.8	-27.3	30.3
34	0	45	147	54.1	69	168	54.1	81.9	0	-7.8	-4	-8	27.6
35	0.5	46	147	56.9	73.6	170	56.9	85.6	6.8	0.1	-0.5	-4.5	23.6
36	0.5	56	147	62.7	82	168	62	99.3	-3.6	-10.1	-9	-12.6	17.8
17	1	60	147	58.4	82.4	168	58.4	95.8	-5	-12	-9.4	-10.6	13.4
25	1	56	146	54.2	72.7	168	54.2	90.5	-13.7	-6.5	-13.7	-12.6	15.1
18	2	53	147	57.8	76	167	57.8	91.5	-4	-10.3	-7.3	-8.4	14.3
26	2	50	145	55.1	70.4	168	55.1	86	-8.3	-2	0	0	13.6
19	5	60	147	60.9	88	168	60.9	104.8	-4	-11.3	-5	-5.4	10.8
27	5	53	147	58.1	75.4	168	58.1	91.3	-7.6	-1.2	-2.8	-2.1	14.1
20	10	65	147	64.4	92.5	168	64.4	111.4	-4.7	-10.5	-6.5	-7.6	9.2
28	10	51	147	58.8	73.9	168	58.8	90.6	-2.3	2	0.2	0.95	10.8
21	15	66	147	67.3	94.4	168	67.3	111	-5.5	-10.3	-6.6	-7.8	8.5
29	15	51	146	60.8	76	168	60.8	91.5	0.4	4	1.12	2.4	10.6
22	25	57	147	59.6	77	168	59.6	96.5	0	-3.2	-1.1	-2.1	7.7
30	25	51	147	60.9	76	168	60.9	92	1.9	3.96	3	3.9	6.4
23	40	53	146	59.6	81.7	168	59.6	96.6	1.7	3.4	1.7	2.1	3.6
31	40	43	146	55.1	70.2	168	55.1	84.3	6.6	8	0	0	3.2
24	60	61	146	64.9	88.5	168	64.9	107.8	0.3	1.7	0	0	2.1
32	60	68	147	68.8	89.3	169	68.8	109.3	-3.7	-2.5	0	0	2.0
37	90	50	147	57.9	76.7	168	57	90	2.3	1.6	0	0	1.4
38	90	41	146	50.7	68.6	168	50.7	79.4	5.5	5.2	0	0	0.6

Paste C:

Sample	HoldingTime (min)	Weight (mg)	Eu Melt.Temp (°C)	Eu Endo Start (mW)	Eu Endo End (mW)	φ Melt. Temp (°C)	φ Endo Start (mW)	φ Endo End (mW)	φ Exo Start (mW)	φ Exo End (mW)	Eu Exo Start (mW)	Eu Exo End (mW)	% Remaining In [(Integration ratio)*27]
S1C	0	56	147	48.7	71.4	170	48.7	66.2	-6.8	-15.7	0	0	22.1
S2C	0	63	148	54.8	78.5	170	54.8	71.1	-7.2	-17	0	0	24.5
S3C	0.5	65	147	56.3	81.6	171	56.3	71	-8.1	-17.8	0	0	24.3
S4C	0.5	61	147	49.9	67	171	49.9	71.9	-8.2	-17.2	0	0	23.0
S5C	1	51	147	48.3	70	171	48.3	65.2	-1	-9.5	0	0	22.0
S6C	1	46	147	47.6	67.3	170	47.6	63	1.1	-5.2	0	0	17.9
S7C	2	67	147	53.7	72.5	172	53.7	76	-10.4	-16.6	0	0	15.1
S8C	2	52	147	50.7	75.2	171	50.7	60.8	-2	-6.5	0	0	13.0
S9C	5	59	147	56.7	84.5	171	56.7	67	-4.4	-7	-3.7	-4.6	9.2
S10C	5	64	147	59.1	93.1	171	59.1	68.2	-6.6	-9.5	-5.1	-6.2	9.3
S11C	10	62	147	57.9	93.8	172	28.7	55.5	-4.6	-6.2	-3.3	-4.2	4.0
S12C	10	64	147	59.8	86.4	171	59.8	74.8	-3	-3.9	0	0	2.2
S13C	15	65	147	62.3	94.8	172	57.4	63.5	-5.7	-6.5	0	0	2.1
S14C	15	53	147	55.2	88.7	171	50.9	56.4	0.6	-0.1	0	0	1.8
S15C	25	46	147	47.9	62.7	170	47.9	71.7	5.7	5.3	0	0	1.0
S16C	25	60	146	48.5	73.9	172	48.5	69.2	-7.5	-8	0	0	1.1
S17C	40	54	147	46.2	72.5	172	46.2	57.7	-2.9	-3.2	0	0	0.8
S18C	40	49	146	43.8	57.9	170	43.8	65.8	-0.7	-0.88	0	0	0.5
S19C	60	69	147	56.8	74.9	170	56.8	85.4	0	0	0	0	0.0
S20C	60	70	147	56.7	91.4	171	40	56.5	0	0	0	0	0.0

Appendix 2. Kinetics model for Pastes A and B:

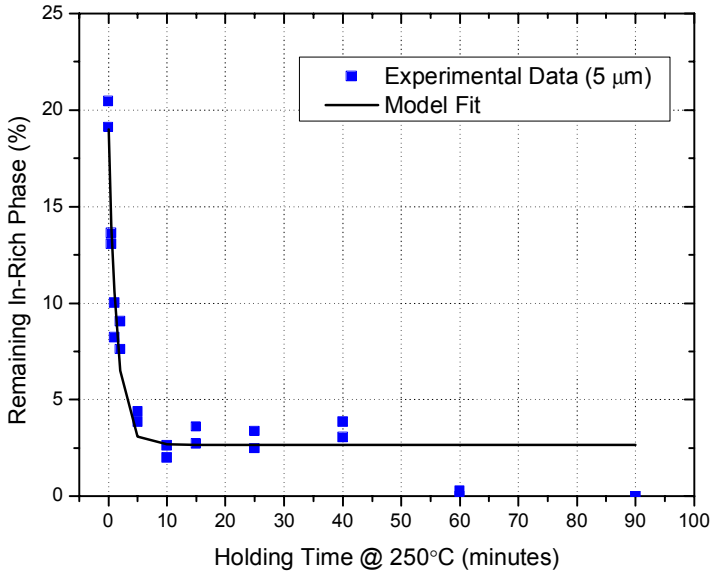

Prediction of the Remaining In-rich material by model fitting the experimental data from Paste A (5 μm silver particle size). Markers denote complete Paste A DSC data from the experiment, the solid line is the prediction from the model.

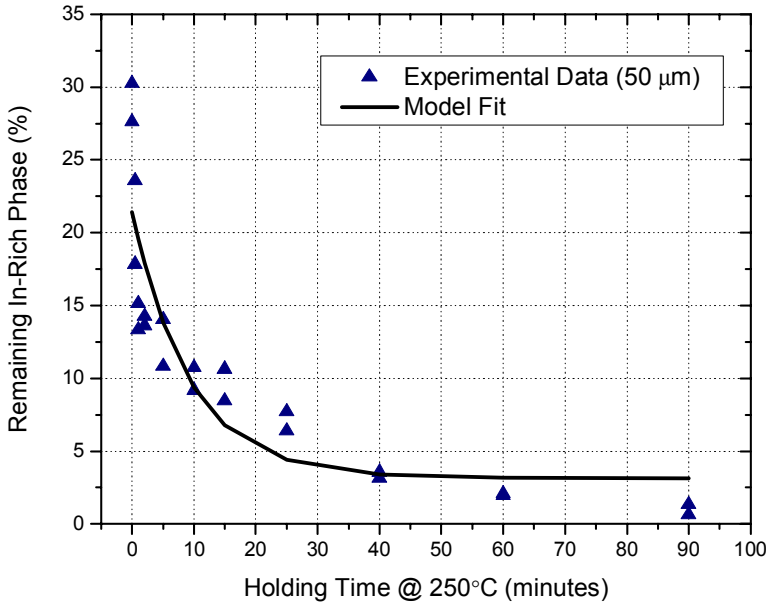

Prediction of the Remaining In-rich material by model fitting the experimental data from Paste B (50 μm silver particle size). Markers denote complete Paste B DSC data from the experiment, the solid line is the prediction from the model.

Appendix 3. Correlation of empirical constants and Ag particle size:

Scatter plot of y_o and silver particle size (μm):

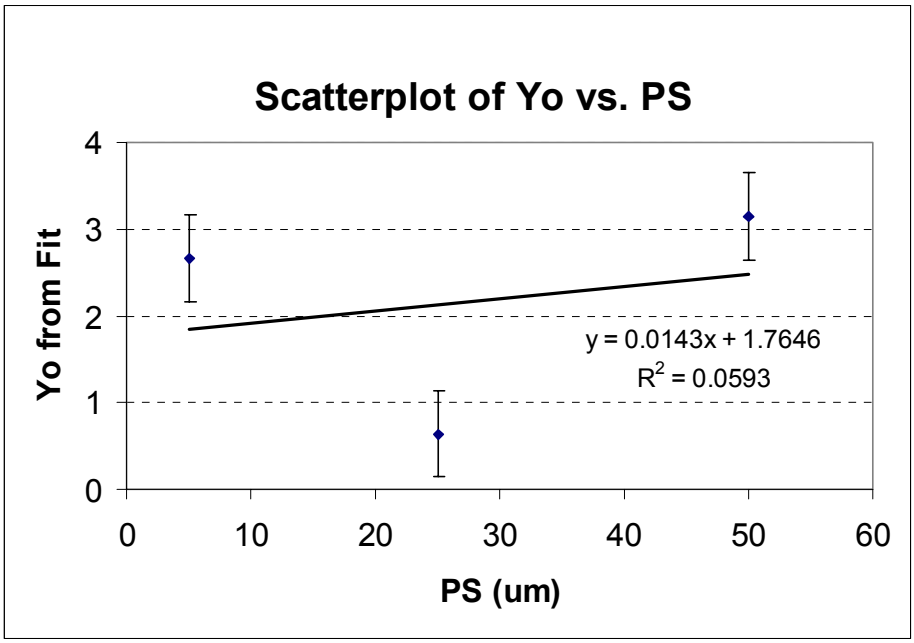

Scatter plot of A_1 and silver particle size (μm):

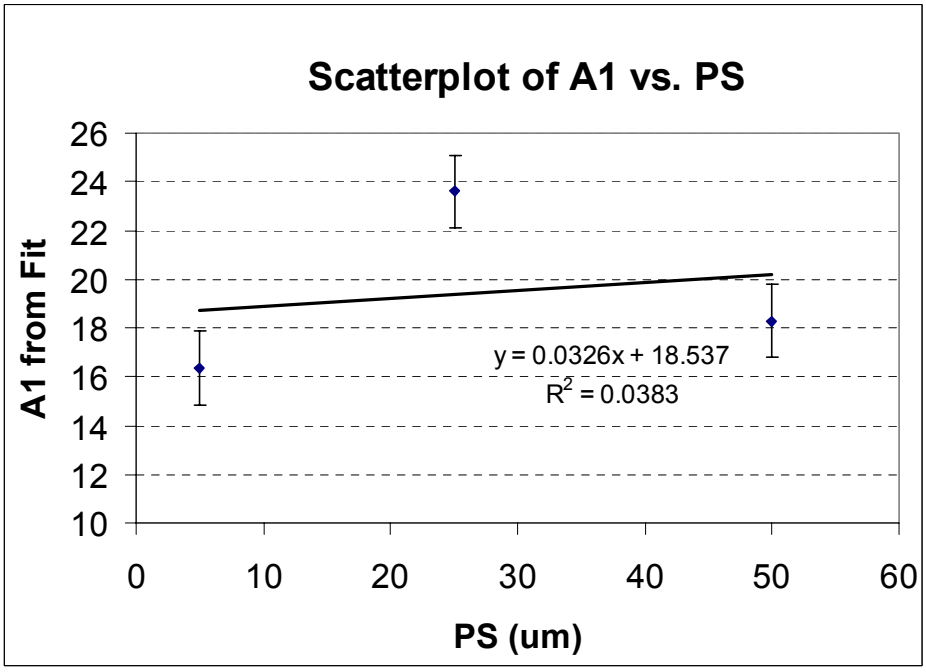

Scatter plot of τ and silver particle size (μm):

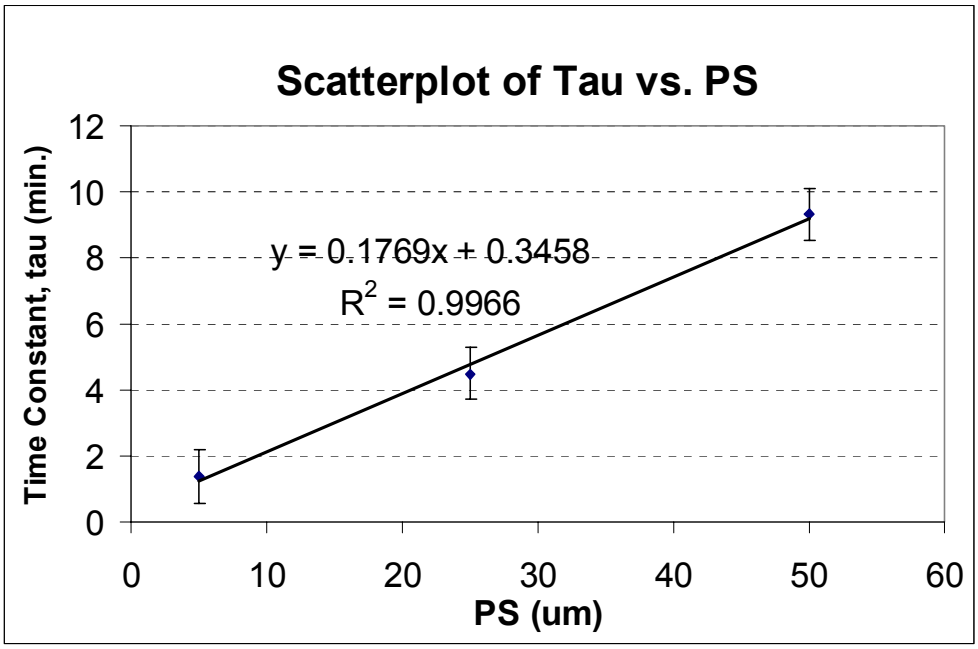

Appendix 4. DSC data for phase II DOE:

Data for isothermal time = 0

Sample	HoldingTime (min)	Weight (mg)	Eu Melt.Temp (°C)	Eu Endo Start (mW)	Eu Endo End (mW)	φ Melt. Temp (°C)	φ Endo Start (mW)	φ Endo End (mW)	φ Exo Start (mW)	φ Exo End (mW)	Eu Exo Start (mW)	Eu Exo End (mW)	Normalized % Remaining In [(Integration ratio)*Initial In Wt%]
1	0	30	156	35.21	50.12	170	35.21	38.22	7.16	5.76	6.68	6.5	8.8
2	0	52	146	31.45	53.47	166	31.45	86.6	-8	-16.73	-5.1	-7.6	14.6
3	0	35	146	38.26	45	166	38.26	78.88	1.48	-7.18	0	0	18.3
4	0	43	156	42.35	72.4	170	34.6	37.5	4.16	3.54	0	0	1.9
5	0	35	146	29.5	35.9	166	29.5	80	6.9	-0.12	6.2	5.5	13.6
6	0	50	146	43	60.6	166	43	85.4	0.91	-11.7	-2.2	-23.5	56.5
7	0	46	156	45.17	69.5	170	45.17	52.2	2.45	1.83	0	0	2.0
8	0	57	146	51.2	81.3	168	51.2	104	-5	-13.1	-4.1	-23.6	33.3
9	0	52	146	48.1	50.8	166	48.1	113.1	0.98	-9.8	-1.1	-5.5	22.4
10	0	50	156	35.1	54.4	166	35.1	53.5	2.1	1.8	0	0	0.8
11	0	45	146	33.8	39.8	166	33.8	94.7	2	-7.9	0	0	14.8
12	0	42	156	34.5	57.3	170	27.6	32.1	7.3	5.8	0	0	5.5
13	0	48	146	34.2	40.2	167	34.2	97.6	1.5	-9.9	0	0	16.4
14	0	50	146	47.2	51.82	170	47.2	110.5	0	-14.5	0	0	21.3
15	0	50	146	35.2	60.5	167	35.2	88.2	4.4	-9.9	1.2	-11.6	34.6
16	0	50	156	37.6	57.2	166	37.6	48.1	4.5	4	0	0	1.7
17	0	55	156	37.8	66.6	170	28.3	35.2	0.7	0.07	0	0	1.8
18	0	43	156	48	69.2	170	48	53	7.5	6.9	0	0	2.3
19	0	45	146	46.7	74.2	167	46.7	87.4	9.2	-2.9	4.6	-15.2	46.8
20	0	41	156	46.5	68.4	170	38	43.7	11.4	8.5	0	0	10.5
21	0	35	156	35.6	51.2	170	35.6	45.4	11.8	10.6	0	0	4.7
22	0	41	146	45.7	79.8	169	45.7	86.7	6	0	6.83	-3.5	21.7
23	0	38	156	47.7	70	170	38.7	45.5	15.9	13.8	0	0	7.2
24	0	42	156	48	71.5	170	39.9	46.2	9	7.8	0	0	4.0
25	0	38	146	34.8	40	166	34.8	83	13.96	6.5	9.9	7.6	18.3
26	0	44	156	37.1	60.1	170	30.7	39.1	8.2	7.6	0	0	1.9
27	0	52	156	51.9	80.2	170	40.9	48.1	9	5.6	0	0	9.6
28	0	40	156	38.6	57.9	170	29.6	40	12	9.6	10.6	9.9	10.4
29	0	57	146	40.4	84.9	166	40.4	107.6	8.2	-8.1	3.4	-13.3	29.5
30	0	50	146	40.2	77.7	170	40.2	97.1	4.8	-6.4	4.3	1.1	15.3
31	0	57	146	65.2	81.1	168	65.2	133.5	14	0.7	6.3	0.46	22.7
32	0	45	156	37.6	57.5	170	37.6	45.6	8.1	6.5	0	0	5.7

Data for isothermal time = 0.5

Sample	HoldingTime (min)	Weight (mg)	Eu Melt.Temp (°C)	Eu Endo Start (mW)	Eu Endo End (mW)	φ Melt. Temp (°C)	φ Endo Start (mW)	φ Endo End (mW)	φ Exo Start (mW)	φ Exo End (mW)	Eu Exo Start (mW)	Eu Exo End (mW)	Normalized % Remaining In [(Integration ratio)*Initial In Wt%]
1	0.5	35	146	38.7	47.7	166	38.7	78.2	5.2	0	2.2	0	15.3
2	0.5	43	146	47.4	57.6	166	47.4	97.3	7.4	-5.2	0	0	21.0
3	0.5	57	146	35.1	74.1	166	35.1	92.5	-1.8	-11.4	-6.6	-18	21.8
4	0.5	53	146	39.8	56.5	166	39.8	102.6	3.7	-7.5	0	0	14.1
5	0.5	57	146	30.7	72.2	166	30.7	98.3	1.4	-15.3	0	0	15.3
6	0.5	47	156	37.1	57.6	170	27.3	38.7	8.01	7	0	0	3.2
7	0.5	63	156	57.7	89.9	170	45.5	52.2	1.4	-0.11	0	0	3.9
8	0.5	50	146	47.9	63	166	47.9	110.7	13.1	3.3	0	0	12.6
9	0.5	37	156	31.6	45.1	170	30	40.5	9	7.7	0	0	5.4
10	0.5	40	156	45.5	65	170	30.8	42.1	9.4	7.6	0	0	5.8
11	0.5	57	146	45.8	95.4	166	45.8	100.2	-8.5	-19.5	-12.1	-41	38.4
12	0.5	40	156	39.7	56.6	170	39.7	52.7	16	14.4	0	0	5.4
13	0.5	48	156	53.1	77.5	170	34	53	11.1	9.8	0	0	3.0
14	0.5	43	156	39.5	55.1	166	39.5	55.8	13.9	13	0	0	2.8
15	0.5	38	156	43.8	63.6	170	20	43.3	6.7	5.8	0	0	2.1
16	0.5	36	146	30.6	59.5	166	30.6	74.8	5.7	-4.6	4.5	4	14.8
17	0.5	40	146	43.2	63	166	43.2	100.3	3.5	-10.2	3.1	2.6	18.5
18	0.5	43	146	32.3	51.5	166	32.3	92.8	1.7	-4.3	1.8	1.4	8.0
19	0.5	42	156	43.7	68.4	170	22.3	41.5	2.9	1.9	0	0	2.3
20	0.5	43	146	45.2	69.8	166	45.2	99	1	-5.1	0.2	-3.3	12.2
21	0.5	30	146	28.4	44.5	166	28.4	74.4	9.2	1.5	0	0	12.4
22	0.5	40	146	44.8	85.6	166	44.8	86.7	5.9	-5.3	4.4	-1.7	20.9
23	0.5	33	146	32.5	60.5	166	32.5	75.9	9.9	4.9	5.4	-4.7	21.1
24	0.5	38	146	43.5	80.4	166	43.5	85.1	7.6	-4	6	0.3	22.0
25	0.5	45	156	46.5	69.5	170	36.1	47.9	5.3	3.3	0	0	5.7
26	0.5	50	146	49.4	94.2	167	49.4	100.1	1.4	-5.2	-4.7	-26.3	29.5
27	0.5	56	156	37.7	60.6	170	37.7	46.1	2	0.9	0	0	3.5
28	0.5	35	156	41.5	60.4	170	32.6	41.4	0	0	0	0	0.0
29	0.5	30	156	29.8	41	166	29.8	37.6	0	0	0	0	0.0
30	0.5	45	156	47.3	74	170	38.9	46.1	0	0	0	0	0.0
31	0.5	30	156	29	42.4	170	29	37.7	11.1	10.2	0	0	4.1
32	0.5	40	156	33.5	50.6	170	33.5	42.5	0	0	0	0	0.0

Data for isothermal time = 1

Sample	HoldingTime (min)	Weight (mg)	Eu Melt.Temp (°C)	Eu Endo Start (mW)	Eu Endo End (mW)	φ Melt. Temp (°C)	φ Endo Start (mW)	φ Endo End (mW)	φ Exo Start (mW)	φ Exo End (mW)	Eu Exo Start (mW)	Eu Exo End (mW)	Normalized % Remaining In [(Integration ratio)*Initial In Wt%]
1	1	36	156	23.4	32.7	166	23.4	41.9	8.2	7.4	0	0	2.9
2	1	53	146	27.5	60.6	166	27.5	81.8	0.11	-6.9	-4.3	-21	27.1
3	1	48	156	28.1	44.1	170	28.1	38.1	0	0	0	0	0.0
4	1	43	146	30	53.6	166	30	86.9	4.7	-3.8	0	0	10.6
5	1	35	146	32.9	52.3	166	32.9	71.7	5.7	-2.7	0	0	14.4
6	1	46	156	40.3	65.2	170	13.1	33.1	2.7	2.2	0	0	1.1
7	1	40	156	36.9	58.5	170	11	32.8	0	0	0	0	0.0
8	1	55	145	39.3	91.9	166	39.3	96.8	-0.2	-21	-1.7	-7.1	23.8
9	1	39	145	37.1	63.8	166	37.1	81	4	-0.9	2.2	0.6	9.2
10	1	37	156	33.4	45.4	170	33.4	39.7	5.9	4.9	6.6	6.5	6.0
11	1	36	156	34.3	53.4	170	10.6	34.8	7.8	7.6	0	0	0.5
12	1	38	146	21.7	44.5	166	21.7	77.6	6.4	-1.4	0	0	9.9
13	1	28	156	23.8	36	170	23.8	31.8	11.7	11.3	0	0	2.0
14	1	31	156	19.6	24.9	166	19.6	43.6	10.7	10.6	0	0	0.3
15	1	34	156	21.6	29.8	166	21.6	44.5	9.5	9.3	0	0	0.6
16	1	52	146	43.5	73.2	166	43.5	111.3	-1.9	-9.3	-7	-10.4	11.1
17	1	41	146	27.2	61.9	167	27.2	78.9	6.7	-6.3	0	0	15.0
18	1	38	146	31.4	73.3	167	31.4	74.5	5.5	0.5	2.4	-13.1	24.1
19	1	32	156	23.8	32.4	170	23.8	40.9	8.6	8.4	0	0	0.8
20	1	25	156	29.3	41.2	170	15	30.5	11.7	11.3	0	0	1.5
21	1	28	146	24.3	49.6	166	24.3	60.2	10.5	6.7	8.6	-2	23.5
22	1	29	156	20.5	25.8	166	20.5	41.8	11.9	11.2	0	0	2.6
23	1	23	145	22.2	36.5	166	22.2	56.8	11.1	8.1	8.7	8.4	6.7
24	1	52	146	26.9	63.9	166	26.9	85.2	0	-15.3	0	0	16.1
25	1	23	146	28.4	47.7	167	28.4	58.3	12.8	6.5	0	0	12.8
26	1	37	146	32.9	69.9	167	32.9	72.2	7.7	-5.2	6.2	3.6	20.3
27	1	43	156	38.5	53.3	170	38.5	45	5.7	4.4	6.1	5.9	7.0
28	1	38	146	35.1	72	166	35.1	72.3	5.5	0.7	1.3	-13.1	25.9
29	1	35	156	33.4	45.6	170	33.4	41	0	0	0	0	0.0
30	1	30	146	23.2	42.4	166	23.2	68.7	10	5.8	10.1	9.9	6.8
31	1	31	156	32.5	45.7	170	32.5	36.3	0	0	0	0	0.0
32	1	34	156	25.2	36.9	166	25.2	36.5	0	0	0	0	0.0

Data for isothermal time = 5

Sample	HoldingTime (min)	Weight (mg)	Eu Melt.Temp (°C)	Eu Endo Start (mW)	Eu Endo End (mW)	φ Melt. Temp (°C)	φ Endo Start (mW)	φ Endo End (mW)	φ Exo Start (mW)	φ Exo End (mW)	Eu Exo Start (mW)	Eu Exo End (mW)	Normalized % Remaining In [(Integration ratio)*Initial In Wt%]
1	5	50	156	42.4	60.2	170	30.2	45	4	3.8	0	0	0.6
2	5	31	156	23.7	34.3	170	23.7	40.7	11	10.8	0	0	0.7
3	5	32	146	26.3	44.2	166	26.3	70.6	0	0	0	0	0.0
4	5	35	146	28	53.6	166	28	68	9.7	4.1	0	0	8.5
5	5	40	146	38.9	81.8	166	38.9	82.1	7.8	2.1	3.3	1.8	8.4
6	5	40	156	43.2	64.4	170	31.5	42.1	7.7	7.6	0	0	0.3
7	5	31	156	34.3	47.7	170	34.3	40.5	12.2	11.9	11.5	11	4.1
8	5	31	156	28.1	40	170	28.1	34.6	0	0	0	0	0.0
9	5	24	146	35.5	51.4	168	35.5	52.1	22	20.3	20.7	20.5	5.8
10	5	36	156	32.5	45	170	32.5	38.6	11.5	11.4	0	0	0.5
11	5	35	156	33.8	45.5	170	24.6	35.7	0	0	0	0	0.0
12	5	41	156	23.4	32.7	166	23.4	42.5	8	7.7	0	0	1.1
13	5	29	156	31.6	44	170	31.6	37.4	0	0	0	0	0.0
14	5	36	146	29	61.7	166	29	75.8	13.9	11.5	0	0	3.0
15	5	44	146	27	50.2	166	27	90.5	0	0	0	0	0.0
16	5	35	146	27.3	60	166	27.3	73.8	11.7	9.3	0	0	3.0
17	5	48	156	27.1	44.3	170	27.1	42.2	5.4	5.2	0	0	0.6
18	5	30	146	32.7	57.1	167	32.7	78.3	10.9	6.9	9.3	9.2	5.9
19	5	39	146	39	61.9	166	39	85.4	0	0	0	0	0.0
20	5	49	156	23.3	35	166	23.3	54.1	0	0	0	0	0.0
21	5	32	146	27.7	50	166	27.7	78	13	9.3	10.7	10.1	5.9
22	5	30	156	24	38.2	170	24	38.7	13.2	13	0	0	0.7
23	5	45	156	42.8	68.6	170	29.2	42.3	0	0	0	0	0.0
24	5	36	156	37.4	57.2	170	28.8	38.9	0	0	0	0	0.0
25	5	32	146	25.7	56.5	167	25.7	68.9	12.5	8	8.1	7.8	6.5
26	5	37	146	26.8	51.6	166	26.8	85.8	7.6	3	5.2	4.2	6.7
27	5	44	155	24.3	35.5	166	24.3	50.3	0	0	0	0	0.0
28	5	35	146	33.8	60.4	168	33.8	90.3	10.5	5.1	0	0	6.5
29	5	36	146	35.5	57.9	167	35.5	80.7	0	0	0	0	0.0
30	5	36	145	35.5	75.5	168	35.5	76	9.5	4.3	6	2	11.4
31	5	36	156	23.8	30.9	166	23.8	44.2	0	0	0	0	0.0
32	5	34	146	35.5	73.3	166	35.5	67.8	14	11.5	12.7	12.5	3.9

Data for isothermal time = 10

Sample	HoldingTime (min)	Weight (mg)	Eu Melt.Temp (°C)	Eu Endo Start (mW)	Eu Endo End (mW)	φ Melt. Temp (°C)	φ Endo Start (mW)	φ Endo End (mW)	φ Exo Start (mW)	φ Exo End (mW)	Eu Exo Start (mW)	Eu Exo End (mW)	Normalized % Remaining In [(Integration ratio)*Initial In Wt%]
1	10	37	146	35.4	61.8	166	35.4	85.8	7.8	5	9	7.8	5.2
2	10	36	145	35.2	60.7	168	35.2	84.9	0	0	0	0	0.0
3	10	35	156	34.4	48	170	34.4	40.1	0	0	0	0	0.0
4	10	51	146	29.7	52.8	166	29.7	97.7	3	-1	5.2	4.5	5.2
5	10	26	155	26.3	36.8	170	26.3	34.2	0	0	0	0	0.0
6	10	30	146	26.5	54.1	166	26.5	65.2	0	0	0	0	0.0
7	10	30	156	21	25	166	21	47.7	0	0	0	0	0.0
8	10	38	156	38.1	56.7	170	25.8	38.7	0	0	0	0	0.0
9	10	32	156	25	37.1	170	25	38.7	0	0	0	0	0.0
10	10	43	146	27.5	50.9	166	27.5	85.7	0	0	0	0	0.0
11	10	36	146	35	69	168	35	70	10	5.6	8	6.8	8.1
12	10	39	146	37.2	78.9	168	37.2	80	9.1	3	0	0	7.2
13	10	36	146	27.3	58.1	167	27.3	72	9.4	5.2	0	0	5.6
14	10	40	146	39.2	81.2	167	39.2	77.8	0	0	0	0	0.0
15	10	39	146	37.6	61.7	168	37.6	86.2	0	0	0	0	0.0
16	10	32	156	31.4	42.6	170	31.4	41.2	13.3	13.2	0	0	0.5
17	10	50	146	29.3	54.5	166	29.3	94.7	0	0	0	0	0.0
18	10	33	156	23.9	35.1	170	23.9	38.9	11.7	11.6	0	0	0.4
19	10	34	156	24.3	35.3	170	24.3	41.8	0	0	0	0	0.0
20	10	30	146	27.5	55.6	168	27.5	64.6	0	0	0	0	0.0
21	10	30	146	35.5	51.2	168	35.5	67.7	14.9	12.7	0	0	4.6
22	10	31	156	35.4	46.1	171	35.4	41.5	0	0	0	0	0.0
23	10	29	156	24.9	33.8	171	24.9	33.8	0	0	0	0	0.0
24	10	32	156	21.2	29.1	170	21.2	45.1	11.3	11.28	0	0	0.1
25	10	33	156	34.2	46.5	170	34.2	38.9	0	0	0	0	0.0
26	10	29	156	31.8	40.9	170	31.8	39.8	15	14.9	0	0	0.6
27	10	27	156	24.2	32.4	170	24.2	24.3	0	0	0	0	0.0
28	10	35	146	36.2	72.5	170	36.2	72	0	0	0	0	0.0
29	10	37	146	26.6	48.7	166	26.6	80.6	7.9	4.8	7.2	6.9	4.5
30	10	34	156	33.4	47.1	170	33.4	43.5	0	0	0	0	0.0
31	10	28	156	31.4	44.3	170	31.4	40	0	0	0	0	0.0
32	10	47	146	35.4	60.5	167	35.4	75	12	6.1	0	0	9.1

Data for isothermal time = 25

Sample	HoldingTime (min)	Weight (mg)	Eu Melt.Temp (°C)	Eu Endo Start (mW)	Eu Endo End (mW)	φ Melt. Temp (°C)	φ Endo Start (mW)	φ Endo End (mW)	φ Exo Start (mW)	φ Exo End (mW)	Eu Exo Start (mW)	Eu Exo End (mW)	Normalized % Remaining In [(Integration ratio)*Initial In Wt%]
1	25	34	156	24.5	35.3	168	24.5	42.9	0	0	0	0	0.0
2	25	44	146	40.7	82.5	168	40.7	78.2	0	0	0	0	0.0
3	25	42	146	39.2	64.2	168	39.2	92.1	0	0	0	0	0.0
4	25	31	156	33.2	45.7	171	33.2	40.1	0	0	0	0	0.0
5	25												
6	25	30	156	32.9	43.7	170	32.9	40	0	0	0	0	0.0
7	25	44	155	29.4	42.8	170	29.4	40.8	0	0	0	0	0.0
8	25	55	146	33.3	75	168	33.3	91.6	0	0	0	0	0.0
9	25												
10	25												
11	25												
12	25	37	156	33.6	37.9	168	33.6	50.1	0	0	0	0	0.0
13	25	49	146	42.9	64	170	42.9	87.6	3.5	2.1	6.6	5.7	3.5
14	25	36	156	36.3	44.2	170	36.3	46.8	0	0	0	0	0.0
15	25	32	156	24.3	32.6	170	24.3	39.2	0	0	0	0	0.0
16	25												
17	25	29	146	34.1	58.5	170	34.1	57.8	12.7	11.1	13.3	12.7	4.6
18	25	36	146	36.5	58.3	170	36.5	82	8	7	10.8	9.5	3.4
19	25	35	146	27.7	45.6	168	27.7	77.6	9.9	8.8	11.8	11.3	2.4
20	25	25	146	33.4	58	168	33.4	56	13.6	12.1	13.9	13.4	4.2
21	25	38	156	20.6	24.5	170	20.6	49.5	0	0	0	0	0.0
22	25	26	146	25.8	40.1	166	25.8	64.6	12.6	11.9	14	13.6	2.1
23	25												
24	25												
25	25												
26	25												
27	25												
28	25	30	146	28.2	44.1	168	28.2	67.9	0	0	0	0	0.0
29	25	34	146	29.4	55.3	169	29.4	66.6	11.1	9.2	12	10.1	6.0
30	25												
31	25												
32	25	25	146	25.9	47.6	170	25.9	55.8	13	11.6	13.5	12.9	3.9

Data for isothermal time = 40

Sample	HoldingTime (min)	Weight (mg)	Eu Melt.Temp (°C)	Eu Endo Start (mW)	Eu Endo End (mW)	φ Melt. Temp (°C)	φ Endo Start (mW)	φ Endo End (mW)	φ Exo Start (mW)	φ Exo End (mW)	Eu Exo Start (mW)	Eu Exo End (mW)	Normalized % Remaining In [(Integration ratio)*Initial In Wt%]
1	40	26	156	31.8	40.8	170	31.8	38.9	0	0	0	0	0.0
2	40	28	156	30.2	40.3	170	30.2	39.2	0	0	0	0	0.0
3	40	28	146	25.3	42.1	166	25.3	66.1	0	0	0	0	0.0
4	40	31	146	37.2	54.3	168	37.2	72.3	13	12	0	0	1.9
5	40	36	146	37.5	71.3	169	37.5	71	7.6	6.6	11	9.1	4.3
6	40	50	156	38.3	51.2	170	38.3	52.3	0	0	0	0	0.0
7	40	37	156	23.6	31.2	170	23.6	49.7	0	0	0	0	0.0
8	40	40	146	30.3	57.6	166	30.3	71.7	9.3	7.8	10.6	9.6	3.6
9	40												
10	40	35	146	35.5	70.3	168	35.5	70.8	0	0	0	0	0.0
11	40	41	156	38.2	51.8	170	38.2	49.1	0	0	0	0	0.0
12	40												
13	40												
14	40												
15	40	36	146	38.9	59.1	168	38.9	79.7	0	0	0	0	0.0
16	40	43	156	25.2	36.5	168	25.2	48.6	0	0	0	0	0.0
17	40												
18	40												
19	40	25	156	24.7	32.6	170	24.7	34.8	0	0	0	0	0.0
20	40	42	146	27.7	47.1	170	27.7	84.5	8.8	7.8	0	0	1.3
21	40	36	146	35.8	71.1	170	35.8	69.1	11.8	10.3	13.6	11.3	5.5
22	40												
23	40												
24	40	43	146	30.5	66.1	168	30.5	80.5	0	0	0	0	0.0
25	40	43	156	26.2	37.3	170	26.2	50.9	0	0	0	0	0.0
26	40												
27	40												
28	40												
29	40	42	146	41.4	70.5	170	41.4	97.5	10	9.3	12	11.3	1.6
30	40												
31	40	46	146	30.6	54.6	169	30.6	90.9	7.4	6.3	0	0	1.3
32	40	33	146	28.6	56.1	168	28.6	68	11.9	10.8	13	11.8	3.4

Data for isothermal time = 60

Sample	HoldingTime (min)	Weight (mg)	Eu Melt.Temp (°C)	Eu Endo Start (mW)	Eu Endo End (mW)	φ Melt. Temp (°C)	φ Endo Start (mW)	φ Endo End (mW)	φ Exo Start (mW)	φ Exo End (mW)	Eu Exo Start (mW)	Eu Exo End (mW)	Normalized % Remaining In [(Integration ratio)*Initial In Wt%]
1	60	48	156	24.5	35.4	170	24.5	50	0	0	0	0	0.0
2	60	42	156	21	25	170	21	55.3	0	0	0	0	0.0
3	60	40	156	38.9	50.9	170	38.9	49.1	0	0	0	0	0.0
4	60	40	146	30.4	53.5	170	30.4	85.3	11.2	10.7	0	0	0.6
5	60	34	146	37.4	63.1	170	37.4	83.7	14	13.3	0	0	1.0
6	60	44	146	31.3	47.2	166	31.3	78.1	9.3	8.8	0	0	0.8
7	60	42	146	30.9	65.8	167	30.9	76.8	8	7.2	9.9	8.6	2.6
8	60	54	156	21.7	26.5	170	21.7	48.4	0	0	0	0	0.0
9	60	44	146	40.2	68.2	170	40.2	67.3	0	0	0	0	0.0
10	60												
11	60	43	146	30.5	44.8	166	30.5	77.4	0	0	0	0	0.0
12	60	34	146	36.5	60	170	36.5	61.7	11.3	10.3	13	11.9	4.3
13	60	44	156	26.6	34.5	166	26.6	48.5	0	0	0	0	0.0
14	60												
15	60												
16	60												
17	60	43	146	32.2	56.3	168	32.2	68.3	9.7	8.1	11	9.5	5.1
18	60												
19	60	40	146	33	57.1	168	33	67.7	0	0	0	0	0.0
20	60	47	156	39.1	44.6	172	39.1	50.3	0	0	0	0	0.0
21	60	55	146	46.7	80.5	170	46.7	77.3	2.8	0.8	6	4	6.2
22	60	45	146	41.5	58.8	168	41.5	81	0	0	0	0	0.0
23	60												
24	60												
25	60												
26	60												
27	60												
28	60	39	156	36.3	45.5	170	36.3	41.6	0	0	0	0	0.0
29	60	43	146	40.8	58.9	170	40.8	80.3	8.3	7.7	0	0	1.0
30	60	45	156	36.4	43.2	170	36.4	54.4	0	0	0	0	0.0
31	60												
32	60												

Appendix 5. ANOVA for second phase DOE:

Global Model:

Factorial Fit: % In-Rich Re versus Composition, Ag Particle , ...

Estimated Effects and Coefficients for % In-Rich Remaining (coded units)

Term	Effect	Coef	SE Coef	T	P
Constant		4.142	0.2803	14.77	0.000
Composition	6.362	3.181	0.2803	11.35	0.000
Ag Particle Size	2.502	1.251	0.2803	4.46	0.000
Processing Temperature	-2.721	-1.361	0.2803	-4.85	0.000
Heating Rate	1.278	0.639	0.2803	2.28	0.024
Holding Time	-12.867	-6.434	0.4008	-16.05	0.000
Composition*Ag Particle Size	1.895	0.947	0.2803	3.38	0.001
Composition*Processing Temperature	-1.517	-0.758	0.2803	-2.70	0.007
Composition*Heating Rate	1.011	0.506	0.2803	1.80	0.073
Composition*Holding Time	-9.004	-4.502	0.4008	-11.23	0.000
Ag Particle Size* Processing Temperature	-1.564	-0.782	0.2803	-2.79	0.006
Ag Particle Size*Heating Rate	0.542	0.271	0.2803	0.97	0.335
Ag Particle Size*Holding Time	-3.347	-1.673	0.4008	-4.17	0.000
Processing Temperature*Heating Rate	-0.238	-0.119	0.2803	-0.43	0.671
Processing Temperature*Holding Time	2.014	1.007	0.4008	2.51	0.013
Heating Rate*Holding Time	-2.286	-1.143	0.4008	-2.85	0.005
Composition*Ag Particle Size* Processing Temperature	-1.207	-0.604	0.2803	-2.15	0.032
Composition*Ag Particle Size* Heating Rate	0.290	0.145	0.2803	0.52	0.605
Composition*Processing Temperature* Heating Rate	-0.073	-0.037	0.2803	-0.13	0.896
Composition*Ag Particle Size* Holding Time	-2.298	-1.149	0.4008	-2.87	0.005
Composition*Processing Temperature* Holding Time	-0.289	-0.145	0.4008	-0.36	0.719

```
Composition*Heating Rate*              -1.771  -0.886   0.4008   -2.21
0.028
  Holding Time
Ag Particle Size*                      -0.160  -0.080   0.2803   -0.29
0.775
  Processing Temperature*
  Heating Rate
Ag Particle Size*                       1.859   0.929   0.4008    2.32
0.021
  Processing Temperature*
  Holding Time
Ag Particle Size*Heating Rate*         -0.972  -0.486   0.4008   -1.21
0.226
  Holding Time
Processing Temperature*Heating Rate*    0.215   0.107   0.4008    0.27
0.789
  Holding Time
Composition*Ag Particle Size*          -0.040  -0.020   0.2803   -0.07
0.943
  Processing Temperature*
  Heating Rate
Composition*Ag Particle Size*           1.309   0.654   0.4008    1.63
0.104
  Processing Temperature*
  Holding Time
Composition*Ag Particle Size*          -0.615  -0.307   0.4008   -0.77
0.444
  Heating Rate*Holding Time
Composition*Processing Temperature*    -0.048  -0.024   0.4008   -0.06
0.952
  Heating Rate*Holding Time
Ag Particle Size*                       0.218   0.109   0.4008    0.27
0.786
  Processing Temperature*
  Heating Rate*Holding Time
Composition*Ag Particle Size*           0.117   0.058   0.4008    0.15
0.884
  Processing Temperature*
  Heating Rate*Holding Time


S = 4.37318     PRESS = 5640.41
R-Sq = 77.27%   R-Sq(pred) = 70.07%   R-Sq(adj) = 74.13%


Analysis of Variance for % In-Rich Remaining (coded units)

Source               DF   Seq SS   Adj SS   Adj MS      F      P
Main Effects          5  10128.6  8319.78  1663.96  87.01  0.000
2-Way Interactions   10   3846.4  3612.61   361.26  18.89  0.000
3-Way Interactions   10    524.8   480.90    48.09   2.51  0.007
4-Way Interactions    5     63.9    63.78    12.76   0.67  0.649
5-Way Interactions    1      0.4     0.40     0.40   0.02  0.884
Residual Error      224   4283.9  4283.94    19.12
  Lack of Fit        96   4001.9  4001.95    41.69
  Pure Error        128    282.0   281.99     2.20
Total               255  18848.1
```

Main Effects Model:

```
The regression equation is (uncoded units)
```

```
% In-Rich Remaining = 8.64 + 0.121 Ag Particle Size + 0.518 Composition
                     - 0.0607 Processing Temperature + 0.0544 Heating Rate
                     - 1.66 Holding Time


Predictor                   Coef  SE Coef       T      P
Constant                   8.638    4.529    1.91  0.058
Ag Particle Size         0.12091  0.02953    4.09  0.000
Composition              0.51753  0.04921   10.52  0.000
Processing Temperature  -0.06070  0.01476   -4.11  0.000
Heating Rate             0.05445  0.02461    2.21  0.028
Holding Time             -1.6603   0.1397  -11.89  0.000


S = 5.90577   R-Sq = 53.7%   R-Sq(adj) = 52.8%

PRESS = 9155.17   R-Sq(pred) = 51.43%


Analysis of Variance

Source           DF       SS      MS      F      P
Regression        5  10128.6  2025.7  58.08  0.000
Residual Error  250   8719.5    34.9
  Lack of Fit   122   8437.5    69.2  31.39  0.000
  Pure Error    128    282.0     2.2
Total           255  18848.1
```

Model I: (t: 0→1 minutes)

Factorial Fit: % In-Rich Re versus Composition, Ag Particle , ...

All possible effects considered (31)

```
Estimated Effects and Coefficients for % In-Rich Remaining (coded units)

Term                                  Effect    Coef  SE Coef       T      P
Constant                                       11.948   0.2417   49.43  0.000
Composition                           17.144   8.572   0.2417   35.46  0.000
Ag Particle Size                       6.565   3.283   0.2417   13.58  0.000
Processing Temperature                -4.834  -2.417   0.2417  -10.00  0.000
Heating Rate                           4.214   2.107   0.2417    8.72  0.000
Holding Time                          -6.094  -3.047   0.2841  -10.72  0.000
Composition*Ag Particle Size           4.772   2.386   0.2417    9.87  0.000
Composition*Processing Temperature    -0.868  -0.434   0.2417   -1.80  0.077
Composition*Heating Rate               3.334   1.667   0.2417    6.90  0.000
Composition*Holding Time              -2.852  -1.426   0.2841   -5.02  0.000
Ag Particle Size*                     -4.174  -2.087   0.2417   -8.64  0.000
  Processing Temperature
Ag Particle Size*Heating Rate          1.710   0.855   0.2417    3.54  0.001
Ag Particle Size*Holding Time         -0.473  -0.237   0.2841   -0.83  0.408
Processing Temperature*Heating Rate   -0.582  -0.291   0.2417   -1.20  0.233
Processing Temperature*Holding Time    3.328   1.664   0.2841    5.86  0.000
Heating Rate*Holding Time             -2.060  -1.030   0.2841   -3.63  0.001
Composition*Ag Particle Size*         -3.270  -1.635   0.2417   -6.76  0.000
  Processing Temperature
Composition*Ag Particle Size*          1.133   0.566   0.2417    2.34  0.022
  Heating Rate
Composition*Processing Temperature*   -0.154  -0.077   0.2417   -0.32  0.751
  Heating Rate
Composition*Ag Particle Size*         -0.614  -0.307   0.2841   -1.08  0.284
```

Holding Time					
Composition*Processing Temperature*	1.729	0.864	0.2841	3.04	0.003
Holding Time					
Composition*Heating Rate*	-1.458	-0.729	0.2841	-2.57	0.013
Holding Time					
Ag Particle Size*	-0.421	-0.210	0.2417	-0.87	0.387
Processing Temperature*					
Heating Rate					
Ag Particle Size*	0.992	0.496	0.2841	1.75	0.086
Processing Temperature*					
Holding Time					
Ag Particle Size*Heating Rate*	-1.039	-0.520	0.2841	-1.83	0.072
Holding Time					
Processing Temperature*Heating Rate*	0.957	0.478	0.2841	1.68	0.097
Holding Time					
Composition*Ag Particle Size*	-0.300	-0.150	0.2417	-0.62	0.537
Processing Temperature*					
Heating Rate					
Composition*Ag Particle Size*	1.230	0.615	0.2841	2.17	0.034
Processing Temperature*					
Holding Time					
Composition*Ag Particle Size*	-1.597	-0.799	0.2841	-2.81	0.007
Heating Rate*Holding Time					
Composition*Processing Temperature*	0.903	0.452	0.2841	1.59	0.117
Heating Rate*Holding Time					
Ag Particle Size*	0.241	0.121	0.2841	0.42	0.672
Processing Temperature*					
Heating Rate*Holding Time					
Composition*Ag Particle Size*	0.784	0.392	0.2841	1.38	0.173
Processing Temperature*					
Heating Rate*Holding Time					

S = 2.33687 PRESS = 915.843
R-Sq = 97.01% R-Sq(pred) = 92.16% R-Sq(adj) = 95.56%

Analysis of Variance for % In-Rich Remaining (coded units)

Source	DF	Seq SS	Adj SS	Adj MS	F	P
Main Effects	5	9205.5	9464.36	1892.87	346.62	0.000
2-Way Interactions	10	1627.9	1693.56	169.36	31.01	0.000
3-Way Interactions	10	397.5	427.79	42.78	7.83	0.000
4-Way Interactions	5	84.4	85.65	17.13	3.14	0.014
5-Way Interactions	1	10.4	10.39	10.39	1.90	0.173
Residual Error	64	349.5	349.50	5.46		
Lack of Fit	16	98.3	98.34	6.15		
Pure Error	48	251.2	251.16	5.23		
Total	95	11675.2				

Factorial Fit: % In-Rich Re versus Composition, Ag Particle , ...

Reduced model after ANOVA, only considering statistically significant effects

Estimated Effects and Coefficients for % In-Rich Remaining (coded units)

Term	Effect	Coef	SE Coef	T	P
Constant		11.948	0.2534	47.15	0.000
Composition	17.144	8.572	0.2534	33.83	0.000
Ag Particle Size	6.500	3.250	0.2501	13.00	0.000

Processing Temperature	-4.834	-2.417	0.2534	-9.54	0.000
Heating Rate	4.214	2.107	0.2534	8.31	0.000
Holding Time	-6.094	-3.047	0.2979	-10.23	0.000
Composition*Ag Particle Size	4.687	2.344	0.2501	9.37	0.000
Composition*Heating Rate	3.334	1.667	0.2534	6.58	0.000
Composition*Holding Time	-2.852	-1.426	0.2979	-4.79	0.000
Ag Particle Size* Processing Temperature	-4.037	-2.019	0.2501	-8.07	0.000
Ag Particle Size*Heating Rate	1.567	0.783	0.2501	3.13	0.002
Processing Temperature*Holding Time	3.328	1.664	0.2979	5.59	0.000
Heating Rate*Holding Time	-2.060	-1.030	0.2979	-3.46	0.001
Composition*Ag Particle Size* Processing Temperature	-3.270	-1.635	0.2534	-6.45	0.000
Composition*Ag Particle Size* Heating Rate	1.133	0.566	0.2534	2.24	0.028
Composition*Processing Temperature* Holding Time	1.564	0.782	0.2939	2.66	0.010
Composition*Heating Rate* Holding Time	-1.458	-0.729	0.2979	-2.45	0.017
Composition*Ag Particle Size* Processing Temperature* Holding Time	1.230	0.615	0.2979	2.07	0.042
Composition*Ag Particle Size* Heating Rate*Holding Time	-1.597	-0.799	0.2979	-2.68	0.009

S = 2.45003 PRESS = 753.820
R-Sq = 96.04% R-Sq(pred) = 93.54% R-Sq(adj) = 95.12%

Analysis of Variance for % In-Rich Remaining (coded units)

Source	DF	Seq SS	Adj SS	Adj MS	F	P
Main Effects	5	9205.5	9471.09	1894.22	315.56	0.000
2-Way Interactions	7	1609.8	1633.99	233.43	38.89	0.000
3-Way Interactions	4	329.0	358.24	89.56	14.92	0.000
4-Way Interactions	2	68.8	68.76	34.38	5.73	0.005
Residual Error	77	462.2	462.20	6.00		
Lack of Fit	29	211.0	211.04	7.28		
Pure Error	48	251.2	251.16	5.23		
Total	95	11675.2				

Model II: (t: 1→10 minutes):

Factorial Fit: % In-Rich Re versus Composition, Ag Particle , ...

All possible effects considered (31)

Estimated Effects and Coefficients for % In-Rich Remaining (coded units)

Term	Effect	Coef	SE Coef	T	P
Constant		4.535	0.2094	21.66	0.000
Composition	7.518	3.759	0.2094	17.95	0.000
Ag Particle Size	3.272	1.636	0.2094	7.81	0.000
Processing Temperature	-2.840	-1.420	0.2094	-6.78	0.000
Heating Rate	0.984	0.492	0.2094	2.35	0.022
Holding Time	-7.440	-3.720	0.2550	-14.59	0.000
Composition*Ag Particle Size	2.430	1.215	0.2094	5.80	0.000
Composition*Processing Temperature	-1.414	-0.707	0.2094	-3.38	0.001

Composition*Heating Rate	0.549	0.274	0.2094	1.31	0.195
Composition*Holding Time	-5.934	-2.967	0.2550	-11.63	0.000
Ag Particle Size* Processing Temperature	-1.369	-0.684	0.2094	-3.27	0.002
Ag Particle Size*Heating Rate	0.387	0.193	0.2094	0.92	0.359
Ag Particle Size*Holding Time	-3.061	-1.531	0.2550	-6.00	0.000
Processing Temperature*Heating Rate	0.033	0.017	0.2094	0.08	0.937
Processing Temperature*Holding Time	-0.557	-0.279	0.2550	-1.09	0.279
Heating Rate*Holding Time	-0.993	-0.496	0.2550	-1.95	0.056
Composition*Ag Particle Size* Processing Temperature	-0.562	-0.281	0.2094	-1.34	0.184
Composition*Ag Particle Size* Heating Rate	-0.059	-0.030	0.2094	-0.14	0.888
Composition*Processing Temperature* Heating Rate	0.504	0.252	0.2094	1.20	0.233
Composition*Ag Particle Size* Holding Time	-2.297	-1.149	0.2550	-4.50	0.000
Composition*Processing Temperature* Holding Time	-1.880	-0.940	0.2550	-3.69	0.000
Composition*Heating Rate* Holding Time	-0.595	-0.297	0.2550	-1.17	0.248
Ag Particle Size* Processing Temperature* Heating Rate	-0.016	-0.008	0.2094	-0.04	0.969
Ag Particle Size* Processing Temperature* Holding Time	1.341	0.671	0.2550	2.63	0.011
Ag Particle Size*Heating Rate* Holding Time	-0.100	-0.050	0.2550	-0.20	0.845
Processing Temperature*Heating Rate* Holding Time	-0.242	-0.121	0.2550	-0.47	0.637
Composition*Ag Particle Size* Processing Temperature* Heating Rate	0.556	0.278	0.2094	1.33	0.189
Composition*Ag Particle Size* Processing Temperature* Holding Time	0.629	0.315	0.2550	1.23	0.222
Composition*Ag Particle Size* Heating Rate*Holding Time	0.253	0.127	0.2550	0.50	0.622
Composition*Processing Temperature* Heating Rate*Holding Time	-0.692	-0.346	0.2550	-1.36	0.180
Ag Particle Size* Processing Temperature* Heating Rate*Holding Time	-0.197	-0.098	0.2550	-0.39	0.701
Composition*Ag Particle Size* Processing Temperature* Heating Rate*Holding Time	-0.732	-0.366	0.2550	-1.44	0.156

S = 2.04778 PRESS = 540.709
R-Sq = 93.39% R-Sq(pred) = 86.68% R-Sq(adj) = 90.19%

Analysis of Variance for % In-Rich Remaining (coded units)

Source	DF	Seq SS	Adj SS	Adj MS	F	P
Main Effects	5	2597.03	2715.79	543.157	129.53	0.000
2-Way Interactions	10	973.36	983.99	98.399	23.47	0.000
3-Way Interactions	10	189.97	191.56	19.156	4.57	0.000
4-Way Interactions	5	22.23	23.13	4.627	1.10	0.368
5-Way Interactions	1	8.64	8.64	8.637	2.06	0.156
Residual Error	64	268.38	268.38	4.193		
Lack of Fit	16	226.11	226.11	14.132		

```
  Pure Error        48    42.27    42.27    0.881
Total               95  4059.60
```

Reduced model after ANOVA, only considering statistically significant effects

Estimated Effects and Coefficients for % In-Rich Remaining (coded units)

Term	Effect	Coef	SE Coef	T	P
Constant		4.535	0.2110	21.50	0.000
Composition	7.518	3.759	0.2110	17.82	0.000
Ag Particle Size	3.272	1.636	0.2110	7.76	0.000
Processing Temperature	-2.867	-1.434	0.2106	-6.81	0.000
Heating Rate	0.935	0.467	0.2106	2.22	0.029
Holding Time	-7.440	-3.720	0.2570	-14.48	0.000
Composition*Ag Particle Size	2.430	1.215	0.2110	5.76	0.000
Composition*Processing Temperature	-1.414	-0.707	0.2110	-3.35	0.001
Composition*Holding Time	-5.934	-2.967	0.2570	-11.55	0.000
Ag Particle Size* Processing Temperature	-1.369	-0.684	0.2110	-3.24	0.002
Ag Particle Size*Holding Time	-3.061	-1.531	0.2570	-5.96	0.000
Composition*Ag Particle Size* Holding Time	-2.297	-1.149	0.2570	-4.47	0.000
Composition*Processing Temperature* Holding Time	-1.880	-0.940	0.2570	-3.66	0.000
Ag Particle Size* Processing Temperature* Holding Time	1.341	0.671	0.2570	2.61	0.011

```
S = 2.06318     PRESS = 471.293
R-Sq = 91.40%   R-Sq(pred) = 88.39%   R-Sq(adj) = 90.04%
```

Analysis of Variance for % In-Rich Remaining (coded units)

Source	DF	Seq SS	Adj SS	Adj MS	F	P
Main Effects	5	2597.03	2718.08	543.616	127.71	0.000
2-Way Interactions	5	942.49	952.30	190.460	44.74	0.000
3-Way Interactions	3	171.03	171.03	57.010	13.39	0.000
Residual Error	82	349.05	349.05	4.257		
Lack of Fit	34	306.78	306.78	9.023		
Pure Error	48	42.27	42.27	0.881		
Total	95	4059.60				

Model III: (t: 10→60 minutes):

Factorial Fit: % In-Rich Re versus Composition, Ag Particle , ...

All possible effects considered (31)

Estimated Effects and Coefficients for % In-Rich Remaining (coded units)

Term	Effect	Coef	SE Coef	T	P
Constant		1.003	0.04748	21.13	0.000
Composition	1.956	0.978	0.04748	20.59	0.000
Ag Particle Size	0.699	0.349	0.04748	7.36	0.000

Processing Temperature	-2.007	-1.003	0.04748	-21.13	0.000
Heating Rate	0.151	0.075	0.04748	1.59	0.116
Holding Time	-0.923	-0.462	0.06429	-7.18	0.000
Composition*Ag Particle Size	0.648	0.324	0.04748	6.82	0.000
Composition*Processing Temperature	-1.956	-0.978	0.04748	-20.59	0.000
Composition*Heating Rate	0.130	0.065	0.04748	1.37	0.175
Composition*Holding Time	-0.833	-0.416	0.06429	-6.48	0.000
Ag Particle Size* Processing Temperature	-0.699	-0.349	0.04748	-7.36	0.000
Ag Particle Size*Heating Rate	0.021	0.010	0.04748	0.22	0.829
Ag Particle Size*Holding Time	0.095	0.047	0.06429	0.74	0.463
Processing Temperature*Heating Rate	-0.151	-0.075	0.04748	-1.59	0.116
Processing Temperature*Holding Time	0.923	0.462	0.06429	7.18	0.000
Heating Rate*Holding Time	0.074	0.037	0.06429	0.58	0.566
Composition*Ag Particle Size* Processing Temperature	-0.648	-0.324	0.04748	-6.82	0.000
Composition*Ag Particle Size* Heating Rate	-0.000	-0.000	0.04748	-0.00	0.997
Composition*Processing Temperature* Heating Rate	-0.130	-0.065	0.04748	-1.37	0.175
Composition*Ag Particle Size* Holding Time	0.185	0.093	0.06429	1.44	0.153
Composition*Processing Temperature* Holding Time	0.833	0.416	0.06429	6.48	0.000
Composition*Heating Rate* Holding Time	0.111	0.056	0.06429	0.86	0.390
Ag Particle Size* Processing Temperature* Heating Rate	-0.021	-0.010	0.04748	-0.22	0.829
Ag Particle Size* Processing Temperature* Holding Time	-0.095	-0.047	0.06429	-0.74	0.463
Ag Particle Size*Heating Rate* Holding Time	0.070	0.035	0.06429	0.54	0.590
Processing Temperature*Heating Rate* Holding Time	-0.074	-0.037	0.06429	-0.58	0.566
Composition*Ag Particle Size* Processing Temperature* Heating Rate	0.000	0.000	0.04748	0.00	0.997
Composition*Ag Particle Size* Processing Temperature* Holding Time	-0.185	-0.093	0.06429	-1.44	0.153
Composition*Ag Particle Size* Heating Rate*Holding Time	0.107	0.053	0.06429	0.83	0.409
Composition*Processing Temperature* Heating Rate*Holding Time	-0.111	-0.056	0.06429	-0.86	0.390
Ag Particle Size* Processing Temperature* Heating Rate*Holding Time	-0.070	-0.035	0.06429	-0.54	0.590
Composition*Ag Particle Size* Processing Temperature* Heating Rate*Holding Time	-0.107	-0.053	0.06429	-0.83	0.409

S = 0.536176 PRESS = 56.3170
R-Sq = 94.54% R-Sq(pred) = 88.85% R-Sq(adj) = 92.77%

Analysis of Variance for % In-Rich Remaining (coded units)

Source	DF	Seq SS	Adj SS	Adj MS	F	P
Main Effects	5	272.789	281.442	56.2884	195.80	0.000
2-Way Interactions	10	175.850	179.290	17.9290	62.37	0.000

3-Way Interactions	10	27.576	27.132	2.7132	9.44	0.000
4-Way Interactions	5	1.093	1.092	0.2184	0.76	0.581
5-Way Interactions	1	0.198	0.198	0.1976	0.69	0.409
Residual Error	96	27.598	27.598	0.2875		
Lack of Fit	32	12.147	12.147	0.3796		
Pure Error	64	15.452	15.452	0.2414		
Total	127	505.102				

Factorial Fit: % In-Rich Re versus Composition, Ag Particle , ...

Reduced model after ANOVA, only considering statistically significant effects

Estimated Effects and Coefficients for % In-Rich Remaining (coded units)

Term	Effect	Coef	SE Coef	T	P
Constant		1.003	0.04723	21.24	0.000
Composition	1.956	0.978	0.04723	20.70	0.000
Ag Particle Size	0.703	0.351	0.04715	7.45	0.000
Processing Temperature	-2.007	-1.003	0.04723	-21.24	0.000
Holding Time	-0.923	-0.462	0.06396	-7.22	0.000
Composition*Ag Particle Size	0.656	0.328	0.04715	6.96	0.000
Composition*Processing Temperature	-1.956	-0.978	0.04723	-20.70	0.000
Composition*Holding Time	-0.833	-0.416	0.06396	-6.51	0.000
Ag Particle Size* Processing Temperature	-0.703	-0.351	0.04715	-7.45	0.000
Processing Temperature*Holding Time	0.923	0.462	0.06396	7.22	0.000
Composition*Ag Particle Size* Processing Temperature	-0.656	-0.328	0.04715	-6.96	0.000
Composition*Processing Temperature* Holding Time	0.833	0.416	0.06396	6.51	0.000

S = 0.533413 PRESS = 40.8106
R-Sq = 93.47% R-Sq(pred) = 91.92% R-Sq(adj) = 92.85%

Analysis of Variance for % In-Rich Remaining (coded units)

Source	DF	Seq SS	Adj SS	Adj MS	F	P
Main Effects	4	272.03	280.96	70.2409	246.87	0.000
2-Way Interactions	5	174.24	178.40	35.6806	125.40	0.000
3-Way Interactions	2	25.83	25.83	12.9147	45.39	0.000
Residual Error	116	33.01	33.01	0.2845		
Lack of Fit	20	11.41	11.41	0.5707		
Pure Error	96	21.59	21.59	0.2249		
Total	127	505.10				

Appendix 6. Point-count data for Fractional Density Study:

Data for 10 Wt.% In Paste:

Field No.	P (pore hits)	(P / Po) X 100	(Pi - Ppavg)^2
1	7	35	25.00
2	8	40	0.00
3	8	40	0.00
4	8	40	0.00
5	7	35	25.00
6	9	45	25.00
7	7	35	25.00
8	9	45	25.00
9	10	50	100.00
10	7	35	25.00
11	9	45	25.00
12	8	40	0.00
13	7	35	25.00
14	10	50	100.00
15	7	35	25.00
16	7	35	25.00
17	8	40	0.00
18	9	45	25.00
19	8	40	0.00
20	7	35	25.00
Sum	160		500

Po	20.00		
Fractional Porosity (Ppavg)	40.00	Fractional Density	60.00
s(Ppavg)	5.13		
CV	12.82		
95% Confidence Interval	2.46		
% Relative Accuracy	6.16		

Data for 20 Wt.% In Paste:

Field No.	P (pore hits)	(P / Po) X 100	(Pi - Ppavg)^2
1	6	30	1.56
2	7	35	39.06
3	6	30	1.56
4	6	30	1.56
5	5	25	14.06
6	6	30	1.56
7	6	30	1.56
8	5	25	14.06
9	5	25	14.06
10	5	25	14.06
11	6	30	1.56
12	7	35	39.06
13	5	25	14.06
14	5	25	14.06
15	6	30	1.56
16	5	25	14.06
17	5	25	14.06
18	6	30	1.56
19	7	35	39.06
20	6	30	1.56
Sum	115		243.75

Po	20.00		
Fractional Porosity (Ppavg)	28.75	Fractional Density	71.25
s(Ppavg)	3.58		
CV	12.46		
95% Confidence Interval	1.72		
% Relative Accuracy	5.98		

Data for 30 Wt.% In Paste:

Field No.	P (pore hits)	(P / Po) X 100	(Pi - Ppavg)^2
1	3	15	12.25
2	2.5	12.5	1.00
3	2	10	2.25
4	1.5	7.5	16.00
5	2	10	2.25
6	1.5	7.5	16.00
7	2.5	12.5	1.00
8	3	15	12.25
9	1.5	7.5	16.00
10	3	15	12.25
11	3	15	12.25
12	2	10	2.25
13	2	10	2.25
14	1.5	7.5	16.00
15	3	15	12.25
16	2	10	2.25
17	2	10	2.25
18	3	15	12.25
19	2	10	2.25
20	3	15	12.25
Sum	46		167.5

Po	20.00		
Fractional Porosity (Ppavg)	11.50	Fractional Density	88.50
s(Ppavg)	2.97		
CV	25.82		
95% Confidence Interval	1.43		
% Relative Accuracy	12.40		

Data for 40 Wt.% In Paste:

Field No.	P (pore hits)	(P / Po) X 100	(Pi - Ppavg)^2
1	2	10	20.25
2	1	5	0.25
3	0.5	2.5	9.00
4	2	10	20.25
5	1	5	0.25
6	0.5	2.5	9.00
7	1.5	7.5	4.00
8	1	5	0.25
9	0.5	2.5	9.00
10	0	0	30.25
11	1.5	7.5	4.00
12	2	10	20.25
13	2	10	20.25
14	1	5	0.25
15	1	5	0.25
16	0.5	2.5	9.00
17	1	5	0.25
18	0.5	2.5	9.00
19	1	5	0.25
20	1.5	7.5	4.00
Sum	22		170

Po	20.00		
Fractional Porosity (Ppavg)	5.50	Fractional Density	94.50
s(Ppavg)	2.99		
CV	54.39		
95% Confidence Interval	1.44		
% Relative Accuracy	26.11		

Appendix 7. ANOVA for densification screening DOE (Equation 59):

Factorial Fit: Fractional D versus In-Compositi, Ag Particle , ...

Estimated Effects and Coefficients for Fractional Density (1-Porosity) (coded units) considering all possible effects.

Term	Effect	Coef
Constant		73.626
In-Composition	23.657	11.829
Ag Particle Size	-3.908	-1.954
Processing Temperature	7.783	3.891
Heating Rate	1.470	0.735
In-Composition*Ag Particle Size	-1.688	-0.844
In-Composition* Processing Temperature	-2.438	-1.219
In-Composition*Heating Rate	-1.185	-0.593
Ag Particle Size* Processing Temperature	1.937	0.969
Ag Particle Size*Heating Rate	3.375	1.688
Processing Temperature*Heating Rate	2.125	1.062
In-Composition*Ag Particle Size* Processing Temperature	1.033	0.516
In-Composition*Ag Particle Size* Heating Rate	-1.345	-0.673
In-Composition* Processing Temperature* Heating Rate	-2.405	-1.203
Ag Particle Size* Processing Temperature* Heating Rate	-4.405	-2.202
In-Composition*Ag Particle Size* Processing Temperature* Heating Rate	1.000	0.500

Analysis of Variance for Fractional Density (1-Porosity) (coded units)

Source	DF	Seq SS	Adj SS	Adj MS	F	P
Main Effects	4	2550.70	2550.70	637.674	*	*
2-Way Interactions	6	119.41	119.41	19.902	*	*
3-Way Interactions	4	112.25	112.25	28.063	*	*
4-Way Interactions	1	4.00	4.00	4.000	*	*
Residual Error	0	*	*	*		
Total	15	2786.36				

Factorial Fit: Fractional D versus In-Compositi, Ag Particle , ...

Reduced analysis considering statistically significant parameters, note that no interactions were identified as significant.

Estimated Effects and Coefficients for Fractional Density (1-Porosity) (coded units)

Term	Effect	Coef	SE Coef	T	P
Constant		63.626	1.157	63.63	0.000

In-Composition	23.657	10.234	1.157	10.22	0.000
Ag Particle Size	-3.908	-1.744	1.157	-1.69	0.119
Processing Temperature	7.783	3.421	1.157	3.36	0.006
Heating Rate	1.470	0.635	1.157	0.64	0.538

S = 4.62863 PRESS = 498.600
R-Sq = 94.54% R-Sq(pred) = 91.51% R-Sq(adj) = 92.47%

References:

[1] McCluskey, F. P., Grzybowski, R., Podlesak, T., High Temperature Electronics, CRC Press, Boca Raton, 1997.

[2] Neudeck, P.G., Spry, D.J., Beheim, G.M., Okojie, R.S., "6H-SiC Transistor Integrated Circuits Demonstrating Prolonged Operation at 500°C," Proc of International Conference on High Temperature Electronics (HiTEC 2008), Albuquerque, NM, May 12-15, 2008.

[3] Johnson, R.W., Williams, J., "SiC Power Device Packaging Technologies for 300 to 350°C Applications," *Materials Science Forum*, Vols. 483-485, 2005, pp. 785-790.

[4] Lee, C.C., Wang, C.Y., Matijasevic, G., "Advances in Bonding Technology for Electronic Packaging," *Journal of Electronic Packaging*, Vol. 115, June 1993, pp. 201-207.

[5] Matijasevic, G., Wang, C.Y., Lee, C.C., "Void Free Bonding of Large Silicon Dice Using Gold-Tin Alloy," *IEEE Transactions on Components, Hybrids and Manufacturing Technology*, Vol. CHMT-13, 1990, pp. 1128-1134.

[6] Schwarzbauer, H., Kuhnert, R., "Novel Large Area Joining Technique for Improved Power Device Performance," *IEEE Transactions on Industry Applications*, Vol. 27, No. 1, January/February 1991, pp. 93-95.

[7] Lu, G.Q., Catala, J.N., Zhang, Z., Bai, J.G., "A Lead-Free, Low Temperature Sintering Die Attach Technique for High Performance and High Temperature Packaging," *IEEE CPMT Conference on High Density Microsystem Design and Packaging and Component Failure Analysis*, June-July 2004, pp. 42-46.

[8] "High Temperature Interconnection Joints," Luna Innovations Annual Report for Air Force Contract # FA8650-04-M-5010, Joint collaboration with University of Maryland and University of Alberta.

[9] Quintero, P., McCluskey, P., "High Temperature Lead-Free Attach Reliability," *Proc of ASME-IPACK*, Vancouver, BC, July. 2007.

[10] Quintero, P., Oberc, T., McCluskey, F.P., "Reliability Assessment of High Temperature Lead-Free Device Attach Technologies," Proc of ECTC, Orlando, FL, May, 2008.

[11] R.M. German, Liquid Phase Sintering, Plenum Press, New York, N.Y., 1985.

[12] R.M. German, Sintering Theory and Practice, Wiley-Interscience Publications, New York, N.Y., 1996.

[13] Lu, G.Q., Zhang, Z., "Pressure Assisted Low-Temperature Sintering of Silver Paste as an Alternative Die Attach Solution to Reflow," *IEEE Transactions on Electronic Packaging Manufacturing*, Vol. 25, No. 4, October, 2002.

[14] Palmer, M. A., Erdman, N.S., McCall, D., "Forming High Temperature Solder Joints Through Liquid Phase Sintering of Solder Paste," *Journal of Electronic Materials*, Vol. 28, No. 11, 1999.

[15] Shaw, M.C., "High Performance Packaging of Power Electronics," MRS Bulletin, January, 2003.

[16] Eastman, L.F., Mishra, U.K., "The Toughest," IEEE Spectrum, pp. 28-33, May, 2002.

[17] Schwarzbauer, H., "Method of Securing Electronic Components to a Substrate," US Patent 4 810 672.
[18] Crane, C.H., Lovell, D.T., Baginski, W.A., Olsen, M.G., "Diffusion Welding of Dissimilar Metals," *Welding Res. Supp*., pp. 23-31, January, 1967.
[19] O'Brien, M., Rice, C.H., Olson, D.L., "High Strength Diffusion Welding of Silver Coated Base Metals," *Welding Journal*, pp.25-27, January, 1976.
[20] Lu, G.Q., Calata, J.N., Lei, G., Chen, X., "Low-temperature and Pressurless Sintering Technology for High-performance and High-temperature Interconnection of Semiconductor devices," *8th International Conference EuroSime* 2007.
[21] Bai, J.G., Lu, G.Q., "Thermomechanical Reliability of Low-Temperature Sintered Silver Die Attached SiC Power Device Assembly," *IEEE Transactions on Device and Materials Reliability*, Vol. 6, No.3, September, 2006.
[22] Corbin, S.F., Lucier, P., "Thermal Analysis of Isothermal Solidification Kinetics during Transient Liquid Phase Sintering," *Metallurgical and Materials Transactions A*, Volume 32A, April 2001, pp. 971-978.
[23] Zhou, Y., Kuntz, M.L., Corbin, S.F., "Prediction of the Completion Time for Isothermal Solidification in TLP Bonding," Proceedings from Joining of Advanced and Specialty Materials, 7-9 October 2002, Columbus, OH, ASM International, 2003, pp. 75-82.
[24] MacDonald, W.D., Eagar, T.W., "Transient Liquid Phase Bonding Process," The Metal Science of Joining, *The Minerals, Metals, and Materials Society*, 1992.
[25] Tuah-Poku, I., Dollar, M., Massalski, T.B., "A Study of the Transient Liquid Phase Bonding Process Applied to an Ag/Cu/Ag Sandwich Joint," *Metallurgical Transactions A*, Vol. 19A, March 1988, pp. 675-686.
[26] Cain, S.R., Wilcox, J.R., Venkatraman, R., "A Diffusional Model for Transient Liquid Phase Bonding," *Acta Mater.* Vol 45, No.2, 1997, pp. 701-707.
[27] MacDonald, W.D., Eagar, T.W., "Isothermal Solidification Kinetics of Diffusion Brazing," *Metallurgical and Materials Transactions A*, Volume 29A, January, 1998. pp 315-325.
[28] Turriff, D.M., Corbin, S.F., "Modeling the Influence of Solid-State Interdiffusion and Dissolution on Transient Liquid Phase Sintering Kinetics in a Binary Isomorphus System," *Metallurgical and Materials Transactions*, Volume 37A, May 2006, pp 1645-1655.
[29] Crank, J., The Mathematics of Diffusion, Claredon Press, Oxford, 1976.
[30] Zhou, Y., Gale, W.F., North, T.H., "Modeling of transient liquid phase bonding," *International Materials Reviews*, Vol. 40 No.5, (1995), pp. 181-196.
[31] Kuntz, M.L., Corbin, S.F., Zhou, Y., "Quantifying Metallurgical Interactions in Solid/Liquid Diffusion Couples using Differential Scanning Calorimetry," *Acta Materialia*, Vol. 53, 2005, pp. 3071-3082.
[32] Lesoult, G., Center for Joining of Materials Report, Carnegie Mellon University, Pittsburgh, PA, September, 1976.

[33] Nakagawa, H., Lee, C.H., North, T.H., Metallurgical Transactions A, 22A, 543-555, 1991.
[34] Robert E. Reed-Hill, Reza Abbaschian, Physical Metallurgy Principles, 3rd Edition, 1994, PWS Publishing Company, Boston, pp. 502-504.
[35] Sakamoto, A., Fujiwara, C., Hattori, T., Sakai, S., Welding Journal, Vol. 68, 1989, pp. 63-71.
[36] Illingworth, T.C., Golosnoy, I.O., Clyne, T.W., "Modeling of transient phase bonding in binary systems-A new parametric study," Materials Science and Engineering A, 445-446 (2007), pp. 493-500.
[37] Nakao, Y., "Advanced Transient Liquid Insert Metal Diffusion Bonding Using Alloyed Powder," The 5th International Symposium of the Japan Welding Society, 1990, pp. 139-144.
[38] Savitskii, A.P., "Liquid Phase Sintering of the Systems with Interacting Components," Advanced Science and technology of Sintering, edited by Stojanovic et al., Kluwer Academic, Plenum Publishers, New York, 1999, pp.19-28.
[39] Corbin, S.F., McIsaac, D.J., "Differential Scanning Calorimetry of the Stages of Transient Liquid Phase Sintering," *Materials Science and Engineering A*, Vol. 346, 2003, pp. 132-140.
[40] Kuntz, M.L., "Quantifying Isothermal Solidification Kinetics during Transient Liquid Phase Bonding using Differential Scanning Calorimetry", PhD Thesis, University of Waterloo, Canada, 2006.
[41] Bernstein, L., "Semi-Conductor Joining by Solid-Liquid Interdiffusion (SLID) Process," *Journal of Electrochemical Society*, Vol. 113, No. 12, 1966, pp. 1282-1288.
[42] William F. Smith, Foundations of Materials Science and Engineering, Second Edition, McGraw-Hill, Inc., New York, 1993.
[43] Vladislav Zinovev, Handbook of Thermophysical Properties of Metals at High Temperatures, Nova Science Publishers, Inc., New York, 1996.
[44] http://www.matweb.com/index.asp?ckck=1
[45] William D. Callister, Jr., Materials Science and Engineering an Introduction, Sixth Edition, John Wiley and Sons, Inc., New Jersey, 2003.
[46] Max Hansen, Constitution of Binary Alloys, Second Edition, McGraw-Hill Book Company, Inc., New York, 1958.
[47] M.R. Baren, in: T.B. Massalski (Ed.), Binary Alloy Phase Diagrams, ASM International, Material Park, OH, 1990, p.47.
[48] Rita R., Sen, S.K., "The Kinetics of Formation of Intermetallics in Ag/In Thin Film Couples," *Thin Solid Films*, Vol. 197, 1991, pp. 303-318.
[49] Keppner, W., Weshe, R., Klas, T., Voigt, J., Schatz, G., *Thin Solid Films*, Vol. 143, 1986, pp. 201-215.
[50] Simic, V., Marinkovic, Z., "Room Temperature Interactions in Ag- Metals Thin Film Couples," *Institute of Physics*, Vol. 12, 1978.
[51] Lin, J.C., Huang, L.W., Jang, G.Y., Lee, S.L., "Solid-Liquid Interdiffusion Bonding Between In-coated Silver Thick Films," *Thin Solid Films*, Vol. 410, 2002, pp. 212-221.

[52] So, W.W., Lee, C.C., "High Temperature Joints Manufactured at Low Temperatures," *Electronic Components and Technology Conference*, 1998, pp. 284-291.
[53] Chen, Y.C., So, W.W., Lee, C.C., "A Fluxless Bonding Technology Using Indium-Silver Multilayer Composites," *IEEE Transactions on Components, Packaging, and Manufacturing Technology-Part A*, Vol. 20, No. 1, March 1997, pp. 46-51.
[54] Chuang, R., Lee, C.C., "Silver-Indium Joints Produced at Low Temperature for High Temperature Devices," *IEEE Transactions on Components and Packaging Technologies*, Vol. 25, No.3, September 2002, pp.453-458.
[55] White, C.E.T., Okamoto, H., Phase Diagrams of Indium Alloys and Their Engineering Applications, ASM International, Materials Park, OH, pp. 15
[56] Colin C. Johnson, Joseph Kevra, Solder Paste Technology: Principles and Applications, First Edition, TAB Professional and Reference Books, 1989.
[57] Quiao, X., Corbin, S.F., "Development of Transient Liquid Phase Sintered Sn-Bi Solder Paste," *Materials Science and Engineering*, A283, 2000, pp. 38-45.
[58] Corbin, S.F., "High Temperature Variable Melting Point Sn-Sb Lead-Free Pastes Using Transient Liquid Phase Sintering Processing," *Journal of Electronic Materials*, Vol. 34, No. 7, 2005.
[59] Ulrich, R.K., Brown, W.D., Advanced Electronic Packaging, 2nd edition, John Wiley and Sons, Inc., NJ, 2006.
[60] Randal M. German, Powder Metallurgy Science, Metal Powder Industries Federation, Princeton, New Jersey, 1989.
[61] Rao, C.N.R., Rao, K., Phase Transitions in Solids, McGraw Hill, New York, NY, 1978.
[62] Raymond H. Myers and Douglas C. Montgomery: Response Surface Methodology, Process and Product Optimization Using Designed Experiments, Second Edition, John-Wiley and Sons, Inc. 2002.
[63] Corbin, S.F., "Diffusion-Based Model for Isothermal Solidification Kinetics during Transient Liquid Phase Sintering," *Metallurgical and Materials Transactions A*, Volume 33A, January, 2002, pp. 117-124.
[64] Vander Voort, G.F., Metallography, Principles and Practice, ASM International, Ohio, 1999.
[65] Danniger, H., "Homogenization and Pore Formation During Sintering with Transient Liquid Phase," *Powder Metallurgy International*, Vol. 20, No. 1, 1988, pp. 21-25.
[66] Maraki, A.E., Colombo, P., Clyne, T.W., "Highly Porous Metals and Ceramics," in Encyclopedia of Condensed Matter Physics, vol. 2. G. Bassani, G.L. Liedl, P. Wyder eds., Elsevier, Oxford, (2005), pp. 318-332.
[67] Montes, J.M., Rodriguez, J.A., Herrera, E.J., "Thermal and electrical conductivities of sintered powder compacts," *Powder Metallurgy*, Vol. 46, No. 3, 2003, pp. 251-256.
[68] Schulz, B., High Temp. – High Press., 1981, 13, pp. 649-660.
[69] Fan, H., et al., "Modulus-density scaling behavior and framework architecture of nanoporous self-assembled silicas," *Nature Materials*, Vol. 6, June 2007.

[70] Underwood, E.E., Quantitative Stereology, Addison-Wesley, Massachusetts, 1970.
[71] Pecht, M.G., et al., Electronic Packaging: Materials and Their Properties, CRC Press, Boca Raton, Fl., 1999.
[72] Ashcroft, N.W., Mermin, N.D., Solid State Physics, 1976. Holt, Rinehart, and Winston.
[73] Indium Corporation Solder Alloy Directory, Technical Bulletin.
[74] MIL-STD-883G Method 2019.7 "Die Shear Strength"
[75] JEDEC Standard No. 22-A104C, Test Method A104C "Temperature Cycling"
[76] Oberc, T., Quintero, P., McCluskey, "Viability of an Alternative High Temperature Surface Mount Attach," Proc of International Conference on High Temperature Electronics (HiTEC 2008), Albuquerque, NM, May 12-15, 2008.
[77] D'Hondt, T., Corbin, S.F., "Thermal Analysis of the Compositional Shift in a Transient Liquid Phase during Sintering of a Ternary Cu-Sn-Bi Powder Mixture," *Metallurgical and Materials Transactions A*, Vol. 37A, January, 2006, pp. 217-224.
[78] Hu, C., Baker, T.N., "An analysis of the capillary force and optimum liquid volume in a transient phase sintering process," *Materials Science and Engineering A*, 190 (1995), pp. 125-129.
[79] Liu, Y.M., Chen, Y.L., Chuang, T.H., "Interfacial Reactions between Liquid Indium and Silver Substrates," *Journal of Electronic Materials*, Vol. 29, No. 8, 2000, pp. 1047-1051.
[80] Moser, Z., et al., "Studies of the Ag-In Phase Diagram and Surface Tension Measurements," *Journal of Electronic Materials*, Vol. 30, No. 9, 2001, pp.1120-1127.
[81] German, R.M., "Phase Diagrams in Liquid Phase Sintering," *Journal of Metals*, August 1986.
[82] Illingworth, T.C., Golosnoy, I.O., Gergely, V., Clyne, T.W., "Numerical modeling of transient liquid phase bonding and other diffusion controlled phase changes," *Journal of Materials Science*, Vol. 40, (2005), pp. 2505-2511.
[83] Zhou, Y., North, T.H., "Process Modeling and Optimized Parameter Selection During Transient Liquid Phase Bonding," Z. Metalkd, 85 (1994), pp. 775-780.
[84] Zhou, Y., North, T.H., "Kinetic modeling of diffusion controlled, two phase moving interface problems," *Modeling Simulation Material Science Engineering*, (1993), pp. 505-516.
[85] Lorenz, A., Sachs, E., Allen, S., "Freeze-Off Limits in Transient Liquid Phase Infiltration," *Metallurgical and Materials Transactions A*, Vol. 35A, February, 2004, pp. 641-653.
[86] Anestiev, L.A., Froyen, L., "Model of primary rearrangement processes at liquid phase sintering and selective laser sintering due to biparticle interactions," *Journal of Applied Physics*, Vol. 86, No. 7, (1999), pp. 4008-4017.

[87] Yeheskel, O., Shokhat, M., Ratzker, M., Dariel, P., "Elastic constants of porous silver compacts after acid assisted consolidation at room temperature," *Journal of Materials Science*, Vol. 36, (2001), pp. 1219-1225.
[88] Lorenz, A., Sachs, E., Allen, S., Rafflebeul, L., Kernan, B., "Densification of a Powder-Metal Skeleton by Transient Liquid Phase Infiltration," *Metallurgical and Materials Transactions A*, Vol. 35A, February, 2004, pp. 631-640.
[89] Danninger, H., "Homogenization and Pore Formation During Sintering with Liquid Phase." *Powder Metallurgy International*, Vol. 20, No. 1, 1998.
[90] Faust, N., Messler, R.W., Khatri, S., "Alternatives for Joining Si Wafers to Strain-Accommodating Cu for High Power Electronics," *Journal of Electronic Materials*, Vol. 30, No. 10, 2001.
[91] Lumley, R.N., Schaffer, G.B., "The Effect of Solubility and Particle Size on Liquid Phase Sintering," *Scripta Materialia*, Vol. 35, No.5, 1996, pp. 589-595.
[92] Turker, M., "Effect of production parameters on the structure and morphology of Ag nanopowders produced by inert gas condensation," *Materials Science and Engineering A*, Vol. 367, (2004), pp. 74-81.